Deciphering the role of varying iceberg source in abrupt climate change

Rachel Tanya North

Thesis submitted for the degree of Doctor of Philosophy

Cardiff University

September 2015

Deciphering the role of varying iceberg source in abrupt climate change

Heinrich events involve the massive release of icebergs from continental ice sheets into the sub-polar North Atlantic, which travel as far south as 40°N and deposit large quantities of Ice Rafted Debris (IRD) in marine sediments. Determining the distribution of IRD sources across the Atlantic during Heinrich events is a vital step in ascertaining the sequence of iceberg rafting, and the relative involvement of circum-North Atlantic ice sheets in this release of freshwater to the North Atlantic.

This study examines evidence from multiple radiogenic isotope (Nd, Sr and Pb) analyses on the detrital clay size fraction (<2μm), and stable isotopes in the detrital <63 μm fraction of a Hudson Strait (HS) source ($\delta^{18}O$ of <-2.5 and εNd of <-19) in the clay and fine fraction deposited at the IRD belt site during Heinrich events. At the north-eastern British margin changes in detrital $\delta^{18}O$ and εNd are related to small inputs of HS derived material during H4, however during H2 there is no discernible HS source to the fine fraction this is contrary to previous coarse fraction studies at the site. It is proposed that the dominance of the British and Irish Ice Sheet (BIIS) source at the site during H2 is due to the increasing size of the British Ice sheet over the course of the last glacial.

Endmember modelling of particle size distributions demonstrate a coarsening of the silt fraction over the Heinrich events at the IRD belt site. At the margin of the BIIS there is a correspondence between millennial scale IRD events and coarse particle size distributions which is superimposed on increases in the finest endmember over the last glacial in response to the BIIS reaching the shelf edge.

Changes in stable isotopes of surface dwelling foraminifera demonstrate that the surface waters were fresher during H2 and H4 coinciding with fine fraction IRD inputs. At the British ice sheet margin, increasing surface water stratification after 27 ka BP coincides with increases in fine particle size endmember and $\delta^{18}O$ of the fine fraction further indicating the consistent presence of the BIIS at the shelf edge after 27 ka BP.

DECLARATION

This work has not been submitted in substance for any other degree or award at this or any other university or place of learning, nor is being submitted concurrently in candidature for any degree or other award.
Signed …… (candidate) Date

……

STATEMENT 1

This thesis is being submitted in partial fulfillment of the requirements for the degree of PhD

Signed …… (candidate) Date

……

STATEMENT 2

This thesis is the result of my own independent work/investigation, except where otherwise stated.

Other sources are acknowledged by explicit references. The views expressed are my own.

Signed …… (candidate) Date

……

STATEMENT 3

I hereby give consent for my thesis, if accepted, to be available online in the University's Open Access repository and for inter-library loan, and for the title and summary to be made available to outside organisations.

Signed …… (candidate) Date

……

STATEMENT 4: PREVIOUSLY APPROVED BAR ON ACCESS

I hereby give consent for my thesis, if accepted, to be available online in the University's Open Access repository and for inter-library loans **after expiry**

of a bar on access previously approved by the Academic Standards & Quality Committee.

Signed …… (candidate) Date ……

Acknowledgements

Firstly, I would like to thank my supervisors Ian Hall and Steve Barker for giving me the opportunity to work on this project. I would like to say a huge thank you to Lukas Jonkers for his discussions and for reading and discussing the many chapter drafts. I cannot express my gratitude to Sidney Hemming for hosting me at LDEO and both Sidney and Steven Goldstein for their help and insight in using radiogenic isotopes. I would like to say a huge thank you to Cristina Recasens, Merry Yue-Cai for inviting me into their homes, putting up with my incessant questions and for showing me the ropes in the clean lab. I would like to thank Louise Bolge and Emmanuel for teaching me how to use the Neptune I would like to thank Lindsey Owen for all her help and efforts with the coulter counter, and to Sandra Nederbragt for having the patience to teach me how to use the delta V. I would like to thank Elisabet Michel for looking after me at CNRS and giving me the opportunity to work on core SU92-09.

I would like to thank those who made my stay in New York so wonderful in the lab and in the city so thank you Sascha, Hella, Kennet, Hong Chin, Guilliem, and Paola.

I would like to thank Hannah Hughes for reading over my chapter, and Paola Mofffa Sanchez for her support. I would like to say a warm thank you to all of those who shared an office with me over the past four years (you know who you are) and in particular, Anna, Elaine, Jamie and Sam, for the endless stream of tea, cake, jokes and fun.

I would like to thank my partner Dan whose constant encouragement has kept me going and I would like to thank my family for their unwavering love and support.

Contents

List of Figures, Tables and Equations

Acronyms

$\delta^{18}O$	oxygen isotope ratio relative to VPDB
$\delta^{18}O_{FINE}$	$\delta^{18}O$ of the fine (<63mm) fraction
$\delta^{18}O_{sw}$	$\delta^{18}O$ of seawater
AMOC	Atlantic Meridional Overturning Circulation
BIIS	British and Irish Ice sheet
D-O cycle	Dansgaaard Oeschger cycle
EMMA	End member model algorithm
FSIS	Fennoscandian ice sheet
GICC05	NGRIP age model (2005)
GIS	Greenland ice sheet
GISP2	Greenland ice sheet project 2
GNAIW	Glacial North Atlantic Intermediate Water
GS	Greenland Stadial
HS	Hudson Strait
IC	Irminger Current
IIS	Icelandic ice sheet
IODP	International Ocean Drilling Program
IRD	Ice rafted detritus
ISOW	Iceland Scotland Overflow Water
ka BP	thousand calendar years Before Present (1950) CE)
LGM	Last glacial maximum
LIS	Laurentide ice sheet
MIS	Marine isotope stage
NAD	North Atlantic Drift current
NADW	North Atlantic Deep Water
NGRIP	North Greenland Ice core Project
PSD	Particle size distribution
SCW	Southern Component Water
Sv	Sverdrup (106 m^3/s)
VPDB	Vienna Pee Dee Belemnite (oxygen isotope standard for calcite)
VSMOW	Vienna Standard mean ocean water (oxygen isotope standard for water)

1 Introduction

There is increasing global attention on the climate system, and specifically its natural variability and response to major changes in forcing. This results from growing concern about the potential for abrupt climate changes in response to anthropogenic increases in the concentration of greenhouse gases since the industrial revolution. The NRC (The National Research Council) committee on Abrupt climate change (2002) defines abrupt climate change as occurring when:

*"**The climate system is forced to cross some threshold, triggering a transition to a new state at a rate determined by the climate system itself and faster than the cause" (NRC committee on Abrupt climate change (2002), p.14)***

Research into past climate has become a vital way of understanding how the climate system reacts to large-scale changes in climate forcing. The Atlantic Meridional Overturning Circulation (AMOC) plays a key role in the global climate system through its northward redistribution of heat (Rahmstorf, 2002). Current estimates are of 1.33 PW northward ocean heat transport for an overturning circulation of 18.6 Sv (Johns et al., 2010). Changes in the AMOC have been associated with large fluctuations in the Earth's climate in the past and projections of AMOC decline provide a key source of uncertainty regarding future climate change. Recently, a multi-proxy reconstruction of the AMOC index suggests that the weakness of the AMOC since 1975 is unprecedented in the last millennium (Rahmstorf et al., 2015). Further melting of Greenland in the coming decades could contribute to further weakening of the AMOC. Rapid changes in the vigour of the AMOC are associated with abrupt climate changes during the last glacial climate (Rahmstorf, 2002). The North Atlantic region is thought to be sensitive to freshwater perturbations and therefore this region is a crucial study area for cryosphere-ocean interactions, and associated abrupt climate shifts.

1.1 North Atlantic abrupt climate change during the last glacial

Records of $\delta^{18}O$ (a proxy of local air temperature and global ice volume) from Greenland ice cores (Dansgaard et al., 1982; Oeschger et al., 1984; Johnsen et al., 1992; Dansgaard et al., 1993; Grootes et al., 1993; Andersen et al., 2004; NEEM

community, 2013) show large abrupt changes in temperature during the last glacial (between 110 and 12 ka).

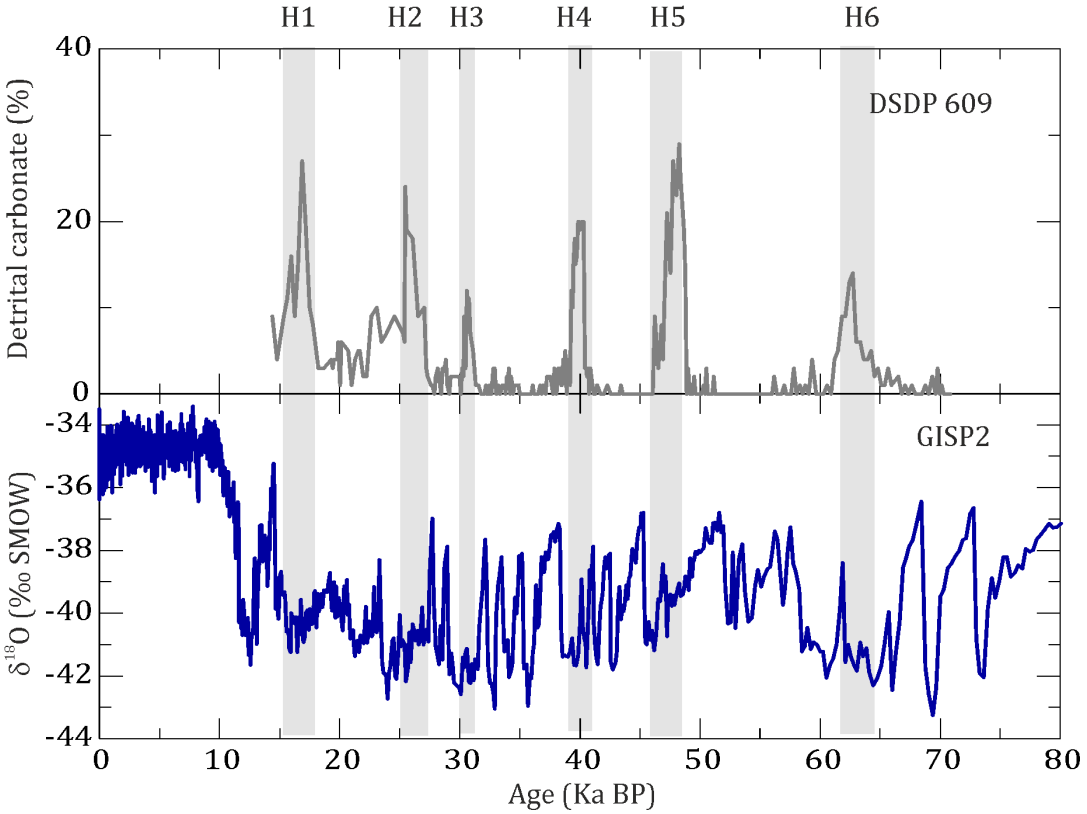

Figure 1.1: Examples of Atlantic abrupt climate change. Top, a record of the percentage detrital carbonate from the DSDP 609 core in the North Atlantic, peaks marked in grey correspond to Heinrich events (H1-H6) (Bond and Lotti, 1995). Bottom, the $\delta^{18}O$ record from the GISP2 ice core in Greenland showing Dansgaard-Oeschger events during the last glacial period (Grootes et al., 1993).

These climate variations, known as Dansgaard-Oeschger cycles (D-O cycles), began with a stadial (cold glacial conditions) lasting centuries to millennia, followed by a rapid warming (5-16 °C) over a period of decades to an interstadial state (warmer glacial conditions). Interstadials mark periods of gradual cooling, ended by a further rapid change back to stadial conditions (Rahmstorf, 2002; Barker et al., 2011) as shown in Figure 1.1. Bond et al. (1993) demonstrated that these cycles are matched by changes in the North Atlantic marine record with cooler stadial periods observed in the Greenland ice cores matching cooler sea surface temperatures (SST's). Additionally these stadial conditions are concomitant with increases in atmospheric dust fluxes (Mayewski et al., 1994), decreasing methane (Chappellaz et al., 1993; Brook et al., 1996; Chappellaz et al., 2013) and carbon dioxide in the atmosphere (Broecker, 1994). D-O events were thought to have an approximate pacing of 1470

years (Schulz, 2002) but evidence from updated age models of the DSDP-609 record suggests a dual periodicity of ~1000 and ~ 2000 years (Obrochta et al., 2012).

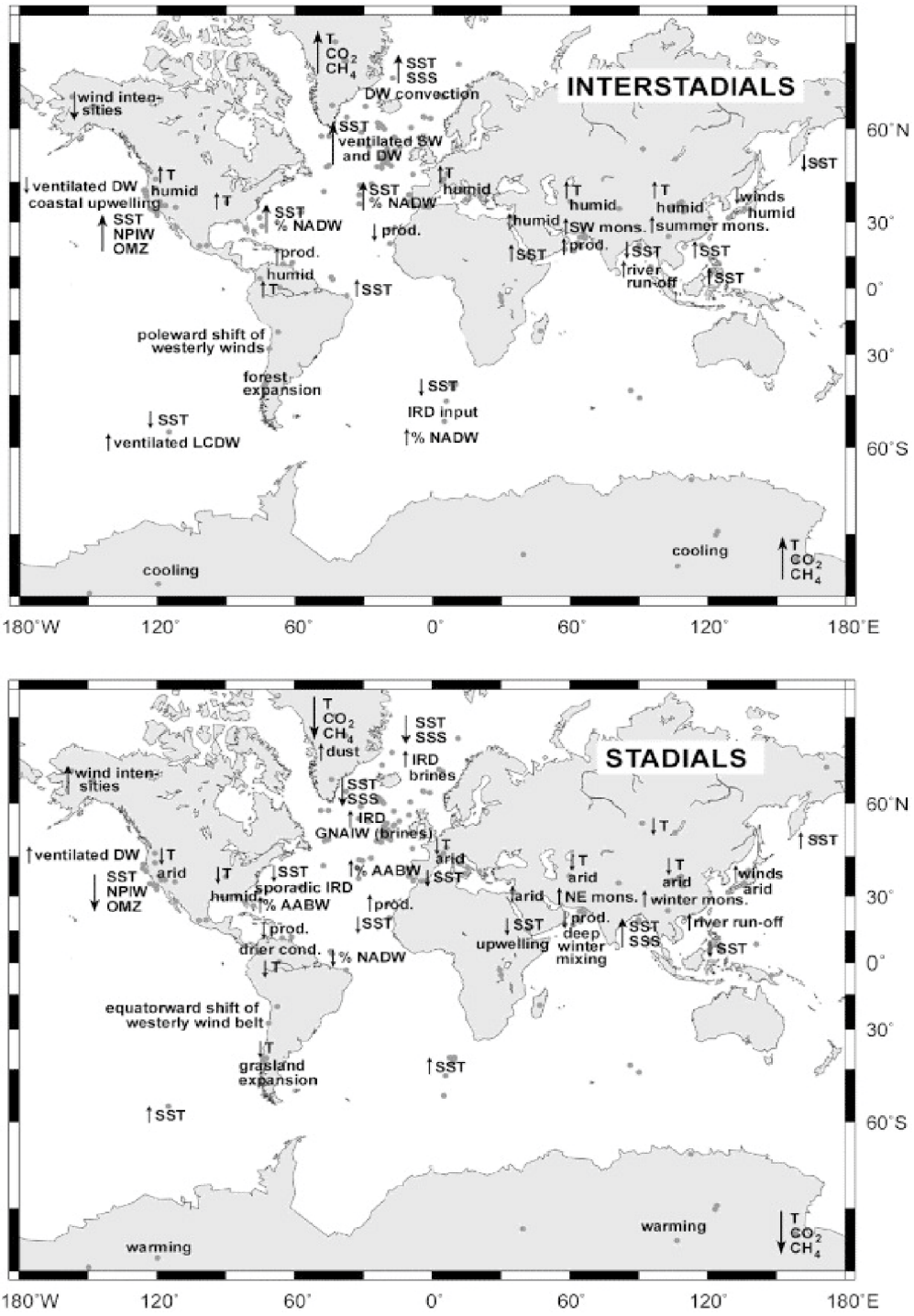

Figure 1.2: Summary maps of key trends in Dansgaard-Oeschger cycles. Top: for interstadial conditions Bottom; for stadial conditions. (Voelker and Workshop participants, 2002) reproduced with permission from Elsevier.

Sites across the North Atlantic exhibit millennial scale variability, attributed to the D-O cycles, in surface ocean conditions and fluxes of ice rafted detritus (IRD), forced

through changing ice sheet dynamics (Bond and Lotti, 1995; Elliot et al., 1998, 2002; de Abreu et al., 2003; Kroon et al., 2000; Peck et al., 2006; Scourse et al., 2009; Hall et al., 2011). Outside of the North Atlantic region there are climate correlatives to D-O variability, (Voelker and Workshop participants, 2002) which are summarised in Figure ***1.2***. Abrupt climate variability is also a feature of Antarctic climate (Jouzel et al. 2007). Many Southern Hemisphere climate records are phased to Antarctica (e.g., Lamy, 2004; Kaiser et al., 2005; Lamy et al., 2007; Caniupán et al., 2011) and indicate that cool North Atlantic conditions are associated with a warming in Antarctic climate. This relationship is known as the thermal bi-polar seesaw (Broecker, 1998; Seidov and Maslin, 2001; Lamy et al., 2007; Landais et al., 2015). Barker et al. (2011) postulate that this is a millennial scale antiphase relationship between warm D-O type events in Greenland climate and the *rate of change* in Antarctica, this enabled the construction of a synthetic Greenland ice core record based on Antarctic climate reaching over 800,000 years.

1.2 Heinrich events

Across the North Atlantic there are several intervals of increased deposition of coarse-grained material (>150 μm) known as ice rafted debris (IRD). These ice rafting events were first documented by Broecker (1994), and named after Heinrich (1988) who identified six Heinrich layers in the last glacial sediments, referred to as H1 (the most recently deposited Heinrich layer) through to H6 (the earliest Heinrich layer during the last glacial). Heinrich layers have been documented at sites across the North Atlantic in particular in the IRD belt between 40° N and 55° N (a belt of increased sand deposition during the last glacial) as defined by Ruddiman (1977), (e.g., Bond et al., 1992, 1993; Bond and Lotti, 1995; Bond et al., 1997; Francois and Bacon, 1994; Thomson et al., 1995; Grousset et al., 1993, 2000, 2001; Andrews et al., 1994; Manighetti et al., 1995; Zahn et al., 1997; Cortijo et al., 1997; McManus et al., 1998; Veiga-Pires and Hillaire-Marcel, 1999; Snoeckx et al., 1999; Bard, 2000; Hemming, 2004; Jullien et al., 2006; Rashid et al., 2012). This IRD material is thought to have been transported by 'armadas' of icebergs supplied by the circum-North Atlantic ice sheets (Broecker, 1994). These layers occur at the end of D-O cold phases with SST cooling events of increased severity (though this change in intensity is not expressed in the Greenland ice core records) (Bond et al., 1993; Rahmstorf, 2002). An additional Heinrich layer (5a) at 52.5 ka BP was identified at eight sites in the Northwest Atlantic

and Labrador sea by Rashid et al. (2003a). The Younger Dryas event at 12.9-11.6 ka BP is thought to have similar characteristics to Heinrich events see Bond et al. (1993), and is often referred to as H0 as in Andrews et al, (1995).

These two types (D-O cycles and Heinrich events) of climate variability characterise the last glacial in the North Atlantic and occurred in earlier glacial periods (e.g., Martrat et al., 2007; Hodell et al., 2008; Barker et al., 2011; Naafs et al., 2013b). The rapid nature of this type of climate variability makes it important to understand the mechanisms that force these abrupt changes, to improve our understanding of the dynamics and the full range of climate variability. The abrupt nature of Heinrich events, the enigma surrounding their cause and the extent of their impact make them a focus for research into cryosphere-ocean-atmosphere interactions.

1.2.1 Characterising Heinrich events

Typically, Heinrich layers of the last glacial are split into Hudson Strait (HS) Heinrich layers, which are classed as cemented marls (Heinrich 1988; Hemming, 2004) and originated in the Hudson Strait, these include H1, H2, H4, and H5. The H3 and H6 events are different to the HS events: in the Labrador Sea and Western Atlantic these have a Hudson Strait origin (Grousset et al., 1993; Bond and Lotti, 1995; Rashid et al., 2003b; Rasmussen et al., 2003). However, in the Eastern Atlantic H3 and H6 consist of IRD from Greenland and European origin (Grousset et al., 1993; Gwiazda et al., 1996a; Snoeckx et al., 1999; Hemming, 2004). As well as the increase in coarse lithic proportions, the Hudson Strait Heinrich events are associated with changes in magnetic susceptibility (Grousset et al., 1993; Dowdeswell et al., 1995; Watkins et al., 2007), inputs of detrital carbonate (e.g. Andrews and Tedesco, 1992; Bond et al., 1992; Andrews et al., 1998; Hodell and Curtis, 2008), and a Paleoproterozoic to Archean age of the sediments deposited (e.g., Gwiazda et al., 1996b; Hemming et al., 1998) and low εNd (<-16) an indicator of an older continental source (Grousset et al., 1993; Hemming et al., 1998; Snoeckx et al., 1999; Revel et al., 1996). Heinrich events cause substantial freshening and cooling of the temperate North Atlantic surface waters (Bond et al., 1993; Maslin et al., 1995; Cortijo et al., 2005; Benway et al., 2010).

Heinrich events are associated with decreases in the strength of the AMOC (Prins et al., 2002; McManus et al., 2004; Hall et al., 2006; Lippold et al., 2012; Jonkers et al., 2012a; Thornalley et al., 2013), reduced influence of Glacial North Atlantic

Intermediate Water (GNAIW) and northward incursion of Southern Component Water (SCW) although the phasing between the ocean and ice sheet is still under debate (Keigwin and Lehman, 1994; Vidal et al., 1997; Zahn et al., 1997; Elliot et al., 2002; Lynch-Stieglitz et al., 2014; Oppo et al., 2015). Heinrich events have been associated with rises in sea level of up to 35 m (e.g., Rohling et al., 2008; Siddall et al., 2008) however this is contested by Arz et al (2007), which suggests that the phasing of the sea level rises is in phase with interstadials. Heinrich events also coincide with changes in global wind patterns (Porter, 1995; Wang et al., 2008), and potentially a global impact on the hydrological cycle (Treble et al., 2007; Rohling et al., 2009; Weldeab, 2012).

1.2.2 Duration of Heinrich events and their position in the last glacial cycle

Heinrich events are irregularly spaced between 5-14 kyr apart but on average approximately 7.2 kyr apart (Sarnthein et al., 2000). Table 1.1 shows the timing of Heinrich events from several studies, though the timing of Heinrich events is surrounded by a great deal of uncertainty (Rohling et al., 2003 Sanchez Goni and Harrison., 2010). Heinrich layers are characterised by sharp bases, an indication of the rapid onset of the Heinrich events (Hemming et al., 1998; Hemming, 2004). As bioturbation of sediment layers acts downwards, dates from the base of the Heinrich events yield maximum ages as the coarse IRD prevents top down bioturbation. Equally, the only age that can be achieved for the end of the Heinrich event is a minimum age because bioturbation mixes the sediments above the event (Hemming 2004), hence it is hard to accurately constrain their duration. However, there are clear indications that the duration of Heinrich events varies at different sites (see summary in Table 1.1): H1 to H6 could have durations of between 0.4k.y to 2.2k.y (Elliot et al., 2001; Rohling et al., 2003; Hemming, 2004, Sanchez Goni et al., 2009).

Heinrich events that occurred at different stages of the last glacial have different initial conditions, and modelling experiments have shown that the initial conditions can affect the duration and source of IRD (Prange, 2004). H6 and H5 occur early in Marine isotope stage (MIS 3), when July insolation at 65°N is relatively high, global ice volume is lower than during the glacial maximum and sea levels are higher (Siddall et al., 2008) and IRD records indicate that the North Western European

Table 1.1 Timing and duration of Heinrich events, n = number of studies included in the mean, * original source is Bond et al.(1992,1993) based on radiocarbon dates [+] original source is Meese et al. (1997). Dates from Sanchez Goni and Harrison (2010) are based on GICC05 chronology and are the length of Heinrich Stadials.

Event	Hemming (2004)	Mean duration (kyr) (n)	range	Elliot et al 2001, 2002 (^{14}C ka BP)	Sanchez Goni and Harrison (2010)	Duration (kyr)
H1	16800*	1410 (8)	531.	13.4-15.1	15.6-18.0	2.4
H2	24000*	1600 (8)	521	20.4-22.1	24.3-26.5	2.2
H3	31000[+]	1800 (3)	800	26.1-27.4	31.3-32.7	1.4
H4	38000[+]	2140 (4)	965	33.9-34.9	38.3-40.2	1.9
H5	45000[+]	434 (1)	-	-	47.0-50.0	3.0
H6	60000[+]	7000 (1)	-	-	60.1-63.2	3.1

ice sheet (NWEIS) is small (e.g., Scourse et al., 2009). H4 occurs mid MIS 3 when there is an intermediate level of ice volume and low level of variation in insolation forcing (Cortijo et al., 2005). H3 and H2 occur in a period of high ice volume, and H1 occurs in a period of high ice volume and increasing insolation values just prior to deglaciation. Differences in the background state of the AMOC also affect the severity of the change in AMOC during Heinrich events (Lynch-Stieglitz et al., 2014).

1.2.3 Potential mechanisms

Since the abrupt variability of the last glacial and Heinrich events were discovered, there has been a lively debate on their potential causes. Potential mechanisms relate to ice sheet dynamics, including internal instability of the Laurentide ice sheet (MacAyeal, 1993; Clarke et al., 1999; Papa et al., 2005; Marshall and Koutnik, 2006), the build-up of buttressing ice shelves during cooling and collapse during climate amelioration (Hulbe, 1997; Hulbe et al., 2004; Alley et al., 2006; Alvarez-Solas and Ramstein, 2011) and internal oscillations in the ice sheet-climate system (e.g., Calov, 2002). Others have suggested that the AMOC acts as an amplifier of the Heinrich events (e.g., Zahn et al., 1997). Marcott et al. (2011), suggests that there is a subsurface ocean warming during a Heinrich event as a result of the reduction in the northward flow of the AMOC, this warms the base of the ice shelf causing a surge of the buttressed ice stream.

1.2.4 Contrasts between the IRD belt and the ice sheet margins

Outside of the IRD belt and the Heinrich event intervals, there are varying sources of IRD; Greenland and European sources dominate the North and Eastern Atlantic, whereas North American inputs dominate the Labrador sea and the Western Atlantic (Revel et al., 1996; Grousset et al., 2001). However, several studies on the European margins have shown an input of LIS material during Heinrich events. Sites at the Goban Spur, the Porcupine Seabight, Rosemary Bank and Celtic Margin all have an input of 'detrital' or 'dolomitic' carbonate during H1, H2, H4 and H5 (H5 is observed at the Porcupine Seabight and Goban Spur only (e.g., Scourse et al., 2000; Peck et al., 2007; Knutz et al., 2007; Hall et al., 2011; Scourse et al., 2009). Dolomitic/detrital carbonate has been found across the North Atlantic during Heinrich events and is thought to correspond to dolomitic carbonate that underlies the Hudson Strait (Andrews and Tedesco, 1992; Bond et al., 1993), however there are local Palaeozoic carbonates that may be identified as dolomite in the British Isles so this is far from conclusive. The interpretation of the carbonate input during Heinrich events is supported by evidence from $^{40}Ar/^{39}Ar$ ages of hornblende grains which have similar ages to sediments underlying the Hudson Strait (Peck et al., 2007), and Nd and Sr isotopes which confirm the presence of a low εNd (<-16) and high Sr input during Heinrich events at the Porcupine Seabight, Barra Fan and Celtic Margin (Auffret et al., 2002; Leigh, 2007; Peck et al., 2007).

Snoeckx et al., (1999) and Grousset et al. (2000) have suggested that there are European 'precursors' to Heinrich events. In this scenario ice rafting from the LIS (the Heinrich event) is preceded by 1-1.5 Ka by deposition of European ice sheet derived material. It is thought that these precursor events acted as a trigger for the release of icebergs from the LIS through atmospheric forcing. Another perspective on the precursor hypothesis is that the European inputs that occur prior to Heinrich events are part of D-O cyclicity (Bond et al., 1992), and many sites from the Nordic seas have records of IRD and $\delta^{18}O$ which have a similar expression to the D-O cycles observed in the Greenland ice core record. Subsequent studies (Peck et al., 2007; Scourse et al., 2009; Haapaniemi et al., 2010) support the proposal that these precursors are likely to be part of D-O cyclicity rather than unique to Heinrich events, as IRD from the BIIS is deposited throughout the stadial with IRD associated with the LIS appearing towards the end of a Heinrich stadial.

1.3 What can we learn from the fine fraction?

The techniques used to characterise the IRD focus largely on the 'operationally' defined classification of coarse fraction material (>150μm), due to the likelihood of post-depositional transport of smaller fractions. However, there is a tacit assumption that no bias is introduced by the exclusion of finer fractions (Hemming 2004). Glacial abrasion results in large amounts of clay and silt-sized particles and in fact, the sand-sized fraction (63 to 2000μm) is the least abundant of glacier derived sediments (Andrews, 2000). Silts and clays can be transported further than sand-sized material and may indicate the presence of ice over a large spatial and temporal range than sand-sized material. For example in distal settings it is likely that the majority of coarse material has already melted out of the icebergs (Dowdeswell et al., 1998), as clay-sized detrital carbonate does not flocculate readily and may be transported greater distances than coarse-fraction IRD (Hodell and Curtis, 2008).

In ice proximal sites (<300 m from the ice sheet) from the Labrador Sea Heinrich events are associated with graded mud facies with IRD grains, indicating the lofting of fine sediment grains (Hesse et al., 2004). These sedimentary facies from the Labrador Sea indicate that Heinrich events start with an input of fine material through melt water and turbidity flows (e.g., Hesse and Khodabakhsh, 1998; Hesse et al., 2004; Rashid et al., 2012). Similar sedimentary facies have been observed during H1 at the Celtic margin (Zargossi et al., 2001). By using the fine fraction, it may be possible to trace sediment plumes and finer IRD near the European margin and across the North Atlantic prior to IRD inputs. Outside the IRD belt where Heinrich layer markers are not evident in coarse-grained lithic proxies, using $\delta^{18}O$ of fine fraction carbonates may help to identify Heinrich events (Hodell et al., 2010).

1.4 *Aim and outline of thesis*

The overall aim of this study is to further the understanding of the sources and deposition of sedimentary inputs transported primarily by ice rafting and meltwater, to the open ocean and how this may impact on surface hydrography and ocean circulation.

This thesis focuses on the temperate North Atlantic during abrupt climate changes, particularly Heinrich events, of the last glacial, and seeks to further the knowledge of

freshwater forcing in the North Atlantic. This will be achieved through geochemical and grain size analysis of fine fraction material from two sites, SU92-09 from the IRD belt, which is expected to show a 'typical' response to Heinrich events. The second site is MD04-2829CQ which is proximal to the BIIS and the coarse fraction petrology of the core demonstrates a LIS input (Hall et al., 2011). This site will provide a record of BIIS variability through the Heinrich events and the last glacial. Comparing changes in the fine fraction alongside co registered proxy records of IRD flux and changes in ocean hydrography will allow further insight into possible mechanisms and impacts for these abrupt climate changes.

The objectives are to:

i. Investigate changes in the supply of fine glaciogenic material to the margins of the BIIS over the last glacial during abrupt climate changes;

ii. Contrast the supply of glaciogenic material between the BIIS margin and the IRD belt;

iii. Understand changes in source of glacial flour over Heinrich event 2 and Heinrich event 4;

The thesis consists of seven chapters. Chapter 2 will provide a description of the two core sites chosen for this study and provide a description, background and justification for the analytical methods used.

The following four chapters will present and discuss the results obtained in this study. Each of the chapters 3,4, and 5 focuses on a different aspect of the fine fraction sediment composition and contrasts the processes and inputs occurring in the IRD belt with those at the margins of the BIIS. Chapter 6 is a mini-chapter, which presents and discusses new contextual proxy data from site SU92-09.

Due to differences in the particle size profiles between hemipelagic and glacially derived material it is possible to identify ice rafted compared to current sorted material. Chapter 3 will examine whether increased IRD and meltwater inputs to the fine fraction have a discernible effect on the particle size distribution of the <63μm fraction.

Inputs of detrital carbonate to the North Atlantic IRD belt are a primary identifying feature of Heinrich events, by using bulk fine fraction $\delta^{18}O$ detrital carbonate transported by meltwater and icebergs. Chapter 4 will identify shifts in the transport of fine fraction (<63μm) detrital carbonate to an ice sheet distal environment (the IRD belt) and ice proximal environment (Rosemary Bank) to better understand the depositional regimes of ice sheet over the last glacial period between 18-41 ka BP in response to abrupt climate change.

Chapter 5 will reconstruct changes in the source of IRD and meltwater sediments of <2μm fraction material over H2 and H4 using radiogenic Nd Sr and Pb at the British Margin and in the IRD belt. Heinrich events are associated with changes in the Nd, Sr and Pb isotope ratios in coarse fraction IRD, which indicate a change to a Paleoproterozoic to Archean aged source thought to be the Hudson Strait of the LIS. Using the <2μm fraction it should be possible to trace inputs of sediment from melt water plumes and ice rafting.

Chapter 6 will present new foraminifera benthic and planktonic stable isotope records from site SU92-09 to reconstruct surface and bottom ocean conditions during the last glacial in response to abrupt climate change.

Chapter 7 is a synthesis of the primary themes in this thesis summarising the main conclusions and opportunities for further work.

2 Materials and methods

2.1 Study sites oceanographic setting

Two sites were examined in this study, the first site consists of marine sediment core MD04-2829CQ from Rosemary Bank in the Northern Rockall Trough. This site is distal to the main ice rafted debris (IRD) deposition belt as defined by (Ruddiman, 1977), but proximal to the British and Irish Ice Sheet (BIIS). The second site, marine core SU92-09, lies within the main IRD belt as shown in ***Figure 2.1***. The two sites were chosen to encompass the large variability in IRD deposition and oceanographic conditions across the eastern North Atlantic.

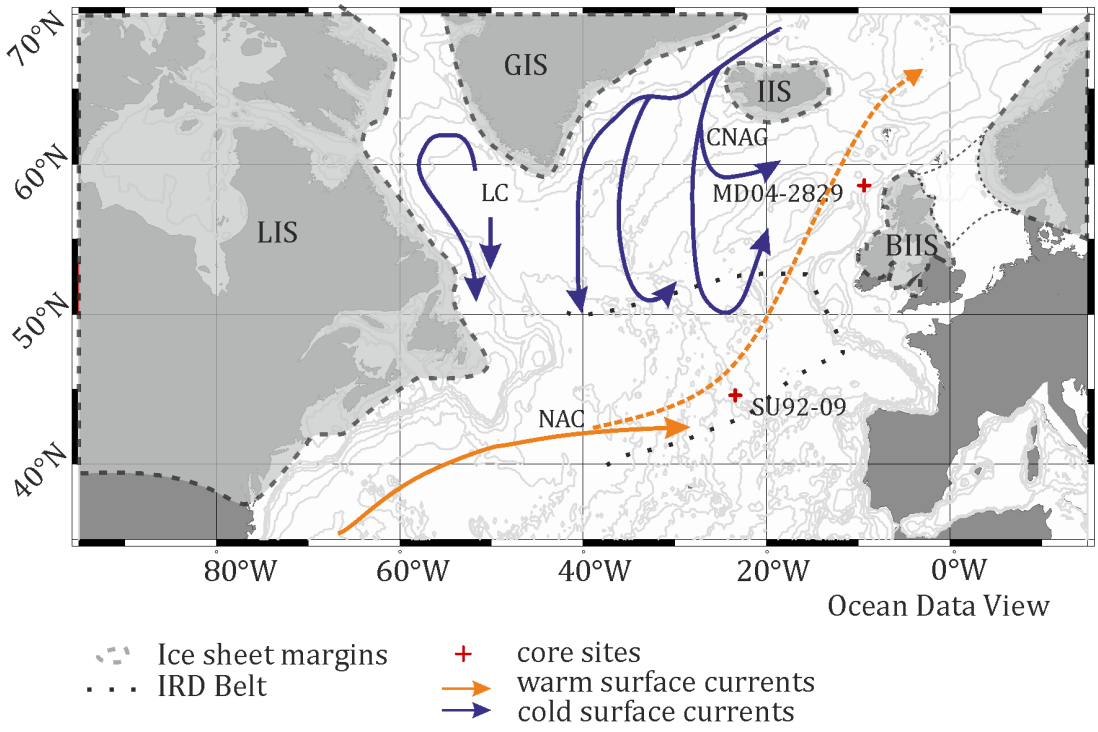

Figure 2.1: Sketch map of the North Atlantic region. Showing the location of core SU92-09 and MD04-2829CQ in relation to the ice sheets (Laurentide ice sheet, (LIS), British and Irish ice sheet, (BIIS), Icelandic ice sheet (IIS), and Greenland ice sheet (GIS)) at the LGM (Bond et al., 1992), the IRD belt (with 200 grains cm-2 ka-1 dotted contours) (Ruddiman, 1977) and the LGM surface circulation (Watkins et al., 2007).

2.1.1 Northern Rockall Trough

Marine sediment core MD04-2829CQ (58º 56.93' N; 09º 34.30' W; 1743 m water depth, (***Figure 2.2***) was recovered during a reoccupation of the DAPC2 site (Hall et al., 2006; Knutz et al., 2007) acquired during the SEQUOIA (Sequencing Ocean

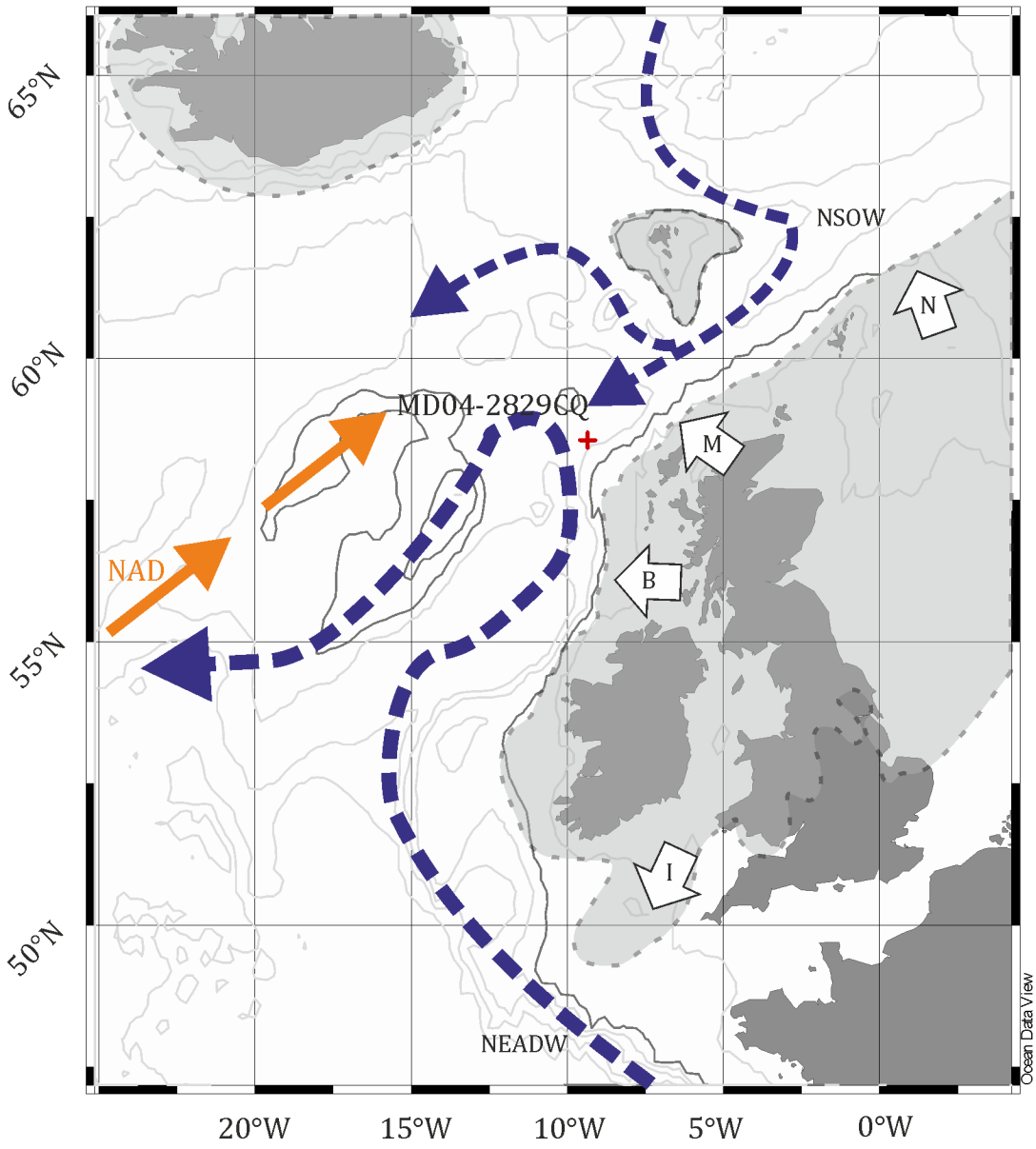

Figure 2.2: Annotated map showing site MD04-2829CQ (red cross) and modern major deep ocean water masses; Nordic Seas Overflow Water (NSOW) and North-eastern Atlantic Deep Water (NEADW), and warm surface water mass the North Atlantic Drift (NAD), from McCartney (1992) and Hall et al.(2011). Maximum extent of the British and Irish Ice sheet from Clark et al. (2012). White arrows denote major ice streams I= the Irish ice stream, B = Barra Fan ice stream, M=Minch ice stream and N=Norwegian channel ice stream from Scourse et al. (2009) and references therein.

Ice Climate Interaction in the NE Atlantic during the Last Glacial) program. The intention was to extend the DAPC2 record beyond MIS (Marine Isotope Stage) 2 (Hall and Scourse, 2005). The site is located on a contourite sediment drift and under the modern ocean configuration, is subject to two main deep-water masses. The Nordic Seas overflow water (NSOW) that flows over the Wyville Thomson ridge and a recirculation of North Atlantic deep water (NADW), which flows from the south (McCartney, 1992) see ***Figure 2.2***. Northward flowing surface waters at the site are sourced from the North Atlantic Drift current (NAD). The MD04-2829CQ core was recovered away from the main continental slope, near to the Sula Sgeir Trough Mouth Fan sourced from the Minch Ice stream (Scourse et al., 2009). The core site is situated in an ideal location to assess sedimentary inputs from the British and Irish Ice Sheet (BIIS) as it is proximal to the Minch ice stream (Bradwell and Stoker, 2007; Stoker and Bradwell, 2005) and the Barra Donegal Fan, a glacially fed trough mouth fan (Armishaw et al., 2000). Previous palaeoclimate reconstructions from the site include those from DAPC2, focused on the last deglaciation (Hall et al., 2006; Knutz et al., 2007), and from MD04-2829CQ published in Hall et al. (2011) extending back to ~41 ka BP. The latter data will be indicated when compared to data from this study, these include; IRD and faunal counts, faunal SST estimates, foraminifera stable isotopes and hornblende ages.

2.1.1.1 Age model for core MD04-2829CQ

The age model for core MD04-2829CQ was originally published in Hall et al. (2011) and is based on 21 radiocarbon dates from samples of *Neogloboquadrina pachyderma (N. pachyderma)* and one from a sample of *Globigerina bulloides (G. bulloides)*. Radiocarbon dates were converted to calendar years using the model of (Fairbanks et al., 2005) assuming a constant reservoir correction of 400 years (www.radiocarbon.ldeo.columbia.edu). This reservoir correction of 400 years is consistent with modern local estimates for 40°–70°N in the North Atlantic (Hall et al., 2011).

2.1.1.2 Age model tuning

Originally, core MD04-2829CQ was tuned to the $\delta^{18}O$ record of the GISP2 ice core in Hall et al. (2011). This differs from the age model constructed in Scourse et al. (2009), which is based on stacked records of the abundance of the planktonic

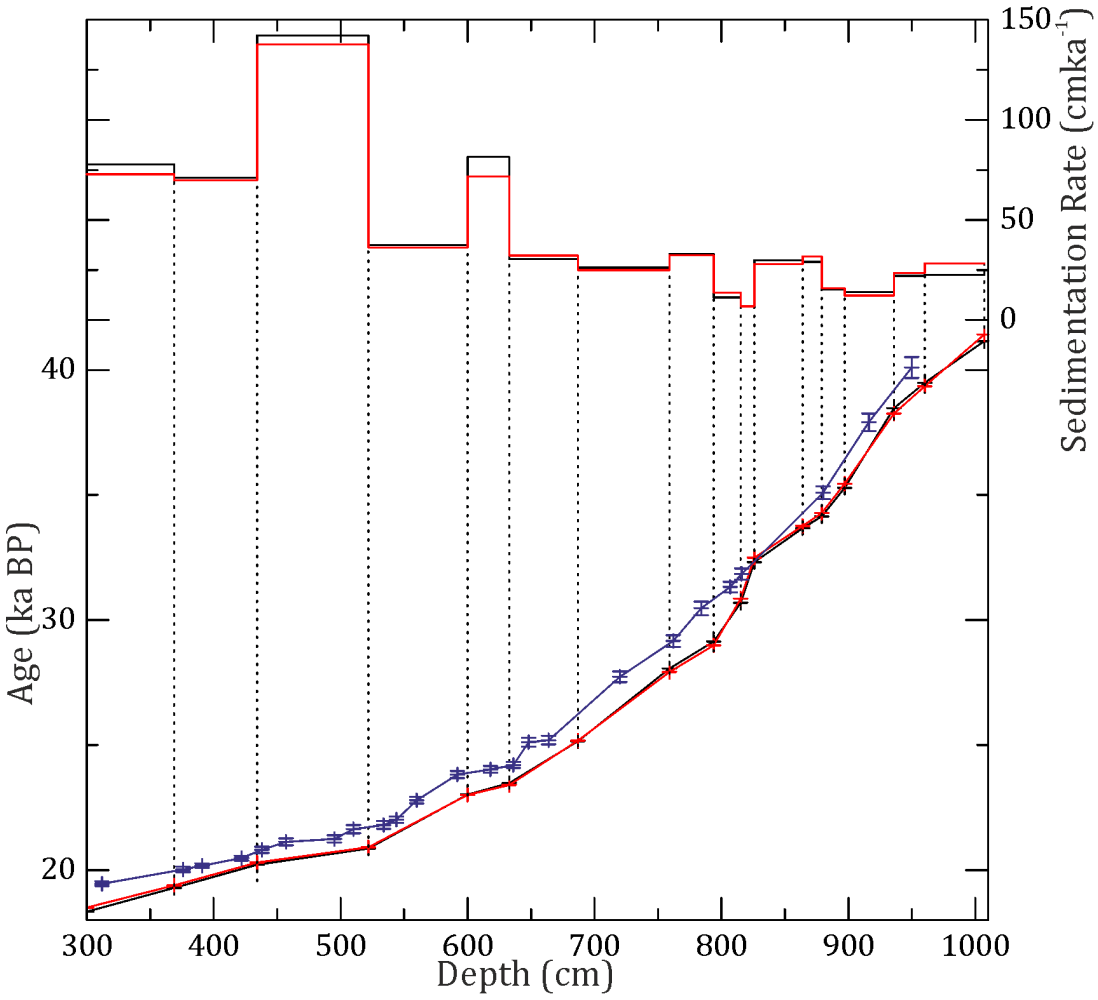

Figure 2.3: Age and sedimentation rate for core MD04-2829CQ. Original GISP2 model in black, GICC05 model in red, calibrated radiocarbon dates in blue.

foraminifera *N. pachyderma*, with differences between the two age models in excess of 3 ka towards the earlier part of the record. The age model of Hall et al. (2011) benefits from independent constraint provided by the Laschamp excursion (~41 ka B.P.) identified in the magnetic record. The Hall et al. (2011) chronology is also closer to the calibrated radiocarbon ages with a reservoir of between 400 and 1700 years. The age model of Scourse et al. (2009) requires a $\Delta^{14}C$ reservoir in excess of 3000 years, whereas glacial marine reservoir estimates for sites close to the British margin are typically ~ 1500, e.g., DAPC2, (Knutz et al., 2007) or 2000 years at MD01-2461, (Peck et al., 2006). Here, minor modification to the Hall et al. (2011) age model for MD04-2829CQ have been made by migrating the tie points of the GISP2 tuned age model from the NGRIP core using the algorithm from Obrochta et al. (2014) as shown in ***Figure 2.3***. The average resolution of the age model is 256 years, and varies between 395 years at its maximum and -216 years at its minimum.

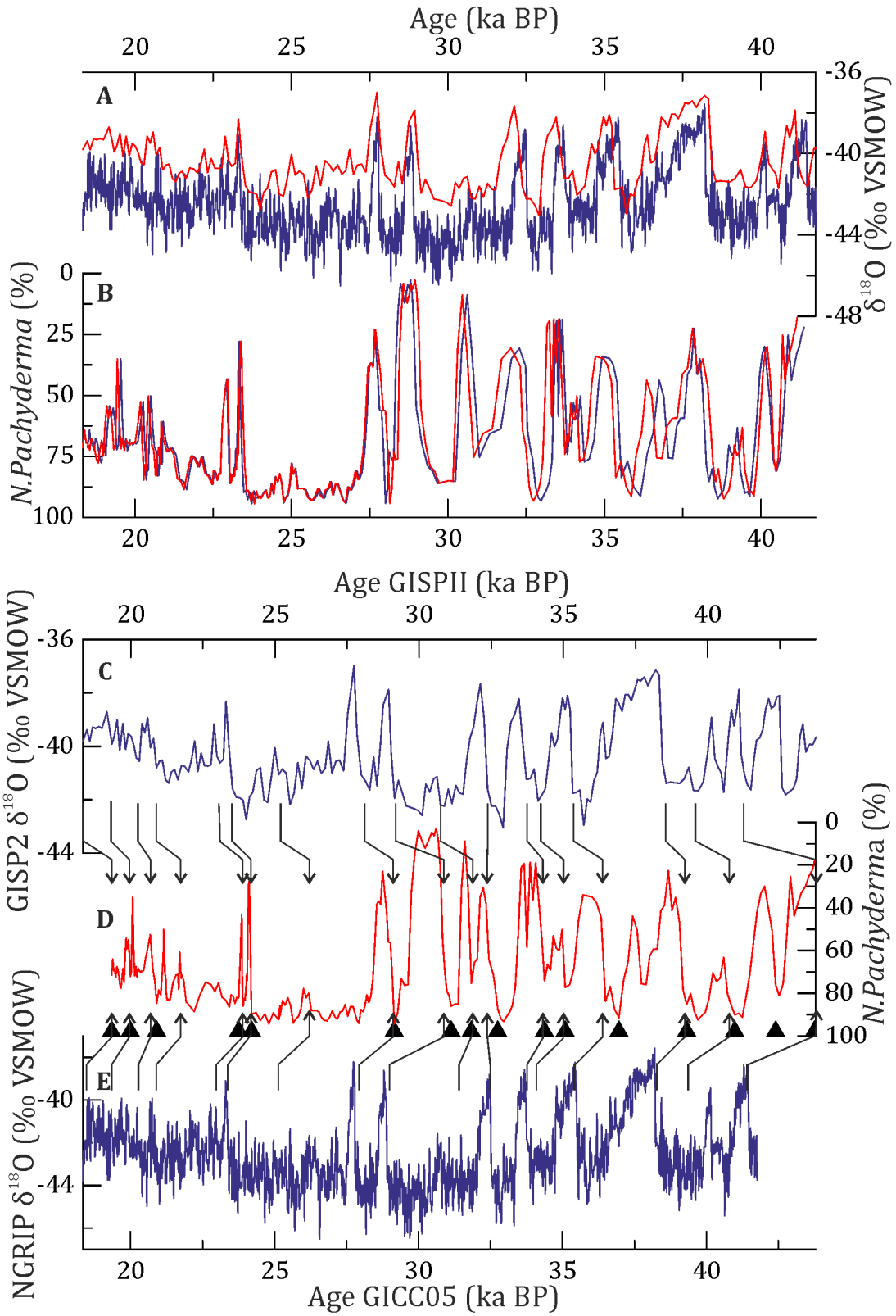

Figure 2.4: Age Model of core MD04-2829CQ updated to GICC05 age model (Andersen et al., 2005) using NGRIP tie points. A; The NGRIP δ^{18}O curve on the GICC05 age model in blue, GISP2 δ^{18}O original age model in red (Grootes and Stuvier, 1997). B; The N. pachyderma abundance (%) (Hall et al., 2011) shown in red using the original tie points to GISP2 and in blue using tie points migrated onto

the GICC05 age model using Obrochta et al. (2014) algorithm; C; GISP2 $\delta^{18}O$ curve with original tie points indicated D:, The N. pachyderma abundance (%) in red with tie points and the radiocarbon ages indicated in triangles, E; NGRIP $\delta^{18}O$ curve on the GICC05 age model with the tie points to the MD04-2829CQ curve indicated.

This is well within the range of uncertainty of the age model for the GISP2 core of 2% (360-800 years.) (Meese et al., 1997). ***Figure 2.4*** also demonstrates that tie points from core. MD04-2829CQ to GISP2 can be tied to corresponding features in the NGRIP $\delta^{18}O$ curve. The age model gives sedimentation rates of between 6 and 32 cm ka^{-1} prior to 23 ka BP and higher sedimentation rates of between 37 and 143 cm ka^{-1} after 23 ka BP (see Figure 2.3).

2.1.2 IRD Belt

Marine sediment core SU92-09 was recovered during the second leg of the PALEOCIMAT cruises and is located at 44°59.70N 23°38.95W and 3270 m water depth (Cortijo et al., 1997). The site is positioned at the south-eastern edge of the IRD belt, and well placed to assess inputs from the Laurentide ice sheet to the Eastern North Atlantic and contributions from the Greenland, Icelandic and Northern European ice sheets (Grousset et al., 1993; Hemming, 2004).

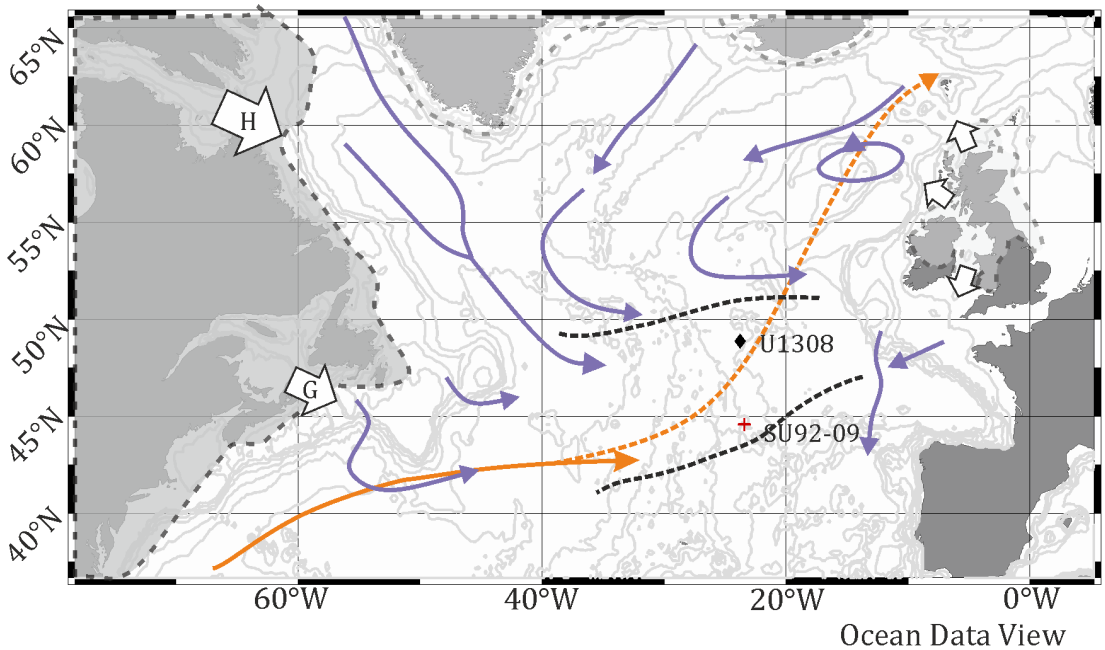

Figure 2.5: Annotated map showing site SU92-09 (red cross), and site U1308 (black diamond) (Hodell et al., 2008). Ice sheets mean IRD paths (purple arrows) (Naafs et al., 2013b) and the IRD belt (black dashed line) (Ruddiman, 1977) the NAD current is shown in orange (Watkins et al., 2007) white arrows are major ice streams H= Hudson Strait ice stream and G is the Gulf of Saint Lawrence ice stream.

Previous study of the core provides magnetic susceptibility data and greyscale for the entire core and % IRD counts over Heinrich event 4, from Elsa Cortijo pers. comm.

2.1.2.1 Age model for core SU92-09

In the absence of radiocarbon dates, the chronology of SU92-09 is based on correlation of the magnetic susceptibility curve from SU92-09 to the magnetic susceptibility curve of nearby core U1308 also in the IRD belt (Hodell et al., 2008) (***Figure 2.5***).

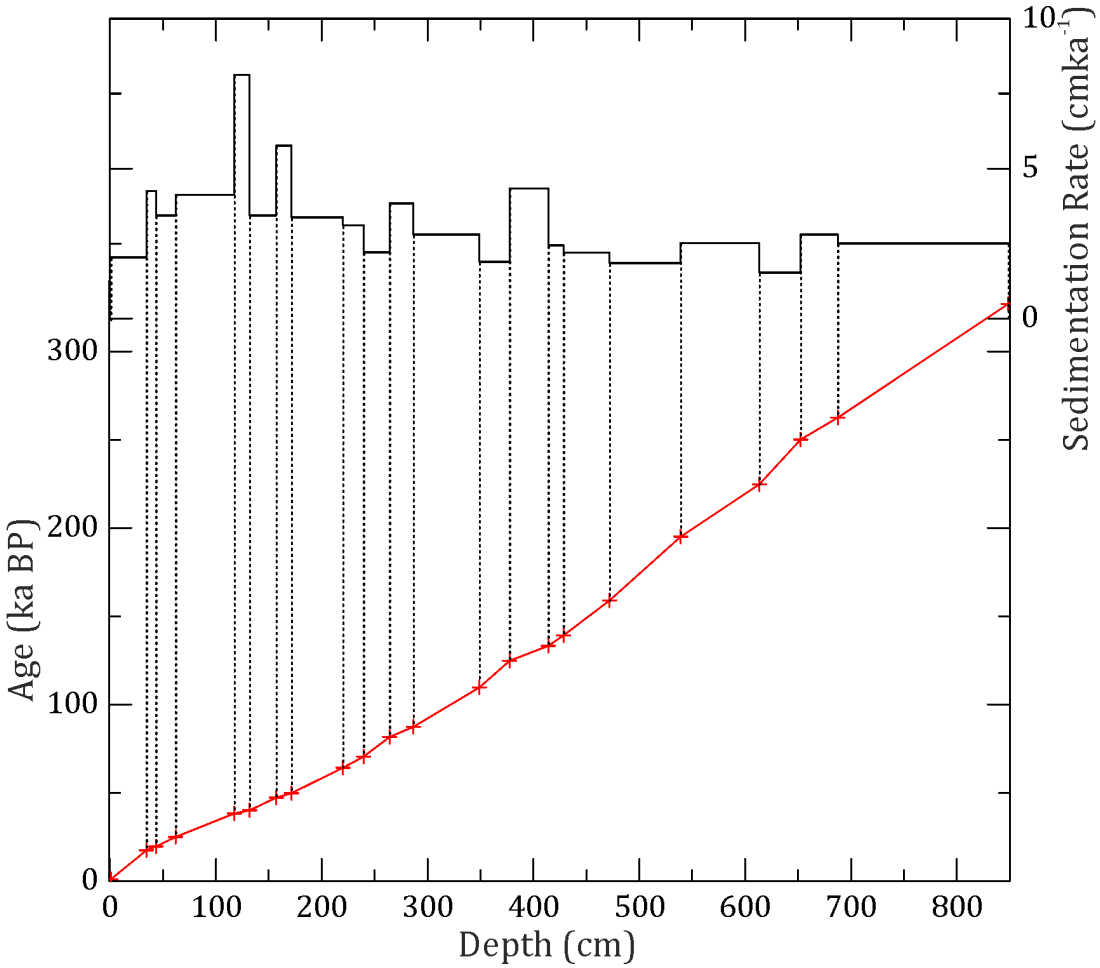

Figure 2.6: Sedimentation rates and age depth model for core SU92-09 tuned to U1308.

Though there is a level of subjectivity in correlating curves in this way, several studies have used changes in magnetic susceptibility to match cores within the IRD belt, as changes in magnetic susceptibility form a distinct marker that in this region the North Atlantic (e.g., Channell et al., 2012). The correlation was achieved by taking

the midpoints of matched peaks and minima in the two magnetic susceptibility curves (***Figure 2.7***). The chronology for U1308 is based on Hodell et al. (2008) which used

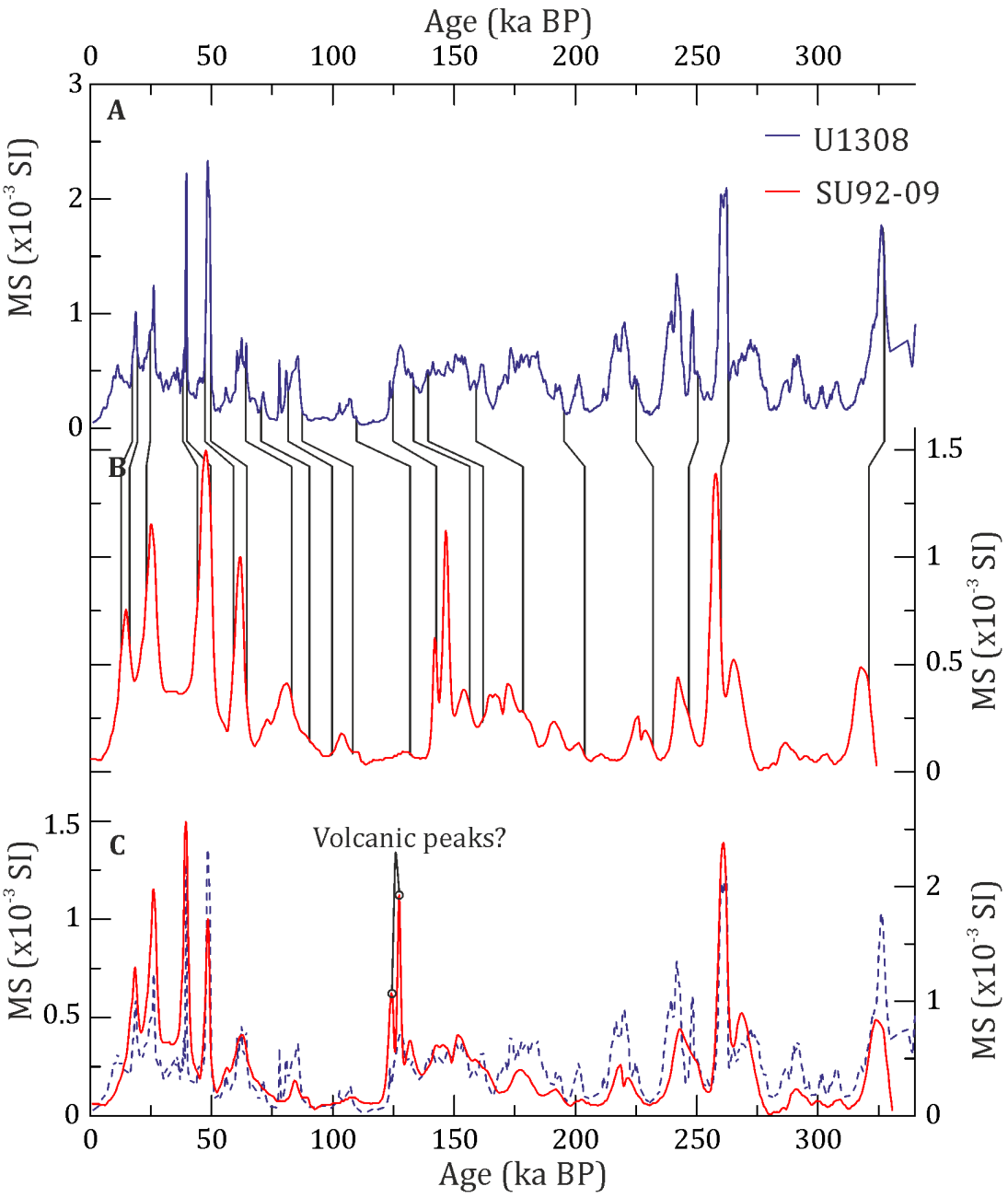

Figure 2.7: Age model tuning for core SU92-09 based on tie points between the magnetic susceptibility records from core U1308 (Hodell et al., 2008) and SU92-09. A: magnetic susceptibility curve from U1308 B: magnetic susceptibility curves from both cores plotted against age, C: floating magnetic susceptibility curve from SU92-09.

radiocarbon dates (Bond et al., 1993) and tuning to the SFCP04 (Shackleton et al., 2004) and LR04, (Lisiecki and Raymo, 2005) model (see Appendix 1). The tuning between the cores was carried out using linear interpolation using the program

Analyseries 2.0 (Paillard et al., 1996); the resulting fit between the two magnetic susceptibility records has an R^2 value of 0.717. The sedimentation rates based on the age model are 2 and 8 cm ka^{-1}, see Figure 2.6.

2.2 Methodology

The aim of this section is to describe and justify the methods that were used to derive the proxy records in the subsequent chapters.

2.2.1 Particle size measurements

Particle size holds diverse information about the sediments deposited in particular in relation to the source of the material and the method of deposition (McCave, 2007). Several instruments infer particle size, the sedigraph, the coulter counter, and Laser particle sizers each with their own advantages/constraints (McCave and Hall, 2006; Jonkers et al., 2009). The coulter counter is a resistance pulse counter, and works on the principle that as a particle passes through the aperture which is in an electric field maintained in electrolyte, there will be a change in voltage proportional to the volume of the particle (Bianchi et al., 1999). There are assumptions associated with this method, i.e. particles are spherical and based on the volume of quartz, which is often not the case, particularly with clays. Measurements of particle size in the 5-63μm decarbonated fraction (removing biogenic carbonates that were produced in situ, and lithic carbonate which only makes up a small proportion of the sediments) were undertaken to evaluate changes in detrital particle size over the last glacial in cores MD04-2829CQ and SU92-09.

2.2.1.1 Sample processing

A total of 163 samples in 1 cm slices at ~2cm resolution were processed from core MD04-2829CQ and 78 samples at between 1 and 2 cm resolution from core SU92-09. Sample preparation follows the method of McCave et al. (1995). In order to remove carbonates between 3 and 4 mg of dried < 63 μm fraction of the samples was leached in 200 ml of 2M acetic acid for at least 24 hours, and settled in glass jars. This was repeated once. The samples were then washed in 500 ml of deionised water to remove traces of acetic acid. To remove biogenic silicates the samples were then leached in sodium carbonate for 5 hours at 85°C and washed in deionised water twice to remove traces of sodium carbonate. A solution of 2% sodium hexametaphosphate (calgon) was added to the remaining terrigenous residues and samples were spun to disaggregate. Each sample was sonicated for 2 minutes prior to duplicate analyses using a Beckman Coulter Multisizer III. Samples were run at a concentration of 2-4%, and 300,000 counts were taken from each sample between 5-63μm in 50

logarithmically spaced size bins. Samples were run in duplicate, if the difference between sample means was greater than 0.3, samples were rerun to ensure fidelity of the results.

2.2.2 Stable isotope analysis

2.2.2.1 Oxygen and carbon isotopes in detrital carbonate

The $\delta^{18}O$ values of sedimentary carbonates become progressively depleted in ^{18}O relative to Pee-Dee Belemnite with age such that, marine carbonates of Cambrian age have $\delta^{18}O$ values of ~ -8 ‰ compared to modern values of > 0 ‰ (Veizer et al., 1999; Faure and Mensing, 2005). This is result of a combination of re-equilibration of $\delta^{18}O$ ratios of carbonate in sedimentary rocks with meteoric water, which acts to deplete ^{18}O in carbonates, and higher ocean temperatures when the calcite was initially precipitated (Faure and Mensing, 2005). Based on the observed difference between Quaternary and Proterozoic aged carbonate oxygen isotopes, bulk oxygen isotope measurements have been previously used to represent the changing proportions of abiotic (lighter $\delta^{18}O$) and biotic components (heavier $\delta^{18}O$) of Quaternary marine (e.g., Balsam and Williams, 1993) and lacustrine sediment (e.g., Leng et al., 2010).

Hodell and Curtis (2008) utilised this concept to identify Heinrich events using changes in oxygen and carbon isotope values of bulk marine sediment samples. The assertion made by Hodell and Curtis (2008) is that during Heinrich events, sediments are characterised by an increased input of IRD from Palaeozoic limestones and dolomite that underlie the Hudson Strait sector of the LIS, which decreases the $\delta^{18}O$ of bulk sediment samples. Hodell and Curtis (2008) found that Hudson strait Heinrich events (1, 2, 4, and 5) had mean $\delta^{18}O$ values of ~ -5 ‰ compared to background glacial values of ~2-3 ‰. Over time changes in $\delta^{18}O$ of *N. pachyderma* (representing the biogenic inputs to the sediment) and in the $\delta^{18}O$ of lithic grains are relatively small in comparison to the shifts in the bulk $\delta^{18}O$ that are observed at site U1308 Hodell and Curtis (2008) as shown in ***Figure 2.8***. This method has been extended to site U1303 (Channell and Hodell, 2013) and site JPC-13 (Hodell et al., 2010) and is able to identify a detrital carbonate input correlative with Heinrich events even when no detrital carbonate is recovered from the >150μm fraction as at site JPC-13.

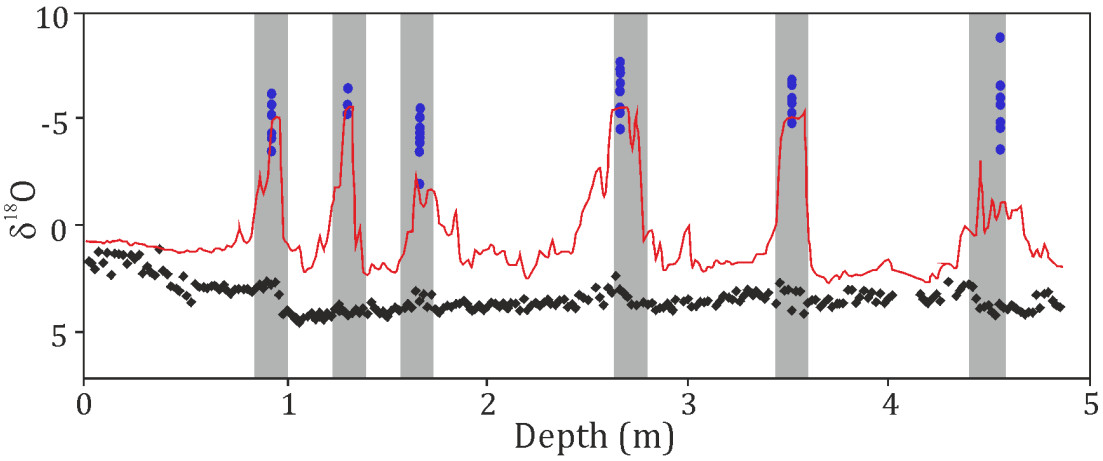

Figure 2.8: $\delta^{18}O$ of bulk carbonate (red) at Site U1308. Black diamonds represent $\delta^{18}O$ of N. pachyderma (sinistral) and blue circles showing the $\delta^{18}O$ of individual detrital carbonate mineral grains picked from Heinrich layers. Redrawn from Hodell and Curtis (2008) with permission from Elsevier.

Chapter 4 of this thesis will use $\delta^{18}O$ of the fine fraction (<63µm) to identify periods of fine-grained carbonate input, building upon the premise of Hodell and Curtis (2008), that the biogenic and lithic components have very different isotopic values and that this can be used to highlight periods when inputs of detrital carbonate are high such as Heinrich events. This will allow the examination of the extent of the Heinrich layers, in <63µm fraction compared to that shown by IRD counts on the coarse lithic fraction.

2.2.2.2 Sample processing for bulk and fine stable isotopes

Samples of pre-dried fine fraction (<63 µm) sediments from core MD04-2829CQ and core SU92-09 were ground to a homogenous powder using a pestle and mortar. Samples of bulk material were excavated at 1 cm intervals dried at 40°C and ground to a homogenous powder. Initially, several samples from each core were analysed on the Thermo Scientific Delta-V isotope ratio mass spectrometer at Cardiff University to roughly estimate the carbonate content of the samples in order to weigh the correct amount of carbonate for analysis. This was approximated by comparing the area curves of initial samples alongside standards with a range of carbonate contents from 100 - 200 µg. Carbonate inputs to core MD04-2829CQ were consistently low around 10 - 20 %, hence 1000 µg ± 200 µg of material was needed for each analysis. Samples form SU92-09 were more variable between 10 and 40% carbonate, by correlating grey-scale values and the area curve of the isotopes it was possible to estimate the % carbonate in samples and weigh out the appropriate amount of between 300 and 1000

µg of sample. Samples from both cores were weighed into cleaned glass vials for stable oxygen and carbon analyses and analysed using the Thermo Scientific Delta-V isotope ratio mass spectrometer at Cardiff University. Six drops of phosphoric acid were injected manually into each vial to dissolve the samples and the analytical procedure was then carried out using a GasBench II auto sampler.

A subset of samples from core MD04-2829CQ was analysed on a second mass spectrometer. In this instance 400 µg ± 40 µg of sample was weighted into cleaned vials, and analysed using a Thermo MAT 252 coupled to a Kiel 2 type carbonate preparation device. An inter-machine comparison was conducted to ensure there was no effect from using a smaller sample size on the MAT 252. In total 32 samples were run on both the MAT-252 and the Delta-V mass spectrometers (see Figure 2.9). To assess the within sample variability a subset of samples were run in duplicate or triplicate (Figure 2.9). In order to assess the consistency of results between batches, replicate samples were analysed. A random strategy was used such that over the each core, one replicate was used for each batch of 48 samples the results are shown in ***Figure 2.10***. The mean difference between samples and replicates for core MD04-2829CQ is 0.09‰ for $\delta^{13}C$ and 0.15‰ (0.18 ‰ including outlier sample 1003) for $\delta^{18}O$, which is <3% of the total variability of the data series. The mean difference between samples and replicates for core SU92-09 is 0.27 ‰ for $\delta^{13}C$ and 0.38‰ for

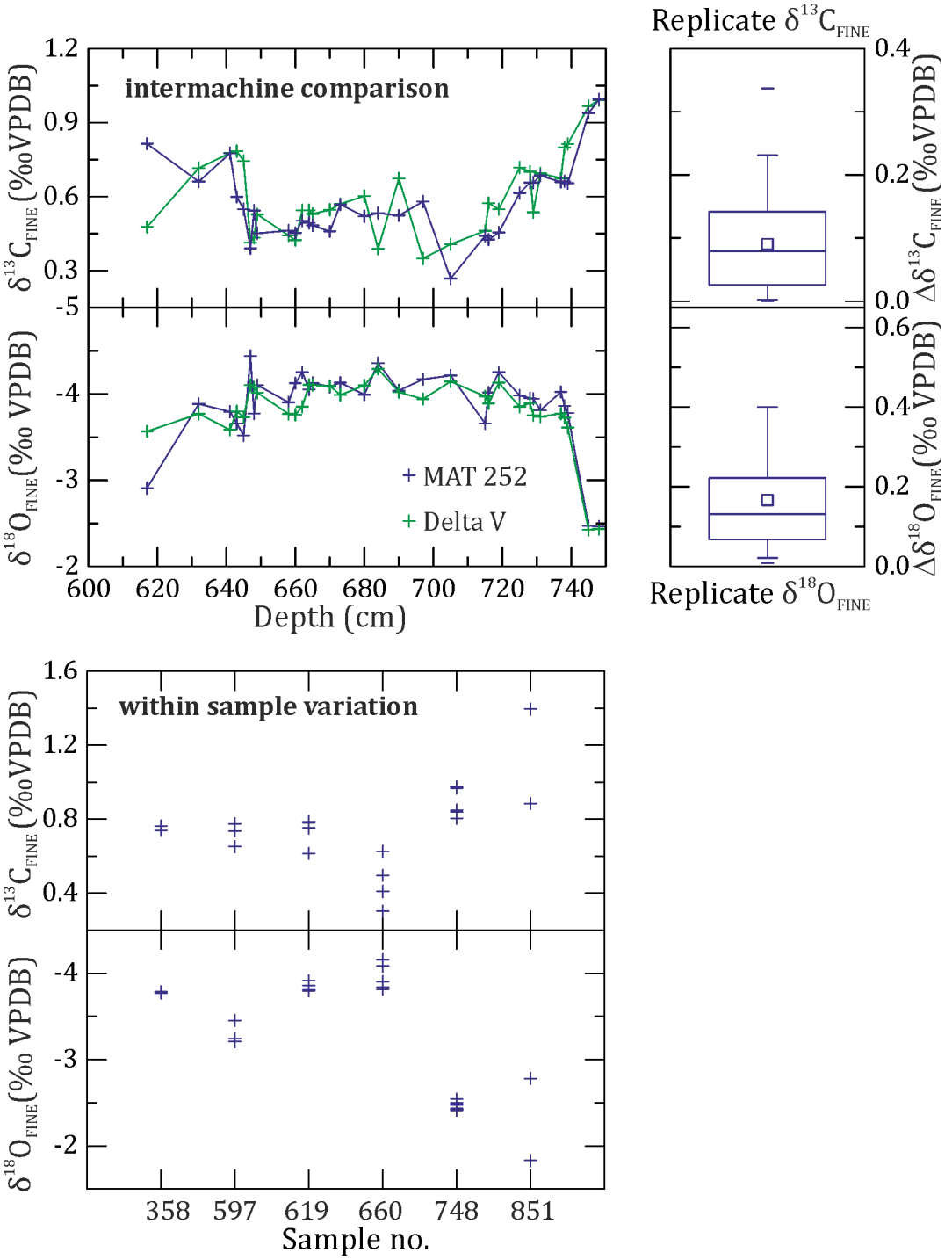

Figure 2.9: Bulk fine oxygen and carbon isotope inter machine comparison and within sample variation. Top: Inter-machine comparison of carbon isotope and oxygen isotope analyses of the fine fraction, run on MAT 252 (blue) and Delta V (green) mass spectrometers. Box plots show the difference between samples run on both machines ($\Delta\delta^{18}O$ and $\Delta\delta^{13}C$). Bottom: variations within the same sample for both carbon isotope and oxygen isotope analyses of the fine fraction.

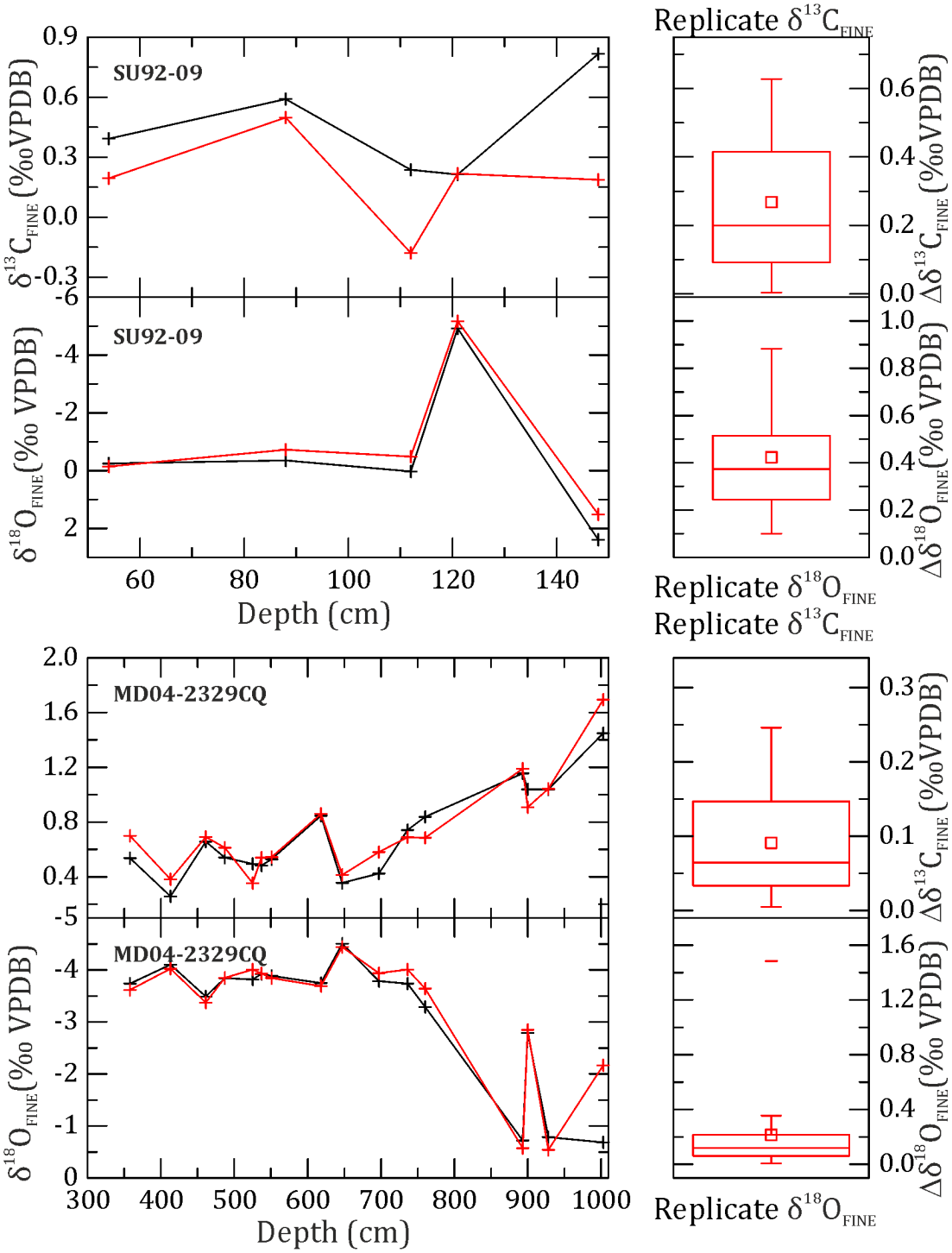

Figure 2.10: Replicate analyses from core SU92-09 and MD04-2829CQ plotted against depth for both $\delta^{18}O_{FINE}$ and $\delta^{13}C_{FINE}$. Boxplots showing the difference between samples and replicates.

$\delta^{18}O$ (0.18 ‰ and 0.26 ‰ excluding sample 148), which is 15% and 5% of the total variability of the two data series respectively. External reproducibility is based on repeat analyses of the School of Earth and Ocean Sciences in house Carrara 1 carbonate standard is better than 0.1 ‰ for $\delta^{18}O$ and 0.07 ‰ for $\delta^{13}C$.

The spectrometers were calibrated through the international standard NBS-19 Equation 2.1. External reproducibility of Carrara 1 carbonate standards was better than 0.1 ‰ for $\delta^{18}O$ and 0.07 ‰ for $\delta^{13}C$.

Equation 2.1: $\delta^{18}O$ notation

$$\delta^{18}O = \left[\frac{\left[\frac{^{18}O}{^{16}O}\right] sample}{\left[\frac{^{18}O}{^{16}O}\right] standard} - 1 \right] x1000‰$$

2.2.3 Foraminifera stable isotope analysis

Planktonic foraminifera are free-floating unicellular eukaryotes with calcite tests (Pearson, 2012). Benthic foraminifera are a diverse group of foraminifera tests that live at the sediment water interface (epifaunal) or in the sediment (infaunal). Foraminifera are abundant in the fossil record since the Cambrian (Culver, 1991) and their fossil assemblages as well as the geochemical properties of individual species tests reflect aspects of the environment in which they grew, making them one of the most widely used tools to study the conditions of past oceans.

2.2.3.1 Stable oxygen isotopes in foraminifera

The fractionation of oxygen isotopes between water and calcite is temperature sensitive, this discovery, led to the proposal that the relationship could be used as a palaeothermometer (Urey, 1947; Epstein et al., 1953). Subsequent work applied this palaeothermometer to the calcite in planktonic foraminifera tests (Emiliani, 1955) and revealed the first isotope stratigraphy of marine sediments. This relationship is complicated by the $\delta^{18}O$ of seawater, in the surface ocean this is affected by the local precipitation budget, local inputs of freshwater (i.e. due to rivers/melting ice), upwelling of water masses with a different $\delta^{18}O$ value and global ice volume (Ravelo and Hillaire-Marcel, 2007). In the deep ocean, the seawater $\delta^{18}O$ is affected by global ice volume and the mixing of deep ocean water masses (Ravelo and Hillaire-Marcel, 2007). In foraminifera, in addition to the temperature dependence on isotope fractionation (Equation 2.2) and the $\delta^{18}O$ of seawater, other factors that affect the $\delta^{18}O$ of foraminifera include changes in the depth habitat, seasonality, ontological effects,

the presence of symbionts and vital effects (Ravelo and Hillaire-Marcel, 2007). Overviews of the $\delta^{18}O$ palaeothermometry techniques and the vital effects and ecological factors that impact the $\delta^{18}O$ (and $\delta^{13}C$ see below) of biogenic carbonates have been recently published (Rohling and Cooke, 1999; Sharp, 2007; Ravelo and Hillaire-Marcel, 2007; Hoefs, 2009).

Equation 2.2: Palaeo temperature equation (Kim and O'Neil, 1997)

$$T = 16.1 - 4.64\ (\delta^{18}Oc\ -\ \delta^{18}Osw)\ +\ (0.09\ (\delta^{18}Oc\ -\ \delta^{18}Osw))^2$$

Where T is temperature, C is calcite and sw is seawater

2.2.3.2 Stable carbon isotopes in benthic foraminifera

The $\delta^{13}C$ of benthic foraminifera tests reflects the $\delta^{13}C$ of dissolved inorganic carbon (DIC) of the water in which the organism calcified (Ravelo and Hillaire-Marcel, 2007). In the ocean, this is a product of nutrient distributions and air sea exchange of carbon, such that low $\delta^{13}C$ corresponds with nutrient-rich waters and high $\delta^{13}C$ corresponds to nutrient poor waters (Lynch-Stieglitz, 2003). This is because photosynthesis incorporates more of the lighter carbon isotope into organic matter and this lighter $\delta^{13}C$ is released as the organic matter decomposes and sinks and enriches the nutrient content of the deep water mass (Lynch-Stieglitz, 2003). The equilibrium exchange between the surface of the ocean and atmospheric CO_2 results in higher $\delta^{13}C$ in cold surface waters and lower $\delta^{13}C$ in warmer surface waters. This has led to $\delta^{13}C$ being used as a tracer in benthic foraminifera typically epifaunal species such as *Cibicidoides wuellerstorfi* and *Planulina* sp., which reflect $\delta^{13}C$ of bottom waters with little or no offset. Factors that might cause an offset include species habitat i.e. epifaunal (living above the sediment) infaunal (living in the sediment) and vital effects of the species, and local productivity (Lynch-Stieglitz, 2003).

2.2.3.3 Sample processing for foraminifera stable isotopes

As down core $\delta^{18}O$ and $\delta^{13}C$ records from the foraminifera *N. pachyderma, G. bulloides* and *C. wuellerstorfi* are already available from core MD04-2829CQ (Hall et al., 2011), only SU92-09 was processed for foraminifera stable isotopes in this study. Three species of foraminifera were identified and picked in each sample to represent different water mass properties; *N. pachyderma*, and *G. bulloides*, to represent the

surface water masses and the benthic foraminifera *C. wuellerstorfi* to represent the isotopic signature of the bottom waters at the site.

Where possible, 30 tests each of *N. pachyderma* from the 150-250 μm fraction and *G. bulloides* from the 250-350 μm fraction to produce a statistical average. Narrow size ranges were used to pick the foraminifera as a significant size effect is observed in the isotope ratios of foraminifera of different sizes (Elderfield et al., 2002; Jonkers et al., 2013). *C. wuellerstorfi* were not abundant in the core and between 1 and 6 tests were run per sample as indicated in Appendix 2. The environment of benthic foraminifera such as *C. wuellerstorfi* is more stable over the year so a statistical average is less important. In some instances, there were too few foraminifera to run or no foraminifera, these samples were excluded. Site SU92-09 has a wide variation in the composition and percentage of detrital carbonate hence to minimise contamination by detrital carbonate, foraminifera tests were crushed between two slides and were cleaned by sonicating in DI water for 20 seconds and again in methanol and further inspected under the microscope to ensure all detrital carbonate had been removed. The tests (shells) were then analysed using the MAT 253 at Cardiff University.

2.2.4 Radiogenic isotope analysis

Decay products of long lived radiogenic systems, including Rb-Sr, Th-U-Pb, Sm-Nd, Lu-Hf and Re-Os are widely used to date and trace geological processes, with a wide range of applications (Goldstein and Hemming, 2003). In palaeo-climate, one of the applications of long-lived isotopes is tracing the dispersal of detrital material throughout the ocean. Long-lived isotope systems are useful due to their conservative nature, retaining the imprint of the original formations age/ geochemical signature and are not altered by deposition in sediment like short-lived isotope systems (Faure and Mensing, 2005). This means that they can be used to locate the original source of the material. Outlined below is the rationale behind the three long-lived isotope systems used in this study.

2.2.4.1 Neodymium/Samarium

Samarium (Sm) and Neodymium (Nd) are rare earth elements (REE) that occur in many silicate and carbonate minerals (Faure and Mensing, 2005). Sm-147 is radioactive and decays by the emission of an α-particle to ^{143}Nd. The isotope

composition of Nd is expressed by the ratio of $^{143}Nd/^{144}Nd$, and is expressed in epsilon (ε) notation (DePaolo and Wasserburg, 1979) as in Equation 2.3

Equation 2.3: εNd notation

$$\varepsilon Nd(t) = \left(\frac{\left(\frac{143Nd}{144Nd}\right) sample(t)}{\left(\frac{143Nd}{144Nd}\right) CHUR(t)} - 1 \right) \times 10000$$

Where ($^{143}Nd/^{144}Nd$) sample (t) is the sample ratio and ($^{143}Nd/^{144}Nd$) CHUR (t) is the CHondritic Uniform Reservior value (0.512638) Faure and Mensing (2005).

The ratio of $^{143}Nd/^{144}Nd$ is dependent on both the age and Sm/Nd ratios being analysed. $^{147}Sm/^{144}Nd$ ratios are based on the concentrations of Sm and Nd measured using ICP-MS (see section 2.2.5) and calculated by Equation 2.4.

Equation 2.4: Calculating $^{147}Sm/^{144}Nd$ ratios

$$\frac{^{147}Sm}{^{144}Nd} = \frac{Sm}{Nd} \times 0.602$$

As Nd and Sm have similar radii they are not readily separated by most sedimentary processes. Hence, the Nd-Sm isotope system provides an average age of the crustal formation of the sediments source. As Nd is more likely to enter magma than Sm, continents have lower $^{143}Nd/^{144}Nd$ than mantle sources (Goldstein and Hemming, 2003). As εNd=0 represents a bulk Earth value over time, more negative values of εNd represent older continental sources and positive values represent younger mantle sources (Goldstein and Hemming, 2003). Late Archean aged terranes have an εNd of approximately -27 ε units (Hemming, 2004).

2.2.4.2 Rubidium/Strontium

Rubidium-87 is radioactive and decays to the stable isotope ^{87}Sr by emission of a β-particle (Faure and Mensing, 2005). The Rubidium (Rb)-Strontium (Sr) system is reset by many geological processes (Hemming, 2004). This is due to the difference in radii between Rb, an alkali metal, found in association with K and abundant in feldspars and micas, and Sr an alkali earth element, which replaces Ca and is enriched in plagioclase and pyroxene. Due to the vulnerability of plagioclase and pyroxene to chemical attack, Sr is removed to the aqueous environment whereas the durability of

micas and K feldspar causes Rb to be retained in the solid system (Faure and Mensing, 2005). The system is also susceptible to resetting by metamorphism (Goldstein and Hemming, 2003), and due to the size dependence of the mineral species, carrying Rb and Sr it is also susceptible to significant mineral sorting and grain size effects such that the $^{87}Sr/^{86}Sr$ ratios become more radiogenic with smaller grain sizes (Garçon et al., 2014). Whilst there is a wide range in variability of Rb-Sr signal, the interpretation is complicated due to the ability of the system to be reset and the implications of grain size (Hemming, 2004).

2.2.4.3 Thorium-Uranium-Lead

Lead (Pb) has four stable isotopes ^{204}Pb, ^{206}Pb, ^{207}Pb, and ^{208}Pb, ^{206}Pb. ^{206}Pb is the decay product of ^{238}U, and ^{207}Pb is the decay product of ^{235}U, and ^{208}Pb is the decay product of ^{232}Th. ^{204}Pb is not a decay product and therefore the ratios are reported are $^{206}Pb/^{204}Pb$, $^{207}Pb/^{204}Pb$ and $^{206}Pb/^{204}Pb$. Each system has several intermediate daughters and are the result of successive emissions of α- and β-particles (Faure and Mensing, 2005). The system is particularly sensitive to dating sources of Archean origin due to the long half-life of ^{238}U. However, the Th-U-Pb system does not discriminate between continental and mantle sources as well as the Sm-Nd and Rb-Sr systems (Goldstein and Hemming, 2003).

Analyses of Nd Sr and Pb isotopes of the clay size < 2 μm fraction material were undertaken in order to assess the changing source of glaciogenic inputs at site SU92-09 and MD04-2829CQ during Heinrich events H2 and H4. Fine-fraction material can be of mixed sources. In order to determine a source of fine fraction material it is crucial to use more than one isotope system to examine the radiogenic signature (Hemming 2004). In this case, Rb-Sr, Sm-Nd and Th-Ur-Pb were used as these isotopic systems distinguish between Archean and Paleoproterozoic provenance which are significant in the North Atlantic (Hemming, 2004).

2.2.4.4 Sample processing

A total of 48 samples of 0.5-1g of sediment, from core MD04-2829CQ were prepared for radiogenic isotope analysis. Samples were taken between core depths of 600-732 cm to represent H2 and from 916-972 cm to represent H4. From core SU92-09 40 samples were taken to cover H2 and H4, between depths of 48-88 cm and 100-146 cm. These were prepared from the <63 μm fraction.

Samples were prepared following Chester and Hughes (1967), and were leached in (i) buffered sodium acetate to remove carbonates, then (ii) 1 M hydroxylamine hydrochloride, and 25% acetic acid solution in order to remove Mn-Fe oxides, leaving the detrital material only. This approach was preferred over a hydrochloric acid leach, as this methodology has been shown to attack the lattice of clay minerals, and potentially bias, in particular, the analyses of detrital Sr. It is therefore is not recommended in low carbonate marine samples (Chester and Hughes, 1967; Clauer et al., 1993; Revel et al., 1996). Biogenic silicates were not removed because organic silicate content is low in samples from the North Atlantic and concentrations of Sr and Nd in biogenic silica are low and would therefore likely have little to no impact on the results (Revel et al., 1996). The samples were split into the following operationally defined size fractions (i) coarse silt (63-20 µm) (ii) silt (20-2 µm) and (iii) clay (<2 µm). The samples were wet sieved through a 20 µm mesh sieve to separate the sample into 63-20 µm and <20 µm and then both fractions were dried. The <20 µm fraction was then settled in a measuring cylinder to 2 µm using Stokes law (Equations 1 and 2) to split it into 20-2 µm and <2 µm fractions (Philpotts and Ague, 2009). This was repeated until the samples were fully settled after the time required by the Stokes law equation. The samples were then centrifuged to remove water and freeze dried overnight.

Equation 2.5: Settling velocity

$$V_S = CD_P{}^2$$

Equation 2.6: Drag co-efficient

$$C = \frac{(\rho_P - \rho)g}{18\mu}$$

From (Philpotts and Ague, 2009) Where V_S is the settling velocity, C is the drag co-efficient, D_P is the particle diameter ρ_P is the particle density, ρ is fluid density, g is the gravitational constant, and μ is the fluid viscosity.

All radiogenic isotope measurements were carried out at Lamont Doherty Earth Observatory, Columbia University, USA. Approximately 50 mg of the <2 µm sediment fraction of each sample was weighed into a Teflon vial. Sample digestion was initially carried out using a solution of 1.5 ml hydrogen fluoride and 2 ml of 8N

nitric acid and heated on a hotplate for 12 hours at 120°C. Following initial dissolution, it was noted that the samples contained an abundance of organic material that could not be dissolved in this solution. In order to remove this organic material, an initial test was carried out on sample 720 (720 cm depth core MD04-2829CQ) to check the effectiveness of a 30% hydrogen peroxide leach overnight followed by heating to 120°C for two hours. The hydrogen peroxide leach was ineffective, hence 0.5 ml of perchloric acid (a stronger reducing agent) was added to all samples, samples were capped and heated at 150°C overnight and left to dry down to a residue at 180- 220°C.

In the further batches, for efficiency, samples were dissolved (i) in a solution of 2 ml hydrofluoric and 0.5ml perchloric acid at 200ºC overnight and dried down, (ii) 0.5 ml of nitric acid and heated at 180ºC overnight and dried down again. After sample dissolution, the Pb, rare earth elements (REE's), Sr and Nd were extracted sequentially from the samples using column chromatography shown in the flowchart in Figure 2.11. Concentrations of the Nd, Sr, and Pb elutions from the samples were diluted prior to analysis, using 3% nitric acid to solutions of 100 ppb (Pb) 80 ppb (Sr) and 50 ppb (Nd) and run using an auto sampler on the Neptune multi-collector inductively coupled mass spectrometer at Lamont Doherty Earth Observatory. Mass discrimination corrections were performed online using an exponential equation as part of the automated program. Blank corrections were not carried out as contamination of blanks was negligible. Samples were normalised to accepted standards; $^{143}/^{144}$Nd values were normalised to JNd-1, ^{87}Sr/^{86}Sr values to NIST-987 and ^{206}Pb/^{204}Pb, ^{207}Pb/^{204}Pb and ^{206}Pb/^{204}Pb values to NIST-981.

Replicate analyses were conducted for core MD04-2829CQ (Figure 2.12). Sr and Nd values are similar to those of the main data series there is a large difference between two of the replicates of Pb data. Whilst contamination of the Pb isotopes may be a possibility, a more likely explanation is that as the provenance age of the sediment that small differences in the settling may result in un-mixing effects that lead to this (pers. comms Hemming, 2015). When samples from the same settling batch are rerun they replicate well (i.e. at depth 642 cm). However, samples that have been resettled i.e. at depths 972 cm and 720 cm show differences. Hence, the Pb isotope ratios from samples including depths including 646, 650, 938, 946 in core MD04-2829CQ and

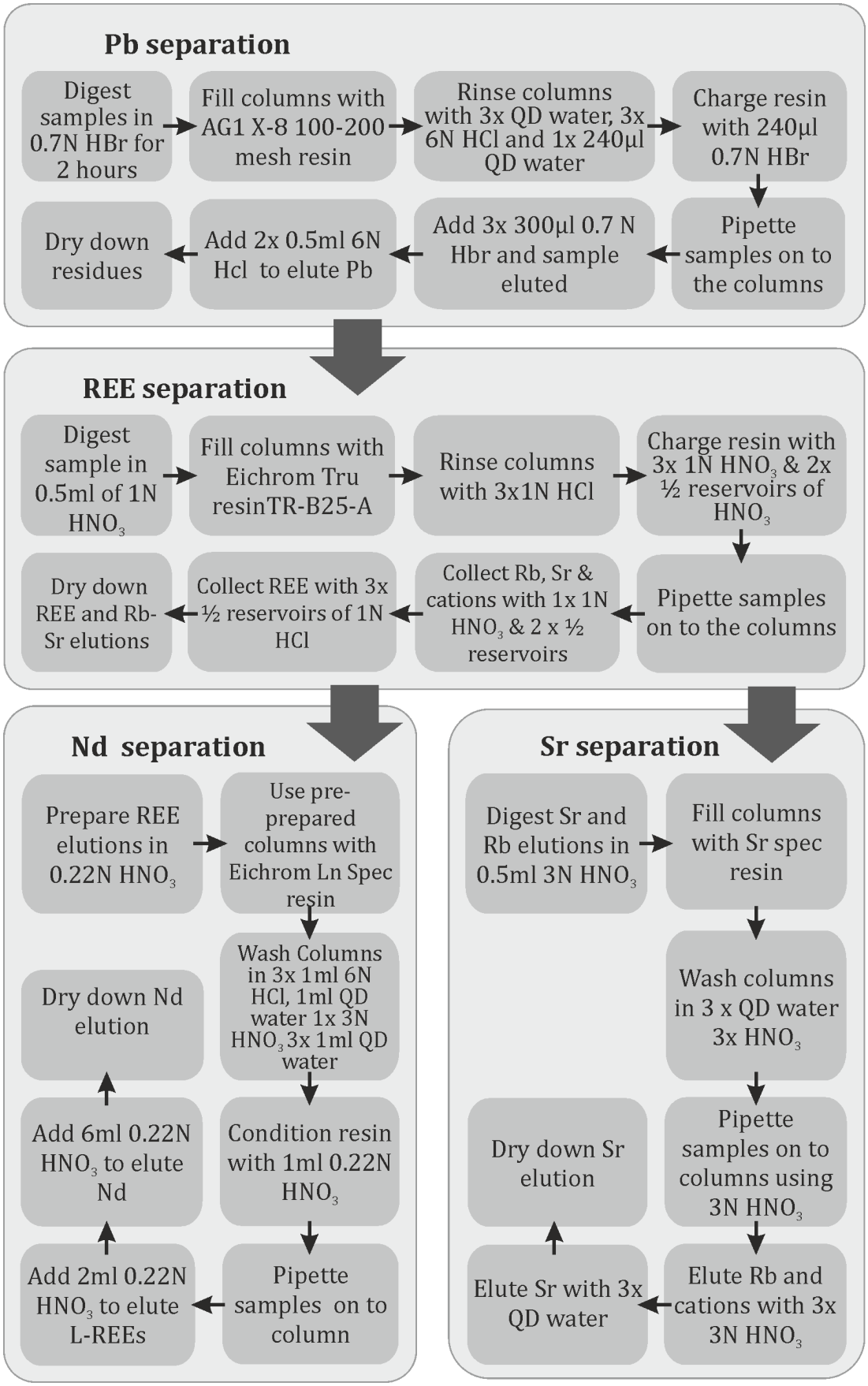

Figure 2.11: Schematic representing the steps in each phase of column chemistry.

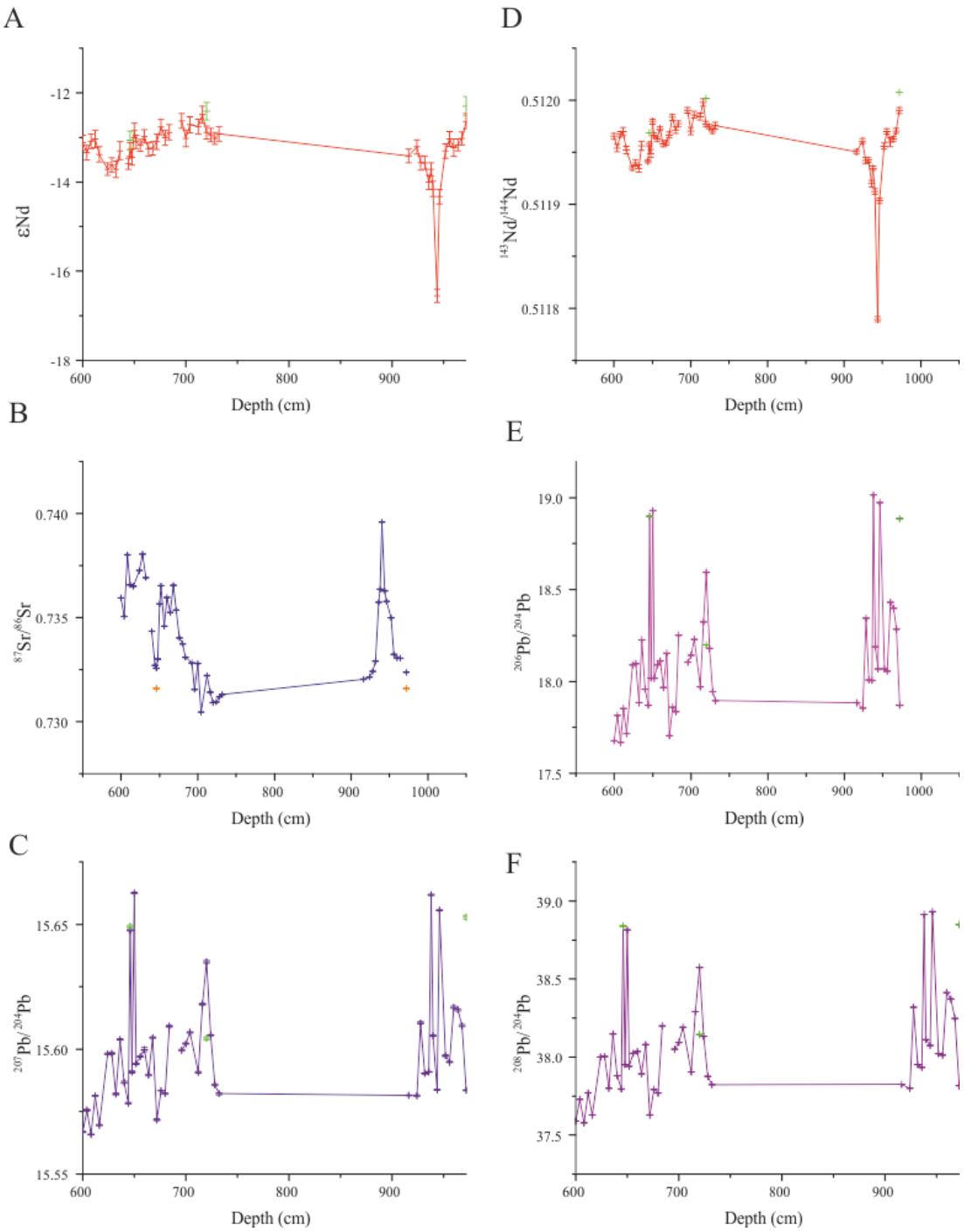

Figure 2.12: Plots of replicate analyses alongside data

samples 64 and 136, which were processed and settled at LDEO prior to dissolution, should be interpreted with caution.

2.2.5 Major and Trace elements

Major and trace elemental analysis complements radiogenic isotope work on sourcing sediments (e.g., Benson et al., 2003). A suite of major and trace elements

were analysed, the main aim was to assess the concentration of Nd Sr and Pb in the samples in order that a mixing model can be used to better define the source and identify when one or more sources were present in the sample. Ratios of K/Ti and Sc/Th were used in order to corroborate the grain size data in Chapter 3 of the clay size fraction at both SU92-09 and MD04-2829CQ.

Samples were dissolved in a solution of 3 ml 8 N nitric acid and 1 ml concentrated (15 N) hydrofluoric acid for each 50 mg of sample, capped and heated at 150°C. The solution was dried down and then fumed in 2 ml perchloric acid at 200°C until all organic material was dissolved. Samples were then transferred to bottles in 2.5 ml 4N nitric acid; a 50 times dilution of the sample. Two samples were initially measured to assess the amount of each element likely to be in the sample set, and a standard solution was prepared based on these concentrations consisting of the elements to be determined (see Appendix 3).

To measure the major and trace elements 250 µl of sample was transferred to a test tube, and a spike of 20µl of 1 ppm Indium solution was added and 10.5 ml of a solution of 3% nitric acid and 0.1% HF. In order to calculate a standard curve a set of 6 standards were prepared with 250 µl of a different sample in each with 0, 100, 250 and 500µl of the standard solution respectively topped up to 10.75 ml with acid. To assess the drift in measurements over the course of the run, a standard was prepared. An aliquot of each sample was run on the Quadrupole ICP-MS for minor element and the ICPMS for major elements at Lamont Doherty Earth Observatory.

2.2.6 Numerical analysis

2.2.6.1 Pearson correlation

Pearson correlation coefficients are widely used to test the level of fit between two variables. However time series data is subject to serial correlation where the time series correlates to previous sections of itself, and data is often non-parametric, estimating confidence in the results is problematic (Mudelsee, 2003). The PearsonT3 programme provides the correlation coefficient between two climate time series with bootstrap confidence intervals to overcome this issue. As persistence reduces the effective data size, substantially more data are required. In this thesis, it will be used in Chapter 3 with data from site MD04-2829CQ.

2.2.6.2 Geochemical mixing model

Geochemical mixing models can be used to constrain the proportions of each source region that is contributing to a sample. A geochemical mixing line will be used to identify the key trends in the data. Using the concentrations of Nd, and Sr, in addition to the $^{144}Nd/^{143}Nd$, $^{87}Sr/^{86}Sr$, ratios from this study and from potential sources an IRD source model will be constructed to better constrain the potential source contributions.

2.2.6.3 Un-mixing grain size data

Sedimentary compositional data such as particle size and magnetic data is a composite of several different processes or sources which can be seen as endmembers (Weltje, 1997). End-members can be viewed as fixed components that when mixed together in various proportions can reproduce the measured data set (Heslop et al., 2007). The aim of un-mixing sedimentary data is to derive environmentally meaningful data by finding the proportion each of the end-members that contribute to a sample. The diffuse reflectance spectrophotometry DRS un-mixer programme uses a non-negative matrix factorisation technique to derive end-members this means it can be used when the end-members are unknown and allows additive estimation of end-members (Heslop et al., 2007). In this study the DRS un-mixer available from http://people.rses.anu.edu.au/heslop_d/ will be used to derive endmembers from grain size compositions in order to identify the relative influence of depositional processes (i.e. ice rafting, sediment sorting) over time at site MD04-2829CQ and SU92-09.

3 Changing grain size as an indicator of IRD in the fine fraction

3.1 Introduction

The large circum-North Atlantic ice sheets, were a significant contributor to the supply of continental material to the North Atlantic Basin during the last glacial (Andrews and Principato, 2002). The glacial erosion associated with these ice sheets supplied sediments to the deep ocean via transport by icebergs, turbidity currents and nepheloid layers (e.g., Dowdeswell and Scourse, 1990; Syvitski et al., 1996; Hesse et al., 2004). Much of the work used to quantify inputs from ice sheets has focused on the >150μm fraction of the sediments (e.g., Bond et al., 1992; 1993; 1997; Grousset et al., 1993; McManus et al., 1994; Bond and Lotti, 1995; Elliot et al., 1998; Auffret et al., 2002, Peck et al., 2007; Scourse et al., 2009; Hall et al 2011; Zumaque et al., 2012). This operationally defined size fraction is used to exclude any non-ice-rafted material, based on the assumption that the only way sediments >150μm can reach the open ocean is through ice rafting (e.g., Hemming, 2004). However, this eliminates the majority of glaciogenic sediments which are derived from the <63μm fraction (Andrews and Principato, 2002; Fagel and Hillaire-Marcel, 2006). This thesis focusses on characterising the source of material in the <63μm and <2μm fraction, presumed to be glacially derived, and transported by ice rafting and associated meltwater plumes. However, it is difficult to exclude other methods of transport of fine sediments such as bottom current remobilisation and aeolian inputs. In this chapter the aim is to use the particle size distributions (PSDs) of the 5-63μm fraction of sediments in conjunction with elemental analyses of the <2μm fraction of the sediments, to elucidate the potential modes of transport of the sediment deposited in the fine fraction at the sites SU92-09 and MD04-2829CQ.

3.1.1 Particle size distributions

Particle size distributions (PSD) reflect the transport and depositional environment of sediments and are potentially useful palaeo environmental tools (Weltje and Prins, 2003). Factors acting upon the final particle size distribution of the sediment include; the mode of deposition, transport, the particle size distribution of the sediment source

and the distance the sediment has been transported (Weltje and Prins, 2007). Processes of transport, deposition and erosion are selective, favouring particular particle sizes therefore sorting sediments into distinct particle size ranges (Weltje and Prins, 2003). This principle can be used to infer changes in oceanographic and atmospheric circulation and depositional regimes over time.

Many approaches have been used to describe PSD, the simplest of which is to use statistical attributes (mean, mode, skewness and kurtosis) (e.g. Folk and Ward, 1957; Folk, 1966; Blott and Pye, 2001). An example that has been widely applied in palaeoceanography, is the use of the mean particle size of the decarbonated sortable silt (10-63μm) fraction to estimate the relative strength of bottom currents (e.g., McCave et al., 1995; Bianchi and McCave, 2000; McCave and Hall, 2006; McCave, 2007). This has been very successful in instances where the sediment is deposited by near bottom currents, as bottom current reworking can process a greater amount of material than is deposited by mechanisms such as ice rafting (McCave, 2007). Sediments that have been ice rafted are largely unsorted (similar to tills), hence, where inputs of ice rafted detritus (IRD) are large, and current sorting is diminished there may be a significant IRD contribution to the sortable silt fraction. This poses a problem for SS studies near the margins of ice sheets or during Heinrich event intervals. Hass (2002), attempted to remove the influence of IRD on the sortable silt variability by subtracting the trend of coarse fraction IRD from the sortable silt proxy. Another approach is to identify the presence of IRD and bottom sorted currents by using the whole particle size distribution. This has previously been achieved using multivariate exploratory techniques including entropy analysis (Forrest and Clark, 1989; deGelleke et al., 2013), principle components analysis (PCA) (Davis, 1970; Andrews and Principato, 2002; Andrews et al., 2003) and factor analysis (Klovan, 1966) however these methods are not designed to deal with compositional non-negative data. Where data are transformed into negative values as part of the matrix they can become difficult to relate back to the original data and processes (Weltje, 1997). The end member modelling algorithm (EMMA) was put forward by Weltje, (1997), the EMMA characterises the PSD using a set of end members which mixed in varying proportions can reproduce the observed PSD. It overcomes the problems in factorisation and PCA by using non-negative factorization of the compositional data.

The end member modelling algorithm is based on the following assumptions about the data from Weltje (1997);

- The order of variables in the model is irrelevant
- The observed variation in composition is as a result of linear mixing with a superimposed measurement error;
- The end member compositions are fixed
- The end member compositions are as close as possible to observed compositions
- The end members are linearly independent, i.e., none of the end members can be expressed as a mixture of the other end members

This method will be used here to examine particle size distributions of the fine fraction.

3.1.2 Particle size distribution; uses in palaeo-environmental studies

End member modelling using the EMMA algorithm has been used in several studies of PSD. It has been used to infer aridity by distinguishing between inputs of fluvial and aeolian material at the Makran continental slope (M. A Prins et al., 2000; M. A. Prins et al., 2000). In another instance it was used to demonstrate changing influence of aeolian and hemipelagic inputs and relating this to aridity and wind strength (Stuut et al., 2002). More recently it has been used to infer the mixing of dust events and background sedimentation from PSD of Loess and Palaeosol sequences in Northern China (Prins et al., 2007). EMMA has also been used to look explicitly at IRD and current sorting from the Reykjanes Ridge in the mid-north Atlantic. This approach was used to distinguish between current sorted and IRD deposited material (Prins et al., 2001, 2002; Jonkers et al., 2012a). However, there are significant differences between their approach and that taken in this study, firstly they used a laser particle size analyser and were able to look at particle sizes between 0.15-1414 μm, and secondly the Reykjanes Ridge site is situated in a drift site which is distal to the source of IRD.

3.1.3 Particle size changes over Heinrich events

Differences in PSDs over Heinrich events have been observed in sediments around the Labrador Sea and the East coast of North America. Hesse and Khodabakhsh

(1998), demonstrate that there are significant changes in the facies composition of Heinrich event layers across the North Atlantic. Sites close to the Hudson Strait having evidence of nepheloid layer deposits and turbidites in contrast to the sites in the North Atlantic where Heinrich layers consist of fine suspended sediment and ice rafted drop stones. deGelleke et al. (2013) were able to infer changes in sediment facies over H1 along the North American margin, using entropy analysis of PSDs. They demonstrated that within 1000 km of the Hudson Strait the Heinrich events are dominated by fine particle sediment plumes with ice rafting becoming more dominant in distal settings, over the course of H1 winnowed deposits become more abundant. Furthermore, studies at the European margin have demonstrated laminations and changes in grainsize are associated with periods of ice rafting (Dahlgren and Vorren, 2003), and in the lead up to Heinrich event 1 in particular at sites in the Southern Norwegian Sea (Lekens et al., 2005) and Celtic margin (e.g., Zargossi et al., 2001; Mojtahid et al., 2005; Toucanne et al., 2008).

3.1.4 Geochemical/sediment composition changes over Heinrich events

Geochemical analysis has a plethora of applications including; characterising the parent material of sediments, the environment of deposition, and to evaluate weathering, sorting, mixing and diagenetic alterations to the sediment (e.g., McLennan et al., 1993; Saito, 1998; Richter et al., 2006; Bloemsma et al., 2012). It is possible to use changing elemental ratios to demonstrate instances of continental mechanically weathered inputs (such as IRD) to a site. For example, XRF derived Si/Sr and Ca/Sr ratios have been employed to identify detrital layers rich in silicate and detrital carbonate respectively (e.g. Hodell et al., 2008; Channell et al., 2012) and K/Ti ratios have been used to demonstrate changing terrigenous sources during IRD events at the Faeroe Drift (e.g., Richter et al., 2006). Previously the ratio of K/Ti and Th/Sc representing shifts from a basaltic to continental source, have been used to validate the end members models of PSD for an IRD related endmember in the North Atlantic (Prins et al., 2001; Jonkers et al., 2012a).

This chapter presents particle size data of the 5-63μm fraction from core SU92-09 and MD04-2829CQ. Previous studies have shown the utility of particle size distributions in understanding the transport mechanisms of sediments (M. A Prins et al., 2000; Stuut et al., 2002; Prins et al., 2002; Arz et al., 2003; Tjallingii et al., 2008).

The aim is to understand the contribution of various transport mechanisms to the sediment at the Rockall trough and IRD belt sites, by un-mixing particle size data from the 5-63μm fraction. It is hypothesised that during Heinrich events particle size will coarsen due to increasing transport of ice rafted debris, which has a coarser grain size profile than hemipelagic sediments (Jonkers et al., 2010), to both sites SU92-09 in the IRD belt, and MD04-2829CQ at Rosemary Bank. By comparing the un-mixed records from these contrasting settings, it will be possible to observe differences between the depositional environments at the margins of an ice sheet and at the IRD belt. This will further the comprehension of changing sediment source at each site. This may allow the assignment of end members to environmentally meaningful processes, and to infer how these change over the glacial and in response to abrupt climate change over H2 and H4. These data will be compared the associated compositions of elements (K/Ti and Th/Sc) from the <2μm fraction, to assess whether there is a continental input to the fine fraction at the same time as IRD inputs over H2 and H4 as a further validation of the PSD based end member model.

3.2 Results

3.2.1 Particle size distributions

In the following figures Heinrich events have been highlighted based on the ages provided by Hemming (2004) as the centre point for H2, H3 and H4. However, at site SU92-09 H4 occurs earlier and is centred on 39 ka BP, H1 is also earlier at SU92-09 and is centred at 17 ka BP, these dates are within the range of estimates shown in Table 1.1. Three main trends can be observed in the contour plot (n=78) of the 5-63µm particle size data from the IRD belt site (SU92-09) in Figure 3.1. Firstly, prior to H4 (46-41 ka BP) and H2 (33 to 25.5 ka BP), the distributions are poorly sorted with similar contributions to the 5-50µm bins and with low volumes recorded in the 50-63µm range. During H4, H2 and H1 (41-38.5, 22.5-25.5 and 16-19 ka BP)

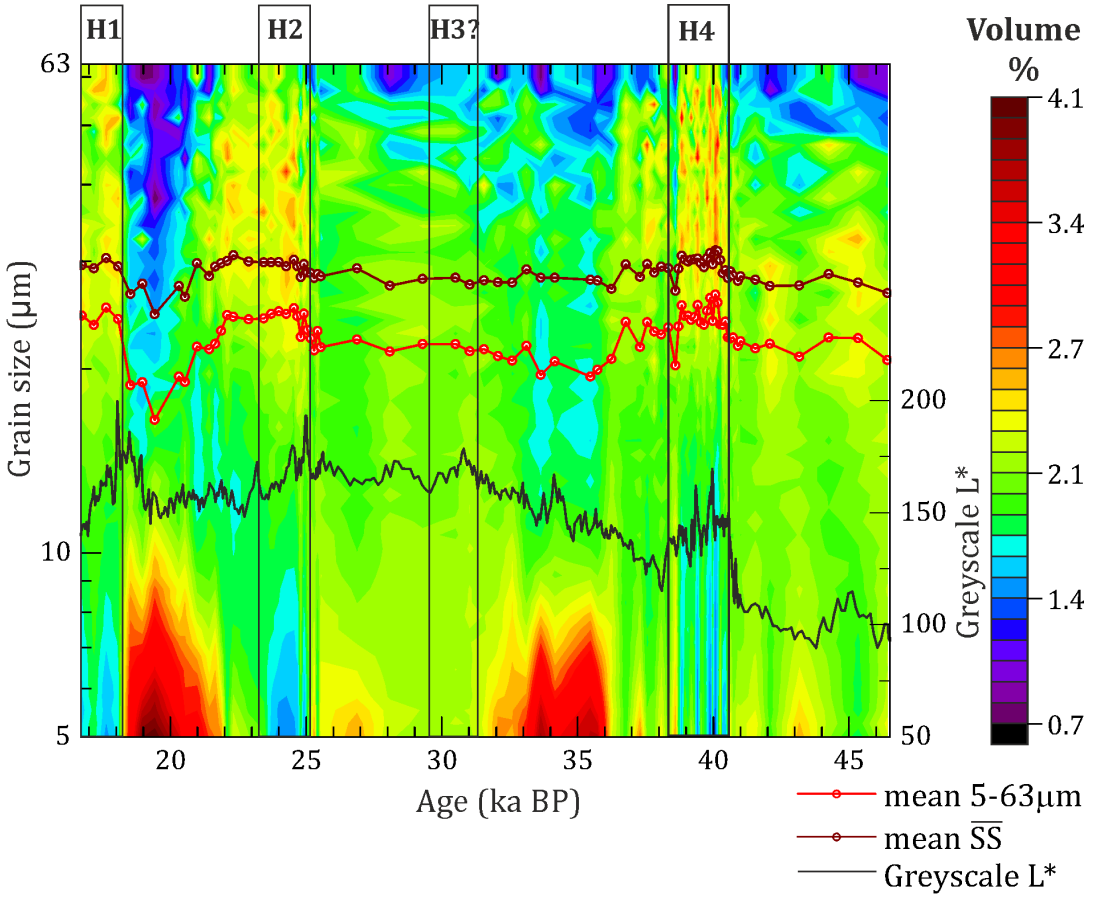

Figure 3.1: Contour plot of the differential volume of particle size vs age from site SU92-09, based on results from the 5-63µm fraction plotted with 50 bins. Particle size is plotted on a logarithmic scale. Heinrich events are highlighted with black outline. Shown in red is mean particle size of the 5-63µm fraction and in brown the mean sortable silt is shown. Greyscale is shown in black for reference.

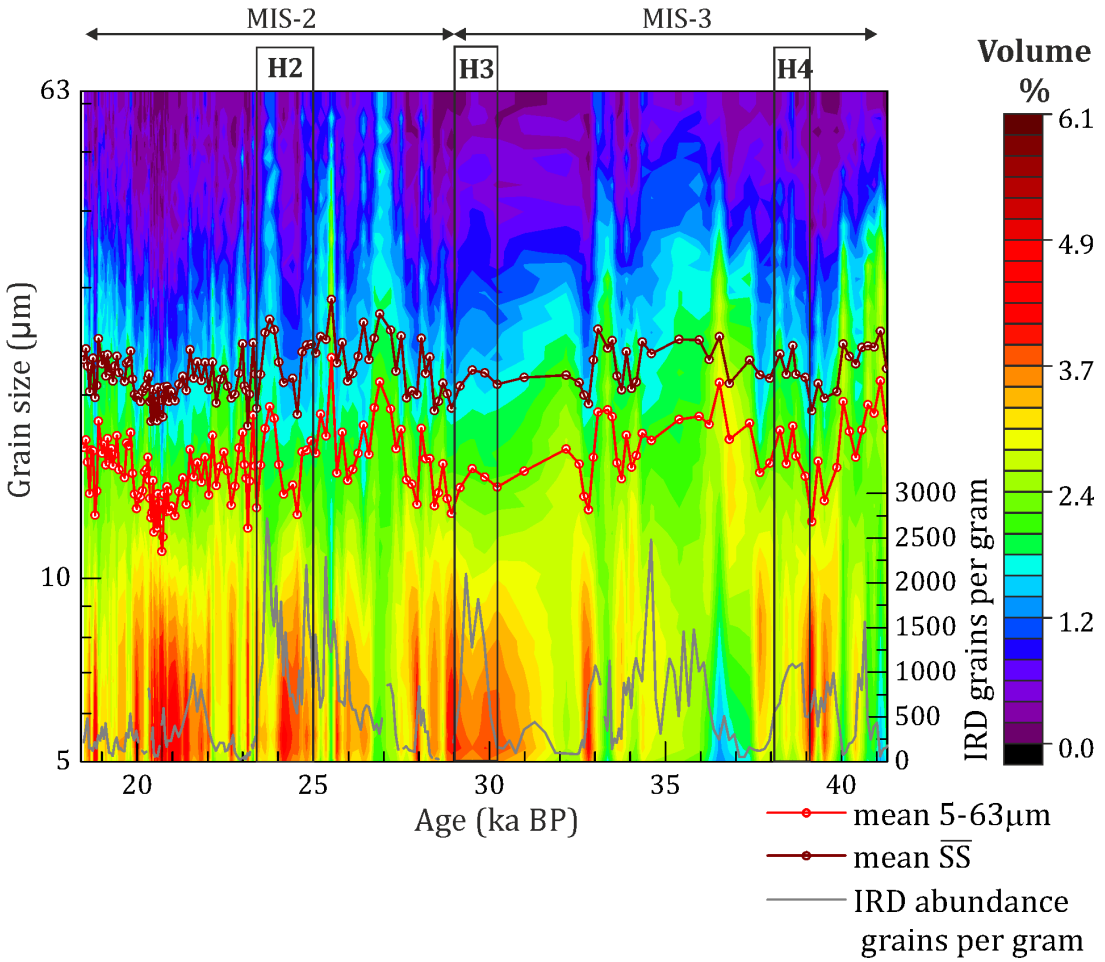

Figure 3.2: Contour plot of the differential volume of particle size vs age from site MD04-2829, 5-63µm fraction plotted with 50 bins. Particle size is plotted on a logarithmic scale. Heinrich events are highlighted with a black outline. Shown in red is mean particle size of the 5-63µm fraction and in brown the mean sortable silt. IRD (>150µm) abundance is plotted in grey for reference.

the particle size coarsens with distinct increases in the 10-63µm fraction to 3.3% volume and decreases in the 5-10µm range to ~1.6 %, which is concurrent with increases in greyscale. After H2 and H4 there is a fining of the particle sizes with a distinct increase in the percentage volume of the <10µm fraction to over 3% and a reduction in the >10µm particle size volumes to <1.2%.

The contour plot in ***Figure 3.2*** shows that at site MD04-2829CQ the particle size distributions are generally finer than those at site SU92-09 with SS and mean particle size of the 5-63µm fraction both lower that at site SU92-09. There is a fining trend during MIS 2 compared to MIS3, and a coarsening of the particle sizes is evident during H2, H3 and H4 and during some but not all ice rafting events, the ice rafting events are indicated by the IRD abundance.

3.2.2 End member model selection

The minimum number of end members sufficient to explain the variability of a dataset can be estimated using the coefficient of determination (R^2), this represents the variance of each particle-size class reproduced by the approximated data (Weltje, 1997; Prins et al., 2002). This is achieved by finding the inflection point of the curve of mean R^2 value plotted against the number of end members that represent the true number of end members that describe the mixture (Prins and Weltje, 1999).

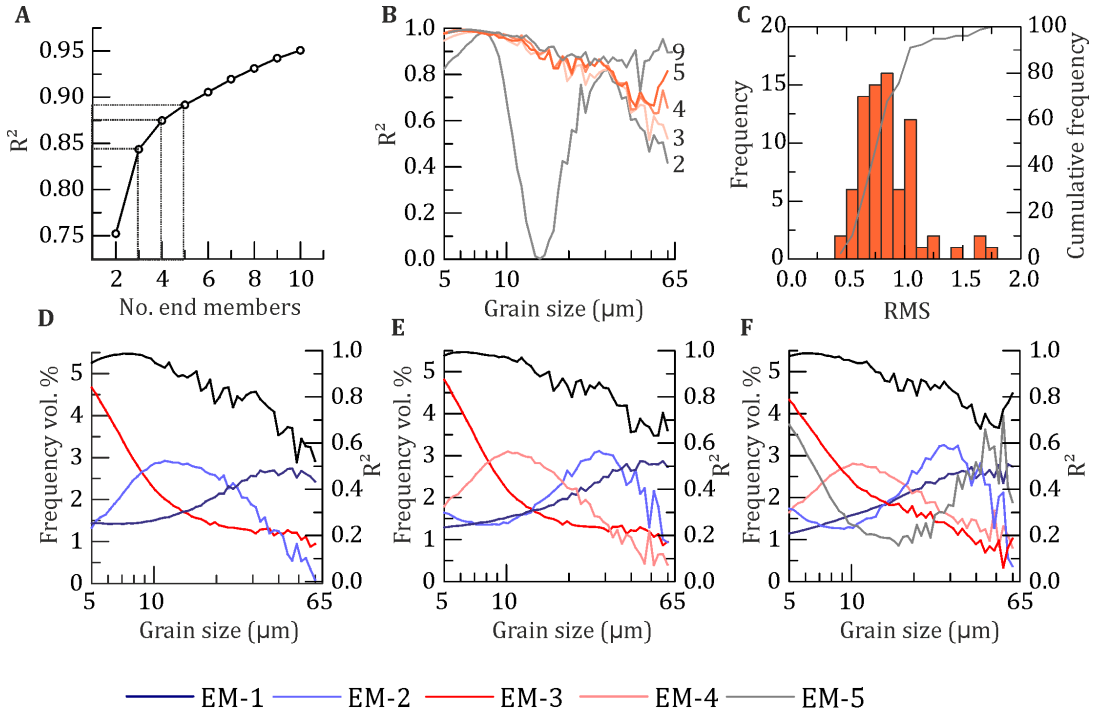

Figure 3.3: End member modelling results for site SU90209. A: R^2 used to estimate appropriate number of end members. B: R^2 per size class for 2,3,4,5 and 9 end member models. C: RMS between the observed particle size distributions and the four end member model D: The size distribution of the end members and R^2 (black line, right axes) per size class for a 3-end member model, E: Four end member model and F: five end member model.

Three potential models with 3, 4 and 5 end members for site SU92-09 from the IRD belt are shown in ***Figure 3.3***. Values of R^2 are 0.84 for a three-end member model, 0.87 for a four end member model and 0.89 for a five end member model. There is no clear inflection point for the SU92-09 data set, however after four end members the increases in R^2 are small (Figure 3.3A). Plotting the R^2 values for each end member model against particle size (***Figure 3.3***B) demonstrates how well the model fits the data at a particular particles size. When the R^2 values are plotted over the different particle sizes, it is clear that the four end member model more adequately describes

the data from the coarser particle sizes than the three end member model, the addition of a fifth end members does not increase the fit of the model greatly. The four end member model shows a good fit to the observed data with 90% of the data having a RMS value of <1 % ***Figure 3.3***C.

At site MD04-2829CQ, (***Figure 3.4***) the inflection point of the mean R^2 curve is much clearer than at SU92-09 and is at four end members (***Figure 3.4***A). The mean

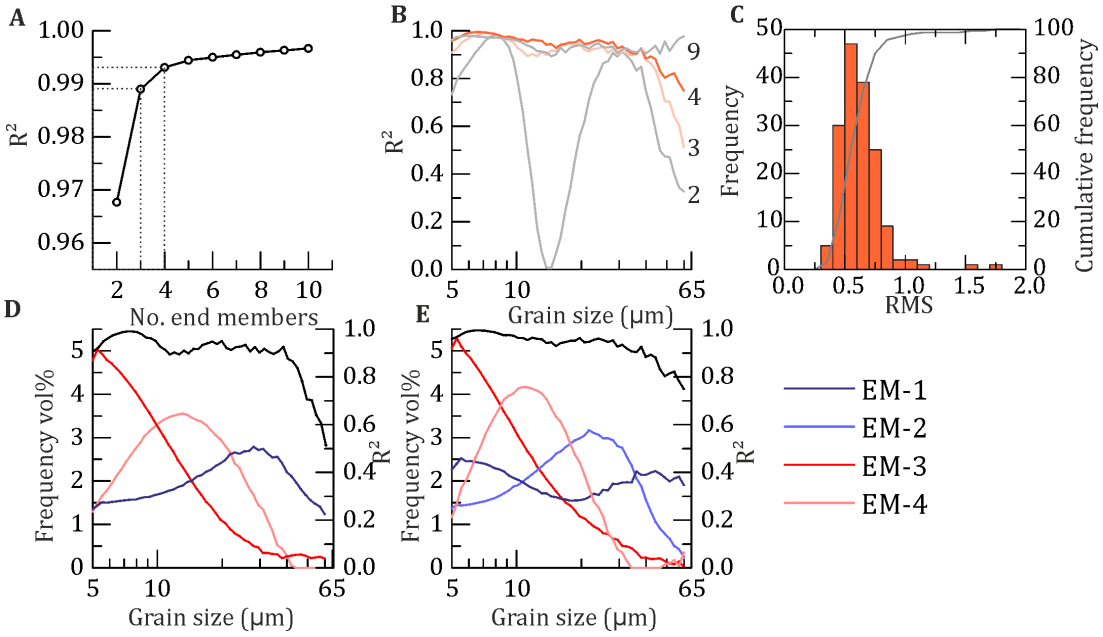

Figure 3.4: End member modelling results for site MD04-2829CQ. A: R^2 used to estimate appropriate number of end members. B: R^2 per size class for 2, 3, 4, and 9 end members models. C: RMS between the observed particle size distributions and the four end member model. D: The variation in end members and R^2 per size class for a three end member model, E: Four end member model.

R^2 value for a three end member model is 0.987 indicating a good fit of the model with just three end members, but a four end member model better describes the coarser fractions than the three end member model. The four end member model shows a good fit to the observed data as 95% of the samples have a RMS value of <1. Therefore, for both site SU92-09 and MD042-829CQ the best model is the four end member model with mean R^2 values of 0.87 for SU92-09 and 0.993 for MD0428-29CQ.

The four end member model of site SU92-09 (***Figure 3.3***E) has an end member (EM-1) with a modal particle size of 57µm (very coarse silt) and three well sorted end members: EM4, fine silt with a modal particle size of 5µm, EM3, medium silt (10µm) and EM2, coarse silt (mode =28µm), based on the classification scheme by Blott and

Pye (2012). When plotted as a time series (Figure 3.5) it is evident that EM-1 of the SU92-09 model increases significantly during the H2, H4, and H1 intervals, to represent 60-70% of the variation at the site.

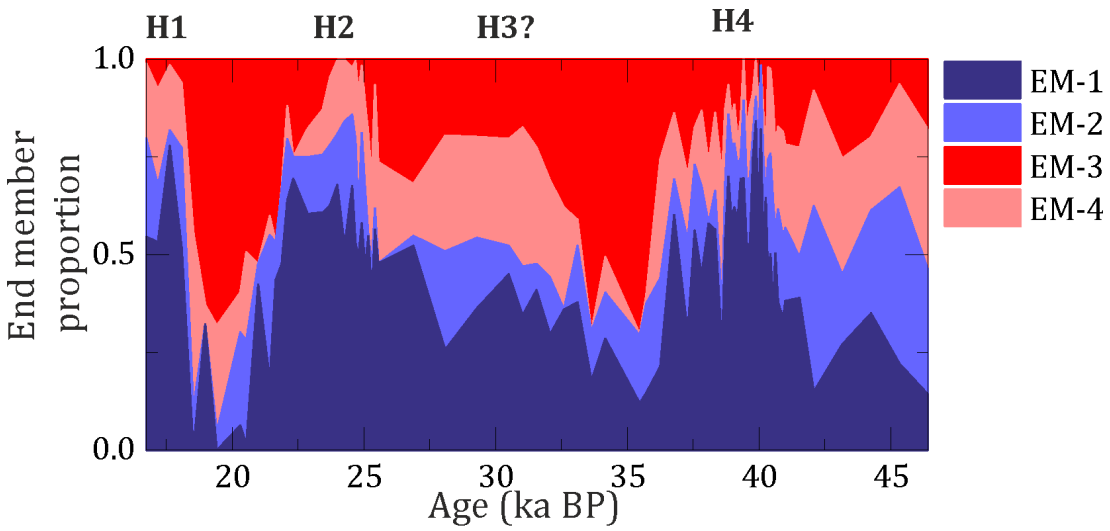

Figure 3.5: Variation in the particle size end member proportions over time at site SU92-09.

The fine silt end member, EM3 dominates in the interval after H4, between 38 -34 ka BP, and H2, between 23 to 19 ka BP (representing over 60 % of the variation). The coarse silt and silt end members are most abundant prior to H4 and between H4 and H2.

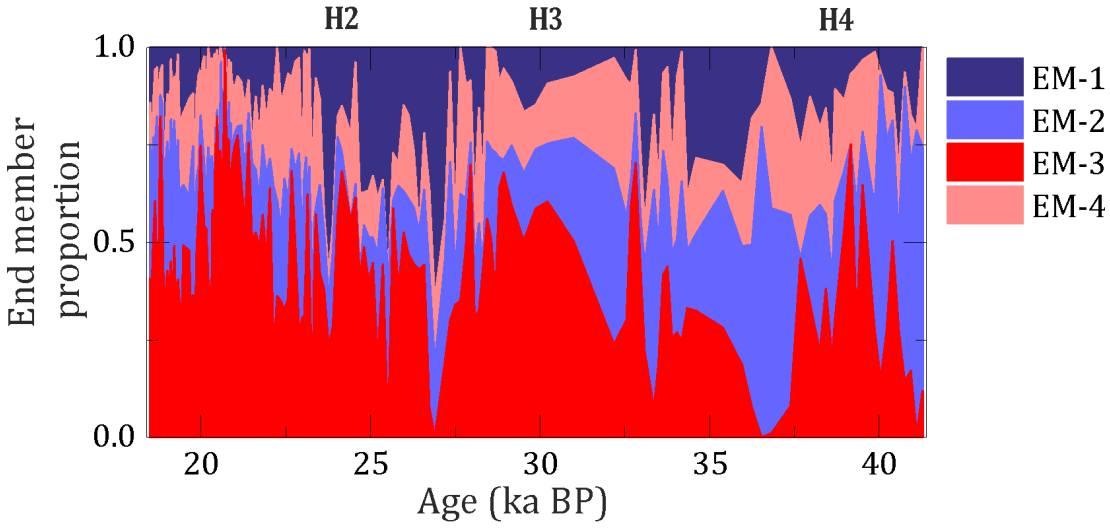

Figure 3.6: Variation in the particle size end member proportions over time at site MD04-2829CQ.

At site MD04-2829CQ the end members exhibit a similar structure to those observed at site SU92-09 with a poorly sorted end member, EM1, (coarse silt), and three well sorted end members: EM3, fine silt (model = 5.2µm), EM4, medium silt (11µm) and EM3, coarse silt (22µm) as shown in ***Figure 3.4***E. In Figure 3.6 it is evident that EM3 the finest end member increases over H4 and then increases over the last glacial. The coarsest end member (EM1) is low at site MD04-2829CQ accounting for less than 50% of the variability.

3.2.3 Elemental analysis

At site MD04-2829CQ (***Figure 3.7***) the K/Ti and Sc/Th ratios are high, ratios of K/Ti peak at the same time as the input of detrital carbonate (DC) IRD to the site during H4 and H2.

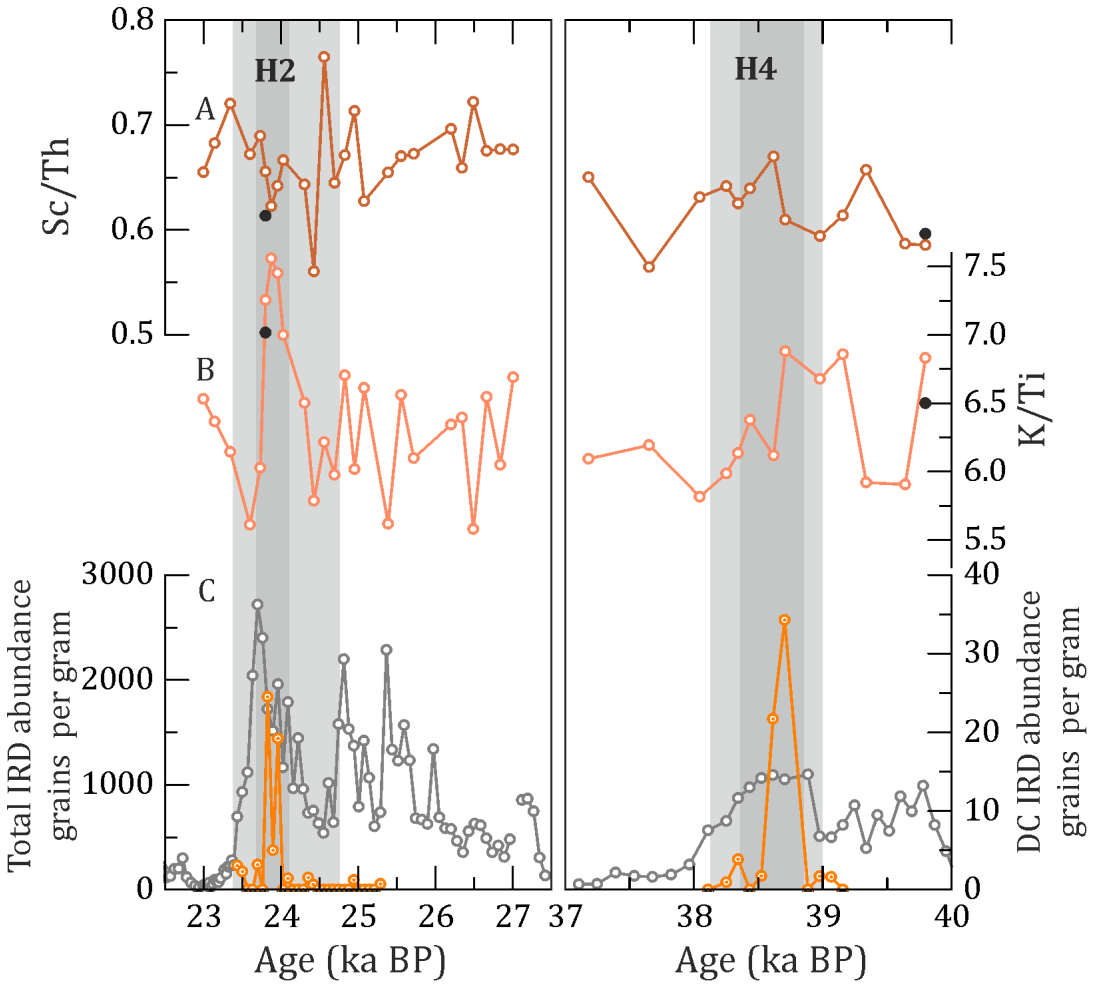

Figure 3.7: ratios of K/Ti and Sc/Th H2 and H4 from the <2µm fraction of site MD04-2829CQ, A; Sc/Th ratio, B; K/Ti ratio, C; the abundance of IRD (grey) per gram and detrital carbonate (DC) abundance (orange) Hall et al. (2011). Replicate analyses are shown in black circles.

At site SU92-09 there is a significant increase in the Sc/Th and K/Ti ratios over H2 and H4, corresponding with changes in fine fraction weight (<63µm), which gives an approximation of the amount of material entering the fine fraction, and magnetic susceptibility and greyscale which give an approximation of the changing composition of the sediments (***Figure 3.8***).

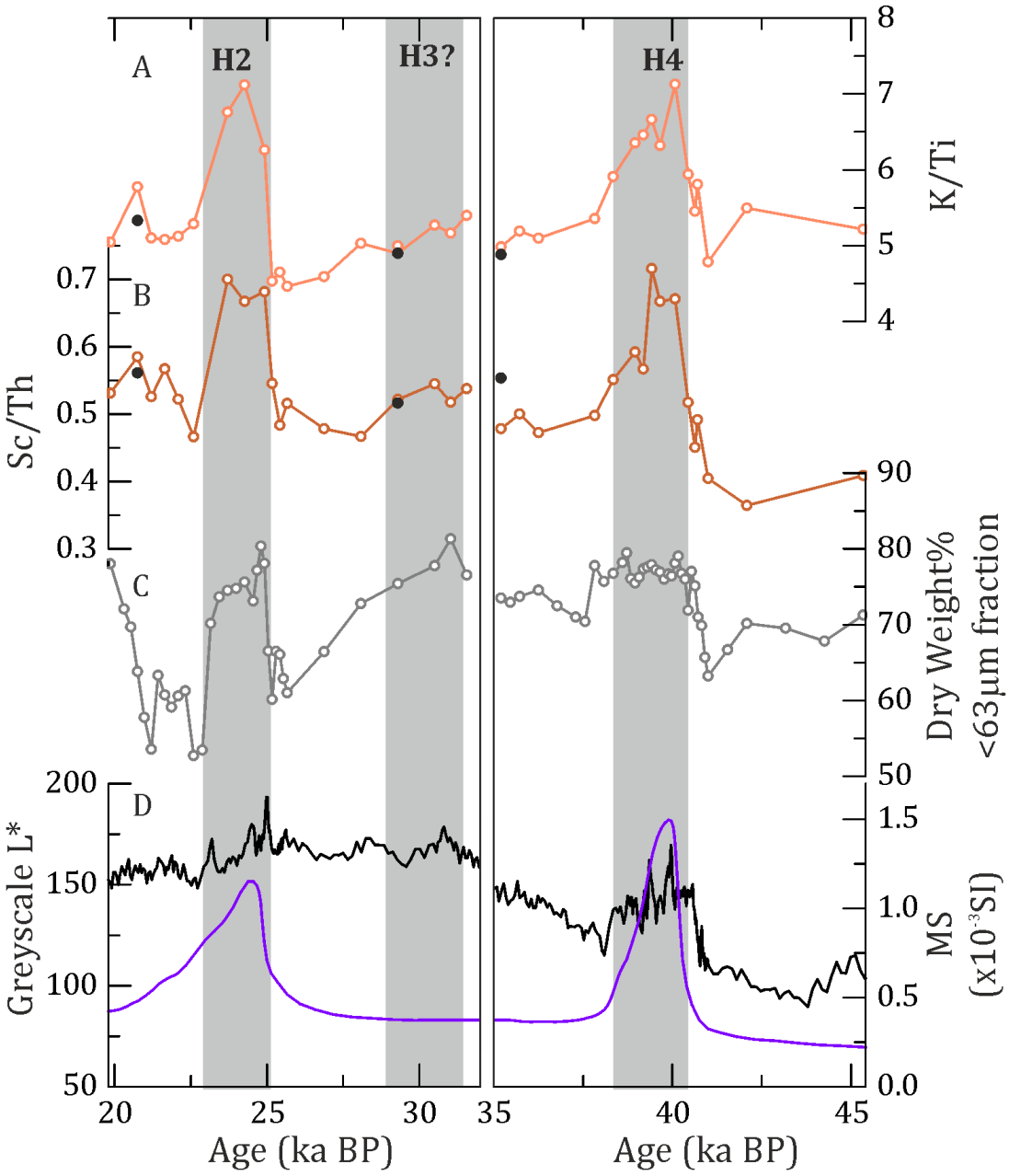

Figure 3.8: Ratios of K/Ti and Sc/Th H2 and H4 from the <2µm fraction of site SU92-09, A; K/Ti ratio, B; Sc/Th ratio, C; dry weight (grey) percentage of the <63µm fraction, D; greyscale and magnetic susceptibility. Replicate analyses are shown in black circles.

3.3 Discussion

3.3.1 Environmental processes contributing to changes in particle size

When attributing environmental processes to the end members the follow assumptions are made:

1. Each end member is a response of the grain size to a single process.
2. The processes that are represented by each endmember are the same over time (i.e. IRD has an invariable composition).
3. The grain size distributions in the endmember model are not overly influenced by single data points (outliers).

There are several processes occurring at the margins of ice sheets that would have an impact on particle size distributions. Site MD04-2829CQ is situated on a contourite drift and is ~50 km away from the shelf break. The processes likely to be active at this site are sorting due to bottom currents, inputs from IRD, meltwater plumes and nepheloid layers associated with the ice sheet, surface currents, hemipelagic drift and aeolian transport (e.g. He et al., 2008) as shown in the schematic in Figure 3.9. At site SU92-09, the potential processes are IRD transport, hemipelagic fluxes, nepheloid layers, aeolian inputs and abyssal currents.

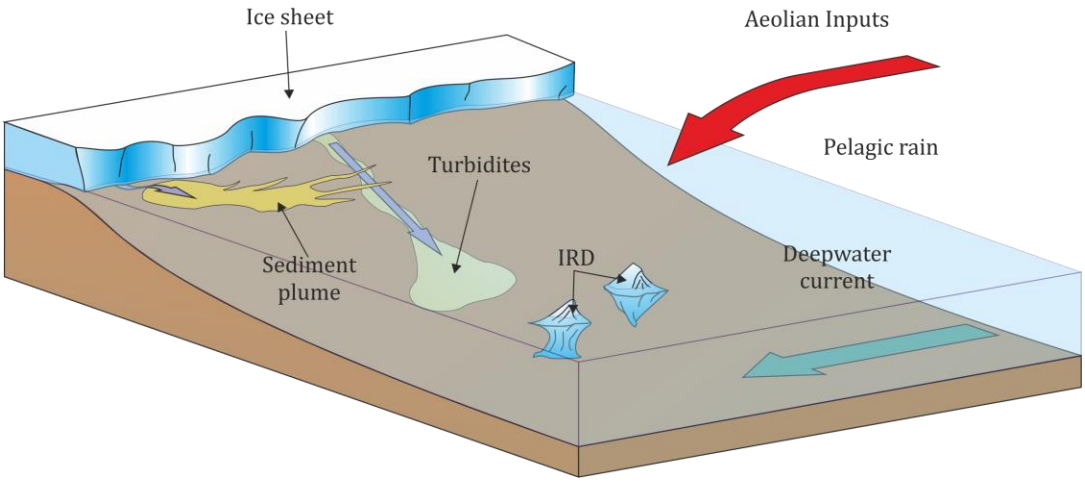

Figure 3.9: possible inputs to ice proximal sites that may have an effect on particle size. Based on the processes discussed in Rebesco (2002) and He et al. (2008).

Englacial and basal transport of sediments within ice exerts little sorting influence and results in the deposition of poorly sorted sediments (tills) (Bennett and Glasser,

2009). As a result, material in icebergs is also poorly sorted. EM-1 at site SU92-09 and site MD04-2829CQ is poorly sorted and coarser than the other end members making it a likely candidate to correspond with IRD. EM-2 is also a coarse end member in both MD04-2829CQ and SU92-09 with a modal particle size of 27 and 30µm respectively. Finer particle size distributions have been associated with ice rafting from ice shelves in modern day studies which entrain sediments from the continental shelf resulting in the entrainment of finer material (Hebbeln, 2000). It is feasible that at least part of the IRD reaching both sites was entrained by this method. Indeed, when the particle size distributions of the two coarsest and poorly sorted end members are compared to the particle size distributions of IRD from modern icebergs (Jonkers et al., 2012a) there are similarities in the grain size distributions (***Figure 3.10***) of which all but BB-2 have a peak in the coarse silt fraction. When EM1 and EM2 are combined at both site SU92-09 and MD04-2829CQ, there is a correspondence between the modelled EM1+EM2 and the ice rafted detritus PSD from BB-3 particularly in MD04-2829CQ. As site MD04-2829CQ is situated on the Feni Drift there is the potential for EM2 to also be representative of coarsening due to increased winnowing of sediments as a result of increased flow speeds of the NSOW. At site DS97-2P (Prins et al., 2001; Jonkers et al., 2012a) mean SS values are between 13-16.5µm, however the mean SS at site MD04-2829CQ is much higher at between 17 and 28 µm. Therefore, it is possible that increases in EM-2 correspond to intervals of faster flow speeds rather than IRD.

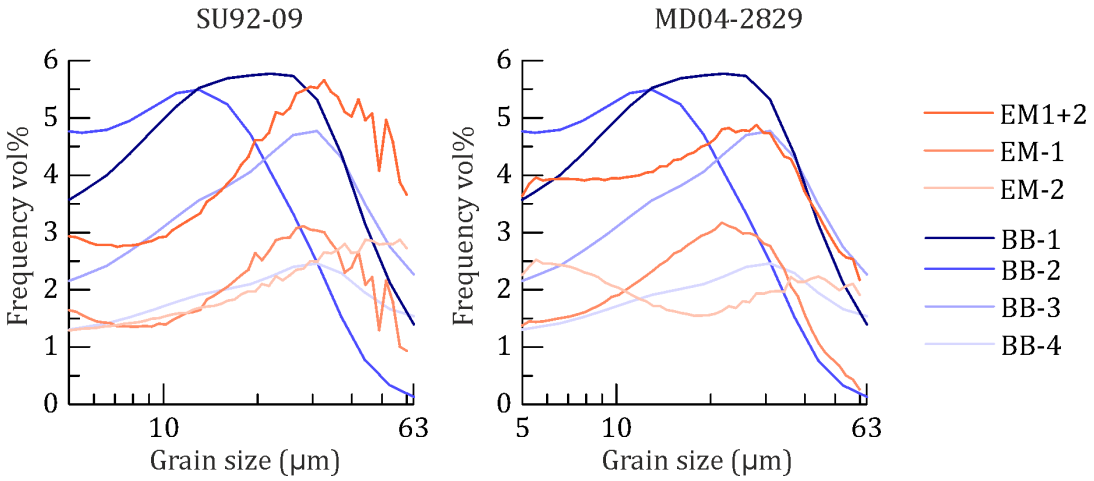

Figure 3.10: Comparison between potential IRD end members at site SU92-09 and site MD04-2829. BB1-BB4 are the particle size profiles of IRD from icebergs in Jonkers et al., (2012). (Note: the BB data is from a larger data set and bins have a larger spacing than the EM from this study).

The Pearson's correlation coefficient calculated using the Pearson's T program (Mudelsee, 2003) between the modelled IRD and IRD indicators from site MD04-2829CQ are shown in Table 3.1. These show a correlation between the abundance of IRD grains and the modelled IRD based on EM-1; however, there is a wide range of error from the bootstrapped confidence interval.

Table 3.1: Pearson T correlation coefficients for endmembers at site MD04-2829CQ

Endmember	Persistence	Proxy	Persistence	correlation co-efficient	confidence interval
Modelled IRD	0.24	$\delta^{18}O_{FINE}$	1.27	0.33	-0.146, 0.68
Modelled IRD	0.24	Total IRD	0.19	0.23	-0.202, 0.58
Modelled IRD	0.24	IRD abundance	0.33	0.53	0.269, 0.72
EM4(fine)	0.274	$\delta^{18}O_{FINE}$	1.27	-0.42	-0.717, 0.01
EM4(fine)	0.274	IRD abundance	0.33	-0.30	-0.578, 0.035

3.3.2 Fine endmember attribution

Site SU92-09 is at 3270 m water depth and is not situated near any known drift site, the sedimentation rate at the site would indicate that it is not affected by increased sediment inputs associated with sediment drifts. Therefore, the inputs to the site must be largely from hemipelagic fluxes, with little inputs from bottom currents. If EM-3 and EM-4 are compared to hemi-pelagic fluxes of particles, which have been shown in previous grain size studies to have a very fine input, it is possible to attribute them to this, rather than flow speeds as was the case in (Prins et al., 2001). In a study of several cores across the North American margin, deGelleke et al. (2013) associated three endmembers with settling from the meltwater plume, turbidity currents and IRD in samples from the <100μm fraction. The smallest grain size endmember was attributed to plume settling and is similar in size to the combined EM3 and EM4. Hence, these could represent settling from hemipelagic sediments.

Site MD04-2829CQ is situated on a contourite drift and therefore the site is likely to experience current sorting. There are two likely scenarios for the finer endmembers of this site, the first is that they represent changes in current sorting, related to the situation of the site on the contourite drift; the second is that the finer endmembers are

related to melt water inputs at the site. The impact of the current on the site has been demonstrated over H1 using $^{231}Pa_{xs}/^{230}Th_{xs}$ (Hall et al., 2006). The fine end members from this study have similar distributions to the finer end members of (Prins et al., 2001, 2002; Jonkers et al., 2012a), these were attributed to low energy bottom currents associated with the ISOW. Fine endmembers have also been associated with meltwater plumes and nepheloid layers within 1000 km of the shelf (deGelleke et al., 2013). Due to the situation of site MD04-2829CQ within 50 km of the BIIS and in a sediment drift, it may be possible that both mechanisms are active at the site. To look at the potential for current sorting, the ratio of EM2 which possibly represents winnowing of the finer sediments by faster bottom currents compared to EM3 and EM4, which represent slow current conditions this is plotted in ***Figure 3.13*** and would indicate reduced current influence over the course of the last glacial.

As is clear from the above discussion of the endmembers there are multiple factors influencing each site that can produce the same particle size profiles it is not possible to attribute a single process exclusively to each endmember which is consistent throughout the records. Therefore, the best approach is to use the modelled end members as a descriptive tool to help understand particle size changes rather than to interpret them as strictly relating to one process in this instance.

3.3.3 Changes in fine fraction deposition over the last glacial

3.3.3.1 SU92-09

At site SU9209 there is a clear trend in the particle size data where EM1, the coarsest endmember, increases during H4, H2 and H1 accounting for over 60% of the material during these events as shown in ***Figure 3.11***C. If EM2 (coarse silt) is added to this as in ***Figure 3.11***B then the coarser silt fraction makes up 80% of the material deposited during the Hudson Strait Heinrich events. However, if this coarsening of particle size is interpreted to be an increase in the supply of IRD then that would indicate that there is a significant amount of IRD outside of the Heinrich event intervals up to 40% (using EM1) and 60% using (EM1+EM2). After H4 the IRD% does not return to 0% therefore there is a demonstrable small supply of IRD outside of Heinrich events to the site. Further evidence at site SU9209 of continental ice rafted

material is the high ratios of K/Ti and Sc/Th at the site, an indication of a continental weathered sediment source. Though these ratios are lower outside of the Heinrich

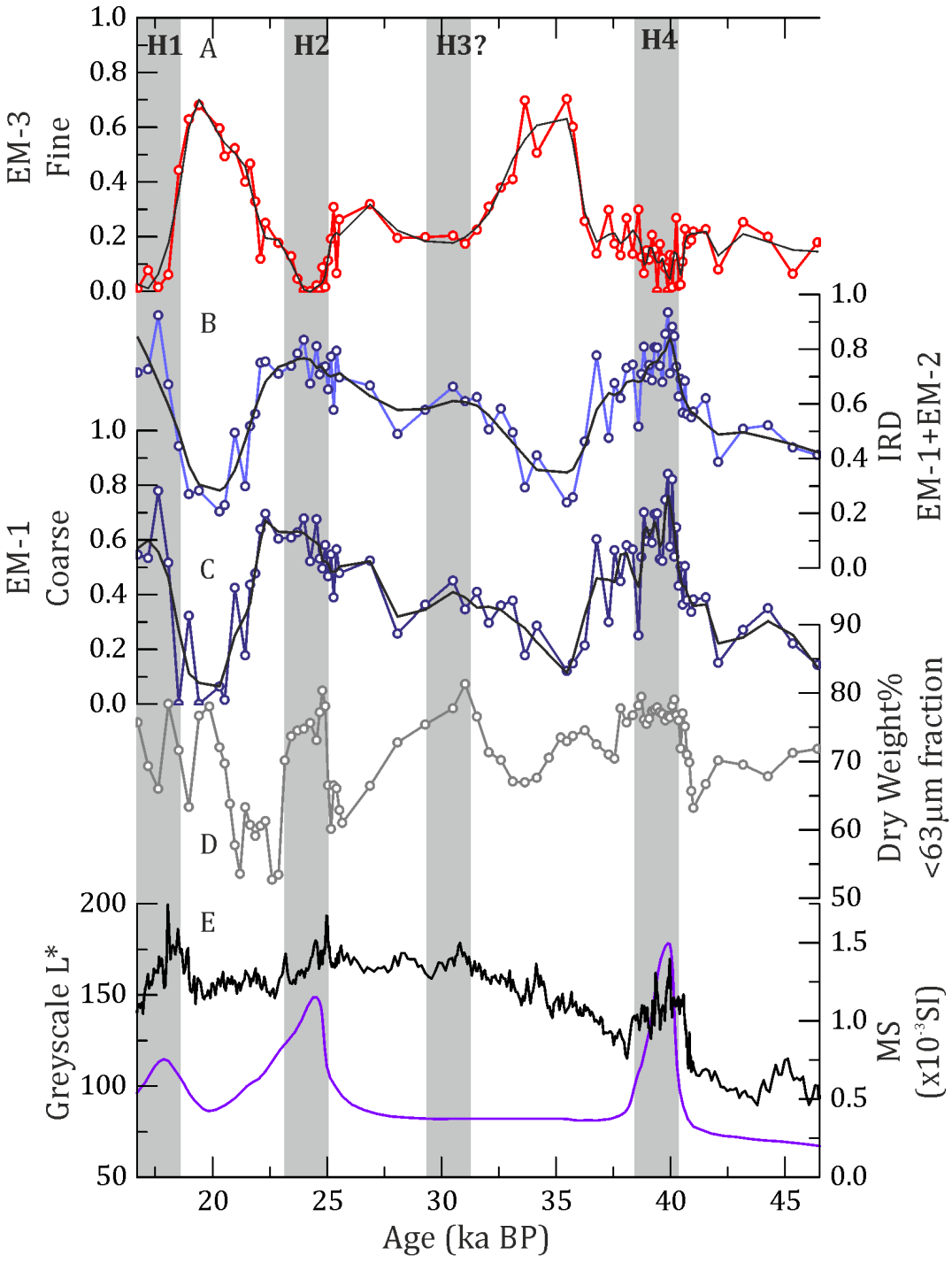

Figure 3.11: Plot of end members from site SU92-09 over time. A; proportion of EM-3 fine, B; proportion of modelled IRD (EM-1+EM-2)C; proportion of EM-1, D; percentage dry weight of the fine (<63µm fraction), E; magnetic susceptibility (purple) and greyscale (black). Black lines are smoothed data trends.

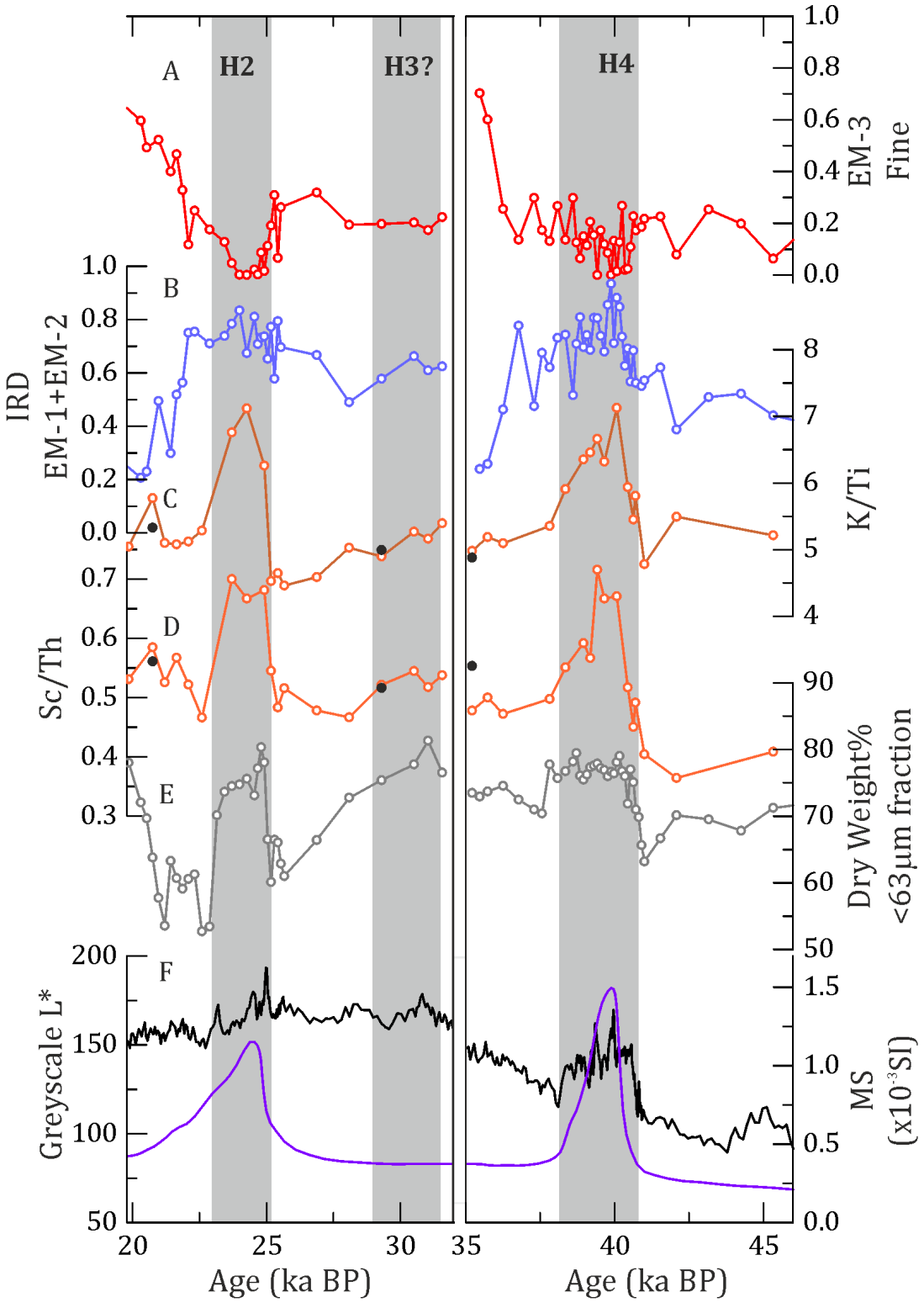

Figure 3.12: Changes in end members and elemental ratios over H2 and H4 for site SU92-09. A; proportion of EM-3 fine, B; proportion of modelled IRD (EM-1+EM-2) C; K/Ti ratio, D; Sc/Th ratio E; percentage dry weight of the fine (<63µm fraction), F;magnetic susceptibility (purple) and greyscale (black).

events they do not reduce to levels that would be expected with low continental inputs to the site.

The circum-North Atlantic ice sheets have been shown to have millennial scale variability that is captured in near ice sheet sites during the last glacial for example at the European margin (e.g., Scourse et al., 2009). Hence, the transport of continental material via ice rafting is feasible throughout the last glacial. At sites within the IRD belt there is evidence of lithics (>150μm) throughout the last glacial, for example at the Driezack seamount (Heinrich 1988) site DSDP609 (Bond et al., 1992; Hodell and Curtis 2008). Another potential scenario is that these changes in grain size outside of Heinrich event intervals are linked to bottom flow speeds, which would indicate an increasing flow speed prior to and immediately after the Heinrich events. Given the low sedimentation rates at the site between 2 and 8 cm ka^{-1}, the extended IRD input scenario is most likely. The large fining events that occur after H2 and H4 could indicate a cessation of IRD input to the site and therefore a site dominated by hemipelagic fluxes.

3.3.3.2 MD04-2829CQ

From a sedimentary perspective site MD04-2829 is much more complex than site SU92-09, situated in a drift and close to the ice sheet, it potentially has several factors controlling particle size at the site as discussed in Section 3.3.2. Increasing proportions of EM3 (fine silt) over the last glacial (***Figure 3.13***), could be interpreted as decreased flow speeds at the site which may be expected over the course of the last glacial, this is interpreted here as increasing supply of fine material from the BIIS throughout MIS 3 as the ice sheet reaches the shelf edge. This is supported by authigenic Pb fluxes of Crocket et al. (2013), which indicate a higher discharge from the BIIS during the period 25 to 18 ka BP after H2. This would support the timing of the expansion of the BIIS put forward by Clark et al. (2012), and the model of BIIS growth from Hubbard et al (2009). EM1+EM2 does not correlate well with IRD abundances (Table 3.1) from site MD04-2829CQ however, EM1 alone shows a reasonable correlation with IRD abundances (0.53) but with a wide confidence interval. Using EM1 it is possible to identify coarsening peaks in

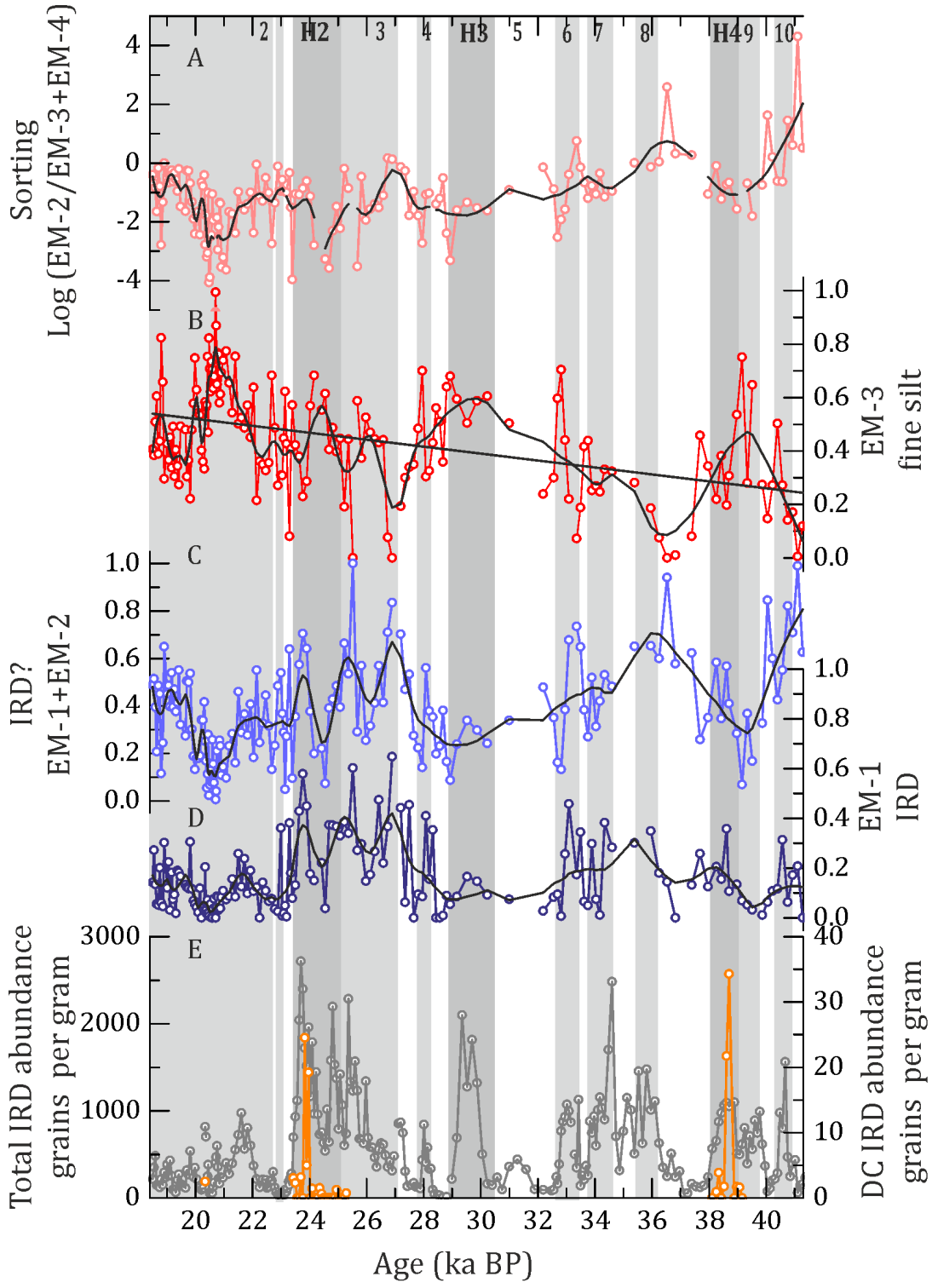

Figure 3.13: Plot of end members from site MD04-2829CQ over time. A; sorting of sediment, B; EM3 (fine silt) C; (EM-1+EM-2) D; proportion of EM-1, E; IRD abundance in grains per gram (grey)and DC abundance (orange) Hall et al. (2011) Black lines are smoothed data trends.

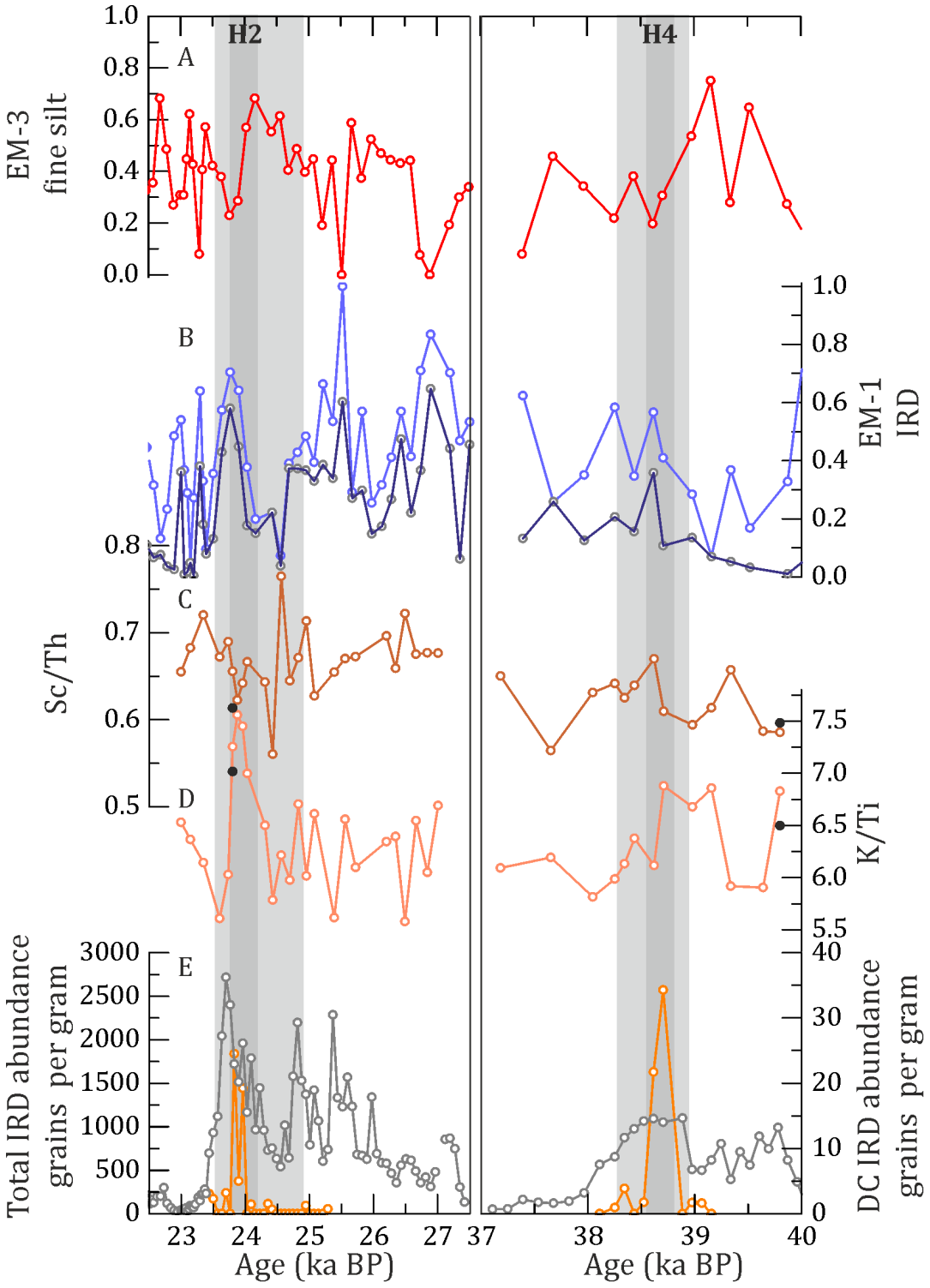

Figure 3.14: Changes in endmembers proportions and elemental ratios over H2 and H4 for site MD04-2829CQ. A; EM3 (fine silt) B;EM1 (dark blue) and EM2 (light blue) C; Sc/Th ratio D; K/Ti ratio, E; IRD abundance in grains per gram and detrital carbonate (DC) grains per gram Hall et al. (2011), (grey).

the fine fraction that correspond to peak IRD inputs in the coarse fraction. In ***Figure 3.14*** peaks in EM1 clearly correspond with DC inputs during H4 and with peaks in the abundance of IRD during H2.

3.3.3.3 Does end member modelling of fine fraction PSD contribute to the knowledge of environmental conditions during the abrupt climate changes of the last glacial?

The aim of this chapter was to characterise the particle size distributions of the fine fraction to better understand inputs to glacial flour. However, there are several cautionary notes to the interpretation here. The first is that it has proved difficult to attribute the end members to actual physical processes. This is likely a result of the narrow size fraction that was observed, in this study that was in part due to the focus of this study on the fine fraction of the sediments in an attempt to trace inputs of glacial flour. A second reason for the narrow size fraction was the use of the coulter counter which was restricted by the aperture size. One potential solution is to rerun a subset of the samples using a wider particle size range (using a laser particle sizer) in order to see if a wider particle size distribution can constrain the interpretation further. The other issue is that there are multiple processes of deposition acting at the core sites, which can cause similar changes to the particle size. This could be better constrained by a multi- core study of the ice margin during the last glacial, as the spatial variability of the PSD will help to inform the interpretation of the endmember model, and modern analogue studies which would allow the interaction between the processes and their particle size distributions to be better understood.

4 Tracing detrital carbonate inputs across the North Atlantic

4.1 Introduction

4.1.1 Detrital carbonate and Heinrich events

A defining feature of the Heinrich layers during the last glacial is the presence of detrital carbonate, both dolomite and limestone, in sediment cores from sites across the North Atlantic IRD belt (Andrews and Tedesco, 1992; Bond et al., 1992; Bond, 1995; Hesse and Khodabakhsh, 1998; Hemming, 2004; Hodell et al., 2008; Channell et al., 2012; Rashid et al., 2012). The layers of detrital carbonate thicken towards the western Atlantic and Labrador Sea where they can be several tens of centimetres thick (Andrews and Tedesco, 1992; Andrews et al., 1994). Comparisons of the composition of the detrital carbonate layers found it was similar to the Palaeozoic sediments that underlay the Hudson Strait sector of the Laurentide Ice Sheet (LIS) (Andrews and Tedesco, 1992; Bond et al., 1992; Broecker et al., 1992). Detrital carbonate has been found to occur at sites across the North Atlantic during Heinrich event intervals (see ***Figure 4.1***), and has been identified as far as the European margin (e.g., Scourse et al., 2000; Peck et al., 2007; Scourse et al., 2009; Hall et al., 2011). However, significant inputs of detrital carbonate are absent from ambient glacial sediments and from sites outside the IRD belt (Bond et al., 1992). Heinrich event 3 (H3) and H6, have been shown to have no detrital carbonate in the eastern North Atlantic but carbonate was present in these layers in the western Atlantic (Bond et al., 1992) as shown in ***Figure 4.1***. Authors often refer to H1, H2, H4 and H5 as Hudson Strait (HS) Heinrich events to mark this distinction (Hemming, 2004).

4.1.2 Characterising carbonate inputs across the North Atlantic

The early work on Heinrich layers often reports carbonate content as a percentage of the coarse fraction (the definition of which varies from >63μm to >150μm (e.g., Bond et al., 1992); however, excluding the fines also excludes a large proportion of material that is potentially carbonate. This could be crucial as at Orphan Knoll and in the Labrador Sea, sedimentation from turbidity currents and meltwater plumes with high fine-grained carbonate concentrations is followed by a brief interval of increased IRD (Clarke et al., 1999; Rashid et al., 2003b, 2012). Another common technique is

to measure the total carbonate content, which easily picks out Heinrich events, (e.g., Weber et al., 2001) but it should be noted that total carbonate includes both biogenic and detrital carbonates. Alternative methods use the changes proportions of biogenic carbonate, which is dominant outside Heinrich layers, to detrital carbonate. This is reflected in parameters such as XRF measurements of Ca/Sr, where high Ca/Sr ratios are representative of intervals where detrital carbonate is high and biogenic carbonate is low (Hodell and Curtis, 2008; Channell et al., 2012). Further studies have tried to distinguish between dolomitic carbonate and limestones by using ratios of Mg/Al on dissolved sediment (Thomson et al., 1995) and Mg/Ca on leachates (Francois and Bacon, 1994).

A further method of characterising the detrital carbonate content is by using the stable oxygen and carbon isotopes ($\delta^{18}O$ and $\delta^{13}C$) of the bulk material (Hodell and Curtis, 2008). This has previously been applied to the fine fraction to look at nepheloid layers along the margins of the LIS in (Balsam and Williams, 1993). By using the large difference between the $\delta^{18}O$ of detrital and biogenic carbonate as explained in Section 2.2.2.1, it is possible to identify periods when biogenic inputs are low and detrital inputs of carbonate are high, as is the case during Heinrich events.

4.1.3 Sources of carbonate in the fine fraction

4.1.3.1 Biogenic and lithic contributions

This chapter will use stable isotopes to identify inputs of detrital carbonate material within the fine fraction (<63 μm) of sedimentary material. Whilst $\delta^{13}C$ of bulk carbonate material varies over time, as past $\delta^{13}C$ values have a similar range to more modern values, it is not possible to distinguish between detrital and biogenic input of carbonate using $\delta^{13}C$ (Veizer et al., 1999; Hodell and Curtis, 2008). Therefore, the following description will focus on $\delta^{18}O$ carbonates found in the <63μm fraction of glacial North Atlantic sediments consist of a mixture of autochthonous biogenic carbonate from coccoliths and small/juvenile/fragmented foraminifera, which have relatively heavy $\delta^{18}O$ values and allochthonous detrital carbonate with much lighter $\delta^{18}O$ (Balsam and Williams, 1993; Hodell and Curtis, 2008). Within both the biogenic and detrital carbonates, there is variation. Detrital carbonate may have different $\delta^{18}O$ values due to the geological age or mineralogy, older and dolomitised carbonates have

lower oxygen isotope values than younger non-dolomitic carbonates (Hodell and Curtis, 2008). The map in ***Figure 4.1*** shows the potential continental carbonate sources around the North Atlantic in relation to the IRD belt and the core sites in this study.

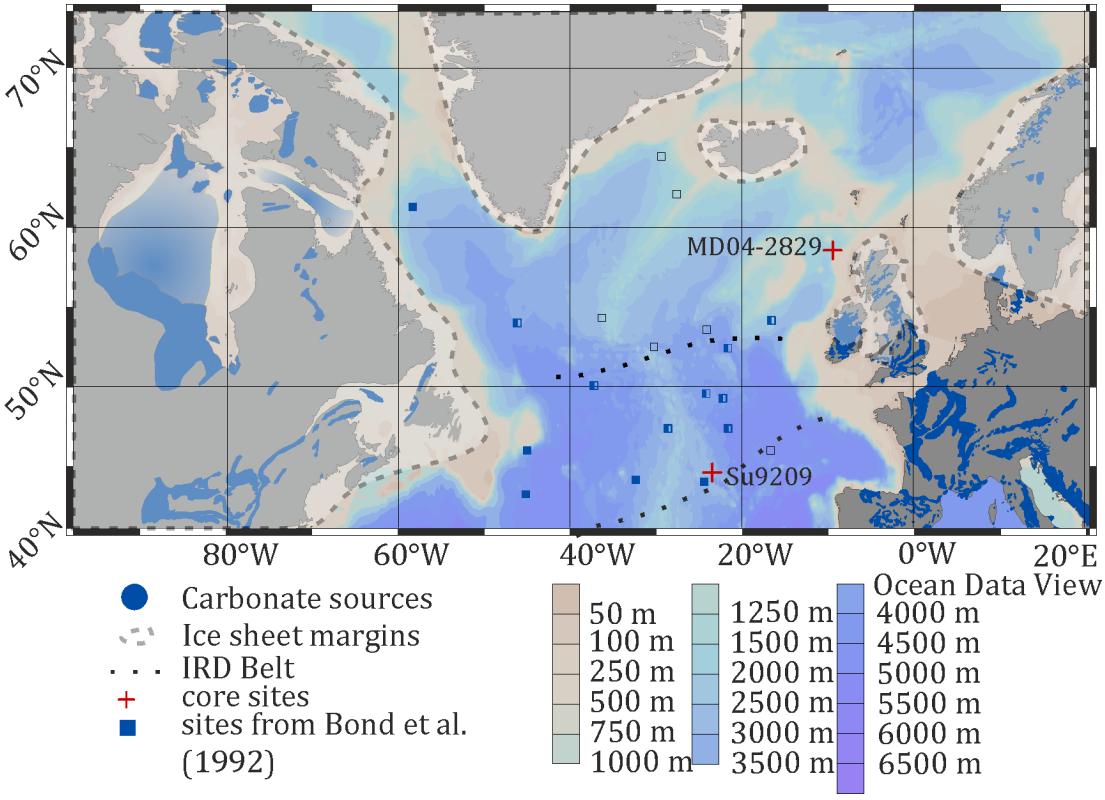

Figure 4.1: Sketch map of the carbonate around the North Atlantic showing sites with carbonate during Heinrich events. Full squares: carbonate is present in all HEs, half squares: carbonate is present in some HEs, open squares: no carbonate is present (Bond et al., 1992). SU92-09, MD04-2829CQ, and the approximate position of the IRD belt (Ruddiman, 1977) are shown for reference. Carbonate provinces around the North Atlantic are reproduced from Williams and Ford (2006).

Previous studies of the $\delta^{18}O$ carbonate measured grains from the >150 µm fraction from Heinrich layers have shown values in the range of -10‰ to -2‰ with a mean of -5.65‰ (Hodell and Curtis, 2008) illustrated in Figure 4.2. Based on the $\delta^{18}O$ curve from Veizer (1999) and values for Archean samples (Veizer et al., 1989, 1999) as shown in Figure 4.2, these low values of $\delta^{18}O$ during Heinrich events would suggest a wide range of geological ages for individual carbonate grains from early Phanerozoic to Archean in age.

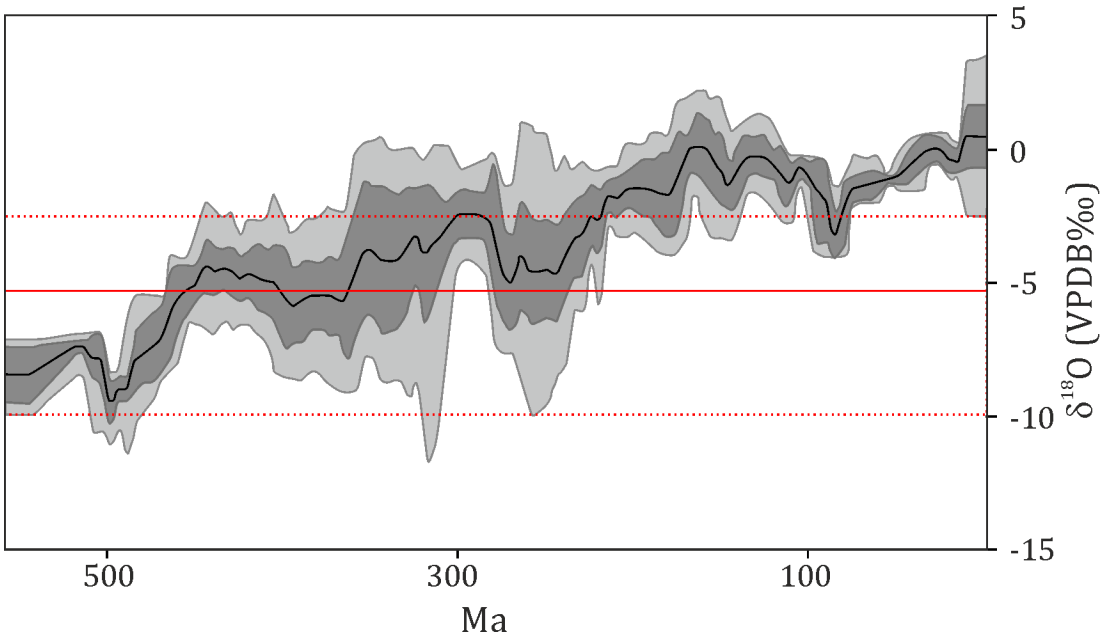

Figure 4.2: The evolution of $\delta^{18}O$ of calcite over time redrawn from Veizer et al, (1999) with permission from Elsevier. The average (solid red line) and range (dotted red line) of $\delta^{18}O$ of individual grains from the >150µm fraction are shown from (Hodell and Curtis, 2008).

The isotopic compositions of biogenic sources of carbonate are dependent on temperature, the $\delta^{18}O$ of the ambient water in which the organism was growing in, and the species that precipitated the calcite. Both foraminifera (e.g., Pearson, 2012) and coccoliths (e.g., Ziveri et al., 2003) have well documented species-specific deviations from the equilibrium fractionation of inorganic calcite. In coccoliths, biological fractionation accounts for differences between $\delta^{18}O$ of coccolith calcite and that of seawater from 2‰ to -2.5‰ depending on the species (Dudley et al., 1986).

4.1.3.2 Constraints on supply of lithic material in the fine fraction

Constraints on the supply of detrital material to the glacial ocean are similar to that of flux of IRD as stated in Peck et al. (2007) and Scourse et al. (2009) these are: the extent of marine ice margins, rate of iceberg calving, surface circulation, iceberg debris content rate of iceberg melt, and sea level (Auffret et al., 2002). Additionally, for detrital carbonates there is an obvious dependence on the presence of carbonate rocks for entrainment by the ice sheet in the source regions. For fine fraction material, other transport mechanisms including redistribution via near bottom currents or aeolian inputs may play an important role (McCave et al., 1995). Finally, at the continental margins and in a drift site, such as the Rosemary Bank site, it is likely that there is some inclusion of carbonates from reworking of sediments and inputs from

slope failures/runoff. Potential changes in any of these parameters could affect the supply of the lithic component of carbonates to the core site and hence the $\delta^{18}O$ of the fine fraction sediment.

This chapter aims to trace detrital carbonate inputs to the fine fraction using the $\delta^{18}O$ of the <63µm fraction ($\delta^{18}O_{FINE}$) in two sites from the North Atlantic and to relate this to ocean conditions during the inputs of detrital carbonate. Outside the IRD belt where Heinrich layer markers are not evident in coarse-grained lithic proxies, using $\delta^{18}O$ of the fine fraction may help identify Heinrich events (Hodell et al., 2010). Using studies of the fine fraction in conjunction with coarse fraction data is expected to reveal more about the nature of delivery of material during the last glacial. In particular during abrupt climate change events and to identify differences between H2 and H4. The approach taken was to compare cores from the European margin and the IRD belt, which are very different depositional environments. A pilot study was undertaken using samples from core MD04-2829CQ to assess the differences between bulk $\delta^{18}O$ and $\delta^{18}O_{FINE}$.

This study will use two sites, MD04-2829CQ from the Rosemary Bank, and SU92-09 from the IRD belt see ***Figure 4.1***. In the IRD belt site SU92-09, it should be possible to observe changes in the $\delta^{18}O$ of the fine fraction that can be directly related to Heinrich events. Comparisons with the north eastern margin of the Atlantic will help characterise the timing of the inputs freshwater forcing and by looking at the fine fraction, it may be possible to identify differences in the phasing of detrital carbonate input related to fresh water plumes from melting icebergs relative to those identified from the coarse fraction material. Such information may provide new insights into the evolution of Heinrich events and the role of smaller, fast reacting ice sheets, such as the British and Irish ice sheet (BIIS), in the millennial scale climate variability of the North Atlantic during the last glacial. In core MD04-2829CQ from the Rosemary Bank, inputs of detrital cream coloured carbonate have been identified during Heinrich intervals, and by looking at changes in the $\delta^{18}O$ of fine fraction material, it may be possible to identify a longer interval of carbonate inputs to the site, with implications for 'precursor' events and the role of the BIIS.

4.2 Pilot study

The pilot study was undertaken to establish the use of $\delta^{18}O_{FINE}$ variations as a proxy for changes in the source and contribution of detrital versus biogenic carbonate at an ice proximal site in the same way as $\delta^{18}O$ has been used on bulk material to trace detrital carbonate inputs in the IRD belt (Hodell and Curtis, 2008) and in distal sites (Hodell et al., 2010).

4.2.1 Pilot sampling strategy

Existing proxy data from core MD04-2829CQ (Hall et al., 2011) including petrological identification of coarse fraction IRD and ANN faunal transfer function SST estimates shown in ***Figure 4.4*** were used to assess which depths should be included in the pilot study. To assess the variation in the proxy over Heinrich events the interval selected needed to encompass a clearly identifiable increase in detrital 'cream coloured carbonate' and also to include a period where IRD input from the BIIS was low (<1000 grains) in order to encompass the full range of variability in the core.

The period spanning H2 was chosen for the pilot study as it meets both of these criteria. Coarse fraction lithic counts show an increase in IRD from the BIIS between 700 and 622 cm depth peaking at 7195 grains cm^{-2} ka^{-1} and an input from the LIS from 690 to 634 cm depth, peaking at 789 grains cm^{-2} ka^{-1}, corresponding to H2. Summer SST estimates are also reduced during this period by approximately 6°C from a maximum of 9ºC to a minimum 3ºC. A period of lowered IRD input is evident between 750 and 700 cm depth and between 600 and 620 cm depth. Of the other potential Heinrich events, H1 was excluded as supporting IRD and SST data are not available for this period from core MD04-2829CQ, and H3 was excluded because it has no identifiable peak in coarse fraction LIS and BIIS sourced IRD at site MD042829CQ. H4 was a potential candidate as it has a peak in LIS sourced IRD of 806 grains cm^{-2} ka^{-1}. However, there is only a small increase in IRD from the BIIS to a peak of 2431 grains cm^{-2} ka^{-1}, and the reduction in estimated SST is less than during H2 approximately 4°C. Hence, it was decided that H2 was a better candidate for the pilot study as the potential change in $\delta^{18}O_{FINE}$ was likely to be larger. The initial study consisted of 150 samples of fine fraction and 150 samples of bulk material that

encompassed H2 at 1 cm intervals from 600-750 cm depth; these were processed as described in Section 2.2.2.2.

4.2.1.1 Pilot Results

Fine fraction samples typically have lower $\delta^{18}O$ values and similar $\delta^{13}C$ values to the bulk material samples as shown in Figure 4.3. The samples of fine fraction material exhibit broadly the same trend as the bulk material as shown in ***Figure 4.4***. The spread of the data points is greater for $\delta^{18}O_{BULK}$ than for $\delta^{18}O_{FINE}$ possibly reflecting the bias introduced by large grains within a sample, although these were ground down and homogenised. Before H2 (prior to the appearance of LIS sourced material) values of $\delta^{18}O_{BULK}$ are between -2.5 ‰ and -1.5 ‰ and values of $\delta^{18}O_{FINE}$ are also higher at -2.5‰.

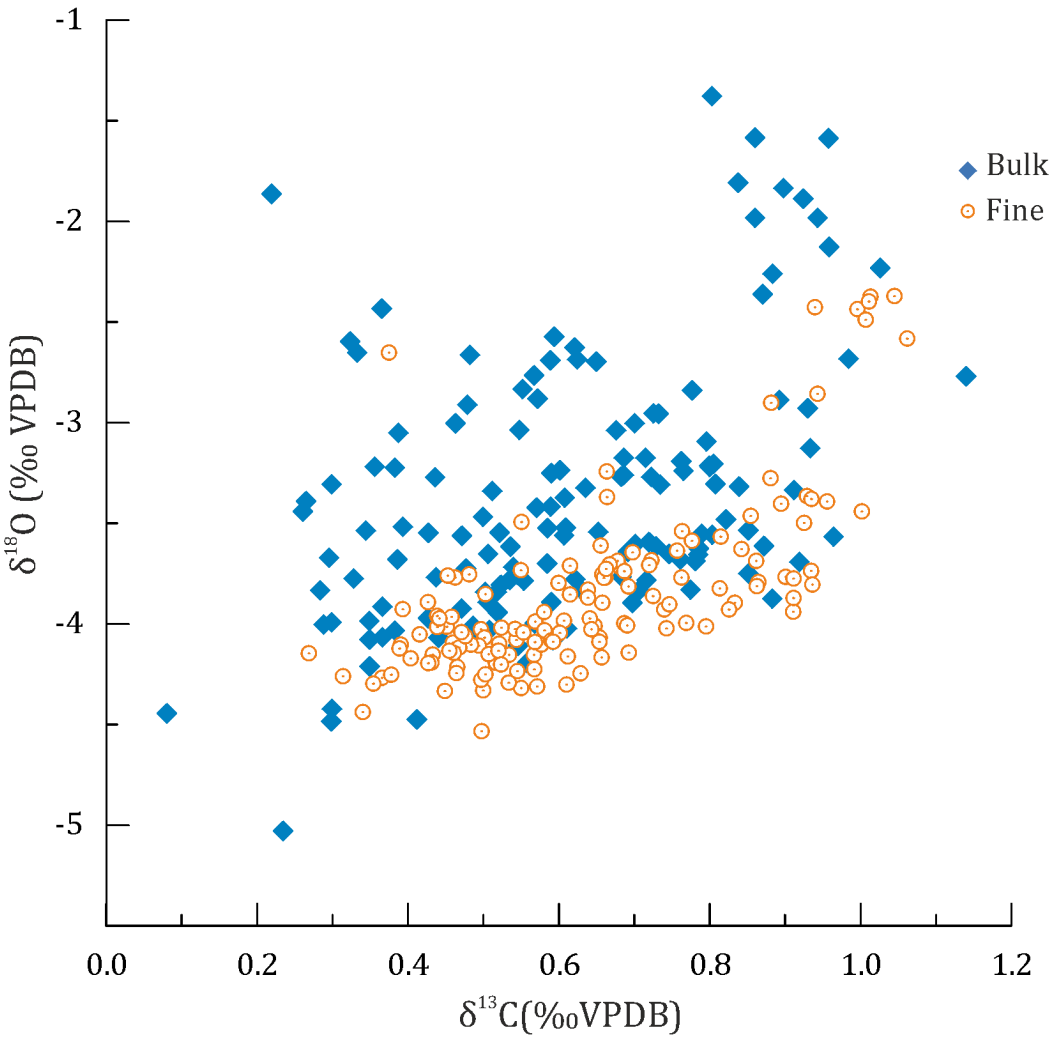

Figure 4.3: Bulk and fine fraction $\delta^{18}O$ plotted against $\delta^{13}C$.

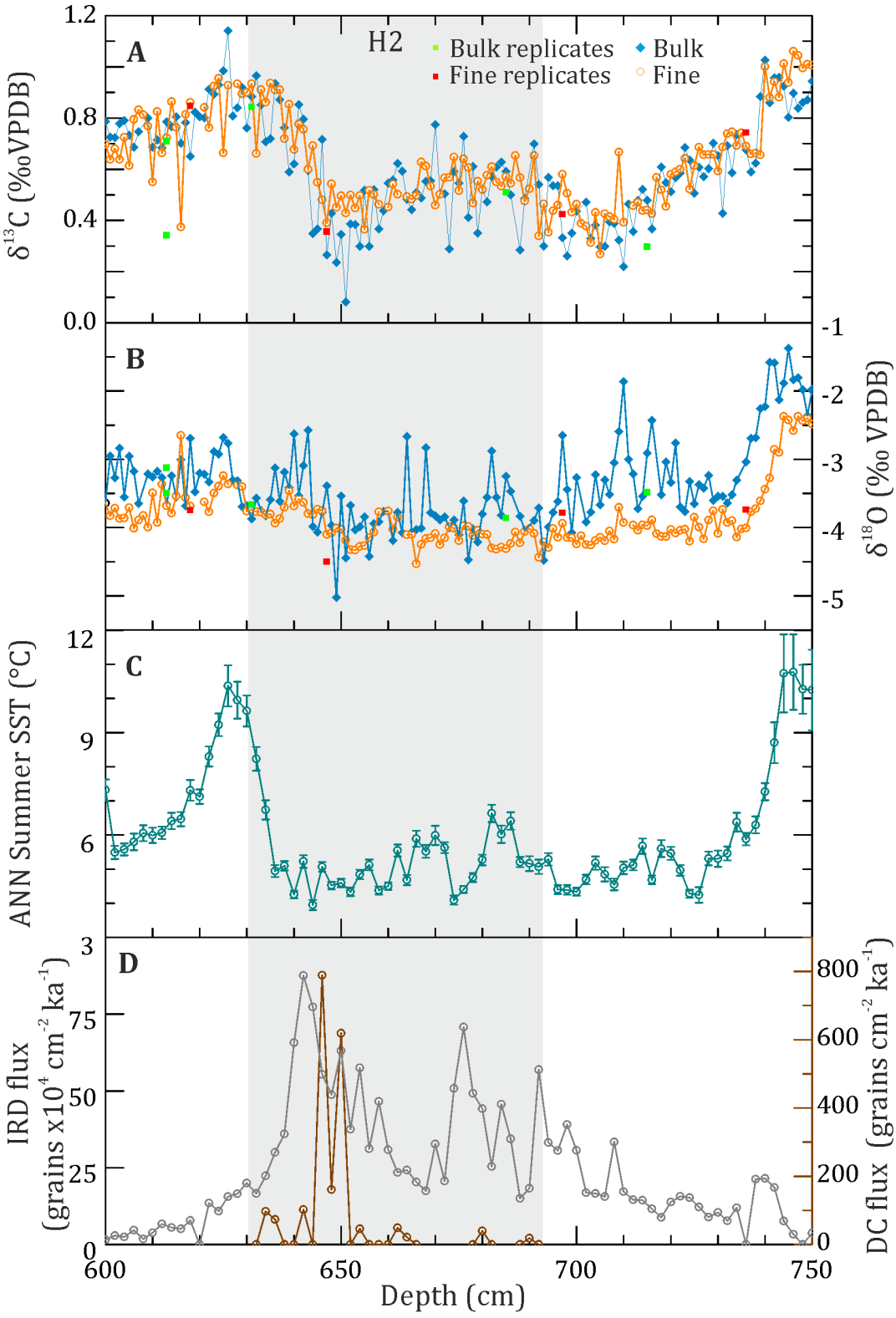

Figure 4.4: Bulk and fine stable isotopes plotted against depth. A; $\delta^{13}C$ from pilot samples of bulk and fine fraction material plotted against depth, B; $\delta^{18}O$ from pilot samples of bulk and fine fraction material C; ANN SST estimates (Hall et al, 2011), D; IRD fluxes, total IRD in grey and detrital carbonate IRD in brown (Hall et al, 2011).

4.2.1.2 Pilot Conclusions

During H2, the $\delta^{18}O_{BULK}$ values become lighter -3.6 ‰ to -5 ‰ this is also the case for $\delta^{18}O_{FINE}$. The initial decrease in $\delta^{18}O_{FINE}$ occurs 3 cm before the change in the $\delta^{18}O_{BULK}$. There is a small change in both $\delta^{18}O_{BULK}$ and $\delta^{18}O_{FINE}$ values after H2 at 630 cm but both are lower than before H2. As $\delta^{18}O_{FINE}$ decreases at the same time as IRD increases this would suggest that the $\delta^{18}O_{FINE}$ signal is linked to the IRD inputs. There is a correspondence between the $\delta^{18}O_{FINE}$ and $\delta^{18}O_{BULK}$, the fine fraction material seems to respond earlier to changing conditions at the start of the Heinrich event as shown in ***Figure 4.4***. There is no correspondence between the input of DC IRD and the $\delta^{18}O$ curve, however the total IRD counts includes limestone and chalk fragments, so a small increase in the amount of carbonate when the detrital carbonate inputs are identified would not necessarily have a large effect on the $\delta^{18}O_{FINE}$. The pilot has shown that fine fraction and bulk $\delta^{18}O$ are similar, and that fine fraction $\delta^{18}O$ can also be used to demonstrate changing proportions of the biogenic and lithic components of carbonates in the fine fraction. Based on this, it was decided to extend the fine fraction study to the whole of core MD04-2829CQ and SU92-09.

4.3 Results

4.3.1 Defining carbonate input using stable isotopes

4.3.1.1 IRD belt site SU92-09

The histogram in ***Figure 4.5*** shows that the population of oxygen isotope data of the fine fraction is bi-modal, the first population has a mean of -4.5 ‰ and corresponds to those samples from H1, H2, and H4 highlighted in the black circle.

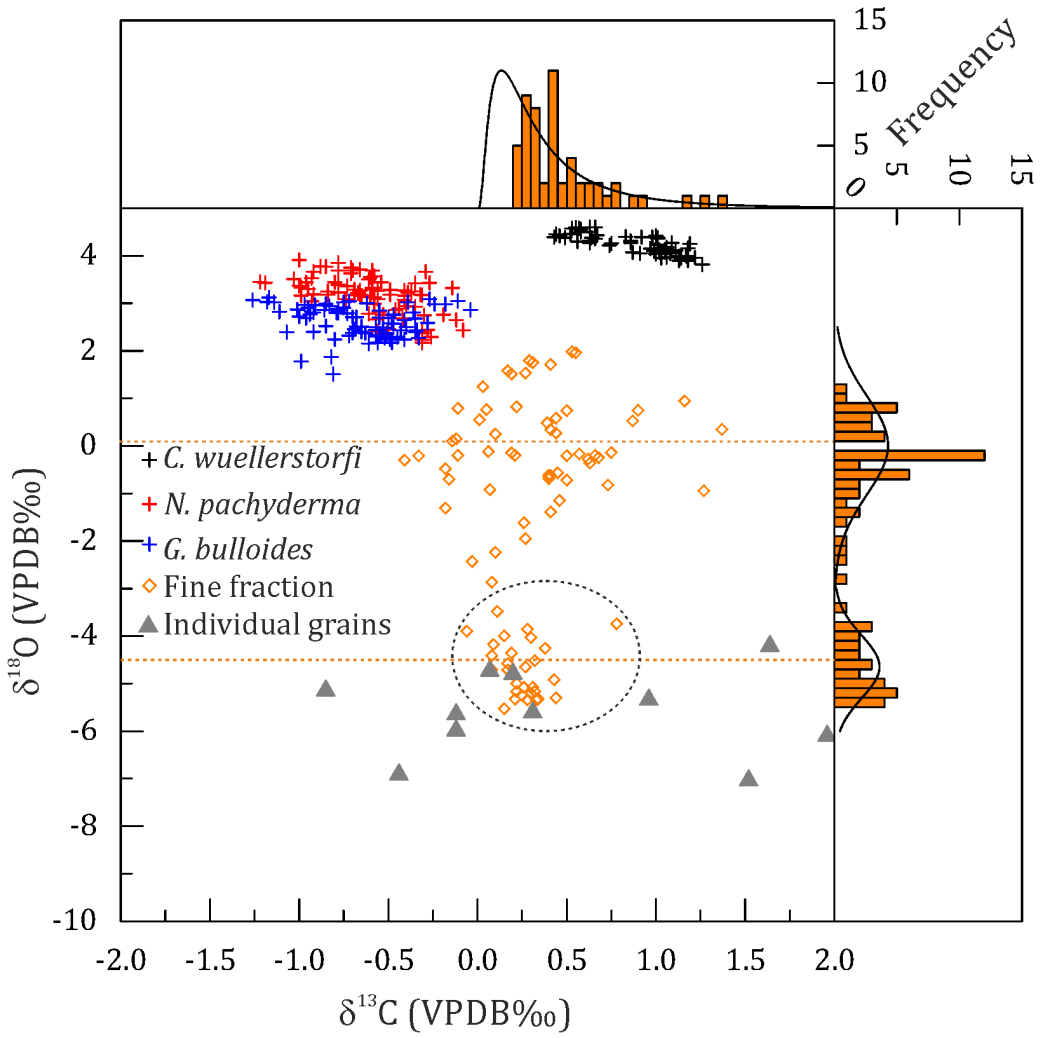

Figure 4.5: Cross plot of $\delta^{13}C$ vs $\delta^{18}O$ ratios from different substrates in core SU92-09 and histograms of the $\delta^{18}O_{FINE}$ (right) and $\delta^{13}C_{FINE}$ (top). Substrates are plotted as follows; N pachyderma in red crosses, G. bulloides in blue crosses, C. wuellerstorfi in black crosses, 63µm fraction in orange diamonds and detrital grains in grey triangles. See text for explanation.

The second population has a mean $\delta^{18}O_{FINE}$ of 0.1‰ and corresponds to the samples from the ambient glacial sediment. When $\delta^{18}O_{FINE}$ and $\delta^{13}C_{FINE}$ is plotted

alongside the $\delta^{18}O$ of foraminifera and the $\delta^{18}O$ of detrital grains picked from core SU92-09, (***Figure 4.5***), it is apparent that $\delta^{18}O$ values of the Heinrich event population are closer to and overlap those of the detrital grains. The ambient glacial $\delta^{18}O_{FINE}$ population is closer to the $\delta^{18}O$ of foraminifera. There is an average difference of ~5.75‰ between detrital and foraminiferal calcite $\delta^{18}O$ measured in this study. $\delta^{13}C_{FINE}$ has a skewed distribution and the $\delta^{13}C$ of detrital grains and foraminifera have a wider range than that of $\delta^{13}C_{FINE}$.

4.3.1.2 Eastern Atlantic margin MD04-2829CQ

Figure 4.6 shows that at site MD04-2829CQ the $\delta^{18}O_{FINE}$ ratio is very low with 70% of the data falling below -3.2 ‰. These low $\delta^{18}O_{FINE}$ ratios circled in black

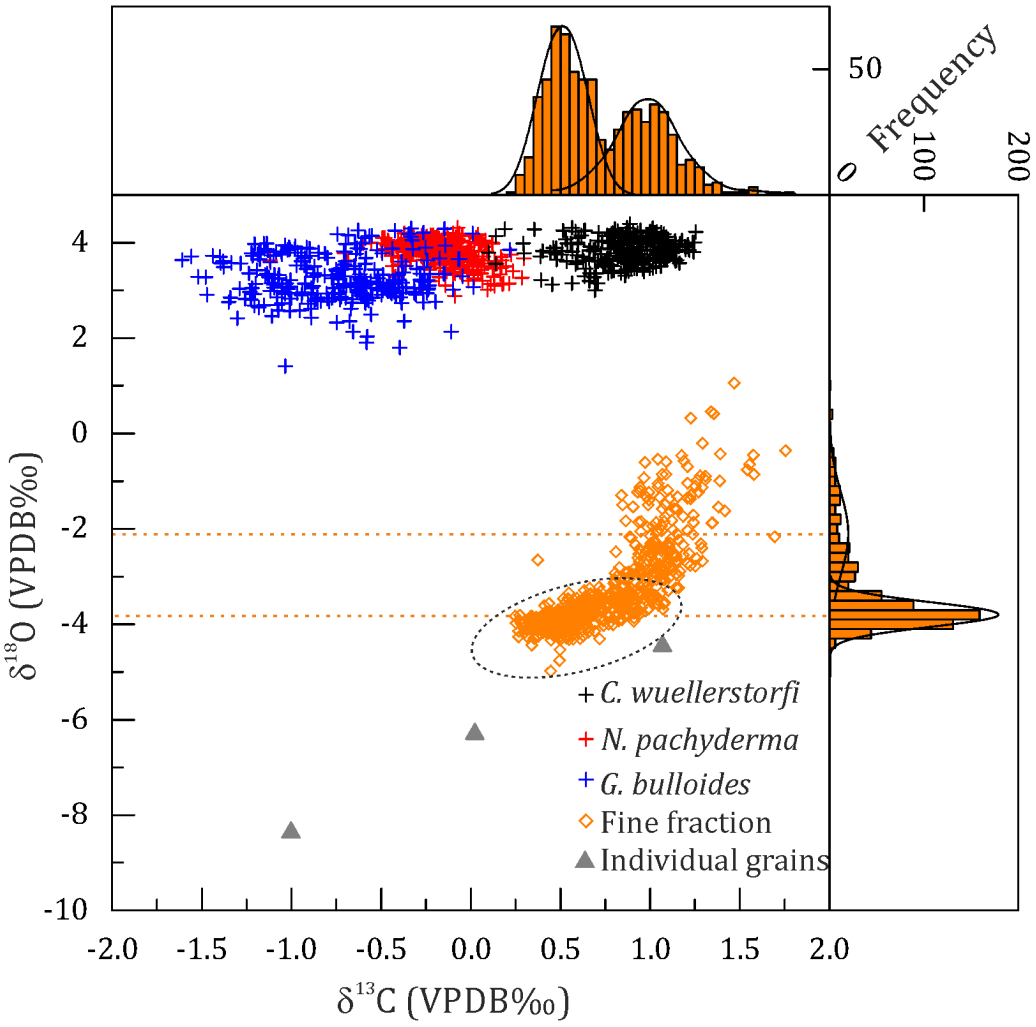

Figure 4.6: Cross plot of $\delta^{13}C$ vs $\delta^{18}O$ ratios from different substrates in core MD04-2829CQ and histograms of the $\delta^{18}O_{FINE}$ (right) and $\delta^{13}C_{FINE}$ (top). Substrates are plotted as follows; N. pachyderma in red crosses, G. bulloides in blue crosses, C. wuellerstorfi in black crosses, 63µm fraction in orange diamonds and detrital grains in grey triangles. See text for explanation.

correspond with samples from H2, H4 and stadial intervals and have a mean of -3.8‰. When plotted alongside other carbonate substrates in the cross plot in ***Figure 4.6*** this low $\delta^{18}O_{FINE}$ group are closer samples of detrital carbonate taken from this core. A smaller number of samples have $\delta^{18}O_{FINE}$ above -3.2 ‰ and these correspond with samples from pre H4 and samples from interstadial intervals, these have a mean of -2.1 ‰ and are closer to the $\delta^{18}O$ of foraminifera from the same core. There are also two populations of $\delta^{13}C$, which are shown in the histogram in the top panel that correspond to the same populations as are seen in the $\delta^{18}O_{FINE}$.

4.3.2 Changes in fine fraction stable isotopes over the last glacial

In ***Figure 4.7*** and ***Figure 4.8***, Heinrich events have been highlighted in grey based on the ages provided by Hemming (2004) as the centre point for H2, H3 and H4. However, at site SU92-09 H4 occurs earlier and is centred on 39 ka BP, H1 is also earlier at SU92-09 and is centred at 17 ka BP. Ratios of $\delta^{18}O_{FINE}$ from site SU92-09 range from 2 ‰ to -5.5‰, and the $\delta^{13}C_{FINE}$ ratios vary from -0.25 ‰ to 1.5 ‰. The ratio of $\delta^{18}O_{FINE}$ is lowered during H1, H2, and H4 to less than -2.5 ‰ and an average of between -4.45‰ and -4.83‰ see ***Figure 4.7***. The $\delta^{18}O_{FINE}$ excursion lasts for a longer period over H4 than over H2. At 31 ka BP thought to correspond with H3, $\delta^{18}O_{FINE}$ is reduced to -1.39 ‰. The reduction in $\delta^{18}O_{FINE}$ over each Heinrich event (except H3) corresponds with peaks in greyscale and reductions in the $\delta^{18}O$ of the planktonic foraminifera *N. pachyderma* of between 0.8 and 1.4‰.

At site MD04-2829CQ, an overall trend of decreasing $\delta^{18}O_{FINE}$ and $\delta^{13}C_{FINE}$ from 41.5 to 18.4.ka BP is evident from ***Figure 4.8***, and $\delta^{13}C_{FINE}$ ranges from in excess of 1 ‰ at 34-41 ka BP to values less than 0.65 ‰ from 27 ka BP to 18 ka BP. During H2, H3, and H4 the $\delta^{18}O_{FINE}$ is below -2.5 and averages -3.5‰. The lowest values in the core are reached during H4 of -4.98‰. During the non-Heinrich event intervals however there are also periods of low $\delta^{18}O_{FINE}$, these correlate to increased IRD input and low SST and occur during stadial periods. The $\delta^{18}O_{FINE}$ ratios in the ambient glacial range from in excess of -1 ‰ between 34 and 41 ka BP to less than -3 ‰ from 26 ka BP to 18 ka BP.

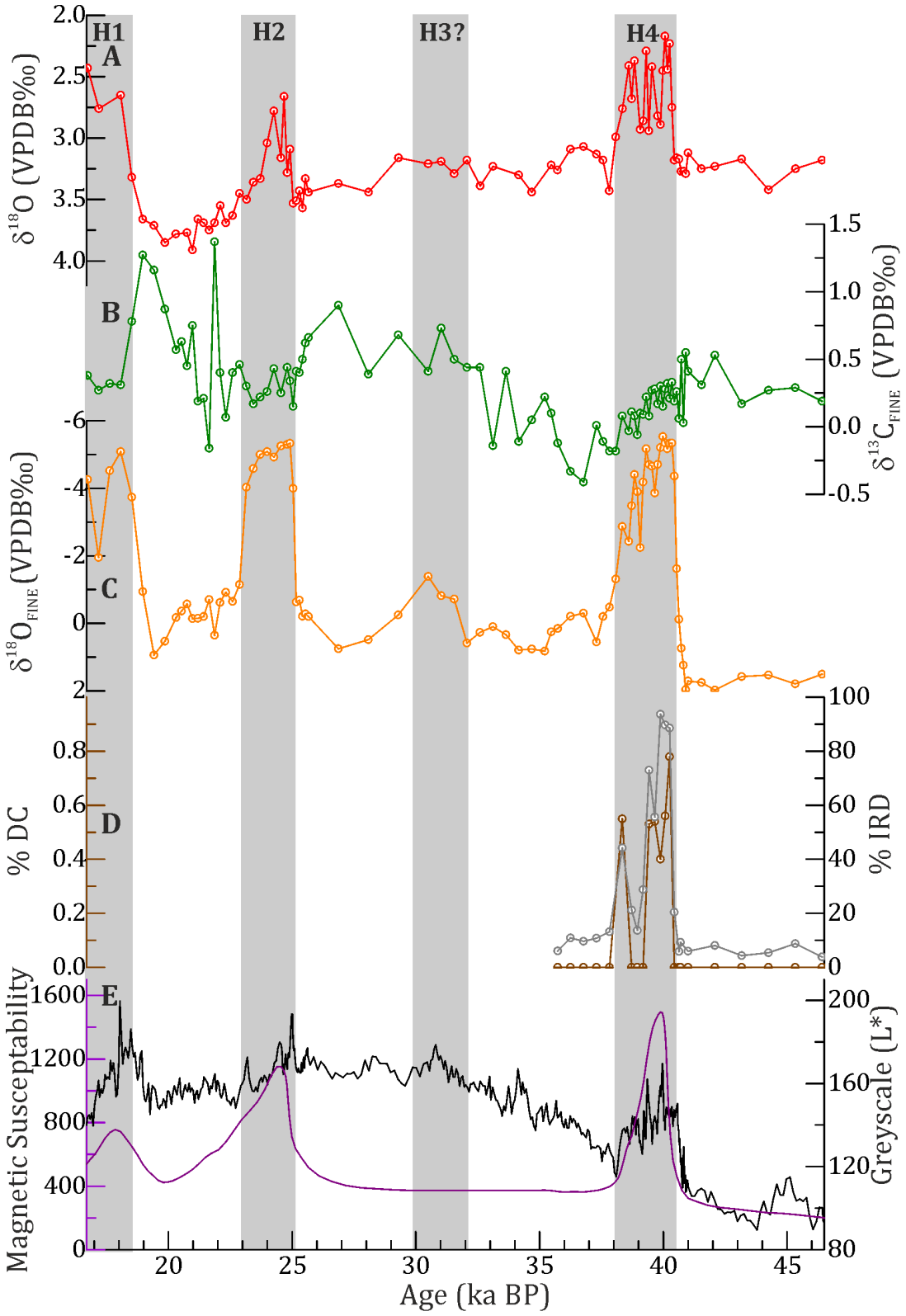

Figure 4.7: $\delta^{18}O_{FINE}$ ratios from core SU92-09 vs age. A; $\delta^{18}O$ <u>N. pachyderma</u> in red, B; $\delta^{13}C_{FINE}$ in green, C; $\delta^{18}O_{FINE}$ in orange, D counts of IRD (grey) and detrital carbonate (brown) as a percentage of the total >150µm fraction, and E; magnetic susceptibility (purple) and greyscale (black), magnetic susceptibility, IRD percentages and greyscale are courtesy of pers. Comms. Elsa Cortijo. Heinrich events are marked in grey.

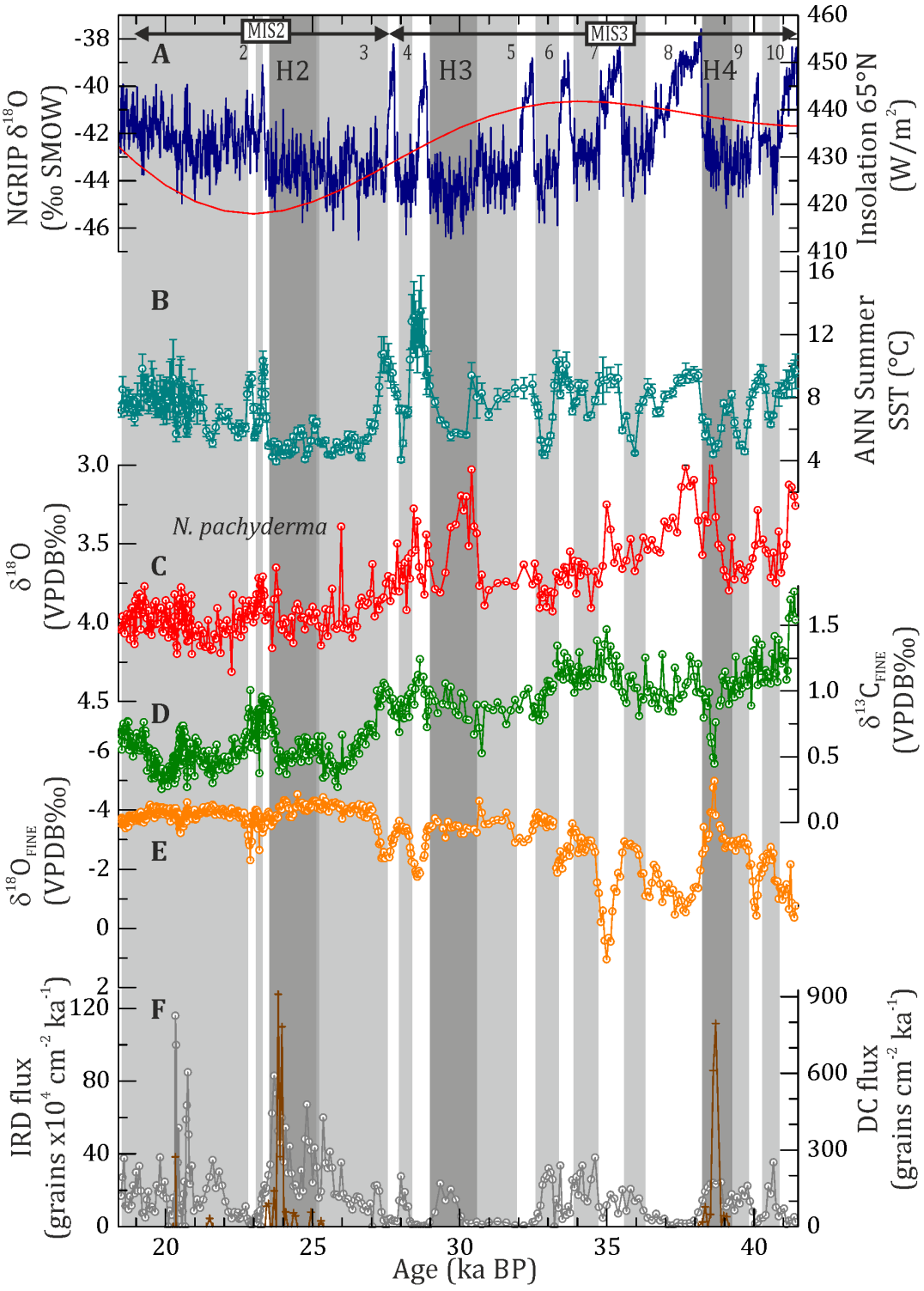

Figure 4.8: $\delta^{18}O_{FINE}$ and $\delta^{13}C_{FINE}$ ratios from core MD04-2829CQ vs age with comparative data from Hall et al. (2011). A; $\delta^{18}O$ NGRIP (Andersen et al., 2006; Svensson et al., 2006) blue, July insolation at 65°N (Berger and Loutre, 1991) red, B; Mean annual SST faunal estimates using ANN (Hall et al., 2011), C; $\delta^{18}O$ of N. pachyderma tests from Hall et al. (2011), D: $\delta^{13}C_{FINE}$, E: $\delta^{18}O_{FINE}$ F: total IRD flux from the >150µm fraction in grey and flux of DC in brown. Stadials are marked in light grey and Heinrich events are marked in dark grey.

4.4 Discussion

4.4.1 Detrital carbonate inputs and $\delta^{18}O_{FINE}$

Measurements of $\delta^{18}O_{FINE}$ at site SU92-09 from the IRD belt, demonstrate that fine fraction carbonates comprise of two distinct populations as shown in the histogram (Figure 4.8). The first of these populations is dominated by heavy $\delta^{18}O$ values with a mean of 0.1 ‰ and is closer to that of foraminifera derived $\delta^{18}O$ values from the same core, hence this is interpreted as the biogenic dominated component of the $\delta^{18}O_{FINE}$ signal. This population of biogenic dominated $\delta^{18}O_{FINE}$ is a feature of ambient glacial sediments in this core. The second population of $\delta^{18}O_{FINE}$ is much lighter with a mean value of -4.5 ‰, this population overlaps with the $\delta^{18}O$ of individual detrital carbonate grains taken from the >150 µm fraction during the Heinrich events intervals. Therefore, it can be said that a significant proportion of the carbonate that makes up $\delta^{18}O_{FINE}$ signal of this population is of lithic origin. The changes in $\delta^{18}O$ of *N. pachyderma* over each Heinrich event are ~1 ‰ and therefore changes in biogenic calcite $\delta^{18}O$ cannot account for the > 6 ‰ shift observed during the Heinrich events. Further support for the lithic origin of the low $\delta^{18}O_{FINE}$ can be found by comparing the $\delta^{18}O_{FINE}$ of core SU92-09 with the coarse fraction lithic counts of detrital carbonate available for H4. The increased percentage of carbonate grains and IRD over H4 corresponds with lighter $\delta^{18}O_{FINE}$ ratios as shown in Figure 4.7. This detrital population of $\delta^{18}O_{FINE}$ is found exclusively during the time intervals of Hudson Strait Heinrich events (H1, H2, and H4). These findings are supported by the earlier work of Hodell and Curtis (2008) who demonstrated that lighter $\delta^{18}O$ of bulk material is linked to changing proportions of detrital to biogenic material over Heinrich events.

At Rosemary Bank, site MD04-2829CQ the range in $\delta^{18}O_{FINE}$ is between -4.98‰ and 1‰, which is smaller than that range at site SU92-09. The $\delta^{18}O$ values, measured as a part of this study, on grains of cream-coloured detrital carbonate are between -4‰ and -8‰ as shown in Figure 4.6. The lighter $\delta^{18}O_{FINE}$, which occurs during stadials and Heinrich events, is more similar to the detrital grains, than the heavier $\delta^{18}O_{FINE}$, which occurs during the interstadials and is closer to the biogenic inputs. Hall et al. (2011), infer the lithic contributions to the MD04-2829CQ site. These include limestone from the Carboniferous formations in Ireland and chalk from the Irish Ice Stream, which are present for much of the last glacial, see the IRD flux in ***Figure 4.8***

and 'cream coloured' carbonates thought to be from the LIS, which only occur during H2 and H4***Figure 4.8***. The low $\delta^{18}O_{FINE}$ during stadials shows the dominance of inputs of detrital carbonate to the fine fraction throughout the last glacial and not just during Heinrich event intervals. As site MD04-2829CQ is situated on the Rosemary Bank it is possible that the fine fraction sediments have undergone some level of reworking, however, the correspondence between previously published IRD fluxes from Hall et al. (2011), would indicate that the dominant component of the fines is related to IRD, rather than sediment sorting associated with post-depositional transport. There are several documented mass movements at the British and Irish shelf that are thought to have occurred during the last glacial (Knutz et al., 2002; Evans et al., 2005; Sacchetti et al., 2007) which may have intermittently re-suspended large volumes of sediment, these cannot be timed precisely but deposition is thought to be local in extent. Whilst inputs such as these cannot be ruled out completely it is likely that over the course of the last glacial inputs from the BIIS dominated the detrital inputs to the fine fraction at this site.

Foraminifera make up the largest proportion of biogenic material in the <63µm fraction. In Figure 4.9, the changes in $\delta^{18}O$ of different substrates ($\delta^{18}O_{FINE}$, $\delta^{18}O$ of foraminifera and derived $\delta^{18}O$ of seawater ($\delta^{18}O_{SW}$) (see Appendix 5 for calculations) are shown over time. Taken together these records demonstrate that, as is the case at site SU92-09, the changes in $\delta^{18}O_{FINE}$ record cannot be accounted for solely by changes in the $\delta^{18}O$ of biogenic calcite at site MD04-2829CQ. Firstly, all of the foraminifera $\delta^{18}O$ values are above 1.7‰. Secondly, the magnitude of the changes in the oxygen isotope curves of individual foraminifera species is small (<1.43 ‰ for *N. pachyderma* and *C. wuellerstorfi* and <2.9 ‰ for *G. bulloides)* relative to the changes in the $\delta^{18}O_{FINE}$ (5.98‰). Finally, the small shifts in $\delta^{18}O$ of the foraminifera are often in opposing directions to that of $\delta^{18}O_{FINE}$. Taken together this means that changing $\delta^{18}O$ signature, and the composition of foraminifera cannot be responsible for the shifts seen $\delta^{18}O_{FINE}$ throughout the last glacial at site MD04-2829CQ. The derived $\delta^{18}O_{SW}$ values also do not co-vary with $\delta^{18}O_{FINE}$ and only have small excursions of ~1.5 ‰ therefore changes in the values of $\delta^{18}O_{SW}$ of the water that biogenic calcite precipitated in are not likely to be responsible for the large shifts in $\delta^{18}O_{FINE}$ observed at site MD042829CQ.

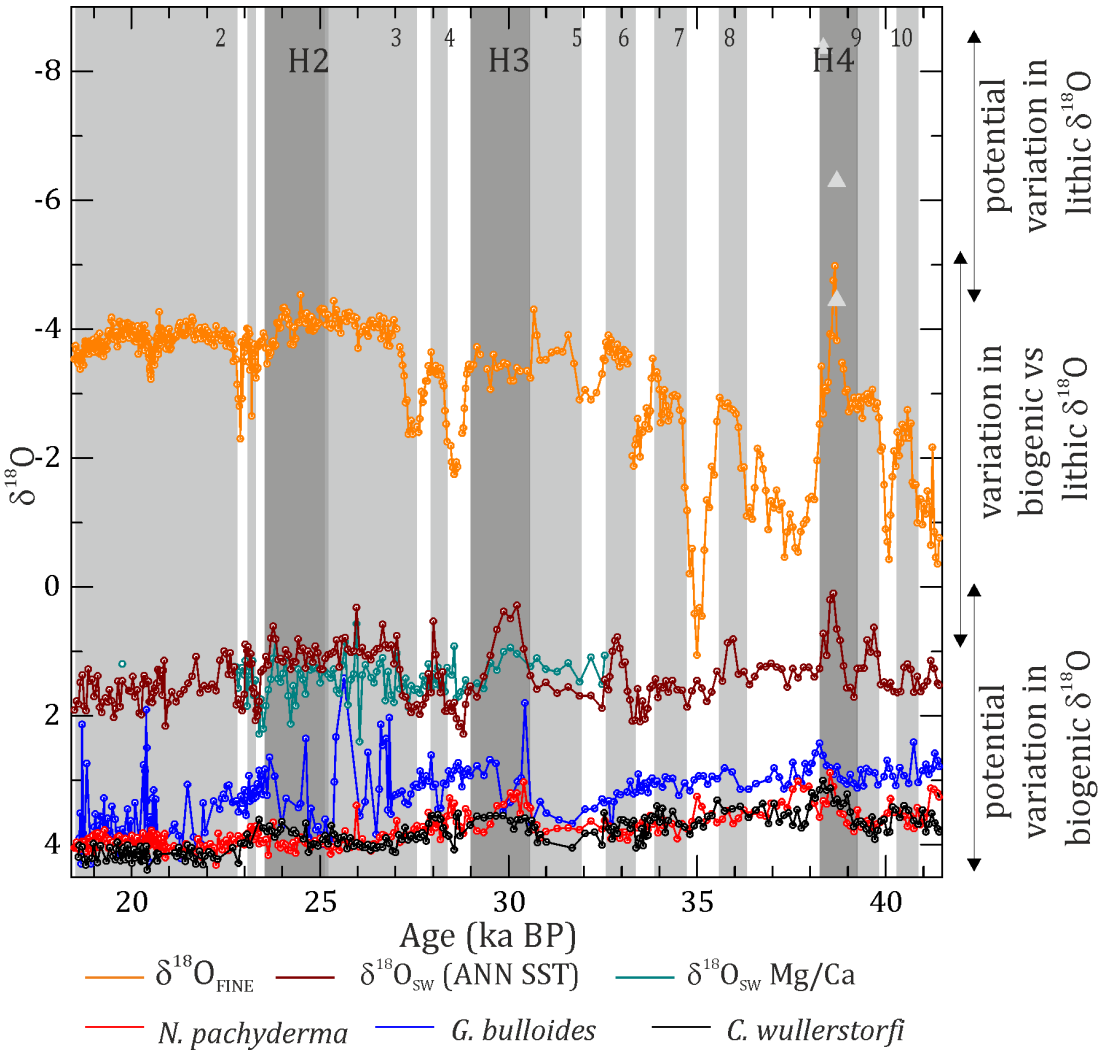

Figure 4.9: $\delta^{18}O$ values of different substrates and estimated $\delta^{18}O_{SW}$ for site MD042829CQ. $\delta^{18}O_{SW}$ calculations were derived as shown in Appendix 5 using MAT SST estimates and N. pachyderma $\delta^{18}O$ and the equation from Kim and O'Neil (1997)

4.4.2 Glacial changes and the impact on $\delta^{18}O_{FINE}$ at contrasting sites

The two sites in this study extend over the periods marine isotope stage (MIS) 3 (57 to 29 ka BP) and MIS 2 (29 to 14 ka BP) (Lisiecki and Raymo, 2005), which are very different in terms of their climate. The portion of MIS 3 that is represented by the cores in this study, 46 to 29 ka BP, is a period of reducing summer insolation at 65 °N; see ***Figure 4.8***, and Northern Hemisphere ice sheet growth and lowering sea level (Siddall et al., 2008). The onset of MIS 2 at 29 ka BP is closely followed by the glacial maximum extent for the northern BIIS at 27 ka BP (Clark et al., 2012), During MIS 2 global ice volume reaches its maximum and sea levels are at their lowest (Clark and Mix, 2000) and July insolation at 65°N is low. In core MD04-2829CQ, this is reflected

in the $\delta^{18}O_{FINE}$ of the sediments; over the course of MIS 3 the $\delta^{18}O_{FINE}$ lowers from -1 ‰ to -3 ‰ indicating increasing supply of detrital material to the core, as the marine margin of the BIIS develops, releasing sediment laden icebergs and meltwater to the site. A possible candidate for this material is the Dalradian limestones which outcrop in Scotland and Northern Ireland these have $\delta^{18}O$ values ranging from -17 to -5.6 ‰ (Thomas et al., 2004) making them indistinguishable from the $\delta^{18}O$ of Hudson Strait detrital carbonate in the IRD belt (Hodell and Curtis, 2008). It is not possible to know if the material found in sediment cores released by ice sheets is due to advance, retreat or changes in the calving regime or ice streaming (Scourse et al., 2009), however the delivery of detrital material to a site indicates the presence of a marine margin of the ice sheet. The continued lowering of $\delta^{18}O_{FINE}$ indicating increased detrital delivery during MIS 3 indicates growth of the marine margin of the BIIS. By 27 ka BP the $\delta^{18}O_{FINE}$ is consistently low and this coincides with the LGM of the BIIS (Clark et al., 2012). Illustrating a continuous supply of fine fraction carbonate to the site at the LGM. This is mirrored by data from bulk $\delta^{18}O$ from the Orphan Knoll near to the Laurentide ice sheet, which shows that after 28 ka BP there is consistently low $\delta^{18}O$ of bulk carbonate below -2.5 ‰ (Figure 4.10) (Channell et al., 2012). This would suggest that near the margins of the ice sheets $\delta^{18}O$ of fine and bulk sediments can indicate inputs from the local ice sheet.

The association seen at site MD04-2829CQ with increasing ice volume over the last glacial and decreasing $\delta^{18}O_{FINE,}$ is not evident at site SU92-09. Prior to H4 in core SU92-09 values of $\delta^{18}O_{FINE}$ are ~1.8 ‰, which is very high and indicates little to no input of detrital material. From 38 ka BP to 19 ka BP the $\delta^{18}O_{FINE}$ of the non Heinrich event intervals the $\delta^{18}O_{FINE}$ average is lower at 0 ‰. This difference in the $\delta^{18}O_{FINE}$ of the ambient glacial could be due to increased lithic carbonate reaching the site as ice volume increases which is supported by an increase in greyscale values over this period. However, due to site SU92-09 ice distal setting and low sedimentation rates during the background glacial there are not large changes in the supply of fine fraction carbonate associated with increasing ice volume over the last glacial a similar pattern is seen in core U3108 from the IRD belt also (see Figure 4.10).

4.4.3 Heinrich event 4

Heinrich event 4 occurs during MIS 3 when global ice volume is still relatively low, and the BIIS is thought to be small and largely limited to Scotland, evidenced

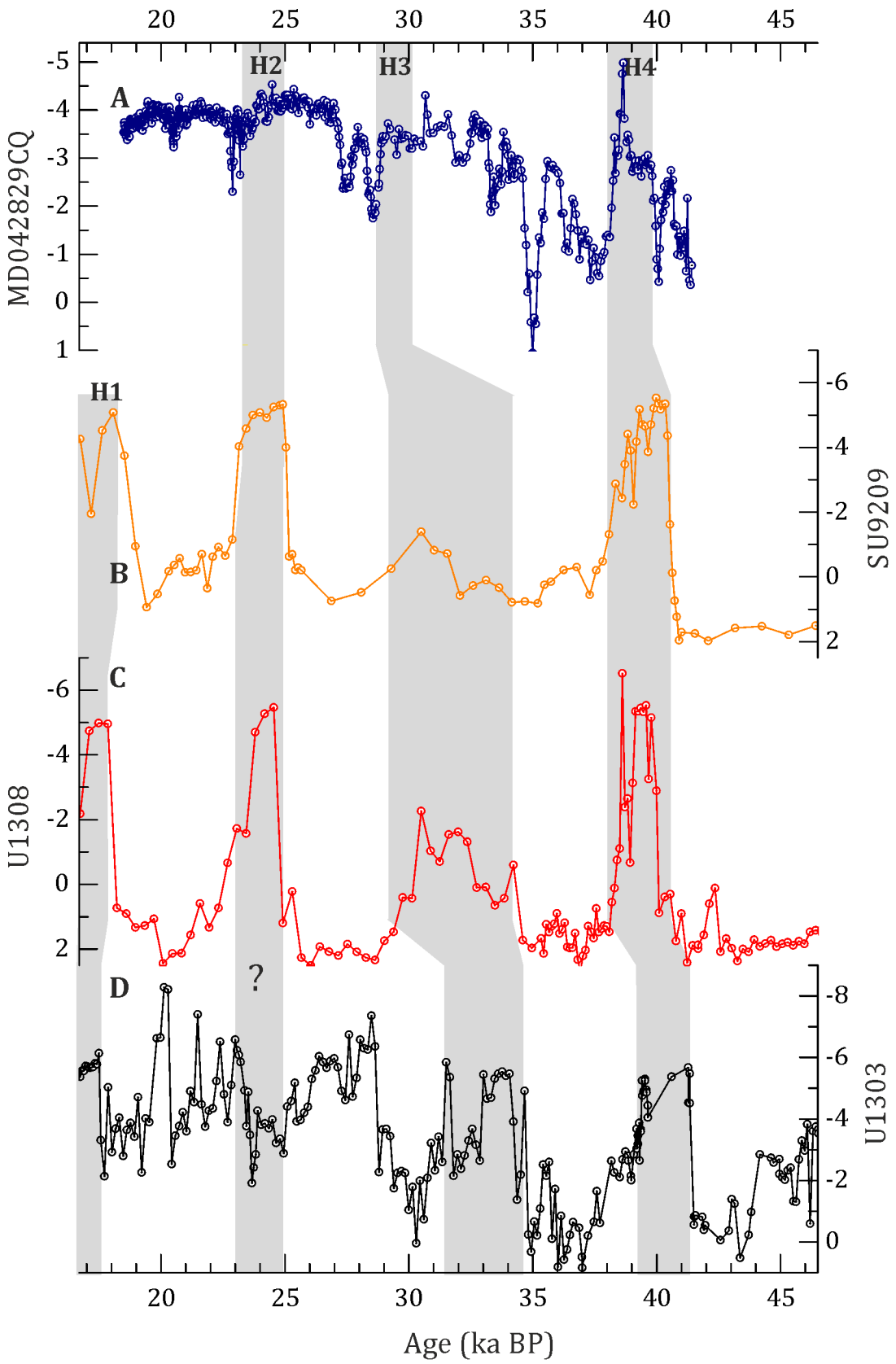

Figure 4.10: $\delta^{18}O$ of bulk material from sites U1302/3 (Channell et al., 2012) and U1308 (Hodell et al., 2008; Hodell and Curtis, 2008) and fine material from cores SU92-09 and MD04-2829CQ.

from IRD identified as Scottish in origin recorded in cores taken from the Porcupine Seabight and the Barra Fan after 46 ka BP, indicating the development of an intermittent marine margin (Knutz et al., 2001; Peck et al., 2007; Peters et al., 2008; Scourse et al., 2009). H4 is the largest of the Heinrich events with estimates of the discharge of 350 km^3 of detrital material, over 2.4 km^2 with an average thickness of 15 cm (Hemming, 2004). It creates a large negative excursion in the $\delta^{18}O$ of *N. pachyderma* thought to represent a large meltwater input across the North Atlantic during H4 (Maslin et al., 1995; Cortijo et al., 1997, 2005). At SU92-09 based on the current chronology, the negative $\delta^{18}O_{FINE}$ excursion during H4 lasts for 2.5 ka, from 40.4 to 38 ka BP, this is with the range of other estimates of the duration of H4 (***Table 1.1***) (Hemming, 2004). The $\delta^{18}O_{FINE}$ record shows a rapid initial change followed by a more gradual return to background conditions. At site MD04-2829CQ the H4 interval 40- 38 ka BP is equivalent to Greenland stadial (GS) 9, and there is a reduction in $\delta^{18}O_{FINE}$ to -2.8 ‰ for the majority of this period. At 39 ka BP there is a further reduction in $\delta^{18}O_{FINE}$ to -4.98‰ which correlates to the input of DC to the >150µm fraction to the site, lasting 500 years, this is usually equated to an input from the LIS in the fine fraction, this is similar to IRD count inputs seen at nearby sites i.e. site MD01-2461 where H4 occurs at 39 ka BP (Peck et al., 2007). At a site from the Faeroe bank a similar peak in Ca/Si and K/Ti at 39 ka BP during H4 is observed and attributed to an input from the Laurentide Ice sheet (Zumaque et al., 2012).

4.4.4 Heinrich event 2

At H2 global ice volume is much greater sea level is thought to be between 80 to 130 m lower than today (Siddall et al., 2003) and there is evidence that global ice sheets are at their maximum shelf extent (e.g., Peltier and Fairbanks, 2006; Clark et al., 2012). Estimates of the size of the release of IRD during H2 are that it covered $2.0x10^6$ km^2 with an average thickness of 15 cm and a volume of 300km^3 of detritus was released (Hemming, 2004). H2 occurs at 25-23 ka BP in core SU92-09 and is expressed by a single reduction in $\delta^{18}O_{FINE}$ to -5.5‰, which lasts for 2 ka. In contrast, during H2 at site MD04-2829CQ there is no discernible peak in $\delta^{18}O_{FINE}$ as $\delta^{18}O_{FINE}$ is already low prior and after H2. There is a significant impact of the LGM on the supply of sediment to MD04-2829CQ, which is not seen in SU92-09.

4.5 Summary

Overall sites close to the margins $\delta^{18}O$ of fine fraction is very dynamic and is not linked to Heinrich events alone but also inputs of carbonates from local ice rafting events. In the distal setting the $\delta^{18}O_{FINE}$ can easily pick out input related to Heinrich events as detrital sediment supply to the site is low. However, at the ice proximal site MD04-2829CQ when carbonate inputs are high such as during MIS 2 it in not possible to pick out an input from a Heinrich event compared to the back ground data however during MIS 3 it is possible to pick out a difference in the $\delta^{18}O_{FINE}$ values when a Heinrich event occurs. At sites close to the margins of the ice sheet $\delta^{18}O_{FINE}$ can help inform us about the input of detrital carbonate to the fine fraction.

5 A comparison between the provenance of the clay size fraction during Heinrich events H2 and H4

5.1 Introduction

5.1.1 Provenance of Heinrich layers across the North Atlantic

The earliest indication of the provenance of ice rafted detritus (IRD) during Heinrich events, came from measuring the thickness of visibly lighter layers containing abundant drop stones. The IRD contained in these layers contain ~20% detrital carbonate (Heinrich layers) in cores from the Driezack Seamount (Heinrich, 1988) and at site DSDP 609 (Bond et al., 1992). The thickening of these layers towards the Hudson Strait was taken as evidence that the source of the icebergs delivering IRD was the Laurentide ice cap centred over Hudson Bay, as limestone deposits cover the Canadian Shield in this region (Andrews and Tedesco, 1992; Bond et al., 1992; Broecker et al., 1992). Since these early observations, other methods have been utilised to better constrain the provenance of the IRD contained within Heinrich layers. These include the petrography of the >150μm sediment fraction (e.g., Bond and Lotti, 1995;Grousset et al., 2001; Auffet et al., 2002; Peck et al., 2007; Scourse et al., 2009; Hall et al., 2011), studies of the magnetic susceptibility (e.g., Grousset et al., 1993; Walden et al., 2007; Channell and Hodell, 2013), and the use of organic biomarkers to trace the input of Hudson Strait material (e.g., Rosell-Melé et al., 1997; Naafs et al., 2013). Long-lived radiogenic isotope systems have also been employed to source IRD, measured in carbonate and authigenic oxide phase free (detrital) material and include. Sm-Nd, Rb-Sr, U-Th-Pb, and K-Ar. These systems allow the source or source age of sediments in the marine environment to be inferred (as described in Section 2.2.4) (Goldstein and Hemming, 2003). As the terranes around the North Atlantic have a variable geological history, this can be linked to potential source areas (PSAs), (Gwiazda et al., 1996b; Revel et al., 1996; Hemming et al., 1998; Grousset et al., 2001; Benson et al., 2003). This suite of techniques has been widely applied to infer the source of IRD during Heinrich events from individual grains (e.g., Gwiazda et al., 1996a, 1996b), bulk sediments (Revel et al., 1996), bulk coarse fraction (>63μm) (Grousset et al., 2001), and the <63μm fraction (Hemming et al., 1998).

In the mid-latitudes between 40°N and 55°N (the IRD belt, after Ruddiman (1977) hereafter referred to as the 'IRD belt') during H1, H2, H4, and H5, detrital inputs were consistently derived from a North Canadian source as identifiable by multiple provenance indicators. For example, values of εNd are low, between -16 and -40, and $^{87}Sr/^{86}Sr$ are high >0.7240 (Revel et al., 1996; Hemming et al., 1998; Snoeckx et al., 1999; Grousset et al., 2000, 2001; Benson et al., 2003; Jullien et al., 2006). Single grain analyses of Pb in feldspar and $^{40}Ar/^{39}Ar$ ages of hornblende grains, from sites in the IRD belt indicate a Paleoproterozoic age of 1650–1900 Ga for sediments deposited during H1, H2, H4, H5. This is consistent with their being derived from the Churchill province (Northern Canada) (Gwiazda et al., 1996a; Hemming et al., 2000a; Hemming et al., 2000b; Barber, 2001; Benson et al., 2003; Hemming and Hajdas, 2003; Downing et al., 2013). Individual grains and bulk >63 μm fraction analyses of Nd and Sr isotopes from as far as the European margin, indicate the presence of sediments from a Canadian source during H1, H2, H4 and H5 (Auffret et al., 2002; Jullien et al., 2006; Leigh, 2007; Peck et al., 2007). This is further supported by a high proportion of Paleoproterozoic hornblende grains observed in Heinrich layers recovered from the Porcupine Seabight and Celtic Sea on the NW European Margin (Peck et al., 2007; Haapaniemi et al., 2010). Nd and Sr isotopes have been used to suggest European 'precursors' to Heinrich events, (Snoeckx et al., 1999; Scourse et al., 2000; Grousset et al., 2000). The deposition of IRD from the European ice sheets prior to the input of Canadian sourced material in a Heinrich layer, and therefore the inference of a European trigger of the Canadian ice-armada (Grousset et al., 2000). However, this mechanism is disputed as not all Heinrich events are preceded by inputs of a European source, and at the European margin IRD is associated with D-O events throughout the last glacial (Peck et al., 2007; Haapaniemi et al., 2010).

Sm-Nd and Pb isotopes and concentrations have been used in the clay size fraction (<2μm) previously to infer the sources of sediments transported by bottom currents in the deep ocean along the Western Boundary Under Current (WBUC) during the Holocene (Fagel et al., 1999, 2002, 2004; Fagel and Mattielli, 2011). However, during glacial intervals there were significant increases in both the relative flux and absolute flux of clay sized sediment to the Labrador Sea from the proximal North American Shield which underlays the Laurentide Ice Sheet (LIS), due to increased glacial erosion (Fagel and Hillaire-Marcel, 2006). Furthermore, during the late glacial, clay size

sediments from the Labrador Sea have similar Nd isotope ratios to those of the coarser fractions implying they have the same source. Therefore, during glacial intervals, inputs to the clay terrigenous fraction of ice proximal sediments are dominated by local sources (Innocent et al., 2000).

The clay-size fraction has not been widely used to infer provenance of the material contained in Heinrich layers across the North Atlantic, largely because of complications related to secondary depositional processes, as the sediment fractions <150μm are potentially reworked by bottom currents in the deep ocean. There is also the potential for mineral sorting across size fractions discussed in Section 5.3.1. But clays can account for a large proportion of glacially derived material (Andrews, 2000), and during the last glacial a large proportion of clays were deposited in glaciomarine environments and derived from glacial erosion (Andrews and Principato, 2002; Benson et al., 2003; Fagel and Hillaire-Marcel, 2006). As the coarse fraction does not account for all of glaciogenic derived material, by overlooking the fine fraction our understanding of the sediment supply during Heinrich events is limited. Indeed, studies that have used the <2μm fraction indicate a changing source of clay material during Heinrich events. Dominant inputs to the <2μm fraction during Heinrich events at the Dreizack Seamounts in the West European Basin have an older age compared to non-Heinrich intervals (Jantschik and Huon, 1992). $^{40}Ar/^{39}Ar$ from <2μm fraction were used to trace the source of Heinrich event 2 from site V28-82 in the IRD belt demonstrating that this fraction had the same provenance as coarser (2-20μm) fractions during H2. Both were consistent with a Labrador Sea ice rafted source (Hemming et al., 2002).

This chapter presents Sr-Nd-Pb element concentrations and isotope ratios, of the <2μm terrigenous fraction from core SU92-09 situated in the IRD belt and MD04-2829CQ from Rosemary Bank. This adds to the growing body of work characterising detrital sediment inputs to the IRD belt and the Northern European Atlantic Margin during Heinrich events. This chapter aims to address the following questions surrounding the origin of clay-sized sediment during Heinrich events.

1. What is the Nd, Sr, and Pb isotopic composition of the clay size fraction of sediments from the IRD belt and European margin?

2. Can these sediments be assigned to a source area and do their relative contributions change over time at each site?
3. Are there significant changes between the composition of Heinrich event 4 (H4) and Heinrich event 2 (H2) given their different initial conditions?
4. Is the clay size fraction similar in composition to coarser fractions from nearby cores?

The study of clay size terrigenous sediments in conjunction with coarse fraction lithic counts, where available, is expected to reveal new information on the source and the nature of delivery of material during Heinrich events H2 and H4. Both H2 and H4 are thought to involve the collapse/surge of the Hudson Strait sector of the Laurentide ice sheet (LIS) through the Labrador Strait (Hemming, 2004). Additionally, both have very different initial conditions; during H4 global ice volume was low, and insolation is high, whereas during H2 global ice volume was high and insolation was low by the time of H2 the European ice sheets had reached their maximum extent (Clark et al., 2012). By comparing changes in the source of detrital material of Heinrich events with different initial conditions the aim is to make inferences about the sources of sediments that will have implications for the local and regional oceanographic conditions during Heinrich events. Comparisons between ice-proximal and ice-distal settings will provide constraints on the sedimentary supply of detrital material in different depositional environments over the course of both Heinrich events.

5.1.2 Chapter Methods

5.1.2.1 Potential source regions and their radiogenic isotope signatures

Robust characterisation of source sediments is needed to be confident of the provenance of deposited detrital sediment, particularly when using bulk or fine sediments that provide an integrated 'signal' from many different sources (Hemming, 2004). This chapter uses data from previous studies to characterise potential source areas (PSAs) for glacially derived material deposited at sites in the North Atlantic Ocean. These are defined by the glacial margins of the major ice sheets during the last glacial and their underlying geology (Gwiazda et al., 1996b; Hemming, 2004) as shown in Figure 5.1. Ideally, isotope ratios from PSAs should be as similar to the

material measured as possible, i.e. they should be from the same size fraction and the same mineral fraction (whole rock, sediments or individual minerals).

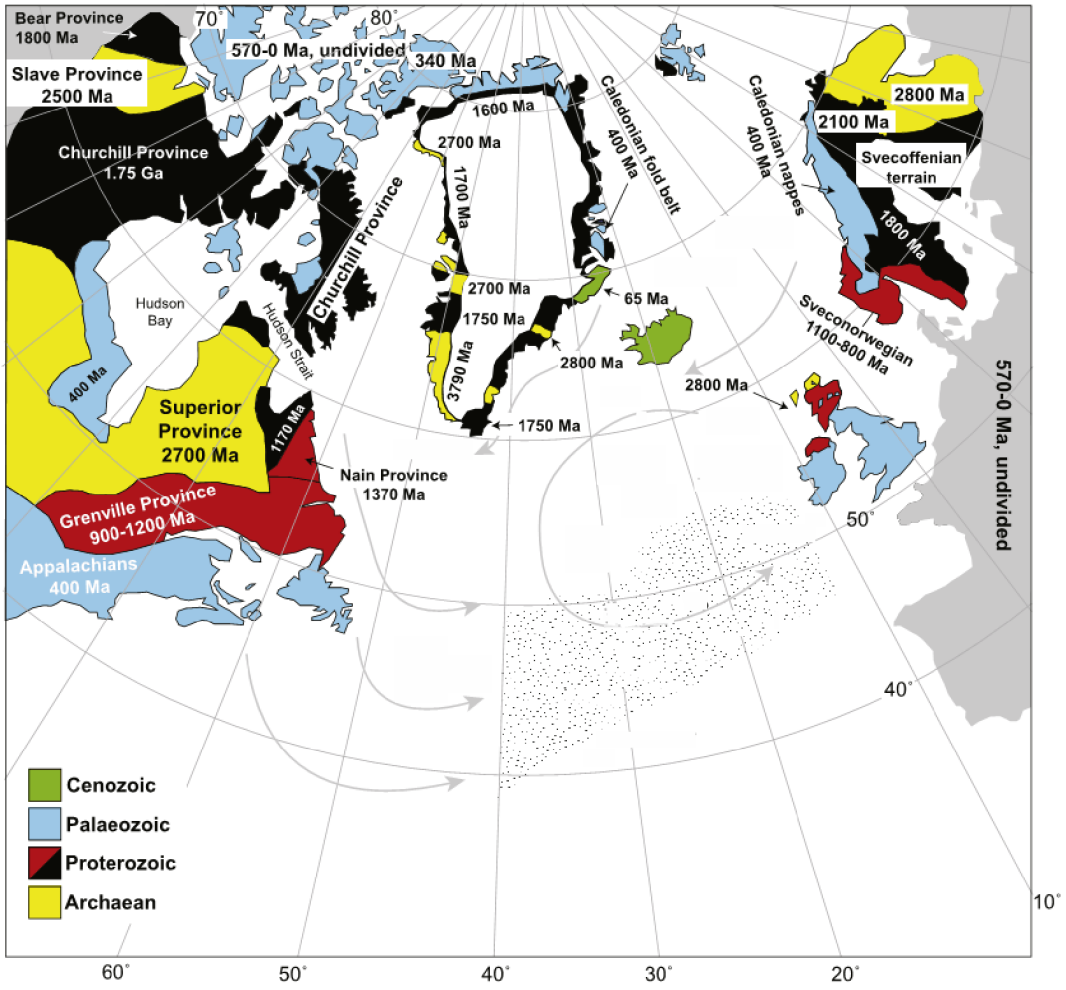

Figure 5.1: Map of simplified source regions taken from Bailey et al. (2013) with permissions from Elsevier. Mean IRD paths are shown by grey arrows and the IRD belt is shown as the 250 grains per cm contour (stippled area) inferred from (Ruddiman, 1977) Geological provinces are based on Gwiazda et al. (1996).

In previous studies PSAs have been characterised using weighted averages of isotope compositions of bedrock terranes from the geochemical literature. For example, Revel et al. (1996) used literature based estimates of $^{143}Nd/^{144}Nd$ and $^{87}Sr/^{86}Sr$, and Fagel et al. (1999) $^{143}Nd/^{144}Nd$ and $^{206}Pb/^{204}Pb$, $^{207}Pb/^{204}Pb$ and $^{208}Pb/^{204}Pb$ to define their source regions. Although this is a good approach, PSA terranes defined by the literature may not characterise the material entrained by the ice sheet and transported to the marine margin. Farmer et al. (2003) suggested that characterisation of PSAs is best achieved using Quaternary sediments from Trough Mouth Fans (TMFs). Such ice-proximal sediments provide the isotopic compositions

of detritus transported by the ice sheet and ice streams to the shelf slope boundary of ocean margins. TMF isotope compositions have been collected from the <63μm by Farmer et al. (2003) and similar PSA data has been collected from fjord, estuarine, and continental shelf for the >63μm fraction (Grousset et al., 2001). More recently εNd data from the <63μm fraction have been compiled from Northern European rivers by Toucanne et al. (2015).

Isotope compositions of the <2μm fraction are not currently available to characterise North Atlantic PSAs and accordingly, this study will use the TMF data from Farmer et al. (2003). Farmer et al. (2003) provide data for Nd, Sr and Pb isotope compositions and concentrations for the <63μm fraction of TMFs from the Canadian margin, Greenland, Iceland and Scandinavia, but not from the British Isles. These have been supplemented in this study by Nd and Sr isotope data from Grousset et al. (2001) and Revel et al. (1996) shown in Figure 5.2. Data from Toucanne et al. (2015) are not included as only the εNd and no Sr isotope values were available. Figure 5.3 shows data from Farmer et al. (2003) which were used for Pb isotope compositions of PSAs, with supplementary data on the mean North Atlantic Pb composition of Mn-Fe oxide phases for comparison from Abouchami et al. (1999) and from the Rockall Trough Crocket et al. (2013) and additional source region data from Fagel et al. (1999). The Northern Hemisphere Reference Line (NHRL) after Hart et al. (1984) (a linear trend composite of Pb isotope data of volcanic islands from the northern Hemisphere) is shown for reference. The coloured envelopes in Figure 5.2 and Figure 5.3 will be used to visually compare the clay size fraction to the PSAs in this discussion. The envelopes integrate samples from studies using the <63μm and >63μm this is necessary as the data from the <63μm fraction only characterise the European source regions using four samples from Scandinavia and this does not encompass the full range of European PSAs. The PSA data and the literature sources are in Appendix 4. Nd and Sr isotopes show large differences among the different PSAs, there are overlaps between the Gulf of Saint Lawrence and Scandinavian margin PSAs particularly in εNd. Pb isotope compositions from Farmer et al. (2003) show a significant degree of overlap between Greenland, Iceland the Gulf of Saint Lawrence and Scandinavia, and whole rock compositions from several North Atlantic provenances clearly overlap in Figure 5.3A.

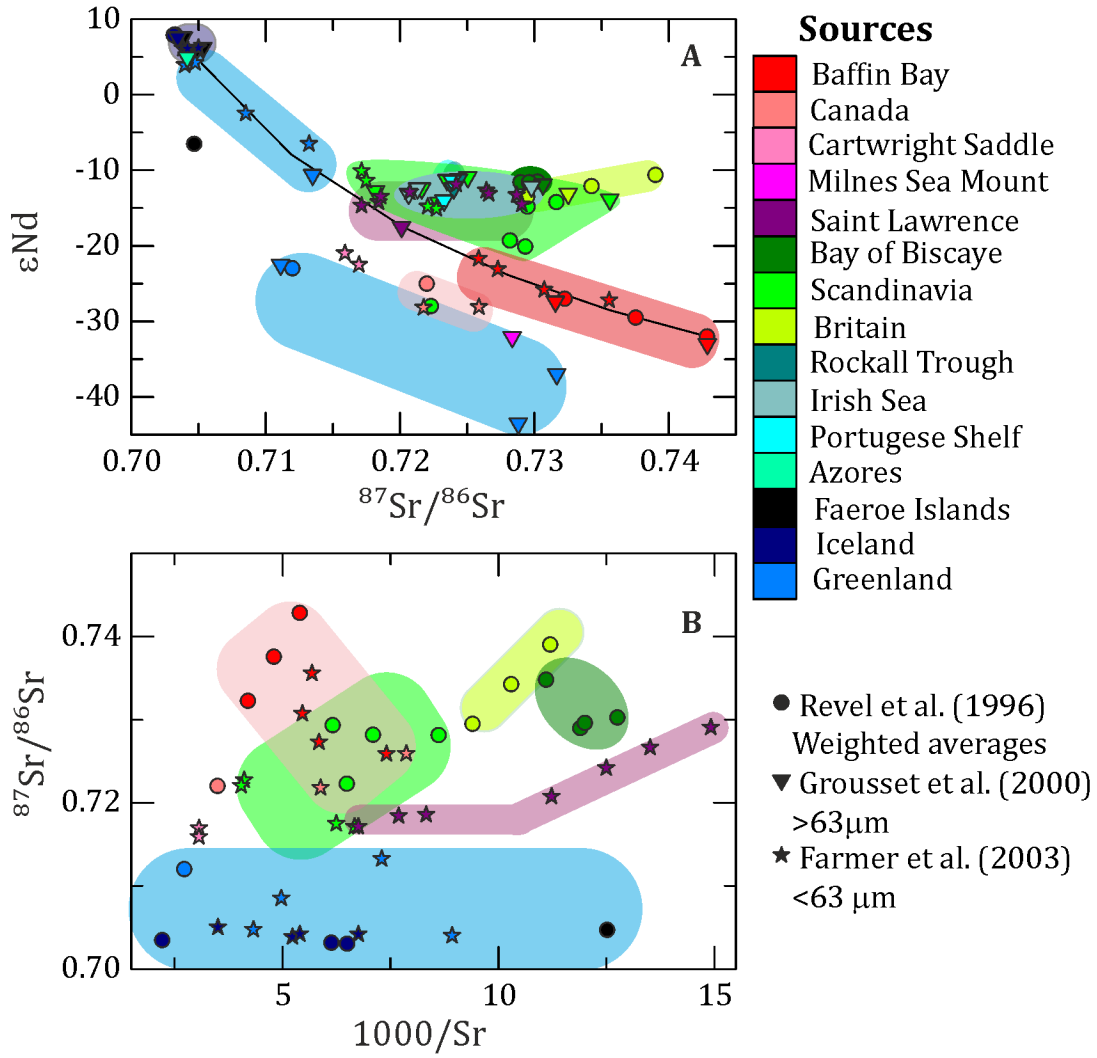

Figure 5.2: Sr and Nd isotope compositions from potential source areas (PSAs). A; εNd and $^{87}Sr/^{86}Sr$ of PSAs and B; $^{87}Sr/^{86}Sr$ and 1000/Sr data from PSAs. Source regions are from Farmer et al. (2003) in the <63µm fraction, Grousset et al. (2000) in the >63 µm fraction and Revel et al. (1996) weighted averages from the literature. Data are highlighted according to provenance see key. PSAs are shown in *Figure 5.1* ***for illustration.***

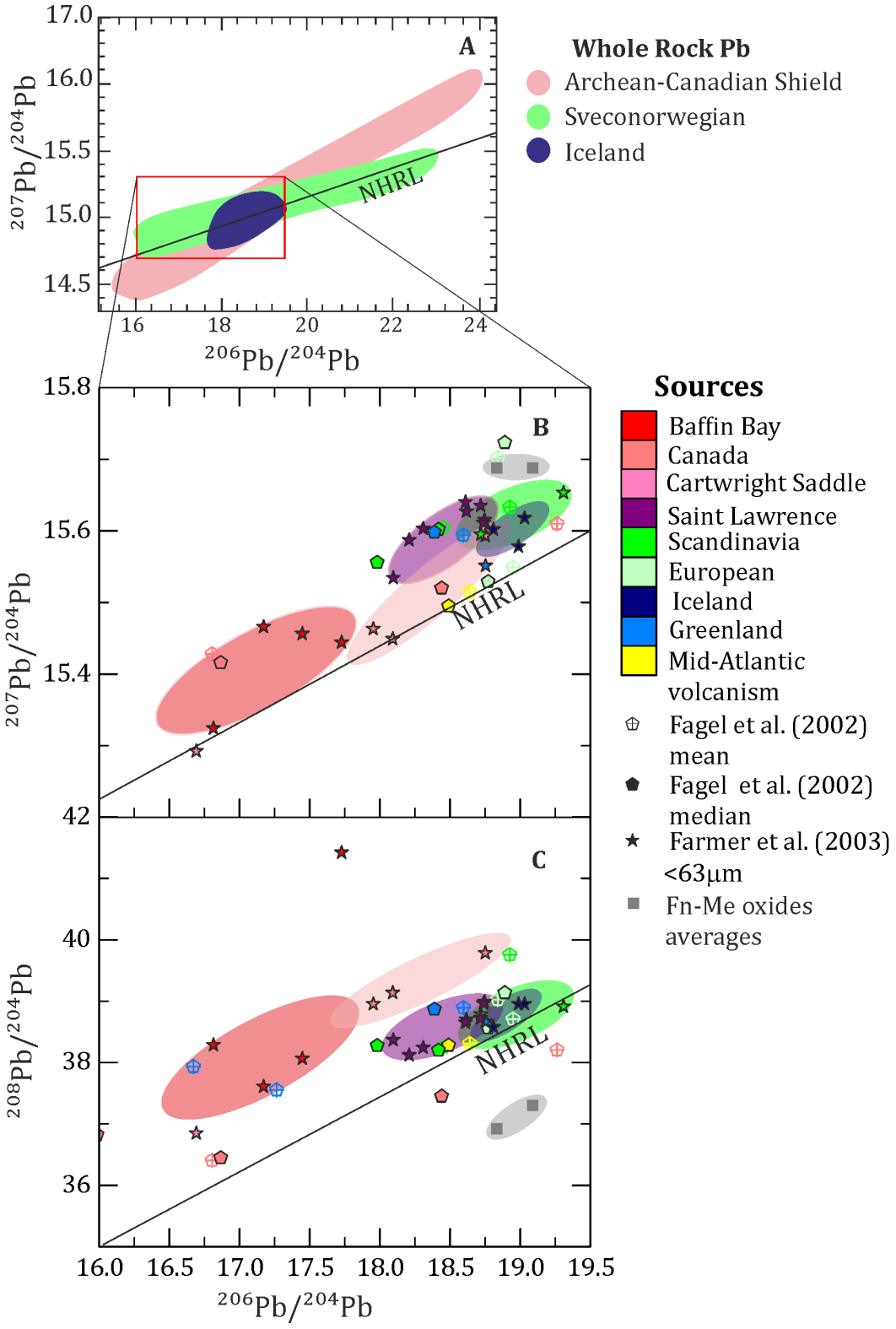

Figure 5.3: Pb isotope ratios from potential source areas (PSAs). A; Whole rock Pb isotope compositions around the North Atlantic. Farmer et al (2003) and references therein. B; $^{206}Pb/^{204}Pb$ vs $^{207}Pb/^{204}Pb$ and C: $^{206}Pb/^{204}Pb$ vs $^{208}Pb/^{204}Pb$ from Farmer et al. (2003), with additional data from Fagel et al. (1999) and average Fn-Me oxide Pb composition from Abouchami et al. (1999) and Crocket et al. (2013) for comparison. NHRL is the Northern Hemisphere reference line after Hart (1984).

5.1.2.2 Geochemical end member modelling

This section provides an estimate of the proportions of each PSA contributing to the clay size terrigenous fraction of sediments deposited in the IRD belt (SU92-09) and Rosemary Bank (site MD04-2829CQ). A three component mixing model examines the contribution of different source areas to the isotopic values presented in this chapter. A mixing model was calculated for isotope ratios of Nd, and Sr of the clay size fraction at each site. Lead isotope compositions were excluded from the mixing model, firstly because the bulk Pb isotope compositions of PSAs show significant overlap, and secondly because replicate analysis of the Pb ratios for core MD04-2829CQ were not consistent, as discussed in Section 2.2.4.4. The mixing proportions were calculated using Equation 5.1 Equation 5.2, and Equation 5.3. The initial compositions of the end members were approximated from the PSA data (Table 5.1).

Table 5.1: Average compositions of PSA

End member	*Sr ppm*	*$^{87}Sr/^{86}Sr$*	*Nd ppm*	*$^{143}Nd/^{144}Nd$*
LIS-Baffin Bay 1	210.33	0.73755	21	0.511123
LIS-Baffin Bay 2	160.67	0.72957333	13	0.511407
LIS-Hudson Strait	148.5	0.72383	15	0.511183
LIS-GSL	62.32	0.725056	11	0.51195
FSIS	200	0.71985	36.325	0.51198
BIIS	97.33333	0.73425	38.33333	0.51202
IIS	202.25	0.7042975	11	0.512948
GIS	170.25	0.7076225	3	0.512625

Based on data from Farmer et al. (2003) Baffin Bay 1 and BIIS are based on data from Revel et al. (1996).

Equation 5.1: determination of mixing fraction for end member 1 of a three component mixing of Nd and Sr

$$f_{EM1}$$

$$= \frac{\left(\frac{^{143}Nd}{^{144}Nd}_{sample} \times Nd_{sample} - \frac{^{143}Nd}{^{144}Nd}_{EM3} \times Nd_{EM3}\right) \times \left(\frac{^{87}Sr}{^{86}Sr}_{EM2} \times Sr_{EM2} - \frac{^{87}Sr}{^{86}Sr}_{EM3} \times Sr_{EM3}\right) - \left(\frac{^{87}Sr}{^{86}Sr}_{sample} \times Sr_{sample} - \frac{^{87}Sr}{^{86}Sr}_{EM3} \times Sr_{Em3}\right) \times \left(\frac{^{143}Nd}{^{144}Nd}_{EM2} \times Nd_{EM2} - \frac{^{143}Nd}{^{144}Nd}_{EM3} \times Nd_{EM3}\right)}{\left(\frac{^{143}Nd}{^{144}Nd}_{EM1} \times Nd_{EM1} - \frac{^{143}Nd}{^{144}Nd}_{EM3} \times Nd_{Em3}\right) \times \left(\frac{^{87}Sr}{^{86}Sr}_{EM2} \times Sr_{EM2} - \frac{^{87}Sr}{^{86}Sr}_{EM3} \times Sr_{EM3}\right) - \left(\frac{^{87}Sr}{^{86}Sr}_{EM1} \times Sr_{sample} - \frac{^{87}Sr}{^{86}Sr}_{EM1} \times Sr_{EM3}\right) \times \left(\frac{^{143}Nd}{^{144}Nd}_{EM2} \times Nd_{EM2} - \frac{^{143}Nd}{^{144}Nd}_{EM3} \times Nd_{Em3}\right)}$$

Equation 5.2: determination of mixing fraction for end member 2 of a three component mixing of Nd and Sr

$$f_{EM2} = \left(\frac{^{87}Sr}{^{86}Sr}_{Sample} \times Sr_{sample} - \frac{^{87}Sr}{^{86}Sr}_{EM3} \times Sr_{EM3} \right) -$$

$$f_{EM1} \times \frac{\left(\frac{^{87}Sr}{^{86}Sr}_{EM1} \times Sr_{EM1} - \frac{^{87}Sr}{^{86}Sr}_{EM3} \times Sr_{EM3} \right)}{\left(\frac{^{87}Sr}{^{86}Sr}_{EM2} \times Sr_{EM2} - \frac{^{87}Sr}{^{86}Sr}_{EM3} \times Sr_{EM3} \right)}$$

Equation 5.3: determination of mixing fraction for end member 2 of a three component mixing of Nd and Sr

$$f_{\mathrm{EM3}} = 1 - f_{EM1} - f_{EM2}$$

Where f = mixing fraction, and EM = end member. Mixing equation is adapted from Franzese et al. (2006).

5.2 Results: radiogenic isotope compositions of the detrital clay size fraction

As detailed in Section 2.2.4.1, εNd ratios reflect the average continental age of the source of the sediment (Taylor and McLennan, 1985; McLennan and Hemming, 1992; Hemming, 2004) and are represented by the εNd notation (the deviation of the $^{143}Nd/^{144}Nd$ from 0.512638 the "bulk earth" value) (DePaolo and Wasserburg, 1979). The clay size (<2μm) fraction of the terrigenous sediments from the IRD belt (site SU92-09) has a wide range of εNd values between -14 and -28 ε units (Figure 5.4B). The lowest values of εNd < -20 are associated with H2 and H4, outlined in grey and are defined by inputs of detrital carbonate (dark grey) and decreased $\delta^{18}O_{FINE}$ (light grey). At the onset of H4 (41 ka BP) εNd values decrease from -15.7 prior to the event to -26.7 at the peak of H4. εNd decreases to -20 by the end of H4 at 38.1 ka BP. Prior to H2, between 32 and 25.5 ka BP, εNd is high >-16.2. εNd values decrease to -26.5 at the onset of H2 and thereafter remain low until the end of H2 when they increase to -16.25 at 23 ka BP. Following the H2 event, εNd values show a slight increase to -14.8 at 19.2 ka BP.

The ratios of $^{87}Sr/^{86}Sr$ also reflect crustal age but the Rb-Sr system is more prone to alteration than Sm-Nd (Dasch, 1969; Biscaye and Dasch, 1971; Goldstein and Jacobsen, 1988) as detailed in Section 2.2.4.2. Higher $^{87}Sr/^{86}Sr$ ratios reflect continental crust and lower $^{87}Sr/^{86}Sr$ ratios reflect younger mantle sources (Faure and Mensing, 2005). The $^{87}Sr/^{86}Sr$ ratios of the terrigenous clay sized sediments from the IRD belt range from 0.7300 to 0.7451 Figure 5.4. High $^{87}Sr/^{86}Sr$ ratios are associated with H2 (0.7384) and H4 (0.7394) but the highest $^{87}Sr/^{86}Sr$ ratios occur during the H3 interval (0.7451) between 31.5 and 29 ka BP (Figure 5.4C).

When the εNd and $^{87}Sr/^{86}Sr$ ratios of the clay size fraction from SU92-09 are cross plotted a common sequence between H2 and H4 is observed Figure 5.5A and Figure 5.5B. Prior to the both H4 and H2 at point 1, $^{87}Sr/^{86}Sr$ is high, 1000/Sr is high and εNd values are high. During H2 and H4 at point 2 εNd decreases to between -20 and -27, 1000/Sr decreases to between 4 and 6 and $^{87}Sr/^{86}Sr$ remains the same excluding H3. After the H2 and H4 events, at point 3 εNd increases to between -15 and -17 with values of 1000/Sr of 7-9 and lower $^{87}Sr/^{86}Sr$ of between 0.730 and 0.738.

Table 5.2 Radiogenic isotope composition data of the clay-sized fraction from the IRD Belt site SU92-09

ID	*Age (ka BP)*	*Nd*	*Sm*	$\frac{Nd}{Sm}$	$\frac{^{143}Nd}{^{144}Nd}$	*2σ*	*εNd*	*2σ*	*TDm*	*Rb*	*Sr*	$\frac{1000}{Sr}$	$\frac{^{87}Sr}{^{86}Sr}$	*2σ*	*Pb*	$\frac{^{206}Pb}{^{204}Pb}$	$\frac{^{207}Pb}{^{204}Pb}$	$\frac{^{208}Pb}{^{204}Pb}$	*2σ*	*2σ*	*2σ*
48	19.865	25.4	4.2	0.0985	0.51188	12	-14.81	0.23	1.2	161	127	8	0.73143	16	38	18.75	15.63	38.76	20	57	16
52	20.758	26.0	4.2	0.0975	0.51183	15	-15.85	0.29	1.3	167	133	8	0.73201	27	42	18.65	15.62	38.70	21	57	16
54	21.204	24.5	4.0	0.0979	0.51182	14	-15.97	0.27	1.3	157	128	8	0.73106	19	47	18.26	15.60	38.28	35	79	21
56	21.65	24.9	4.1	0.0999	0.51186	12	-15.19	0.23	1.3	153	121	8	0.73051	26	111	17.83	15.57	37.79	25	68	18
58	22.097	26.3	4.2	0.0965	0.51181	13	-16.21	0.26	1.3	165	130	8	0.73144	16	113	17.78	15.57	37.74	15	52	14
60	22.599	23.8	3.8	0.0960	0.51180	11	-16.25	0.21	1.3	162	140	7	0.73181	18	98	17.80	15.57	37.78	16	53	15
62	23.157	-	-	-	0.51162	10	-19.94	0.20	-	-	-	-	0.73533	16	-	18.24	15.58	38.45	22	286	62
64	23.715	21.8	3.5	0.0956	0.51141	10	-23.92	0.19	-	168	161	6	0.74087	16	22	18.56	15.58	39.03	0	717	241
66	24.273	25.5	3.9	0.0922	0.51133	16	-25.61	0.31	2.0	173	246	4	0.73695	16	26	17.91	15.53	38.48	18	60	17
68	24.676	-	-	-	0.51128	11	-26.54	0.21	-	-	-	-	0.73835	15	-	17.62	15.55	37.70	14	51	14
70	24.924	-	-	-	0.51131	11	-25.90	0.22	-	-	-	-	0.73772	16	-	17.58	15.55	37.60	14	52	14
72	25.172	24.8	4.1	0.0985	0.51181	12	-16.23	0.23	1.3	172	120	8	0.73468	18	76	18.02	15.59	38.00	18	52	14
74	25.42	22.2	3.7	0.0995	0.51185	11	-15.43	0.22	1.3	166	112	9	0.73525	16	107	17.82	15.58	37.76	41	80	21
76	25.668	23.1	3.8	0.0983	0.51186	11	-15.22	0.22	1.2	166	106	9	0.73571	17	60	18.16	15.60	38.11	19	53	14
78	26.877	21.2	3.5	0.0981	0.51189	12	-14.62	0.23	1.2	163	95	10	0.73731	14	43	18.52	15.63	38.44	19	55	15
80	28.086	22.4	3.7	0.0990	0.51188	12	-14.82	0.23	1.2	183	95	11	0.74091	19	47	18.55	15.63	38.45	15	51	14
82	29.295	26.5	4.3	0.0979	0.51186	10	-15.23	0.19	1.2	192	100	10	0.74279	19	61	18.31	15.62	38.19	17	56	15
84	30.504	25.7	4.2	0.0981	0.51186	12	-15.13	0.24	1.2	183	96	10	0.7439	25	76	18.11	15.61	37.99	40	86	22
86	31.027	23.8	3.9	0.0980	0.51187	12	-15.08	0.23	1.2	175	88	11	0.74506	16	41	18.60	15.65	38.46	17	58	15
88	31.55	27.5	4.5	0.0981	0.51185	11	-15.44	0.22	1.3	187	106	9	0.74242	19	44	18.49	15.63	38.37	26	352	74
100	34.686	24.0	3.9	0.0981	-	0	-	-	-	169	110	9	0.7365	10	37	18.47	15.62	38.48	40	394	82
102	35.209	26.1	4.2	0.0965	0.51182	11	-15.98	0.22	1.3	179	122	8	0.73476	17	83	17.88	15.58	37.84	15	53	15

104	35.732	24.0	4.0	0.0991	0.51182	12	-15.94	0.24	1.3	164	123	8	0.7358	27	44	18.26	15.60	38.30	28	335	71
106	36.255	24.6	4.0	0.0970	0.51181	12	-16.25	0.23	1.3	174	133	7	0.7348	13	40	18.36	15.61	38.39	19	59	16
108	36.777	-	-	-	0.51177	11	-17.02	0.22	-	-	-	-	0.72999	14	-	18.26	15.60	38.37	19	57	15
112	37.823	22.9	3.7	0.0976	0.51177	12	-17.01	0.23	1.4	164	122	8	0.73717	18	43	18.17	15.60	38.20	25	60	17
114	38.346	24.9	4.0	0.0958	0.51161	11	-20.14	0.22	1.6	176	158	6	0.73888	25	33	18.54	15.61	38.72	28	381	80
116	38.723	-	-	-	0.51146	11	-22.89	0.21	-	-	-	-	0.73831	15	-	17.97	15.56	38.13	19	60	16
118	38.956	24.7	3.9	0.0954	0.51149	10	-22.45	0.20	1.8	175	197	5	0.73746	12	92	17.77	15.57	37.81	32	76	21
120	39.189	23.0	3.6	0.0946	0.51148	10	-22.50	0.20	1.8	171	183	5	0.7381	26	67	17.77	15.56	37.84	16	56	15
122	39.422	25.6	3.9	0.0915	0.51135	11	-25.18	0.22	1.9	172	200	5	0.73908	18	63	17.89	15.57	38.06	35	79	22
124	39.654	25.7	4.0	0.0931	0.51145	25	-23.19	0.49	1.8	169	192	5	0.73835	19	33	18.31	15.61	38.68	25	66	16
128	40.073	25.7	4.0	0.0926	0.51127	10	-26.68	0.20	2.1	176	249	4	0.73784	27	26	17.87	15.51	38.39	27	356	75
132	40.445	24.8	3.9	0.0946	0.51161	10	-20.10	0.20	1.6	180	163	6	0.73938	27	201	17.61	15.56	37.55	22	311	67
134	40.631	24.3	3.9	0.0971	0.51183	10	-15.72	0.20	1.3	182	113	9	0.73876	26	65	17.93	15.58	37.88	27	363	77
136	40.7	18.7	3.2	0.1016	0.51185	11	-15.44	0.21	-	160	76	13	0.74154	15	18	19.05	15.67	39.05	0	522	176
138	41.003	-	-	-	0.51186	11	-15.17	0.22	-	-	-	-	0.73362	20	-	17.75	15.57	37.70	34	73	21
140	42.086	18.8	3.0	0.0970	0.51184	12	-15.49	0.23	1.3	165	110	9	0.7344	20	110	17.67	15.57	37.62	24	64	18
146	45.337	21.4	3.4	0.0952	0.51185	11	-15.31	0.22	1.2	165	117	9	0.73347	28	81	17.75	15.57	37.71	23	268	59

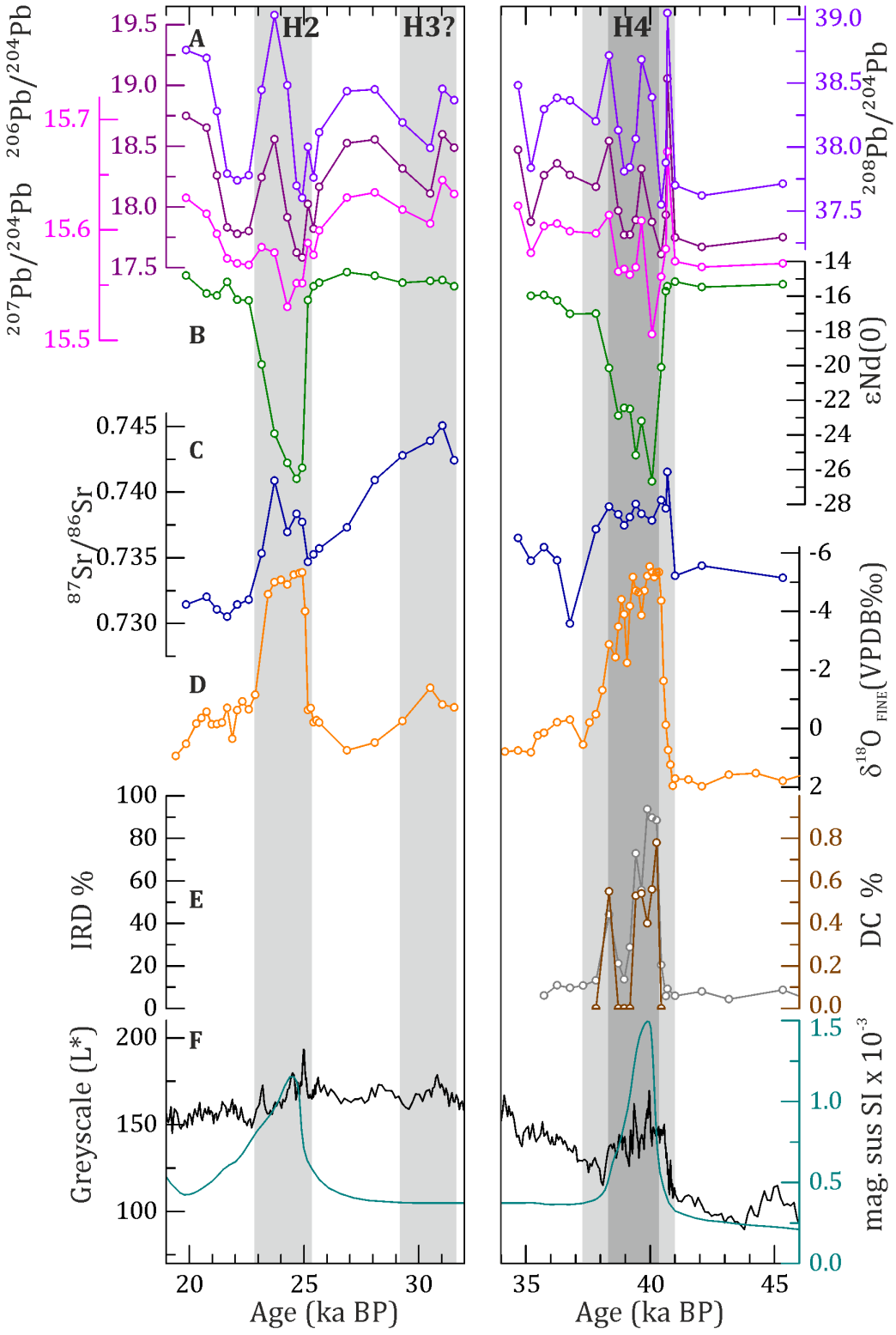

Figure 5.4: Isotope ratios of the <2µm fraction from the IRD belt (site SU92-09) from H2 and H4 and the surrounding intervals. Error bars are smaller than symbols. A; $^{206}Pb/^{204}Pb$ in pink, $^{207}Pb/^{204}Pb$ in purple, $^{208}Pb/^{204}Pb$ in dark purple, B; εNd in green, C; $^{87}Sr/^{86}Sr$ in blue, D; $\delta^{18}O_{FINE}$ in orange, E: percentage IRD in grey and percentage DC of the total >150µm fraction in brown, F: greyscale values in grey and magnetic susceptibility in dark green. Heinrich events are marked in grey. A, B, C, D, this study E and F, pers. comm. Elsa Cortijo.

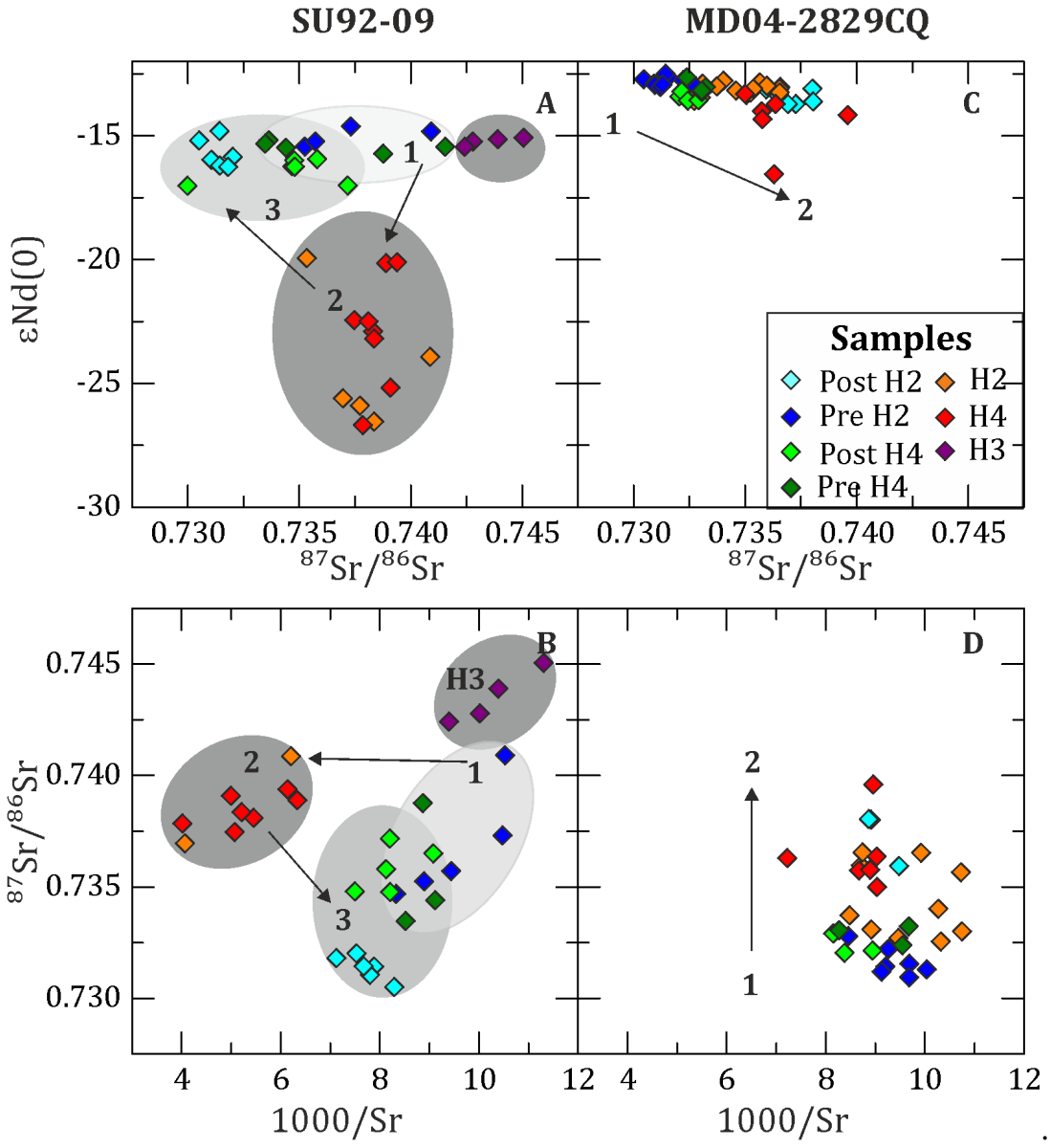

Figure 5.5: Cross plots of Sr and Nd isotope ratios of the clay size terrigenous fraction from the IRD belt and Rosemary Bank. A; $^{87}Sr/^{86}Sr$ vs εNd from SU92-09, B; 1000/Sr vs $^{87}Sr/^{86}Sr$ from SU92-09, C; $^{87}Sr/^{86}Sr$ vs εNd from MD04-2829CQ D; 1000/Sr vs $^{87}Sr/^{86}Sr$ from MD04-2829CQ. Samples are colour coded as shown in the key. Grey circles and lettering are explained in the text.

The clay sized fraction of terrigenous sediments from Rosemary Bank (site MD04-2829CQ have εNd values with a much smaller range between -12.5 and -16.6 (mostly between -12.5 and 14.5) (Figure 5.6B). During H4 from 39.1 to 38.2 ka BP, εNd is lower than in the ambient glacial with the lowest εNd value of -16.6 occurring at the same time as the detrital carbonate input, and decreased $\delta^{18}O_{FINE}$ (-4.98‰). Over H2 from 25.1 ka BP to 23.2 ka BP εNd values gradually decrease but are not significantly different from background glacial values.

$^{87}Sr/^{86}Sr$ ratios of the clay sized terrigenous sediments from Rosemary Bank have a range from 0.7305 to 0.7396 (Figure 5.6C). The $^{87}Sr/^{86}Sr$ ratios are highest during H4 reaching 0.7396. $^{87}Sr/^{86}Sr$ ratios increase during H2 from 0.7328 to 0.7365 and continue to increase after the end of the Heinrich event. Cross plots of εNd and $^{87}Sr/^{86}Sr$ ratios of the <2μm fraction at site MD04-2829CQ (Figure 5.5) show that before both H2 and H4 and after H4 at point 1 in Figure 5.5C and ***Figure 5.5***D $^{87}Sr/^{86}Sr$ is low, εNd is high and values of 1000/Sr between 8 and 11. During H2 and the post H2 interval $^{87}Sr/^{86}Sr$ increase but εNd and 1000/Sr remain constant. During H4 at site MD04-2829CQ only one sample from the H4 interval has lower εNd (-16.55) and lower 1000/Sr than all the samples from site MD04-2829CQ.

Bulk Pb isotopes are useful in detecting Archean sources (Hemming, 2004) (Section 2.2.3.3) but are not currently as widely used as Nd and Sr isotopes in the North Atlantic. This is because bulk isotope compositions of source regions overlap significantly thereby poorly discriminating between different sources (Farmer et al., 2003) see Figure 5.3A. Most comparisons of North Atlantic sediments focus on $^{206}Pb/^{204}Pb$- $^{207}Pb/^{204}Pb$ space and $^{206}Pb/^{204}Pb$- $^{208}Pb/^{204}Pb$ and this will be used here for ease of comparison (Gwiazda et al., 1996b, 1996a; Hemming et al., 1998; Bailey et al., 2012). Three samples were replicated from the Pb isotope data of site SU92-09 (shown in black with links to the original samples (Figure 5.7)), to test the veracity and consistency of the final data point in Figure 5.7A and Figure 5.7B. In the clay size terrigenous fraction of the IRD belt (site SU92-09), there are a range of values in the Pb isotope composition from 17.58 to 19.06 $^{206}Pb/^{204}Pb$, from 15.1 to 15.67 in $^{207}Pb/^{204}Pb$, and from 37.55 to 39.05 in $^{208}Pb/^{204}Pb$. Between 46 and 41 ka BP, the Pb isotope ratios are low (<17.75 for $^{206}Pb/^{204}Pb$, but increase to the highest values of the record just before H4. During H4, Pb compositions are variable with lows of 17.6 and highs of 18.5 for $^{206}Pb/^{204}Pb$. After H4 at 38ka BP the Pb isotope compositions are higher than prior to the H4 interval at ~18.2 for $^{206}Pb/^{204}Pb$. From 31 to 25.5 ka BP Pb isotope ratios are 18.5 for $^{206}Pb/^{204}Pb$. At 25.5 ka BP, the start of H2, they decrease to 17.7 for $^{206}Pb/^{204}Pb$ and then increase over H2 to 18.5 for $^{206}Pb/^{204}Pb$ at 24 ka BP.

Pb isotope compositions of clay-sized sediments from the IRD belt are plotted in $^{206}Pb/^{204}Pb$-$^{208}Pb/^{204}Pb$ space in Figure 5.7B. The dashed line $y = 0.0763x + 14.207$ describes all of the samples (R^2=0.7297). The solid line describes the ambient glacial

sediments $y = 0.0722x + 14.288$ ($R^2 = 0.9248$), and it is clear that the sediments from H2 and H4 are more radiogenic than the ambient glacial sediments plotting above the solid line. In comparison, sediments from H3 are less radiogenic than the ambient glacial sediments plotting below the line. When the sediments are plotted in $^{206}Pb/^{204}Pb$- $^{207}Pb/^{204}Pb$ space (Figure 5.7A), they are described by the dashed line $y = 0.9948x + 20.144$ ($R^2 = 0.8197$) and black line described by the equation $y = 1.0111x + 19.764$ ($R^2 = 0.9745$) is a linear fit to the ambient sediments. The sediments from H2 and H4 deviate from the ambient sediment line towards point 2. Sediments from H3 fall above the line. This is clearly demonstrated in Figure 5.8 where the deviation from the best fit of the ambient glacial sediment is plotted, and a clear trend of higher than ambient glacial $^{207}Pb/^{204}Pb$ values and lower than ambient glacial $^{208}Pb/^{204}Pb$ is evident during H4 and H2.

It should be noted that whilst analytical error is smaller than the symbols for Pb compositions of the clay sized fraction of site MD04-2829CQ, there is a significant sample replication error for the Pb isotope compositions (see Section 2.2.4.4) this is illustrated in Figure 5.6 by the black and red crosses showing the replicates from MD04-2829CQ. The Pb isotope compositions of the clay sized terrigenous fraction from the Rosemary Bank site range from 17.67 to 19.02 in $^{206}Pb/^{204}Pb$, from 15.57 to 15.66 in $^{207}Pb/^{204}Pb$, and from 37.58 to 38.93 in $^{208}Pb/^{204}Pb$. At site MD04-2829CQ, the samples are very similar in composition and do not deviate greatly from the best fit line shown in Figure 5.7C. The fit between $^{206}Pb/^{204}Pb$ vs $^{207}Pb/^{204}Pb$ $y = 0.0697x + 14.336$ ($R^2 = 0.9825$) and Figure 5.7D where the fit between $^{206}Pb/^{204}Pb$ vs $^{208}Pb/^{204}Pb$ is described by $y = 1.0072x + 19.805$ and ($R^2 = 0.995$). Four of the samples from H4 and H2 have very high Pb ratios compared to the other samples.

Table 5.3 radiogenic isotope data for core MD04-2829CQ

ID	*Nd*	*Sm*	*Sm/Nd*	$^{143}Nd/^{144}Nd$	*1σ*	*εNd*	*1σ*	*TDm*	*Rb*	*Sr*	*1000/ Sr*	$^{87}Sr/^{86}Sr$	*1σ*	*Pb*	$^{206}Pb/^{204}Pb$	$^{207}Pb/^{204}Pb$	$^{208}Pb/^{204}Pb$	*1σ*	*1σ*	*1σ*
600	32.8	5.2	0.15862	0.5119653	8	-13.12	0.17	1.04	211	106	9	0.735947	15	144	17.68	15.57	37.59	0.0013	0.0012	0.0032
604	-	-	-	0.5119540	9	-13.34	0.17	-	-	-	-	0.735052	15	-	17.82	15.58	37.73	0.0014	0.0015	0.0044
608	35.4	5.7	0.16148	0.5119671	8	-13.09	0.16	1.06	214	112	9	0.738019	17	156	17.67	15.57	37.58	0.0012	0.0012	0.0031
612	-	-	-	0.5119699	10	-13.03	0.20	-	-	-	-	0.736572	18	-	17.85	15.58	37.77	0.0012	0.0012	0.0030
616	-	-	-	0.5119521	9	-13.38	0.17	-	-	-	-	0.736505	17	-	17.72	15.57	37.63	0.0012	0.0012	0.0031
624	-	-	-	0.5119351	7	-13.71	0.14	-	-	-	-	0.737262	17	-	18.09	15.60	38.00	0.0013	0.0015	0.0044
628	34.6	5.6	0.16058	0.5119399	8	-13.62	0.16	1.10	204	113	9	0.738050	15	42	18.10	15.60	38.00	0.0013	0.0015	0.0044
632	-	-	-	0.5119347	10	-13.72	0.19	-	-	-	-	0.736914	17	-	17.88	15.58	37.80	0.0013	0.0014	0.0042
636	-	-	-	0.5119561	10	-13.30	0.20	-	-	-	-	-	0	-	18.23	15.60	38.15	0.0012	0.0014	0.0043
640	17.0	2.7	0.15917	-	0	-	-	-	107	58	17	0.734342	17	21	17.96	15.59	37.88	0.0014	0.0016	0.0047
644	28.9	4.6	0.16007	0.5119413	6	-13.59	0.12	1.09	178	106	9	0.732708	18	54	17.87	15.58	37.79	0.0013	0.0014	0.0043
646	33.5	5.5	0.16268	0.5119575	8	-13.27	0.16	1.08	201	108	9	0.732556	20	25	18.90	15.65	38.84	0.0012	0.0012	0.0032
648	26.3	4.2	0.16047	0.5119487	9	-13.45	0.18	1.08	215	93	11	0.733012	16	58	18.02	15.59	37.95	0.0014	0.0015	0.0047
650	32.9	5.4	0.16489	0.5119796	8	-12.84	0.16	1.06	216	93	11	0.735655	20	28	18.93	15.66	38.81	0.0013	0.0013	0.0034
652	28.9	4.7	0.16111	0.5119665	8	-13.10	0.15	1.06	212	101	10	0.736535	15	44	18.02	15.59	37.94	0.0013	0.0012	0.0032
656	-	-	-	0.5119626	7	-13.17	0.13	-	-	-	-	0.734590	18	-	18.09	15.60	38.02	0.0012	0.0014	0.0041
660	33.0	5.2	0.15819	0.5119726	8	-12.98	0.15	1.03	222	115	9	0.735963	19	42	18.11	15.60	38.04	0.0022	0.0020	0.0053
664	6.5	1.1	0.16356	0.5119581	8	-13.26	0.15	1.09	35	26	39	0.735240	19	7	17.97	15.59	37.89	0.0013	0.0014	0.0044
668	35.3	5.6	0.16020	0.5119590	8	-13.24	0.15	1.06	209	114	9	0.736546	17	39	18.15	15.60	38.08	0.0013	0.0012	0.0033
672	12.3	2.0	0.15923	0.5119665	9	-13.10	0.17	1.05	84	45	22	0.735361	16	43	17.70	15.57	37.63	0.0013	0.0013	0.0033
676	28.2	4.6	0.16334	0.5119834	9	-12.77	0.17	1.05	208	97	10	0.734025	19	66	17.86	15.58	37.79	0.0012	0.0011	0.0030
680	33.6	5.4	0.15911	0.5119712	9	-13.01	0.17	1.04	211	118	8	0.733730	18	67	17.84	15.58	37.77	0.0012	0.0011	0.0030
684	31.3	5.0	0.15928	0.5119773	9	-12.89	0.17	1.03	226	112	9	0.733088	18	32	18.25	15.61	38.20	0.0013	0.0012	0.0032

692	17.0	2.7	0.16024	-	0	-	-	-	111	61	16	0.732821	17	12	-	-	-	-	-	-
696	29.0	4.6	0.15796	0.5119904	8	-12.63	0.16	1.00	214	103	10	0.731551	20	40	18.11	15.60	38.05	0.0013	0.0013	0.0032
700	31.9	5.1	0.16053	0.5119704	10	-13.02	0.19	1.05	220	118	8	0.732795	19	39	18.14	15.60	38.09	0.0012	0.0012	0.0031
704	-	-	-	0.5119861	9	-12.72	0.18	-	-	-	-	0.730456	17		18.23	15.61	38.19	0.0013	0.0012	0.0033
712	30.8	4.9	0.15975	0.5119843	8	-12.75	0.16	1.02	217	108	9	0.732213	18	60	17.97	15.59	37.90	0.0013	0.0015	0.0043
716	29.3	4.6	0.15634	0.5119976	10	-12.49	0.19	0.98	213	109	9	0.731422	18	25	18.32	15.62	38.29	0.0013	0.0012	0.0032
720	14.4	2.4	0.16966	0.5119772	7	-12.89	0.14	1.10	87	51	20	0.730914	14	14	18.59	15.64	38.57	0.0013	0.0016	0.0048
724	28.5	4.6	0.16022	0.5119744	8	-12.94	0.15	1.04	209	103	10	0.730946	15	35	18.18	15.61	38.13	0.0013	0.0012	0.0033
728	30.3	4.8	0.15864	0.5119704	7	-13.02	0.13	1.04	212	110	9	0.731198	19	53	17.94	15.59	37.88	0.0014	0.0015	0.0044
732	29.2	4.6	0.15768	0.5119756	8	-12.92	0.16	1.02	213	100	10	0.731301	18	70	17.90	15.58	37.82	0.0014	0.0016	0.0046
916	32.2	5.2	0.16046	0.5119504	8	-13.41	0.16	1.08	215	119	8	0.732041	16	59	17.88	15.58	37.83	0.0012	0.0011	0.0029
924	27.9	4.5	0.16220	0.5119607	8	-13.21	0.16	1.08	208	112	9	0.732139	15	44	17.86	15.58	37.80	0.0012	0.0012	0.0030
928	-	-	-	0.5119421	8	-13.57	0.16	-	-	-	-	0.732419	17	-	18.34	15.61	38.32	0.0013	0.0015	0.0049
932	31.5	5.2	0.16363	0.5119425	8	-13.57	0.15	1.11	209	123	8	0.732903	14	43	18.01	15.59	37.95	0.0013	0.0012	0.0032
936	30.3	4.9	0.16275	0.5119200	8	-14.01	0.16	1.14	205	115	9	0.735737	15	52	18.01	15.59	37.93	0.0012	0.0012	0.0032
938	32.2	5.3	0.16371	0.5119347	7	-13.72	0.15	1.13	202	111	9	0.736364	16	23	19.01	15.66	38.91	0.0012	0.0012	0.0032
940	28.3	4.6	0.16396	0.5119123	9	-14.16	0.17	1.16	207	112	9	0.739589	20	37	18.19	15.61	38.11	0.0013	0.0012	0.0032
944	29.3	4.7	0.16117	0.5117895	7	-16.55	0.14	1.34	199	138	7	0.736291	21	42	18.07	15.58	38.07	0.0011	0.0013	0.0042
946	31.2	5.0	0.16167	0.5119034	8	-14.33	0.16	1.16	212	112	9	0.735774	16	21	18.97	15.66	38.93	0.0013	0.0012	0.0030
952	29.4	4.7	0.16078	0.5119559	8	-13.30	0.16	1.07	215	111	9	0.734988	16	39	18.07	15.60	38.02	0.0013	0.0015	0.0045
956	28.9	4.7	0.16179	0.5119698	8	-13.03	0.17	1.06	211	103	10	0.733225	19	40	18.06	15.59	38.01	0.0013	0.0012	0.0046
960	33.3	5.4	0.16260	0.5119598	10	-13.23	0.20	1.08	208	121	8	0.733056	20	23	18.43	15.62	38.41	0.0015	0.0015	0.0045
964	12.1	2.0	0.16245	0.5119628	7	-13.17	0.14	1.07	90	51	20	0.733044	14	12	18.40	15.62	38.37	0.0013	0.0015	0.0045
968	28.5	4.6	0.16317	0.5119704	7	-13.02	0.14	1.07	215	105	10	-	0	58	18.28	15.61	38.25	0.0014	0.0016	0.0047
972	35.9	5.9	0.16366	0.5119902	9	-12.64	0.17	1.04	243	118	8	0.732377	17	24	17.87	15.58	37.82	0.0012	0.0012	0.0030

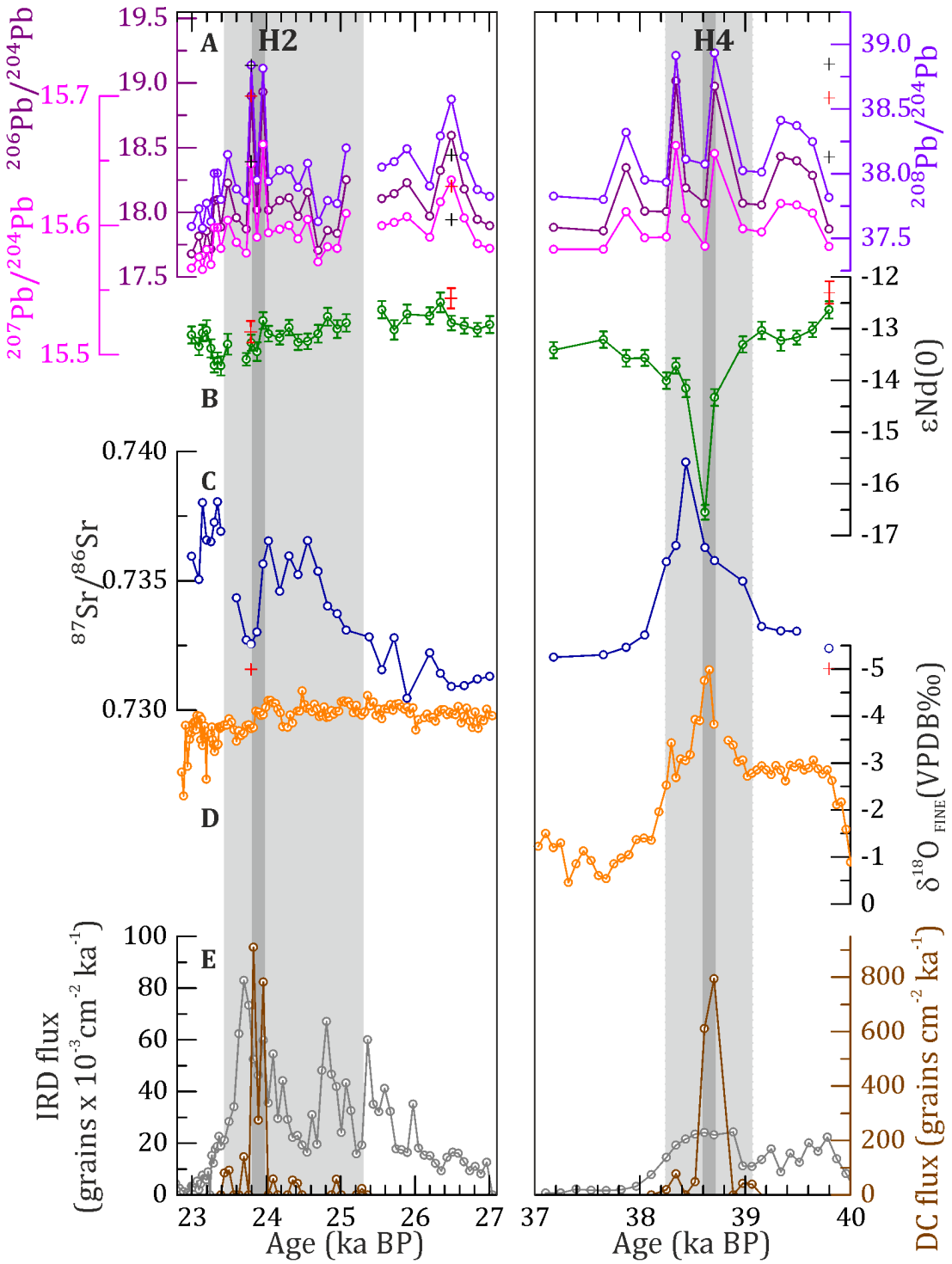

Figure 5.6: Isotope ratios of the clay size terrigenous fraction from Rosemary Bank (site MD04-2829CQ) representing H2 and H4 and the surrounding interval, plotted against age. A; $^{206}Pb/^{204}Pb$ in pink, $^{207}Pb/^{204}Pb$ in purple, $^{208}Pb/^{204}Pb$ in dark purple, B; εNd in green, C; $^{87}Sr/^{86}Sr$ in dark blue, D; $\delta^{18}O_{FINE}$ in orange, E; Total IRD flux in grey and DC flux in brown Hall et al. (2011). Heinrich events are marked in grey. Peak DC input is highlighted in dark grey.

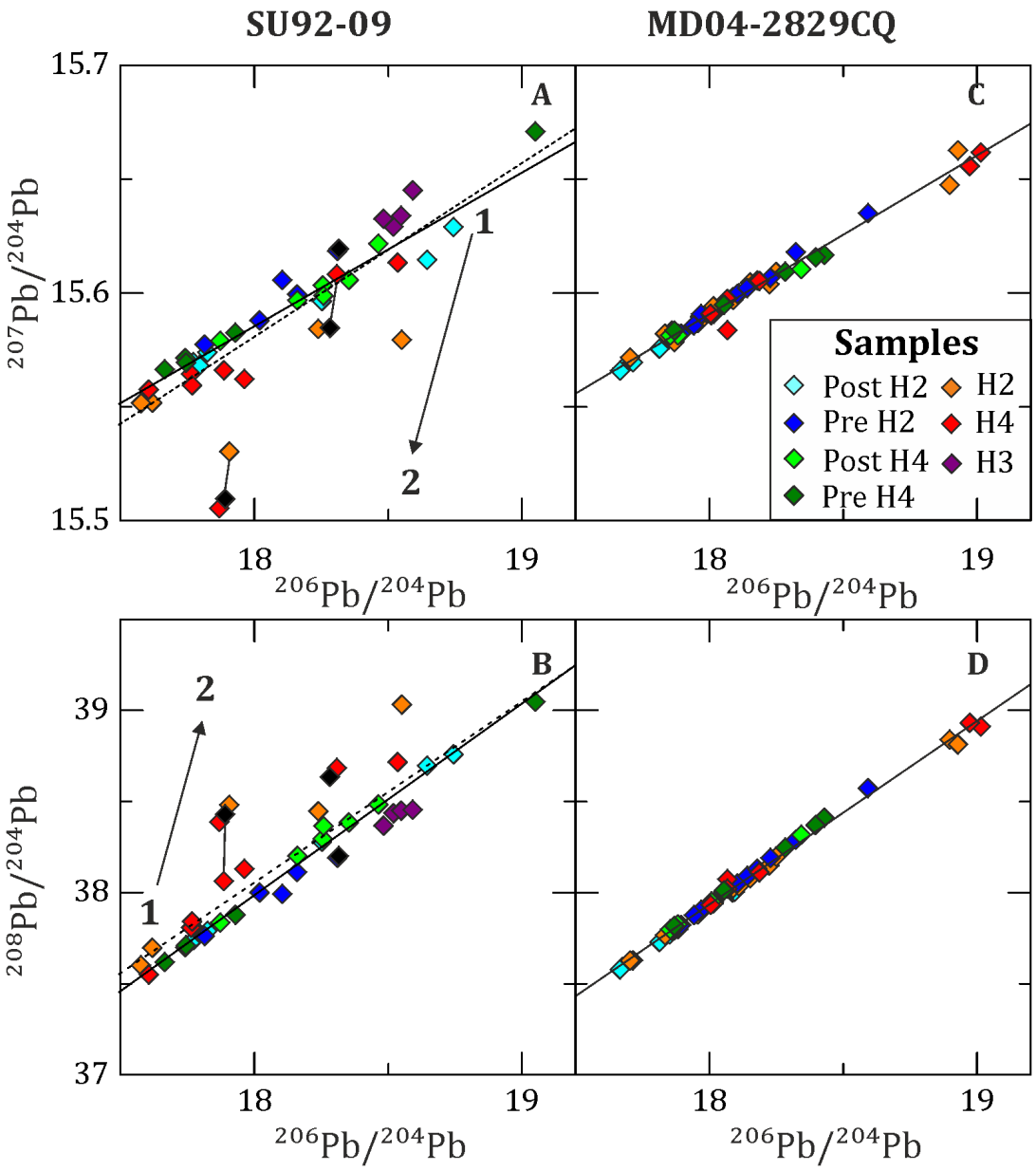

Figure 5.7: Cross-plots of Pb isotope compositions from the clay size terrigenous fraction of sediments from the IRD belt and Rosemary Bank. A; $^{206}Pb/^{204}Pb$ vs $^{207}Pb/^{204}Pb$ from site SU92-09, B; $^{206}Pb/^{204}Pb$ vs $^{208}Pb/^{204}Pb$ from site SU92-09, C; $^{206}Pb/^{204}Pb$ vs $^{207}Pb/^{204}Pb$ from MD04-2829CQ, D; $^{206}Pb/^{204}Pb$ vs $^{208}Pb/^{204}Pb$ from site MD04-2829CQ.

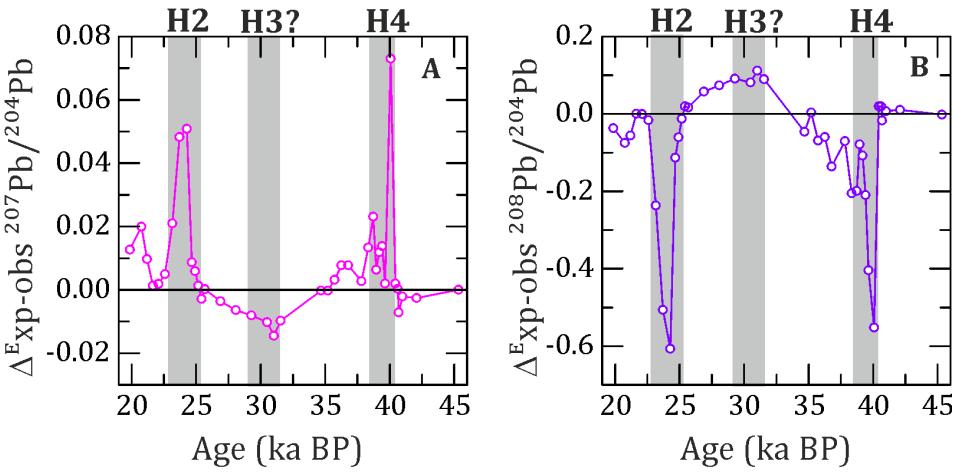

Figure 5.8: plots of the deviation of observed Pb compositions from that expected by the ambient sediment line of site SU92-09 as shown in Figure 5.7. A; ^{207}Pb/^{204}Pb B; ^{208}Pb/^{204}Pb

5.3 Interpretation

5.3.1 Interpreting coarse and fine fraction data; caveats

In both MD04-2829CQ and SU92-09 ratios of $^{87}Sr/^{86}Sr$ are high >0.73 compared to values from the coarse fraction of sites across the North Atlantic which range from 0.72 to 0.73 (see Figure 19 in Hemming, 2004). However, the ratios of $^{87}Sr/^{86}Sr$ in the <2μm fraction from site SU02-09 and MD04-2829CQ compare well to the $^{87}Sr/^{86}Sr$ ratios from the <2μm fraction of site ME-68-89 from the Driezack Seamount in the Western European Basin (Huon and Jantschik, 1993) see Table 5.4. Huon and Jantschik (1993) show that there is a positive offset between the ratios of $^{87}Sr/^{86}Sr$ in the <2μm fraction compared to the $^{87}Sr/^{86}Sr$ ratios in the >63μm from site M6-7A-2441 due to differences in the mineralogy of the sediments across different size fractions (see Figure 5.9). A similar grain size effect on Sr isotopes and concentrations of Rb and Sr has been observed elsewhere (Biscaye and Dasch, 1971; Gaiero, 2007; Garçon et al., 2014).

Table 5.4 $^{87}Sr/^{86}Sr$ ratios from Heinrich events (H-E) and the ambient glacial from <2μm fraction

Core	*H-E $^{87}Sr/^{86}Sr$*	*glacial $^{87}Sr/^{86}Sr$*	*Reference*
MD04-2829CQ	0.734839	0.733615	This study
SU92-09	0.739524	0.733829	This study
ME68-89	0.738235	0.733387	(Huon and Jantschik, 1993)

The causes of the high ratios of $^{87}Sr/^{86}Sr$ in the clay size fraction of the cores in this study compared to those from the North Atlantic is likely mineralogical changes between size fractions. Whilst absolute values may not be comparable between the coarser fractions and the clay sized material, the overall trends are similar between the <2μm fraction material from this study and studies of >63μm fraction material (see Figure 5.16 and Figure 5.17). One approach to reconcile the differences between the coarse and finer fractions is to adjust the $^{87}Sr/^{86}Sr$ of the coarser source region data by a constant (Gaiero, 2007). In Figure 5.9 data are shown from Huon and Jantschik (1993) there is a difference of 0.007 between the <2μm fraction, 2-16μm fraction and the >63μm fraction. Hence, in the absence of <2μm fraction data from the PSA, if the $^{87}Sr/^{86}Sr$ ratios are shifted by 0.007 it is possible to estimate what the source region data may look like in <2μm fraction in Figure 5.12A and Figure 5.13A. However, further analyses from the North Atlantic would be needed to adequately characterise

the difference between the coarser and finer fractions of marine sediments and their source regions.

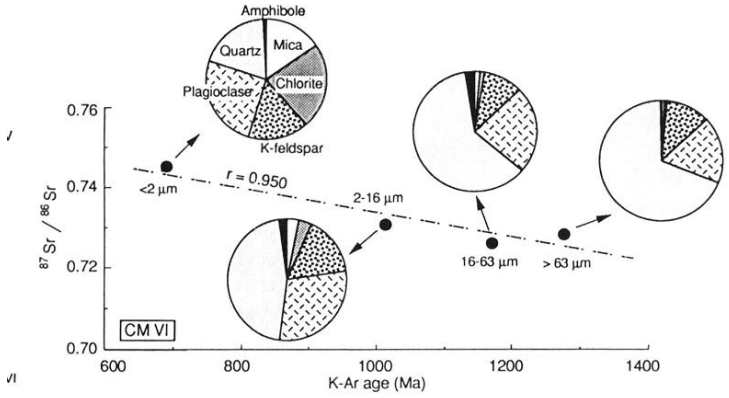

Figure 5.9 The $^{87}Sr/^{86}Sr$ ratio with increasing grain size and changing mineral composition from Huon and Jantschik (1993).

The Pb composition of the <2µm fraction is similar to that of the source regions from Farmer et al. (2003). Yet, it must be noted that Pb tends to be easily biased by substantially more radiogenic heavy minerals such as zircon (Garçon et al., 2014) and therefore is also subject to a grain size effect. The Pb data could be affected by differential settling, as replicates did not compare well with original samples after resettling (Section 2.2.4.4). As the most radiogenic Pb isotope values from core SU92-09 and MD04-2829CQ are from resettled samples (values of $^{206}Pb/^{204}Pb$ above 19 in all cases), the interpretation of these samples should be treated with caution until further repeat analyses can be conducted. However, the same effect was not observed in Nd and Sr isotope ratios, as shown replicate analyses are shown in Figure 5.6 and Figure 5.7.

5.3.2 Radiogenic isotope provenance of clay sized fraction of North Atlantic sediments

5.3.3 Ambient glacial sediments

At site SU92-09, ambient glacial clay sized sediments prior to H2 and H4 and during the H3 interval have high εNd (>-17), and high $^{87}Sr/^{86}Sr$ ratios (>0.735) and after H2 and H4 εNd is high (>-17) and $^{87}Sr/^{86}Sr$ ratios are low <0.737 (Figure 5.5). The modelled age (T_{DM}) see Table 5.2, for ambient glacial sediments, based on the $^{143}Nd/^{144}Nd$ and $^{147}Sm/^{144}Nd$ ratios (see Chapter 2) from the ambient glacial sediments

are consistent with an apparent age of <1.4 Ga, Mesoproterozoic age. When compared to Nd and Sr isotope data from PSA as in Figure 5.10, it is evident that the ambient glacial sediments from post Heinrich event intervals are similar in composition to the TMFs of the Gulf of Saint Lawrence sector of the LIS and the Fennoscandian ice sheet (FSIS) Figure 5.10. Further support of the European source/ southern LIS source region for ambient glacial sediments is derived from the Pb isotope ratios of the ambient glacial sediments, which are also similar to that of GSL and FSIS sediments Figure 5.11.

Ambient glacial clay-sized sediments from the Rosemary Bank site MD0428-29CQ have high εNd >-13 and $^{87}Sr/^{86}Sr$ ratios between 0.731 and 0.74 Figure 5.5 when compared to PSAs the ambient glacial sediments are most similar to the source regions of the Northern European margins, particularly the British Isles, Irish Sea and Bay of Biscay PSA. The Pb isotope ratios of the ambient glacial sediments from Rosemary Bank are almost identical to the Pb isotope ratios of the ambient sediments from the IRD belt site, and indicate a GSL/FSIS source.

5.3.4 Heinrich event 4

The <2μm fraction from core SU92-09 during H4 typically exhibits low εNd < -19, and $^{87}Sr/^{86}Sr$ values between 0.735 and 0.740, similar to the Baffin Bay PSA Figure 5.10. The T_{DM} apparent age for these sediments is 1.8 to 2.1 Ga, Paleoproterozoic in age, which is similar to ages derived from Baffin Bay (Farmer et al., 2003). The Pb isotope compositions during H2 and H4 of the clay size fraction of SU92-09 shift towards higher $^{208}Pb/^{204}Pb$ values and lower $^{207}Pb/^{204}Pb$ relative to the ambient glacial sediments (Figure 5.11). This shift moves the sediments towards the ratios of the Baffin Bay PSA and Hudson Strait PSA (red and pink envelope in Figure 5.11) which is based on data from Farmer et al. (2003).

At Rosemary Bank, during H4, clay size fraction εNd values are high (-14 to -13) similar to the εNd values for British Isles reported in Revel et al. (1996) between (-10 and -13.5). However, at 38.62 ka BP (sample 644) there is a small change from values of -14 to -16 closer to that of the Baffin Bay sediments. This small change coincides with peaks in DC IRD (Figure 5.6) thought to be of LIS origin is coeval with the lowest values of $\delta^{18}O_{FINE}$. Therefore, this could represent a small input of LIS material

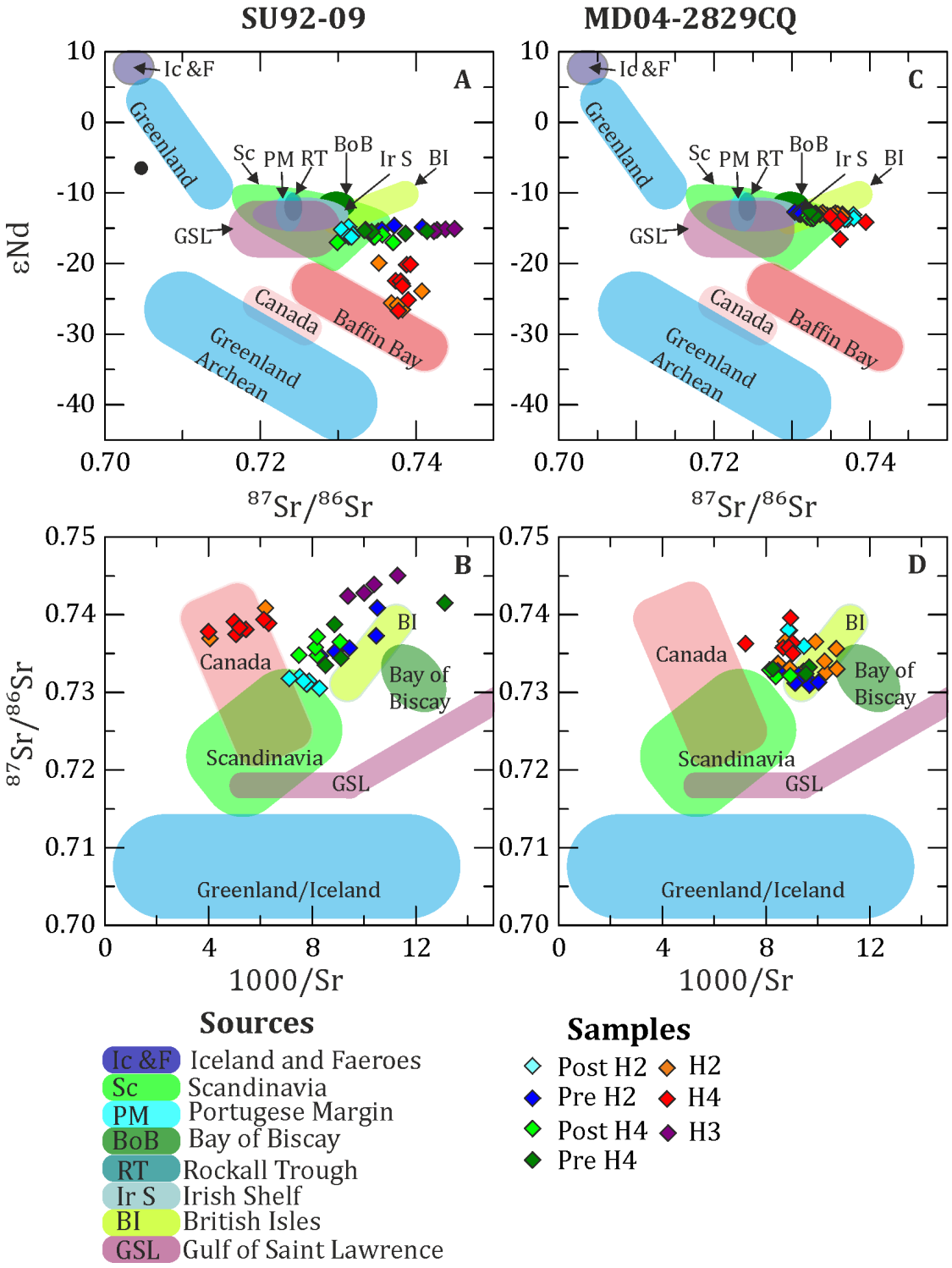

Figure 5.10 Sr and Nd isotope compositions of <2μm fraction samples from site SU92-09 and site MD04-2829CQ plotted alongside envelopes of simplified potential source regions see Appendix 4 and Figure 5.2 for original PSA data.

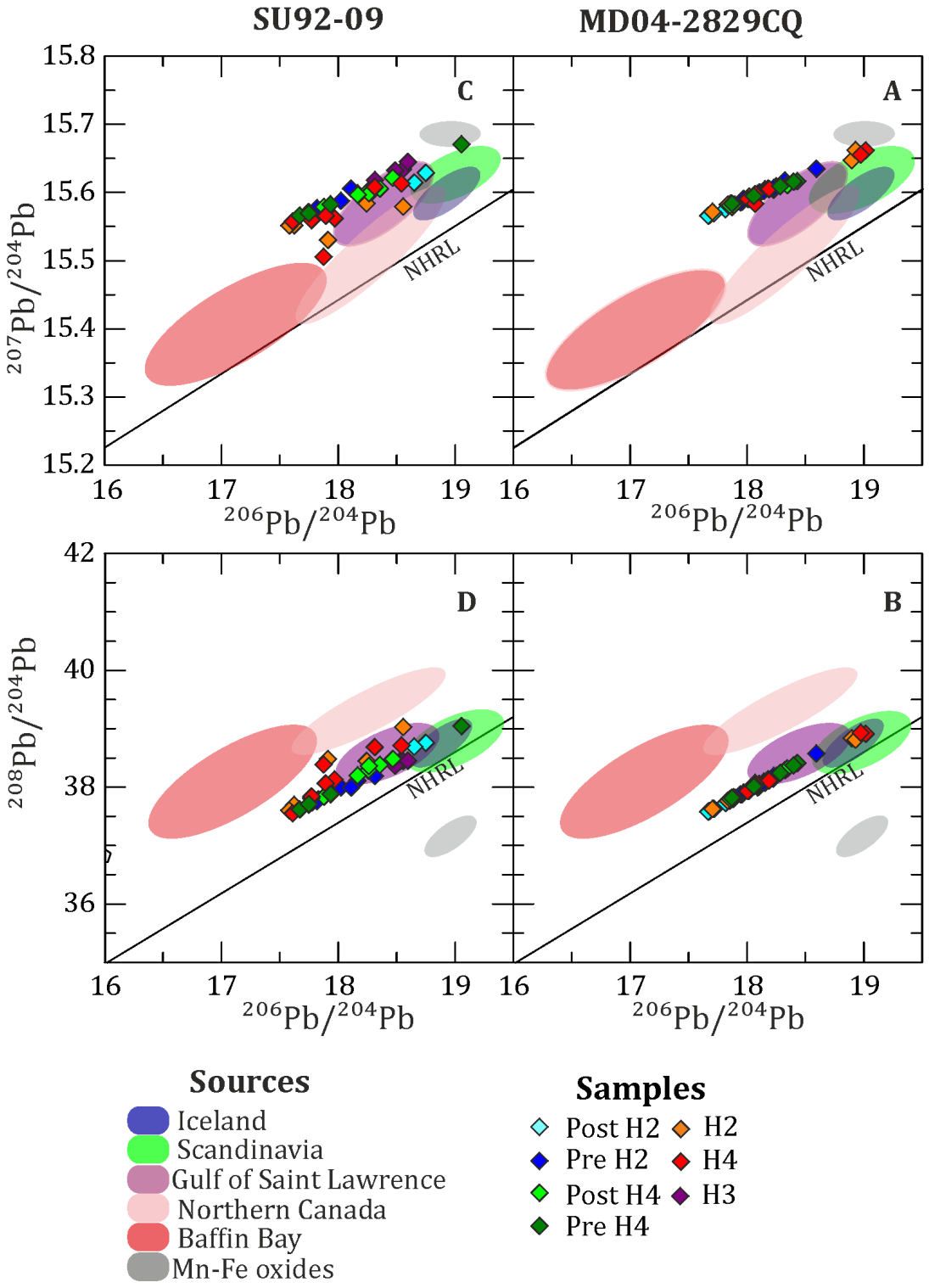

Figure 5.11 Pb isotope ratios of the <2µm fraction form core SU92-09 (A and B) and MD04-2829CQ (C and D) with the envelopes of simplified source region data see Figure 5.3 for original data (Farmer et al., 2003). A and C; $^{206}Pb/^{204}Pb$ vs $^{207}Pb/^{204}Pb$ B and D; $^{206}Pb/^{204}Pb$ vs $^{208}Pb/^{204}Pb$.

mixing with the British ice sheet material, though it is also possible that the lower εNd is from a more local source.

5.3.5 Heinrich event 2

Like H4 at the IRD belt site SU92-09, H2 is characterised by low εNd <-19, and $^{87}Sr/^{86}Sr$ values between 0.735 and 0.74 and deviations in Pb similar to a Baffin Bay/ Hudson Strait source. At the Rosemary Bank site this is not the case, during H2 there is no change in the isotope ratios of the clay sized fraction compared to the ambient glacial and the Nd and Sr isotope ratios conform to those of a British Isles source region.

5.3.6 Sediment mixing

In section 5.3.2 it was established that at least two sources are needed to explain the variation in Nd and Sr isotopes between the ambient glacial sediments and H2 and H4 at site SU92-09. A third source is required to explain the high Sr values observed during H3. Figure 5.12A and Figure 5.12B show that mixing occurs along two axes. Therefore, a three end member model is required. The end member compositions were calculated so that mixing curves produce fields that envelop all of the Sr and Nd isotope and concentration data each core. These end members can then be compared to the average compositions of end members from Table 5.1 to assess the likely source. The three end members are as follows, one similar to the Scandinavian PSA representing inputs from the Fennoscandian ice sheet (FSIS) or GSL PSA representing a Gulf of Saint Lawrence LIS source , another source similar to the Baffin Bay PSA representing sediments from the Hudson Strait sector of the LIS (LIS (HS)) and a third sediment source with high $^{143}Nd/^{144}Nd$ ratios, higher Sr concentrations and $^{87}Sr/^{86}Sr$ than the PSAs described, are illustrated in Figure 5.12A and Figure 5.12B. The final compositions of the end members used for site SU92-09 are shown in Table 5.5. As the end members are approximate, there is a large uncertainty associated with the end members (differences between the end member in the model and the PSA values (Figure 5.12).

Table 5.5 Site SU92-09 end members

End member	*Sr ppm*	*$^{87}Sr/^{86}Sr$*	*Nd ppm*	*$^{143}Nd/^{144}Nd$*
EM1	100	0.7230	15	0.5119
EM2	280	0.7380	28	0.5110
EM3	83	0.7550	28	0.5120

The contributions of the sources (end members) to each sample are shown in the ternary diagram in Figure 5.12C and Table 5.6, the mixing model demonstrates a 38 to 83% contribution to the clay size fraction during H2 and H4 from the LIS (HS) source area. During ambient glacial conditions, sedimentary inputs are a mixture of EM3 and FSIS/GSL sourced sediments. When viewed over time in Figure 5.12B it is evident that the LIS (HS) is only dominant during H2 and H4. It should be noted that H2 is only represented by two data points as trace element data for Nd and Sr was not available for all of the samples from this interval. The FSIS/GSL sediment source is most abundant just prior to H4 and H2 and the undefined end member is most abundant during H3, and after H4, and after H2. This undefined endmember is similar in composition to European sources but has much higher Sr isotope values. Though there is a great deal of uncertainty in the end member model it summarises the initial comparisons between the PSAs and the isotope compositions in Section 5.3.2.

Table 5.6 End member proportions for site SU92-09

Depth (cm)	*Age (ka BP)*	*Heinrich Event*	*EM-1 FSIS/ GSL*	*EM2 LIS (HS)*	*EM3 undefined*
48	19.865		0.2	0.2	0.6
52	20.758		0.15	0.23	0.62
54	21.204		0.31	0.19	0.5
56	21.65		0.23	0.16	0.61
58	22.097		0.15	0.21	0.63
60	22.599		0.31	0.26	0.44
62		H2	-	-	-
64	23.715	H2	0.46	0.36	0.18
66	24.273	H2	0.15	0.81	0.03
68		H2	-	-	-
70		H2	-	-	-
72	25.172		0.23	0.16	0.61
74	25.42		0.46	0.11	0.43
76	25.668		0.38	0.08	0.53
78	26.877		0.54	0.02	0.45
80	28.086		0.46	0.02	0.52
82	29.295	H3	0.15	0.07	0.78
84	30.504	H3	0.15	0.05	0.8
86	31.027	H3	0.31	0	0.69
88	31.55	H3	0.4	0.11	0.89
100			-	-	-
102	35.209		0.15	0.18	0.67
104	35.732		0.31	0.17	0.52
106	36.255		0.23	0.23	0.54
108			-	-	-
112	37.823		0.38	0.16	0.45
114	38.346		0.23	0.36	0.41
116			-	-	-
118	38.956	H4	0.23	0.56	0.21
120	39.189	H4	0.38	0.48	0.14
122	39.422	H4	0.15	0.58	0.26
124	39.654	H4	0.15	0.54	0.31
128	40.073	H4	0.15	0.83	0.02
132	40.445	H4	0.23	0.39	0.38
134	40.631	H4	0.31	0.12	0.57
136			-	-	-
138			-	-	-
140	42.086		0.69	0.08	0.23
146	45.337		0.54	0.12	0.34

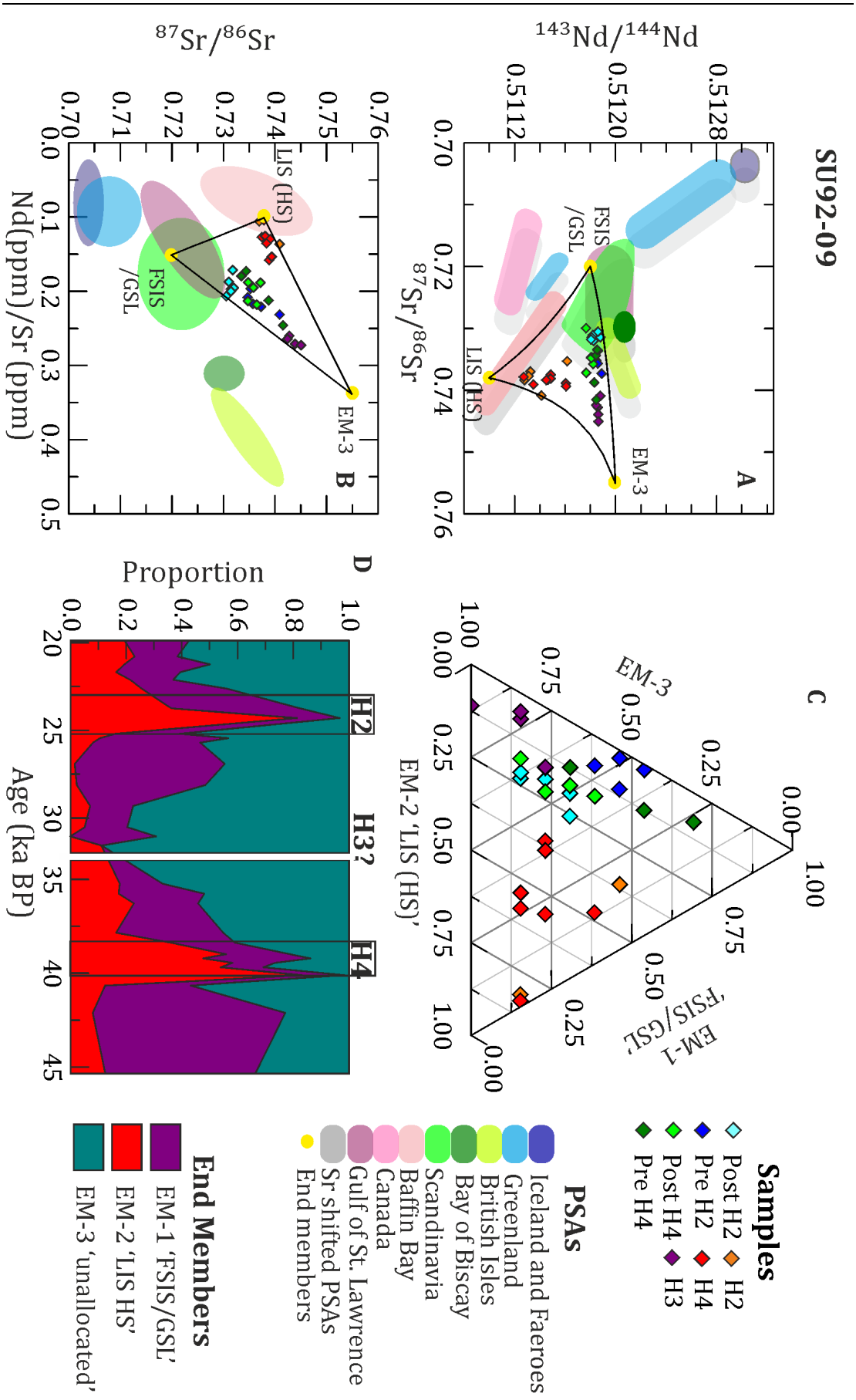
SU92-09
A
$^{143}Nd/^{144}Nd$
$^{87}Sr/^{86}Sr$
FSIS /GSL
LIS (HS)
EM-3
B
$^{87}Sr/^{86}Sr$
Nd(ppm)/Sr (ppm)
C
EM-3
EM-2 'LIS (HS)'
EM-1 'FSIS/GSL'
D
Proportion
Age (ka BP)
H2
H3?
H4
Samples
Post H2
Pre H2
Post H4
Pre H4
H2
H4
H3
PSAs
Iceland and Faeroes
Greenland
British Isles
Bay of Biscay
Scandinavia
Baffin Bay
Canada
Gulf of St. Lawrence
Sr shifted PSAs
End members
End Members
EM-1 'FSIS/GSL'
EM-2 'LIS HS'
EM-3 'unallocated'

Figure 5.12: Mixing model for site SU92-09. A; $^{143}Nd/^{144}Nd$ and $^{87}Sr/^{86}Sr$ ratios of <2µm fraction illustrating the end members used grey areas are PSAs with $^{87}Sr/^{86}Sr$ ratios shifted by 0.007. B; $^{87}Sr/^{86}Sr$ and Nd concentrations/Sr concentrations illustrating end members. C; Ternary plot of the samples relative to their end members. D; End member proportions over time.

The isotope ratios of site MD04-2829CQ can be described by mixing between two sediment sources. The first sediment source is similar in composition to samples from the BIIS PSA and the second is more similar to the isotope composition of sediments from the FSIS/GSL PSA (Figure 5.13A and ***Figure 5.13***B). However, one sample from H4 has lower εNd values than the other samples from site MD04-2829CQ and based on the inputs of detrital carbonate at the same time (Section 5.3.2) this is thought to be due to an input from the Hudson Strait of the LIS. Hence, the LIS (HS) end member was included in this model to judge if this is possible. The model end member compositions are shown in Table 5.7 and the proportions of each end member contributing to each sample is shown in Table 5.8. The proportion that each sediment source contributes to the mixing is shown in Figure 5.13C and Figure 5.13D. The proportions show that the sediments comprise largely of a British source mixing (40 to 89%) with a FSIS/GSL source, the FSIS is the more likely candidate due to the proximity of the FSIS relative to the GSL to site MD04-2829CQ. Prior to H4 the FSIS source dominates, during H4 the British source dominates but there is a small contribution from the LIS (HS) of 30%. The contribution of the LIS (HS) is ~ 10-20% in the ambient glacial, this indicates that the 'Canadian' signal is in part due to a local provenance. During H2 the main component is the BIIS source accounting for 35-89% of the isotope signal during H2.

Table 5.7 Site MD04-2829CQ end members

End member	*Sr ppm*	*$^{87}Sr/^{86}Sr$*	*Nd ppm*	*$^{143}Nd/^{144}Nd$*
EM1	80	0.7265	25	0.512
EM2	280	0.74	26	0.5111
EM3	90	0.74	40	0.512

Table 5.8 modelled end member contributions of sediments from MD04-2829CQ

Depth (cm)	*Age (ka BP)*	*Heinrich event*	*EM1 BIIS*	*EM-2 LIS (HS)*	*EM-3 FSIS/ GSL*
600	22.995		0.41	0.11	0.48
604			-	-	-
608	23.143		0.21	0.15	0.64
612-624			-	-	-
628	23.345		0.26	0.16	0.59
632-640			-	-	-
644	23.731	H2	0.67	0.11	0.22
646	23.799	H2Peak	0.35	0.12	0.53
648	23.876	H2Peak	0.89	0.03	0.08
650	23.956	H2Peak	0.45	0.03	0.52
652	24.032	H2	0.69	0.08	0.23
656		H2	-	-	-
660	24.307	H2	0.36	0.17	0.47
668	24.559	H2	0.21	0.17	0.63
676	24.827	H2	0.75	0.06	0.2
680	24.953	H2	0.30	0.19	0.51
684	25.077	H2	0.48	0.15	0.37
692			-	-	-
696	25.554		0.67	0.09	0.23
700	25.720		0.41	0.19	0.4
704			-	-	-
712	26.200		0.53	0.12	0.35
716	26.344		0.63	0.13	0.25
724	26.662		0.70	0.09	0.2
728	26.839		0.56	0.13	0.31
732	27.006		0.68	0.07	0.25
916	37.181		0.39	0.20	0.42
924	37.653		0.70	0.15	0.14
928			-	-	-
932	38.046		0.42	0.22	0.36
936	38.253	H4	0.53	0.18	0.3
938	38.342	H4	0.43	0.14	0.43
940	38.437	H4	0.67	0.16	0.17
944	38.620	H4Peak	0.49	0.33	0.18
946	38.710	H4Peak	0.49	0.16	0.36
952	38.978	H4	0.61	0.15	0.24
956	39.157		0.68	0.10	0.22
960	39.338		0.31	0.21	0.49
968			-	-	-
972	39.798		0.15	0.19	0.67

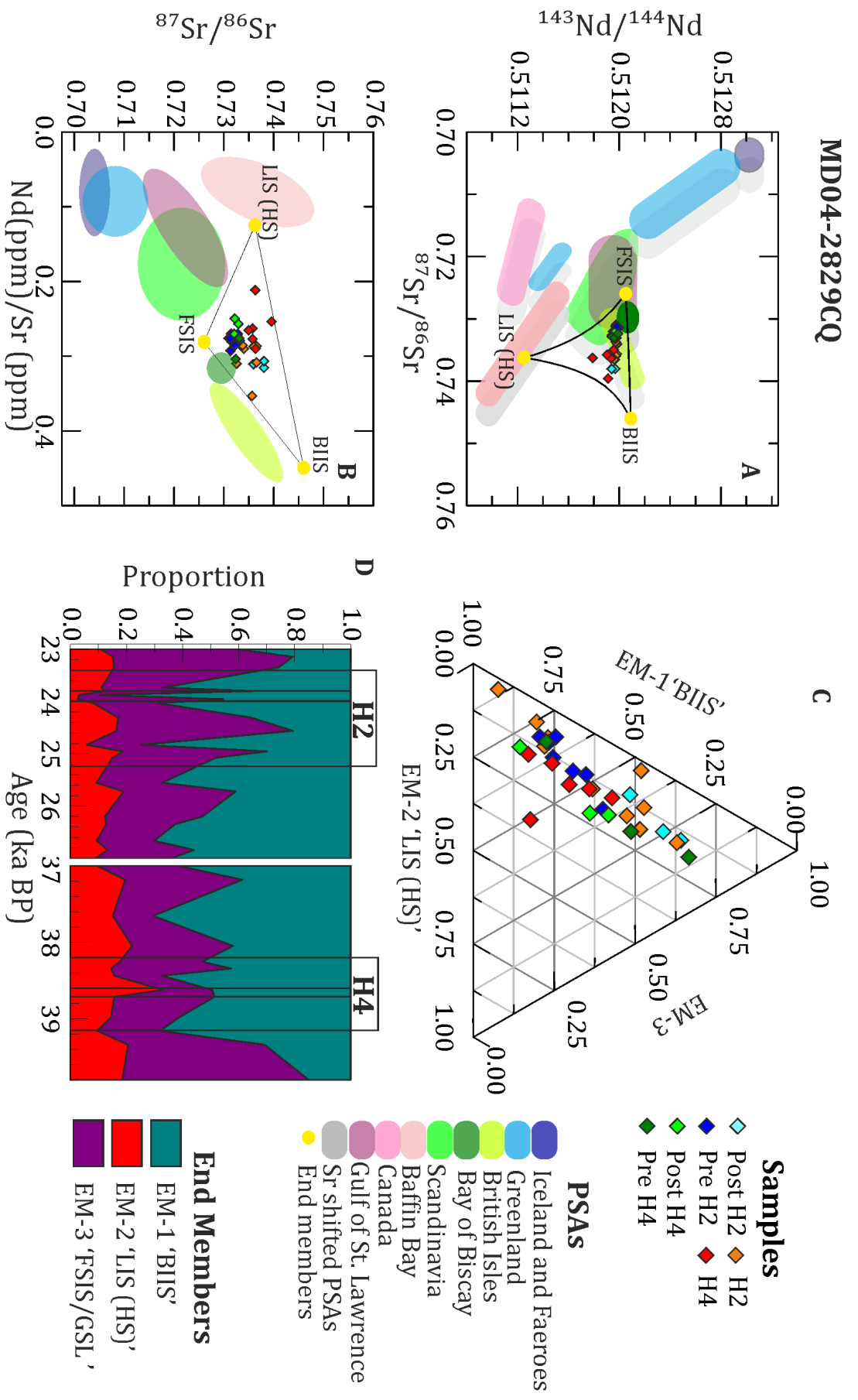
MD04-2829CQ
A
B
C
D
$^{143}Nd/^{144}Nd$
$^{87}Sr/^{86}Sr$
Nd(ppm)/Sr (ppm)
LIS (HS)
FSIS
BIIS
EM-1 'BIIS'
EM-2 'LIS (HS)'
EM-3 'FSIS/GSL'
Proportion
Age (ka BP)
H2
H4
Samples
Post H2
Pre H2
Post H4
Pre H4
PSAs
Iceland and Faeroes
Greenland
British Isles
Bay of Biscay
Scandinavia
Baffin Bay
Canada
Gulf of St. Lawrence
Sr shifted PSAs
End members
End Members
EM-1 'BIIS'
EM-2 'LIS (HS)'
EM-3 'FSIS/GSL'

Figure 5.13: Mixing model for site MD04-2829CQ. A; $^{143}Nd/^{144}Nd$ and $^{87}Sr/^{86}Sr$ ratios of <2µm fraction illustrating the end members used. B; $^{87}Sr/^{86}Sr$ and Nd/Sr concentrations illustrating end members. C; Ternary plot of the samples relative to their end members. D; End member proportions over time.

5.4 Discussion

The following discussion places the provenance of the clay-sized fraction IRD into a regional context for each Heinrich event. The first section of the discussion examines the veracity of using the fine fraction for IRD provenance by comparing the results presented in this chapter with the other coarse fraction data from sites around the North Atlantic and British and Irish margin. The second section examines the implications for using the fine fraction data to elucidate changes in ice volumes and aid in characterisation of the mechanisms that create Heinrich events.

5.4.1 IRD Provenance in the clay size fraction

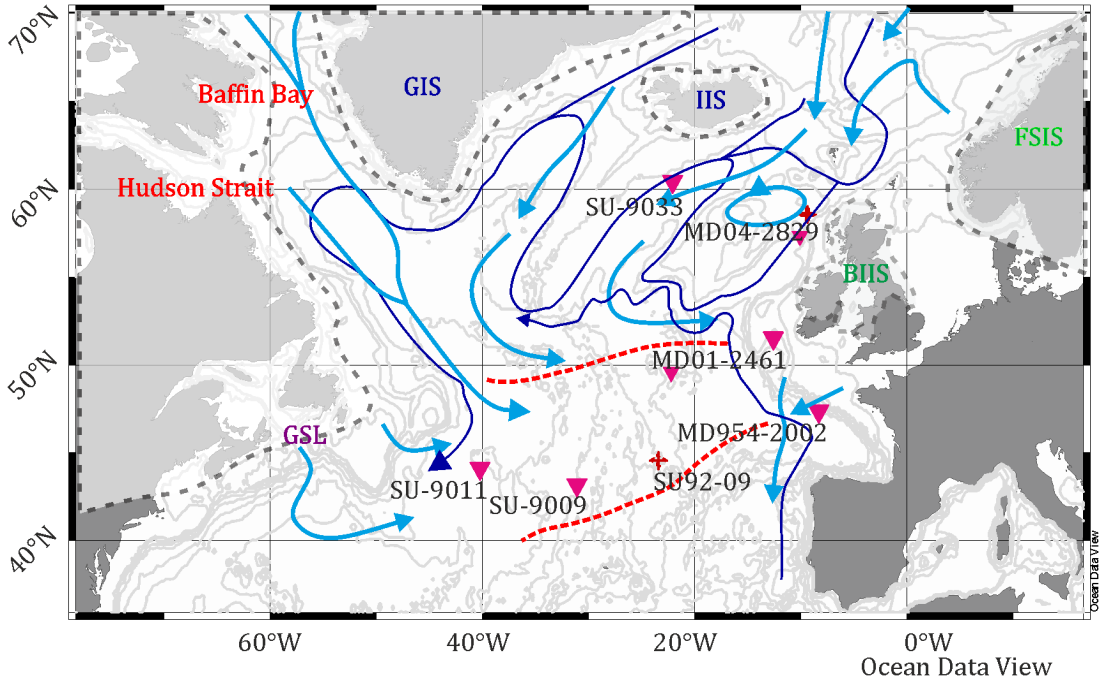

Figure 5.14: Map showing sites referred to in this discussion (pink triangles). Mean IRD pathways in the surface ocean (light blue), and the IRD belt (red) redrawn from (Ruddiman, 1977) bottom currents (dark blue) from Fagel et al. (2004).

Section 5.3.2 demonstrated that the clay-sized radiogenic isotope data from the IRD belt site (SU92-09) is best described by three sources, A GSL/FSIS source during the ambient glacial, and a Hudson Strait/Baffin Bay source during H2 and H4. A further end member, EM3, does not correspond to a PSA but does aid in constraining the mixing between PSAs during the ambient glacial, this end member has high $^{87}Sr/^{86}Sr$

ratios, >0.74 which is similar to those recorded in the western Atlantic during H3 (0.7425) (Hemming, 2004). The data provided from the clay size fraction from the IRD belt in this study is consistent with the Hudson Strait source of the coarser <63 and >63μm fraction across the North Atlantic during H2 and H4 (Revel et al., 1996; Grousset et al., 2001; Hemming, 2004; Jullien et al., 2006).

Table 5.9: The sources and locations of sites referred to in the discussion

Site	Location		water depth (m)	age range kaBP	Size fraction	Sources
SU90-11	Milnes Seamount	44°04N, 40°2 W	3645		Bulk	Revel et al., 996; Jullien et al., 2006)
SU90-09	Mid-Atlantic Ridge	43°.05N, 31°.05W	3375		<63μm	(Grousset et al., 2001)
SU92-09	Eastern Mid Atlantic Ridge	44°60N 23°39W	3270	19-46	<2μm	This study
MD95-2002	Biscay Seamount	47°45′N, 8°53′W	2174		>150μm	(Auffret et al., 2002)
MD01-2461	Porcupine Bank	51°45′N, 12°55′W	1153		>150μm	(Peck et al., 2007)
MD04-2829	Rosemary Bank	58º57'N; 09º34'W	1743		<2μm	This study
SU90-33	Iceland Basin	60°34N 22°05W	2400		Bulk	(Revel et al., 1996)
V28-82	Eastern mid Atlantic	49°27'N 22°16'W	3935	H1-H11	<63μm	(Hemming et al., 1998)
MD95-2006	Barra Fan	57°01'N 10°03'W	2120	20-48	<63μm	(Leigh, 2007)

The Nd-Sr-Pb isotope data from the IRD belt site in this study has substantiated previous assertions in Hemming et al. (2002). Hemming et al. (2002) demonstrated using $^{40}Ar/^{39}Ar$ dates that sediments deposited during Heinrich events are dominated by sediment inputs from the Hudson Strait sector of the Laurentide ice sheet, even in the clay size fraction. This also aptly demonstrates the viability of the clay-sized fraction as a proxy for glaciogenic inputs during the last glacial, and is further supported by the position of the site to the east of the Mid-Atlantic Ridge (MAR), at 3270 m water depth. The MAR is likely to preclude inputs from bottom currents

derived from the LIS as it acts as a topographical barrier to nepheloid layers (Bout-Roumazeilles et al., 1999).

The Pb isotope data from this study when compared with potential source regions for site SU92-09 (Figure 5.7) demonstrate that during both H2 and H4 the Pb isotope ratios of the sediments shift away from the European sources which characterise the source region during the ambient glacial. Though comparable bulk Pb isotope analyses are sparse, where data is available for the <63 across the North Atlantic, a more dramatic shift to lower $^{206}Pb/^{207}Pb$ and lower $^{207}Pb/^{204}Pb$ is observed (Figure 5.15B). It should be noted that the change in Pb isotope ratios from the Barra Fan and V28-82 in the IRD belt are more extreme than is seen in the IRD belt and at site MD042829CQ in the clay size fraction. This could be partly due to changing mineralogy in different size fractions (Garçon et al., 2014).

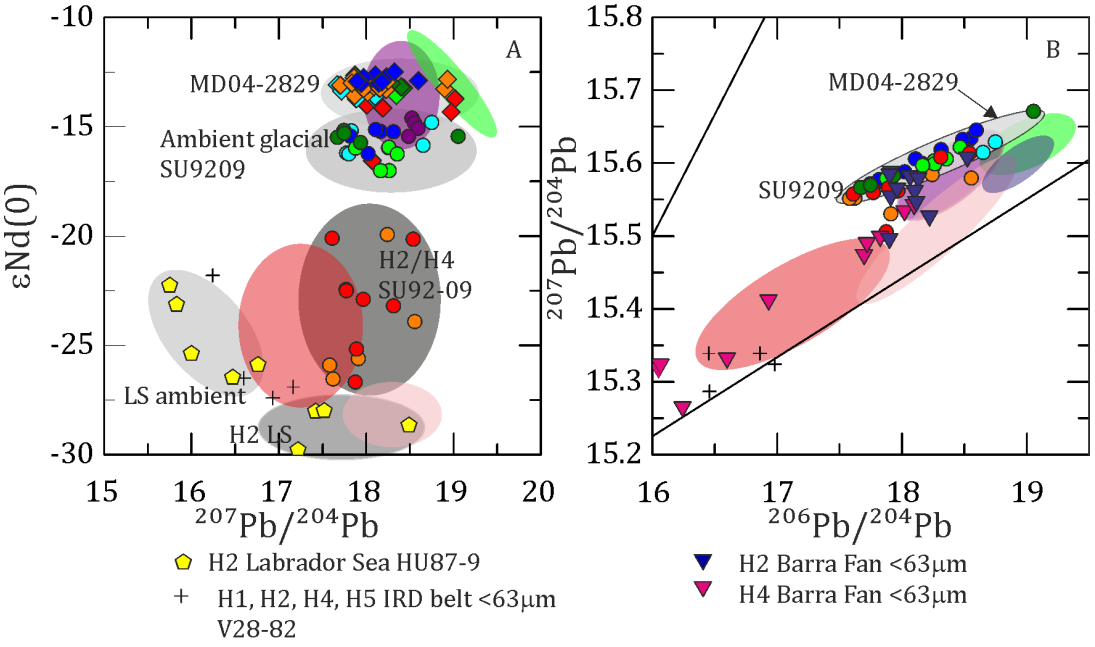

Figure 5.15 Differences between 63 and <2 μm fraction in North Atlantic sites. A εNd vs $^{206}Pb/^{204}Pb$ and B: $^{206}Pb/^{204}Pb$ $^{207}Pb/^{204}Pb$. <2μm fraction from site SU92-09 and MD042828CQ and <63μm fraction from HU87-9 (Barber, 2001; Benson et al., 2003) V28-82 (Hemming et al., 1998) and Barra Fan (Leigh, 2007) and source region envelopes from Figure 5.3**.**

5.4.2 Changing IRD sources over Heinrich event 4 across the North Atlantic

Prior to the H4 interval at site SU92-09 in the IRD belt there is a constant supply from a Scandinavian/GSL source as this study detected in analysis of the interval preceding H4. However this FSIS/GSL input does not constitute a 'European

precursor' but implies a background input, as demonstrated by the low total IRD % at the site prior to H4. (Figure 5.4). The contributions of the Canadian source to the clay-sized fraction correlate well with the increase in inputs of IRD to the coarse fraction and decreases in $\delta^{18}O_{FINE}$ H4. This is consistent with the low Nd and high Sr isotope ratios observed in sites across the North Atlantic (Hemming, 2004). Both site SU90-11, from the western edge of the IRD belt, and MD95-2002 from the eastern edge of the IRD belt, have εNd <-25 and $^{87}Sr/^{86}Sr$ in excess of 0.728 (Figure 5.14, Figure 5.16). During H3 there is an increase in an end with a high Sr isotope ratio and similar εNd values to the European PSA. This could be evidence of a European source, the undefined source shows a similar pattern to that of Si/Sr curve from site U1308 (Channell et al., 2012), which they use as an indicator of detrital silicate and low carbonate inputs.

At the Rosemary Bank site during H4, the isotopic values for εNd and $^{87}Sr/^{86}Sr$ indicate a small input of material of Canadian provenance and increasing contributions from the BIIS. Coarse (>150μm) fraction lithic counts demonstrate an increase in LIS sourced material during H4 which accounts for a maximum of 3.2% of the total coarse fraction IRD at the Rosemary Bank site (Hall et al., 2011). Nd and $^{87}Sr/^{86}Sr$ isotope measurements on coarse fraction material from the margins of the BIIS including sites at the Biscay Seamount, and Porcupine Bank demonstrate that in the coarser fractions there is a significant contribution from a low εNd (-30) and high $^{87}Sr/^{86}Sr$ (0.728) source, consistent with an input from the LIS reaching the margins of the BIIS through ice rafting during H4. Further evidence from the Barra fan also demonstrates a LIS sourced input to the <63μm fraction during H4 using Sr, εNd (-33) and Pb data (Leigh, 2007). However, H2 differs markedly from H4 with high εNd (-12 to -13) and high $^{87}Sr/^{86}Sr$ (0.735 -0.737). This indicates the dominance of BIIS contribution and no LIS input, contrasting not only with the results of H4 from this core (Hall et al., 2011), but also with H2 data from the coarse fraction at the Rosemary Bank site in the North Atlantic and British margin. Across the North Atlantic and at the British Margin, H2 is characterised by increases in the $^{87}Sr/^{86}Sr$ and decreases in εNd values below -16 consistent with a Hudson Strait source (Revel et al., 1996; Hemming et al., 1998; Revel et al., 1996; Snoeckx et al., 1999; Grousset et al., 2001; Peck et al., 2007; Leigh, 2007; Haapaniemi et al., 2010) (Figure 5.16 and Figure 5.17).

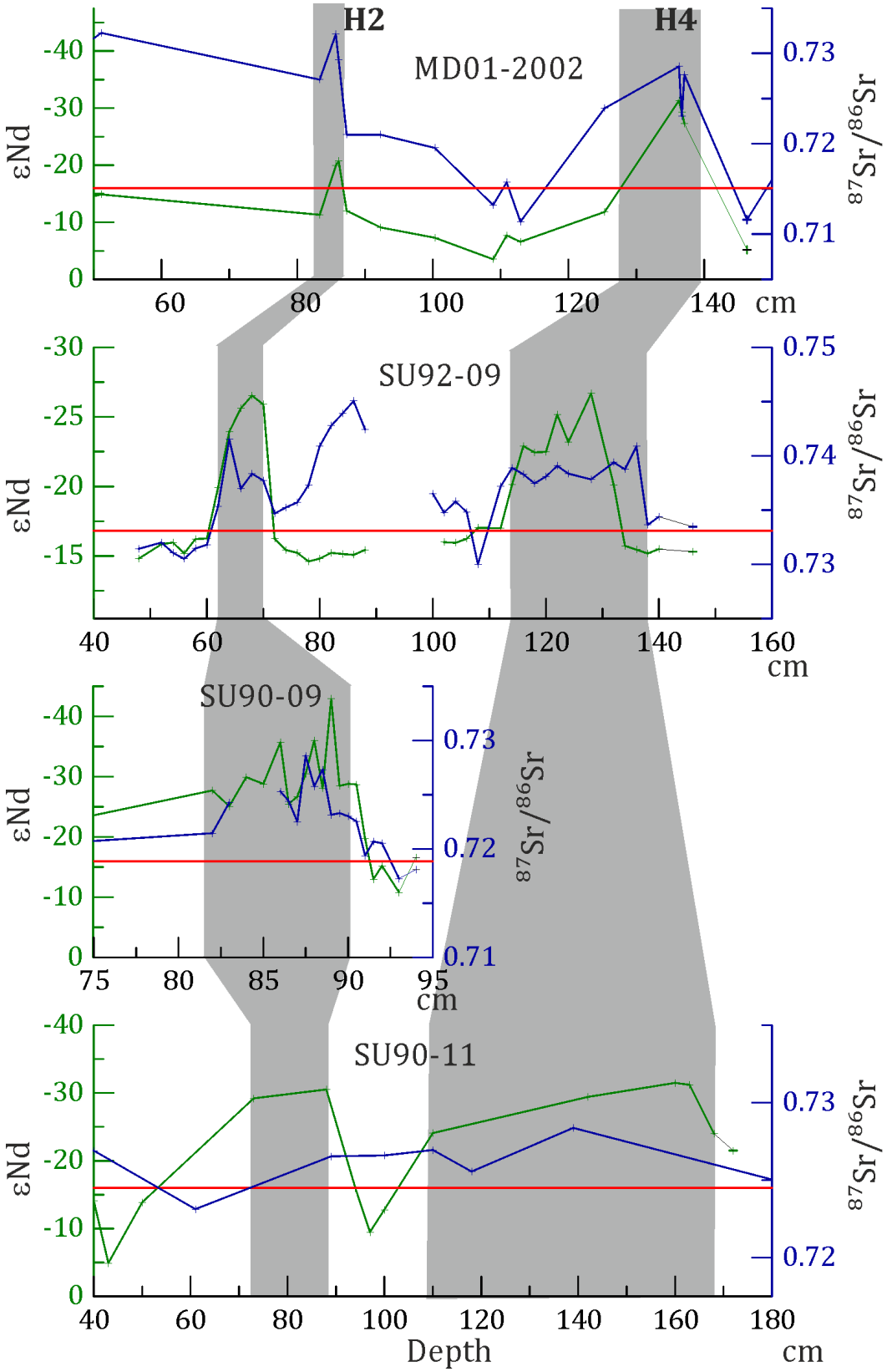

Figure 5.16 εNd and $^{87}Sr/^{86}Sr$ from selected sites along an East to west gradient in the IRD belt, sites are shown in Figure 5.14 ***and data sources are shown in Table 5.9 red line indicates εNd values of -16 thought to deliniate between a Canadian and European source.***

Differences in isotope values between the <2μm fraction and the coarser fractions along the British Margin during H2 and H4 are attributed to variations in grain size and depositional setting, as a function of glacial conditions. Evidence from the British margin suggests that the BIIS was smaller during marine isotope stage 3 (57-29 ka BP) in which H4 occurs (Lisiecki and Raymo, 2005). For example, IRD counts from sites at the Porcupine Seabight, and Barra Fan (Knutz et al., 2001; Peck et al., 2007; Scourse et al., 2009) indicate an intermittent presence of the BIIS throughout MIS 3. H2 occurs after the LGM of the BIIS, which occurred between 27–21 ka BP (Chiverrell and Thomas, 2010; Clark et al., 2012). Maximum IRD supply occurs at different times along the margin of the BIIS (Scourse et al., 2009). At the Donegal Fan it is reached at 30 ka (Knutz et al., 2001), and at 27 ka for other sites including Rosemary Bank and the Porcupine Seabight (Peck et al., 2007; Hall et al., 2011; Clark et al., 2012). This early maximum extent of the northern margin has been interpreted as a curtailment of growth as the northern BIIS as it the shelf break (Clark et al., 2012). Though the background conditions at the European margin differ significantly between H2 and H4, the two Heinrich events are the most similar in their extent and the release of detrital material from the LIS. H4 is the larger of the Heinrich events with an estimated volume of 350 km^3 covering $2.4x10^6$ km^2, compared to H2 which released an estimated volume of 300km^3 covering $2.0 x10^6$ km^2 (Hemming, 2004).

Prior to H2 the BIIS reached its maximum extent at the shelf break, resulting in sedimentary inputs from the BIIS that are much larger during H2, than H4. This has a particular effect on the clay size fraction which makes up the majority of glacially derived sediments (Andrews and Principato, 2002). At the margins of the BIIS, as shown in the schematic diagram in Figure 5.18, there is increased transport of the clay size fraction through mechanisms such as nepheloid layers, turbidites and surface meltwater plumes. This effectively diluted the inputs of LIS derived material in the clay size fractions, meaning that it is not visible in the radiogenic isotope signature of the H2 sediments and represents only a small proportion of the clay sized fraction during H4.

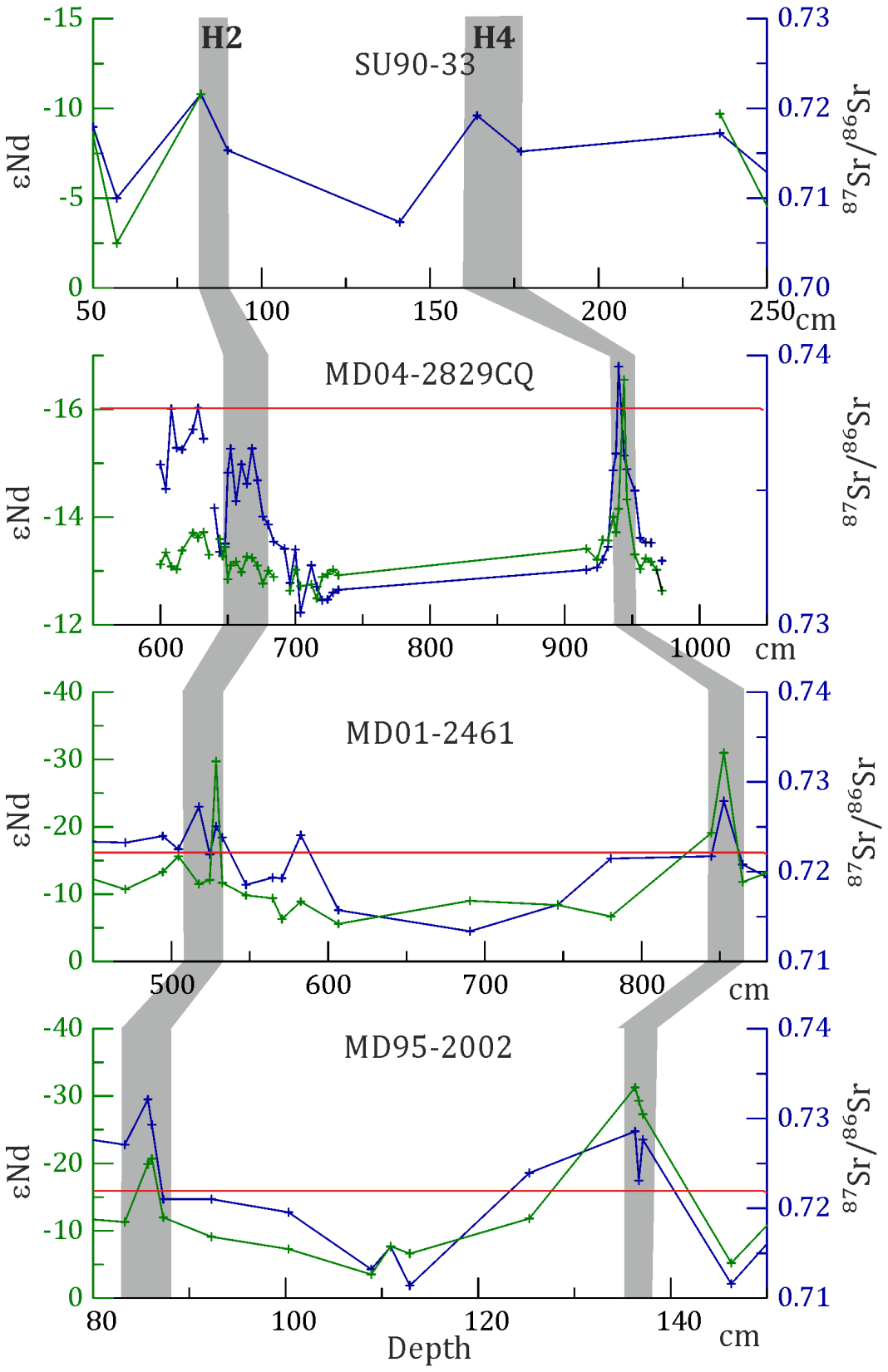

Figure 5.17 εNd and $^{87}Sr/^{86}Sr$ from selected sites along a north to south gradient along the British Margin, sites are shown in Figure 5.14***, data sources are in Table 5.9 red line indicates εNd values of -16 to deliniate between a Canadian and European source.***

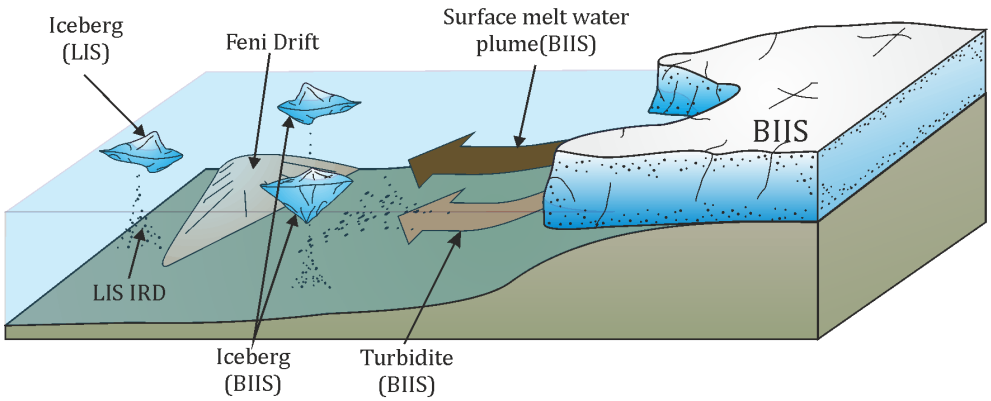

Figure 5.18 Schematic diagram of inputs at the margins of the BIIS

5.5 Summary

This chapter has demonstrated that at the IRD belt the clay size fraction during Heinrich events has a similar source to that observed for the coarse fraction counterparts, with up to 83% of the sediment sourced from the HS sector of the LIS in the central North Atlantic IRD belt. It also demonstrates a change in provenance of clay-sized material prior to H2 and H4 which is close to that of GSL and Scandinavian sources. This finding is consistent with the findings of other studies from across the North Atlantic, which examined coarser size fractions to source the sediments. This common source between different grain sizes indicates that deposition in the NA IRD belt during Heinrich events was dominated by the products of glacial erosion transported by surface currents. During H3 the site is dominated by another end member, which is different in composition to those in the coarse fraction of other studies.

At site MD04-2829CQ the source of fine material is predominantly European, however there may be a small input of an older possibly Canadian source during H4. There are differences between the <2μm fraction from site MD04-2829CQ and the coarse fraction material along the British margin, which may be a result of dilution of distal sources of IRD in the <2μm fraction by meltwater and nepheloid layers. This would not have had a great effect on the coarser fractions.

Finally, further characterisation of source regions for the clay size fraction is required to distinguish between Baffin Bay and Hudson Strait sources, and would enable the robust validation of the assertions made in the literature regarding changing source contributions.

6 Surface and Deep water changes in the North Atlantic during the last glacial

6.1 Introduction

The prevailing paradigm surrounding Heinrich events is that freshening of the North Atlantic surface waters through meltwater inputs, causes a reduction in the vigour of Atlantic Meridional overturning circulation (AMOC) (Bond et al., 1992; Broecker, 1994; Bond et al., 1997; Broecker, 2003; Hemming, 2004). Changes in the benthic $\delta^{18}O$ representing bottom water masses in the North Atlantic over the last glacial have been shown to be in phase with warming in Antarctica (Shackleton and Hall, 2000; Hodell et al., 2010). However, recent evidence from the northern North Atlantic suggests temperature changes were not directly coupled with changes in bottom speeds (Jonkers et al., 2012a).

6.1.1 Surface ocean temperature and salinity changes during Heinrich events

In the ocean, $\delta^{18}O$ of seawater can be lowered by decreases in salinity and increases in temperature (see Section 2.2.3). Across the north-eastern North Atlantic co-registered records of $\delta^{18}O$ of *Neogloboquadrina pachyderma* and sea surface temperature (SST) records demonstrated that during Heinrich events, temperatures cooled and sea surface salinities (SSS) were reduced (Maslin et al., 1995). Decreases of up to 2 ‰ of $\delta^{18}O$ measured on *N. pachyderma* tests demonstrate the widespread impact of this temperature and salinity change over Heinrich events (Cortijo et al., 1997, 2005; Benway et al., 2010). Further evidence for low SST and decreased salinity during Heinrich events is provided using U^{K}_{37}' based sea surface temperature estimates (Madureira et al., 1997; Bard, 2000; Rosell-Melé et al., 2002) see Figure 6.1. Outside of the main IRD belt in the North Atlantic, there are discrepancies where warming SST have been observed over Heinrich events. To the north of the IRD belt for example, at the Reykjanes Ridge a warming over H4 is observed in Mg/Ca derived temperatures (Jonkers et al., 2010). In the north eastern North Atlantic warming of SST was observed during H1 (Cortijo et al., 2005), Furthermore, strong SST seasonality is observed during H4 at the Faeroe Drift in dinoflagellate assemblage

derived SST, and high SST were found concurrent with 80-100% abundances of *N. pachyderma* (a polar indicator) (Zumaque et al., 2012). Towards the southern edge of the IRD belt, at site U1313 there is a warming during Heinrich events suggested by alkenone derived SST (Naafs et al., 2013a),

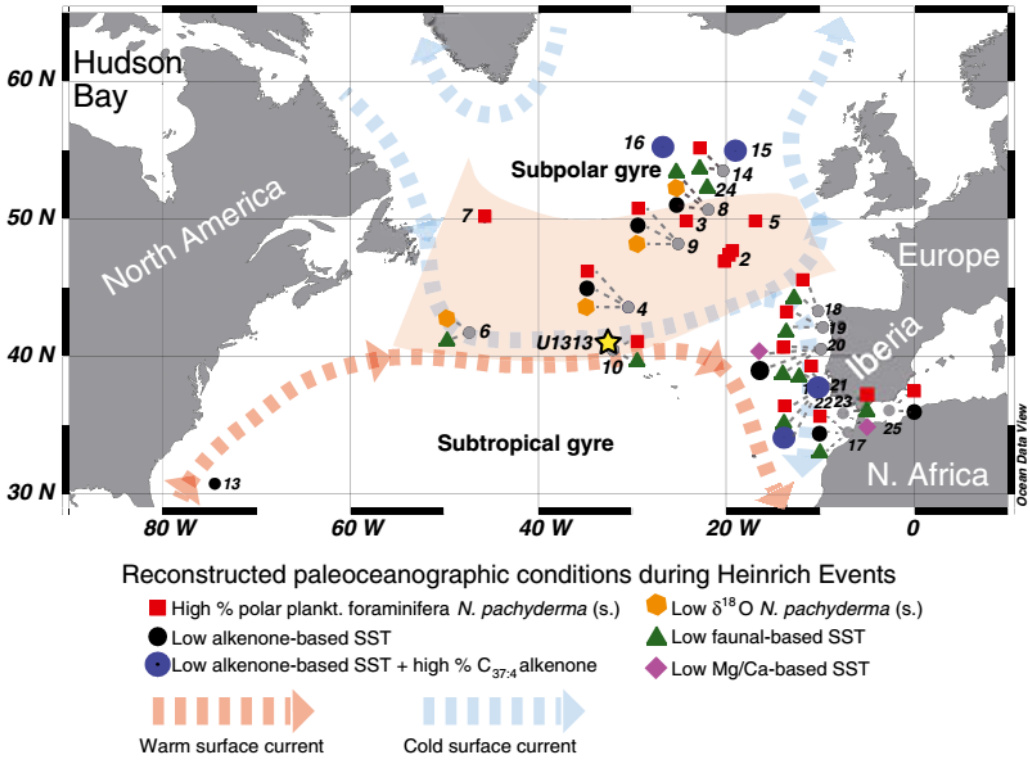

Figure 6.1: summary of proxies relating to palaeoceanographic conditions during Heinrich events from Naafs et al. (2013a) reproduced with permission from John Wiley and Sons.

6.1.2 Response of intermediate and bottom water masses during Heinrich events

The configuration of Last glacial maximum (LGM) deep water masses in the North Atlantic is inferred from $\delta^{13}C$ and dissolved Cadmium (Cd) of benthic foraminifera. At depth, North Atlantic Deep Water shoaled to depths <2 km and was called Glacial North Atlantic Intermediate water (GNAIW); at greater depth Southern Component Water (SCW) expanded northwards as far as the subpolar regions (e.g., Boyle and Keigwin, 1987; Oppo and Fairbanks, 1987; Duplessy et al., 1988; Sarnthein et al., 1994; Curry and Oppo, 2005; Oppo et al., 2015). A slowdown in the Atlantic meridional overturning circulation (AMOC) is thought to be associated with freshwater discharge during Heinrich events (Broecker, 1994;Vidal 1997; Rahmstorf,

2002). Lower overturning rates are indicated by sediment $^{231}Pa/^{230}Th$ ratios (McManus et al., 2004; Hall et al., 2006; Negre et al., 2010; Lippold et al., 2012). However, the use of $^{231}Pa/^{230}Th$ as an AMOC strength proxy is complicated by scavenging of ^{231}Pa by biogenic opal, vertical particle fluxes and AMOC geometry (Lippold et al., 2009; Anderson et al., 2009; Lippold et al., 2012; Jonkers et al., 2015). Further evidence of a reduced AMOC during Heinrich events is demonstrated by lower mean sortable silt (SS) (e.g., Thornalley et al., 2013) and particle size changes (Prins et al., 2002; Jonkers et al., 2012a). Changes in the ventilation of deep water masses are supported by lowered $\delta^{13}C$ of benthic foraminifera across the North Atlantic Basin, supporting a drastic change in the deep circulation associated with these events (Keigwin and Lehman, 1994; Vidal et al., 1997; Zahn et al., 1997; Willamowski and Zahn, 2000; Elliot et al., 2002; Peck et al., 2006). However, not all HEs were identical. Lynch-Stiglitz et al. (2014) for instance demonstrate differences between the change in ventilation between the early glacial H4 and later glacial H2 and H3. They use the $\delta^{13}C$ of benthic foraminifera from several cores from the deep (>2000 m) North Atlantic and intermediate depths (500-900 m) to demonstrate that Heinrich events 2 and 3 have a muted AMOC response to the freshwater forcing in contrast to that which is seen during the early glacial HEs and H1. This is contradictory to modelling experiments that show a greater impact of a freshwater forcing during full glacial conditions (e.g. Bitz et al., 2007; Weber and Drijfhout, 2007).

This chapter will allow inferences to be made about the surface and bottom water dynamics associated with the Heinrich events by presenting planktonic and benthic oxygen and benthic carbon isotope record for site SU92-09 using *N. pachyderma*, *Globigerina bulloides* and *Cibicidoides wuellerstorfi*. By comparing data from site SU92-09 to isotope records from other cores around the North Atlantic it is possible to infer the phasing of changes in surface water mass changes and bottom water mass changes. This could prove informative as previous studies have shown indications of changes in the deep ocean change prior to Heinrich events (e.g., Zahn et al., 1997; Peck et al., 2006; Jonkers et al., 2012a).

6.2 Results

Over the last glacial between 46.5 and 19.5 ka BP there is a trend of increasing $\delta^{18}O$ of the benthic foraminifera *C. wuellerstorfi* from 4 ‰ to 4.6 ‰ (***Figure 6.2***). Most of this increase occurs at 35 ka BP. Over the same period $\delta^{13}C$ of *C. wuellerstorfi* decreases from 1.2 ‰ to 0.5 ‰. During H4 $\delta^{13}C$ of *C. wuellerstorfi* initially decreases to 0.9‰ at one sample point, but thereafter an overall increase to a peak of 1.3 ‰. At H3 there is a drop in benthic $\delta^{13}C$ from 1‰ to 0.6 ‰. During H2 $\delta^{13}C$ initially decreases from a peak of 1 to 0.5%, a hiatus in the deposition of *C. wuellerstorfi* obscures most of H2 however, at the end of H2 $\delta^{13}C$ of *C. wuellerstorfi* is still low and remains low after the event.

The oxygen isotope ratios of *N. pachyderma* gradually increase over the period 46.5 to 16.7 ka BP, this trend is interrupted by excursions to lighter values of ~2.5‰ during H4, 2.9‰ during H2 and 2.5‰ during H1 ***Figure 6.2***. Over H3, there is no change in the $\delta^{18}O$ of *N. pachyderma*. The isotope ratios of *G. bulloides* are lower than those of *N. pachyderma* during the ambient glacial, $\delta^{18}O$ of *G. bulloides* is between 2.1 and 2.8 ‰ until H1 where it decreases to 1.5 ‰. There is a difference of 0.4 to 1.46 ‰ between *G. bulloides* and *N. pachyderma* during the ambient glacial. The decreases in *N. pachyderma* $\delta^{18}O$ during Heinrich events occur at the same time as the large decreases to <-5‰ seen in $\delta^{18}O_{FINE}$.

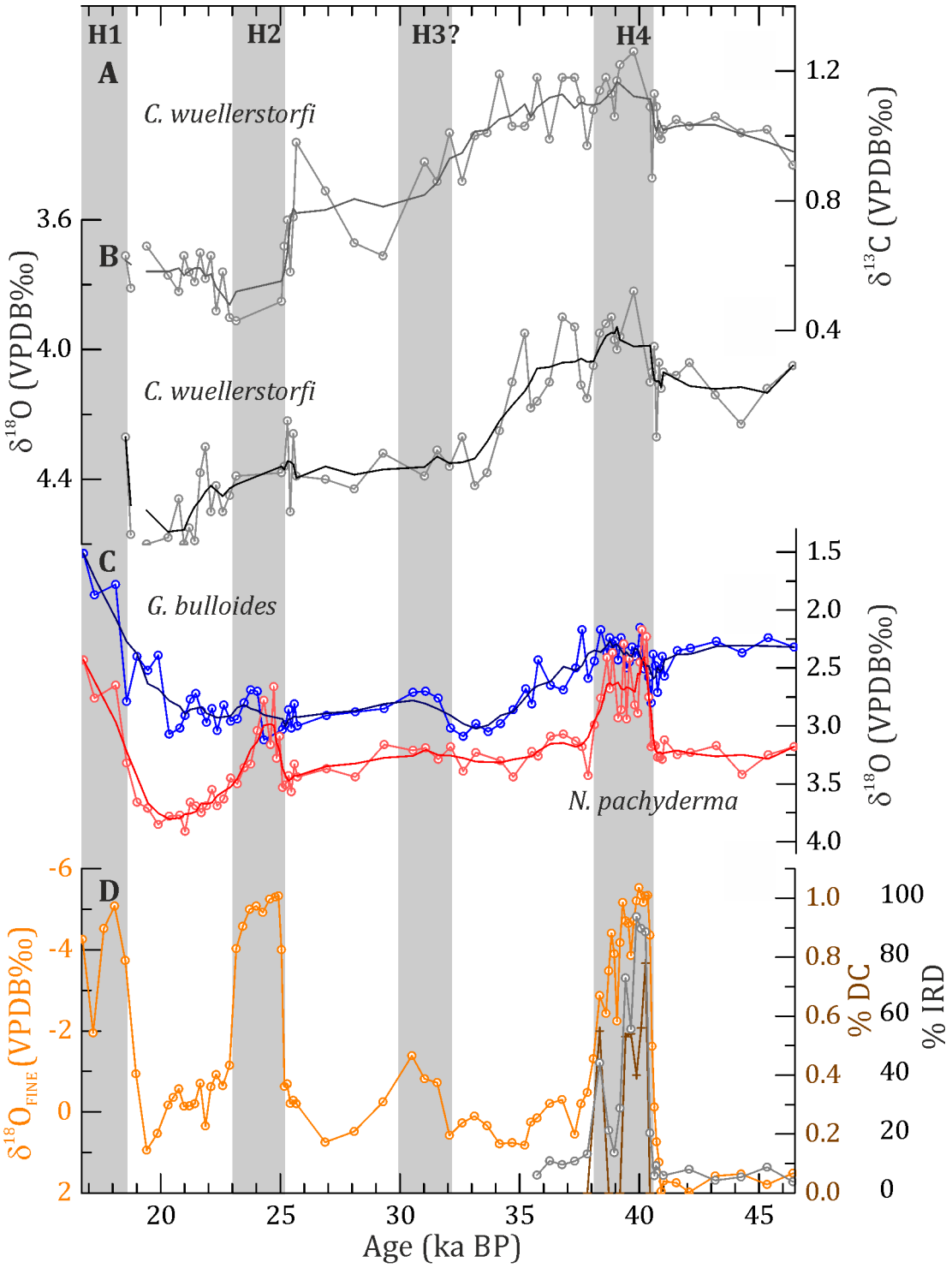

Figure 6.2: Benthic and planktonic foraminifera stable isotope ratios for Core SU92-09. A; $\delta^{13}C$ of C. wuellerstorfi B; $\delta^{18}O$ C. wuellerstorfi, C; $\delta^{18}O$ of planktic foraminifera (labelled), D; $\delta^{18}O_{FINE}$ (orange), percentage IRD (grey) and percentage detrital carbonate (brown) pers. comm. Elsa Cortijo. Heinrich event intervals are marked in grey. Darker lines represent the 5 point averages of foraminifera stable isotopes.

6.3 Discussion

6.3.1 Fresh water input to surface waters

The ambient glacial values of *N. pachyderma* are in the range of 3.5 ‰ and above. During Heinrich events, these are reduced to ~2.5‰ ***Figure 6.2***C. This effect is strongest during H4 where the decrease in $\delta^{18}O$ of *N. pachyderma* matches the timing of the inputs of IRD to the core. During H3 there is no discernible change in the $\delta^{18}O$ of *N. pachyderma*. At the beginning of H2 there is an excursion of ~1‰ that lasts for

Figure 6.3: changes in $\delta^{18}O$ of planktonic foraminifera (before –during) with the 1‰ isoline from Cortijo (2005) . (removed copyright unable to be obtained before submission. see Fig 2 of Cortijo et al (2005)).

1 kyr however the input of IRD (from $\delta^{18}O_{FINE}$) lasts longer than the excursion in *N. pachyderma* $\delta^{18}O$. Lower $\delta^{18}O$ of the tests of planktic foraminifera indicate a decrease in the $\delta^{18}O$ in the water mass in which the foraminifera calcifies or an increase in temperature. In the surface ocean lower $\delta^{18}O$ is indicative of decreasing salinity, and global ice volume changes see Section 2.2.3. In studies across the North Atlantic where the SST effect on $\delta^{18}O$ have been removed, Heinrich events have been shown to have large freshwater anomalies across the IRD belt (Cortijo et al., 1997, 2005). Therefore, it is likely that in core SU92-09 excursions in the $\delta^{18}O$ of *N. pachyderma* is a reflection of lowered SSS during Heinrich events. Comparing the scale of the change in $\delta^{18}O$ at this site with those from (Cortijo et al., 2005) shown in Figure 6.3 demonstrates that this site is consistent with changes across the North Atlantic IRD belt during H4 and during H1. Comparing to sites that data from H2 is available from the excursion is also similar.

6.3.2 Convergence of $\delta^{18}O$ records from G. bulloides and N. pachyderma

The oxygen isotope curves of *N. pachyderma* and *G. bulloides* shown in Figure 6.2 would at first glance support the conclusions of Rashid and Boyle (2007, 2008) that during Heinrich events there is a wind driven mixed layer deepening which results in similar values of $\delta^{18}O$ of *N. pachyderma* and *G. bulloides*. This assertion is based on the depth habitats of the two species: *N. pachyderma* is a subsurface dwelling foraminifera, thought to spend most of its lifecycle near the pycnocline but also found at a wide range of water depths ranging from 50- 80 m as juveniles to 500-600 m at

other life stages, but is found at peak concentration in the modern subpolar ocean at 150 m (Hillaire-Marcel and Bilodeau, 2000). *G. bulloides* is a surface dwelling foraminifera found at depths of 0 - 60 m with a mean calcification depth of 30 m (Schiebel et al., 1997) and peaks during the spring bloom. Studies have used variations in the $\delta^{18}O$ of these two species to examine water mass changes in the surface and sub surface and as an indicator of water mass stratification during IRD events (Hillaire-Marcel and Bilodeau, 2000; Rashid and Boyle, 2007; Peck et al., 2008; Hall et al., 2011). At site SU92-09 the oxygen isotope curves of the two foraminifera during ambient glacial conditions have a difference of 0.4 to 1.46 ‰ Figure 6.4. During Heinrich events however this reduces to a 0.04 to 0.66 ‰ difference between the two foraminifera species as shown in Figure 6.4 This potentially means that the water masses where the foraminifera are growing have similar properties and may be interpreted as mixing of the surface and subsurface water masses. However, there are many considerations in the interpretation of $\delta^{18}O$ between these two species which may mean that this is not the case.

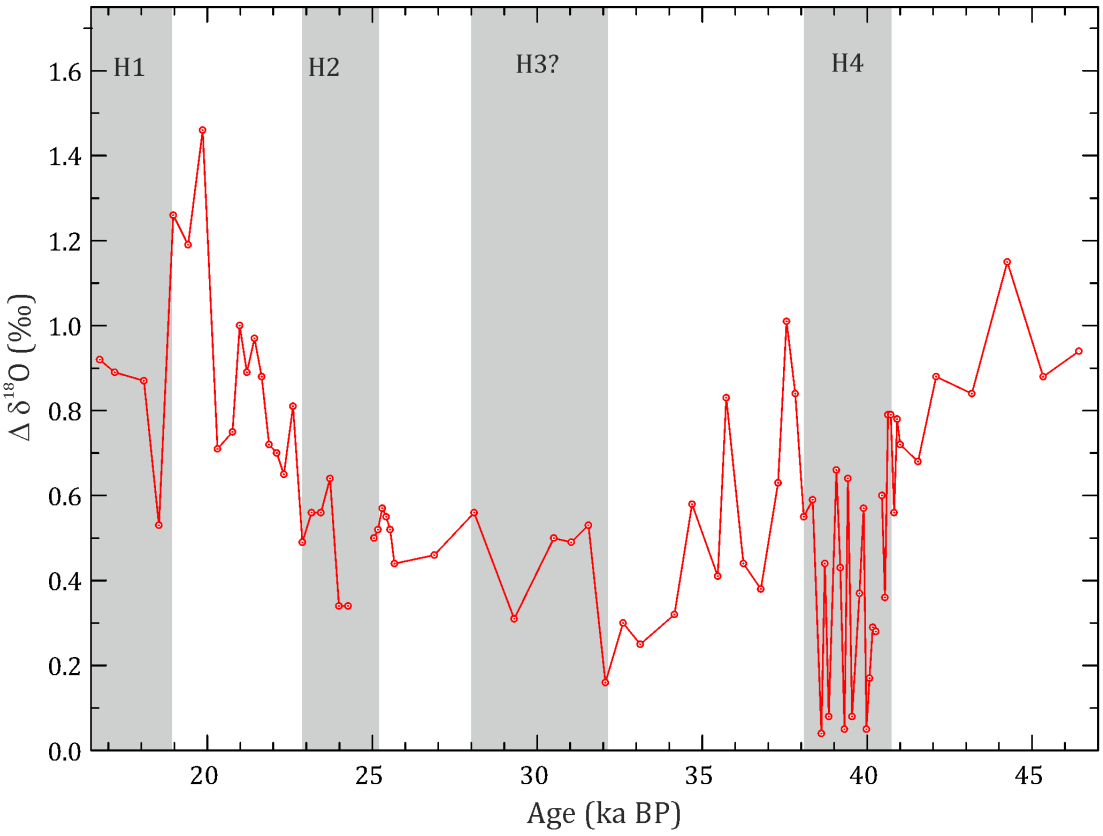

Figure 6.4: plot of the difference (Δ) between the $\delta^{18}O$ values of N. pachyderma and G. bulloides.

Firstly, in modern sediment trap studies, in a N-S transect G. bulloides were found to migrate with the spring bloom reflecting the sea surface conditions of May to June between 40 and 45°N (Ganssen and Kroon, 2000). A further study from the Irminger sea fluxes of N. pachyderma peak earlier in the year during May and again during August compared to G. bulloides which peaks during June –August, and both species are found at the same depth range (Jonkers et al., 2013). This would suggest that the differences in *N. pachyderma* and *G. bulloides* $\delta^{18}O$ in the past are as a result of differences in seasonality rather than depth habitat.

A second consideration is that *G. bulloides* is typically associated with warmer waters whereas *N. pachyderma* is associated with colder SST and have been found to live in sea ice (e.g., Spindler and Dieckmann, 1986). It is the case that each sample at the site integrates time with decades to centuries represented in a single sample. Heinrich events are not once single event but the integration of several meltwater pulses over several hundred years. Therefore, it is possible that the $\delta^{18}O$ of *N. pachyderma* lowers in response to meltwater input from the Heinrich event but that *G. bulloides* is not present at the time of year or during years when meltwater occurs, and does not register the lighter $\delta^{18}O$ values associated with a meltwater pulse during the Heinrich events, resulting in the two records seeming to converge. This is supported by the low inputs of foraminifera during Heinrich events in some cases there were <20 *G. bulloides* per sample. Also during H1 there is a decrease in the *G. bulloides* $\delta^{18}O$ at the same time as the decrease in *N. pachyderma* $\delta^{18}O$ this indicates that if the conditions are favourable *G. bulloides* will register concomitant changes with *N. pachyderma*. Of the scenarios above the third is thought to be the most reasonable considering the evidence provided here. This scenario is also consistent with the interpretation of the *N. pachyderma* $\delta^{18}O$ decrease during HEs predominantly reflecting a (near) surface freshening (and not a warming) since fresh and cold conditions are unfavourable for the growth of *G. bulloides*.

6.3.3 What inferences can be made from changing benthic water masses at the IRD belt site SU92-09?

The records of the benthic foraminifera *C. wuellerstorfi* at site SU92-09 are incomplete with hiatuses during H2 and at the beginning of H4. Potentially, during Heinrich events the benthic conditions were not favourable for the survival of *C.*

wuellerstorfi in large enough numbers for them to be preserved in the sediment sampled. However, inferences about the general changes over the course of the last

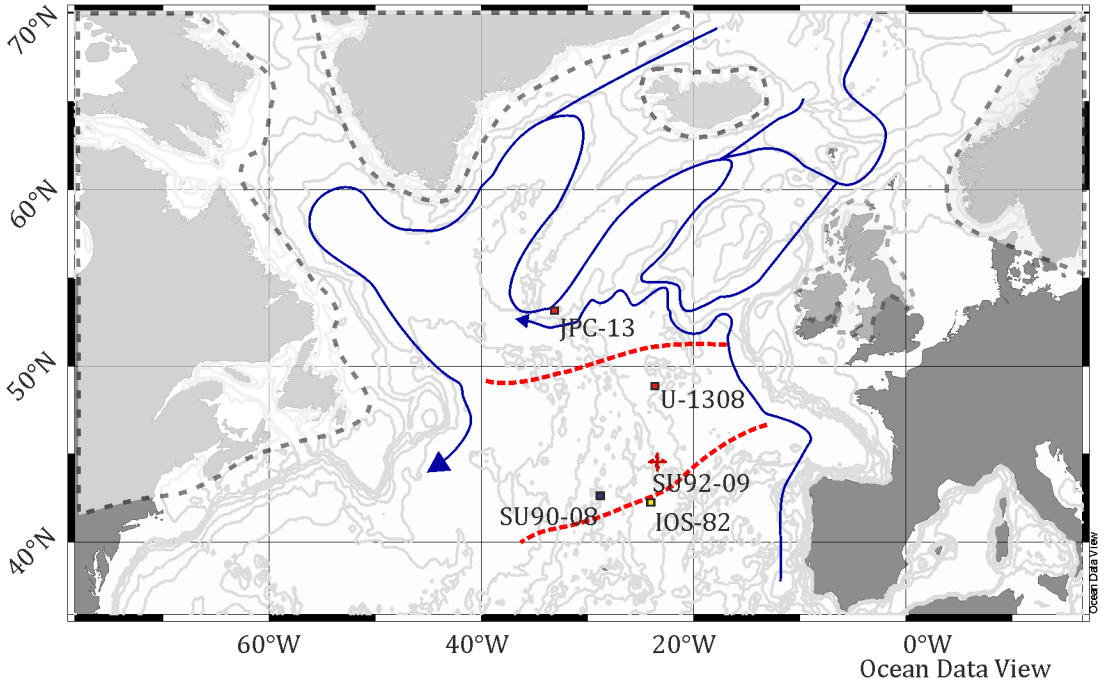

Figure 6.5: Map showing the bottom current circulation adapted from (Fagel et al., 2004) and the sites mentioned in this discussion.

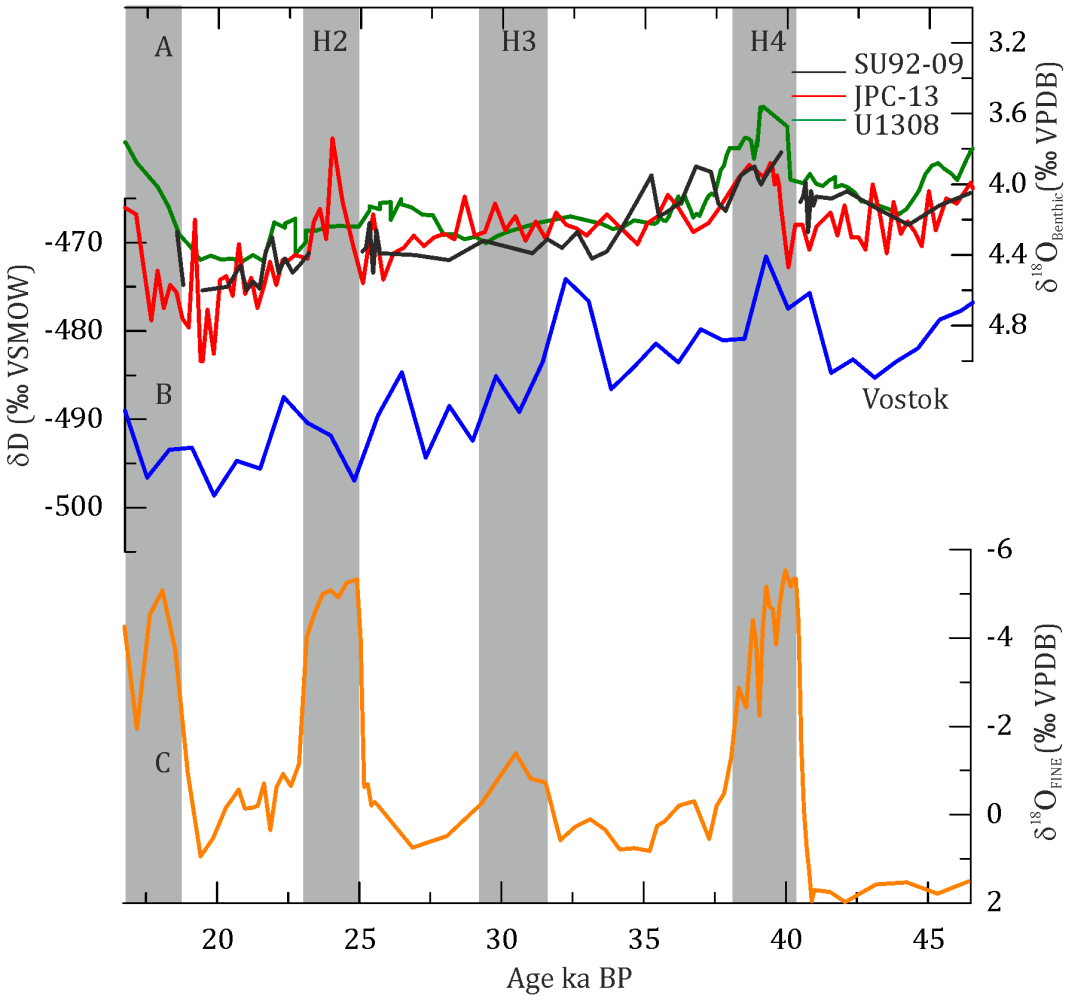

Figure 6.6: $\delta^{18}O$ of C. wuellerstorfi from SU92-09 and North Atlantic records compared to Antarctica δD record. A; $\delta^{18}O$ of C. wuellerstorfi from sites in the mid-Atlantic. B; δD averaged from Vostok (Petit et al., 1999). C; bulk fine fraction $\delta^{18}O$ representing increases in detrital material at site SU92-09 and U1308 (Hodell et al., 2008) are on the same age model JPC-13 (Hodell et al., 2010) and Vostok core are on their own age models.

glacial can be inferred from the data available. $\delta^{18}O$ of benthic foraminifera reflect changes in temperature, global ice volume and local hydrographic conditions (Ravelo and Hillaire-Marcel, 2007) see Section 2.2.3.1. The $\delta^{18}O$ of *C. wuellerstorfi* from site SU92-09 show a general trend of increasing values over the last glacial from 4.1 ‰ to 4.6 ‰. The minimum values correspond with H4, and a stepwise increase occurs at 33.6 ka BP. This general trend is reflected in sites U1308 (Hodell et al., 2008), MD952042 (Shackleton et al., 2004), and JPC-13 (Hodell et al., 2010), locations shown in Figure 6.5 and data in Figure 6.6.

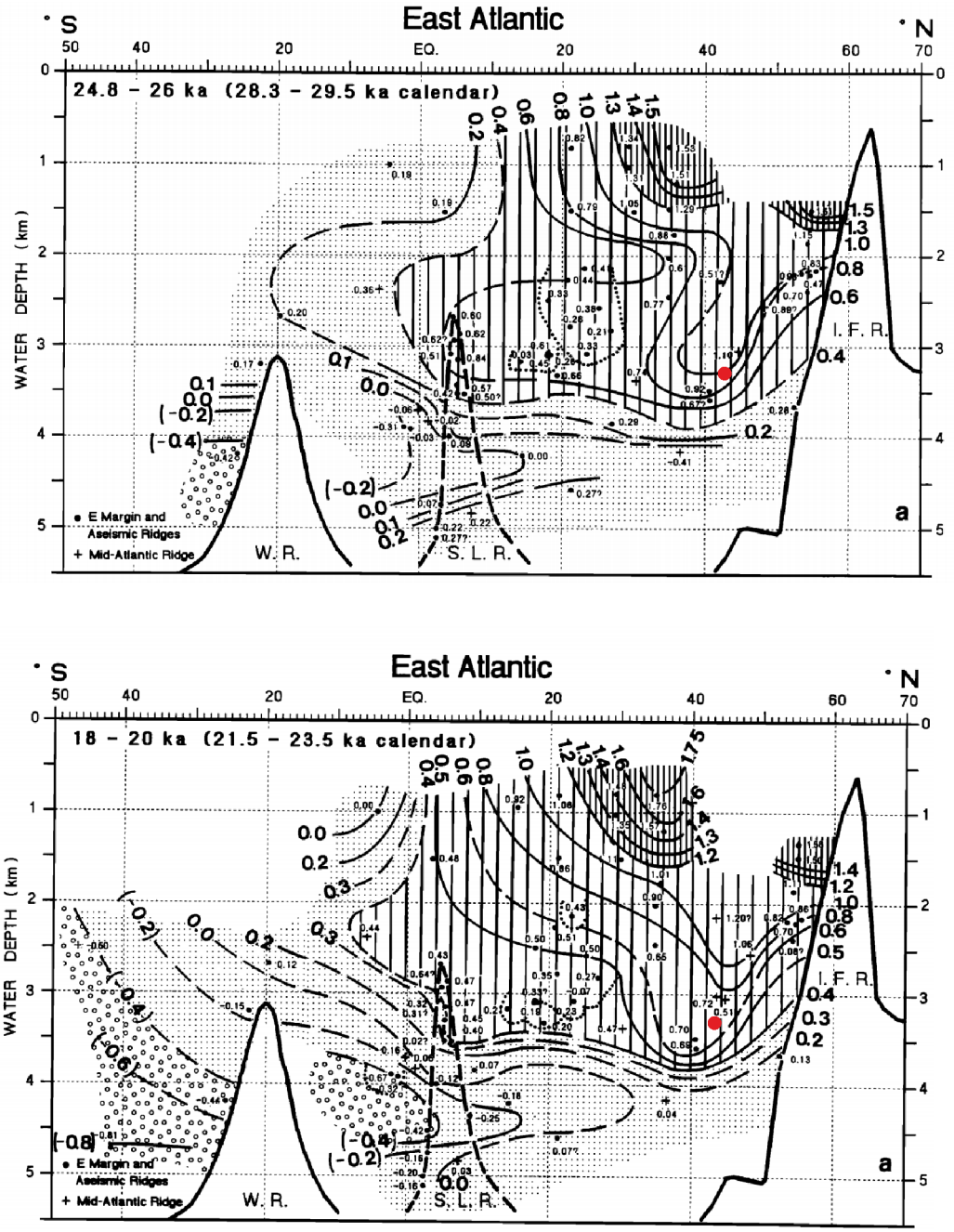

Figure 6.7: Changes in the structure of $\delta^{13}C$ in water-masses in an N-S transect of the North Atlantic from Sarnthein et al (1994) reproduced with permission from Jon Wiley and Sons. Top is early glacial, bottom is last glacial maximum, Red dot indicates the depth of and position of SU92-09.

The increasing values over the last glacial at the sites in Figure 6.6*Error! eference source not found.* demonstrate that this is a wide reaching signal probably linked to changing insolation and ice sheet growth. The excursion during H4 to lighter $\delta^{18}O$ of benthic foraminifera in water depths greater than 3000 m is in phase with warming event A1 in Antarctica (Hodell et al., 2010) also shown in ***Figure 6.6***. The

surface expression of Heinrich events (shown by the $\delta^{18}O_{FINE}$) at site SU92-09 corresponds well with the benthic $\delta^{18}O$ changes at the site.

During the last glacial, benthic $\delta^{13}C$ values at deep sites in the North Atlantic are reduced in response to an incursion of SCW which has a low $\delta^{13}C$ signal (Oppo et al., 2015). At site SU92-09 in the early glacial values of benthic $\delta^{13}C$ match those of the NADW. This supports the assertion of Sarnthein et al.(1994) that during MIS 3, the origin of North Atlantic Deep Water (NADW) was similar to the modern. At site SU92-09, the transition demonstrating the shoaling of NADW to become GNAIW and incursion of SCW occurs between 32 and 28 ka BP where values reduce from ~1‰ to ~0.5‰. Sarnthein et al.(1994) demonstrate the shoaling of NADW by their 21-23 ka BP time step see ***Figure 6.7***, which is consistent with the pattern seen at site SU92-09. The $\delta^{13}C$ of *C. wuellerstorfi* at site SU92-09 during H4 is harder to place into the context of existing data at water depths of >3000 m. During the Heinrich events of the last glacial, across the North Atlantic basin below 2000 m $\delta^{13}C$ values correspond to SCW with values below 0.5 ‰ as far north as the subpolar North Atlantic. At site SU92-09 this is not the case, during H4 values of 1.26 ‰ (the highest in the record) are found at the same time as the IRD is recorded in the core. Vidal et al. (1997) present data from the North Atlantic and demonstrate that in the vicinity of the IRD belt $\delta^{13}C$ values only decrease by <0.25 ‰. Indicating that contrary to other sites in the North Atlantic, local deep water convection occurs at the Ruddiman IRD belt (Vidal et al. 1997).

Table 6.1: comparison between average benthic $\delta^{13}C$ H4 at local sites with data from Vidal et al. (1997), number of samples is in brackets.

Site	Location	Depth (m)	Pre-H4	H4	Post H4
SU92-09	44°N 23°W	3270	1.05 (6)	1.15 (6)	1.11(6)
SU90-08	43°N 30°W	3080	1.13(3)	0.9(4)	1.17 (3)
IOS-82	42°N 23°W	3540	1.05 (4)	0.9 (1)	1 (3)

There is no analytical reason to doubt the values, and as the study was monospecific and from the same size fraction, there should not be variation based on the differences in the rate of incorporation of $\delta^{13}C$ into the shell. If there were misidentification of *C. wuellerstorfi*, this would likely have little effect on the $\delta^{13}C$ value as many studies use a combination of Cibicidodies species to create their benthic

records (e.g., Oppo et al., 2015). Furthermore, contamination via bulk carbonate material would shift the $\delta^{13}C$ to lower not higher values. Early phase diagenesis of calcite has been observed during Heinrich events, and this could have an effect on the $\delta^{13}C$ of the foraminifera calcite, but *C. wuellerstorfi* tests were whole and did not have visible evidence of recrystallization. Therefore, it can be accepted that these data reflect a true change in the $\delta^{13}C$ of the benthic foraminiferal calcite. At the beginning of H4 there is a hiatus in the record of *C. wuellerstorfi*, it could be that the change in $\delta^{13}C$ is missed by this record over H4 and that there is a rapid resumption of the NADW at the site which occurs before the end of the freshwater forcing indicated by IRD and the $\delta^{18}O$ of *N. pachyderma*.

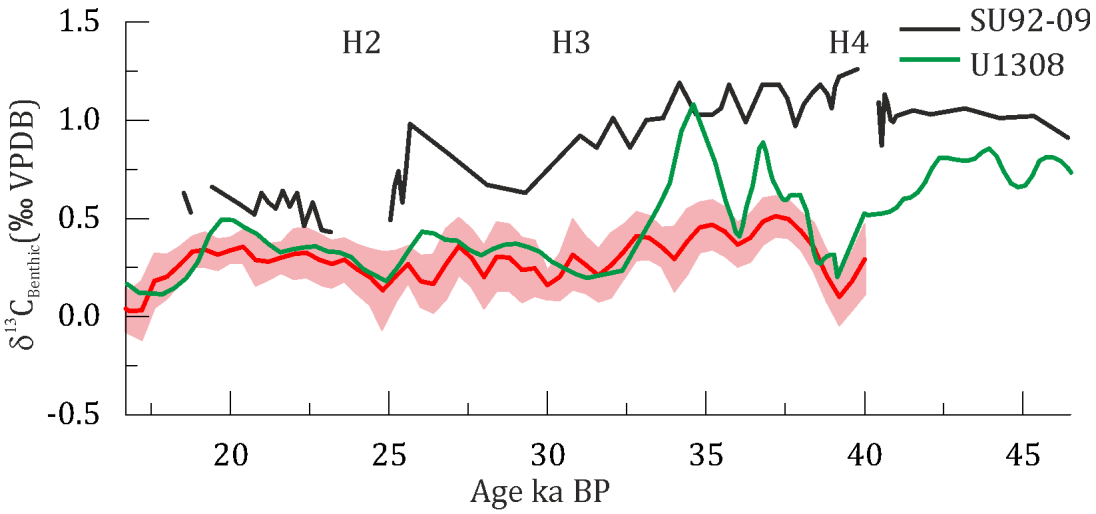

Figure 6.8: $\delta^{13}C$ of benthic foraminifera from North Atlantic sites. SU92-09 in black, average $\delta^{13}C$ from U1308 at 3871 m depth (Hodell et al., 2008) in green and in red is the average $\delta^{13}C$ + 2 standard deviations of 8 sites with >2000 m depth from Lynch-Stiglitz et al.(2014).

6.4 Summary

- The $\delta^{18}O$ of *N. pachyderma* show a similar decrease to other sites across the North Atlantic and demonstrate a freshwater input to the site which is in phase with the increase in $\delta^{18}O_{FINE}$ demarking the start input of fine fraction IRD during the Heinrich event. Over H3 there is no visible decrease in the $\delta^{18}O$ of *N. pachyderma* during H3.
- The $\delta^{18}O$ of *C. wuellerstorfi* shows similar phasing and values to sites JPC-13 and U1308 potentially linking it to Antarctic warming phases.

- The $\delta^{13}C$ of *C. wuellerstorfi* demonstrates a change at 36 ka BP from $\delta^{13}C$ resembling GNAIW to lighter values representing the greater influence of SCW at the site. However over H4 there is no change in $\delta^{13}C$ of *C. wuellerstorfi* which is anomalous for the North Atlantic.

7 Synthesis

The preceding chapters have examined the changing source and supply of glacial flour to the margins of the British and Irish ice sheet (BIIS) and the IRD belt over the last glacial period with particular reference to Heinrich events 2 and 4. This synthesis will summarise the key findings from the previous chapters and then proceed to place them into context of already existing literature.

Chapter 3 revealed changes in the grain size distributions of the 5-63μm fraction. Through a four component end member modelling study of particle size distributions (PSD) it was demonstrated that at site SU92-09 during H1, H2 and H4 the 5-63μm fraction was dominated by a coarser end member with a PSD resembling that expected from IRD. After H2 and H4, the IRD belt site shows a dramatic fining, which is thought to indicate a retreat of the polar front preventing IRD from reaching the site or changes to circulation providing material to the site. At the Rosemary Bank site, there are increases in endmembers with coarser PSD that are associated with an increase in IRD abundance. The finest end member increases over the course of the last glacial, in this case it is attributed to increased input from the BIIS as the shelf edge was reached, this is supported by $\delta^{18}O$ data from Chapter 4 which demonstrated increasing detrital input to the site over MIS 2.

Chapter 4 demonstrated that at site SU92-09 in the central North Atlantic IRD belt there is a significant input of fine fraction detrital carbonate evidenced by low $\delta^{18}O$ of the <63 μm fraction ($\delta^{18}O_{FINE}$) during Heinrich events. This is likely as a result of transport of <63μm fraction carbonates by ice rafting and associated melt water from the Hudson Strait ice stream which is underlain by Palaeozoic carbonates. At the British margin, a distinct impact of the growth of the BIIS calving margin on the $\delta^{18}O_{FINE}$ proxy is observed. Lower values of $\delta^{18}O_{FINE}$ are associated with high IRD input and low SST indicating periods of higher supply of continentally derived carbonate relative to the biogenic supply. Over MIS 3 and 2 the supply of continental carbonate increased as the BIIS established a more permanent marine ice margin. During H4 there was an increase in detrital carbonate associated with the lowest value in the $\delta^{18}O_{FINE}$ record of -4.98‰ and this is thought to be the expression of a Hudson Strait source during H4. During H2, the local BIIS is much larger and masks the

Hudson Strait input to the fine fraction at the site in the $\delta^{18}O_{FINE}$. This chapter demonstrated the usefulness of $\delta^{18}O_{FINE}$ as a tracer for IRD derived from $CaCO_3$. The chapter highlights the presence of carbonate IRD in the fine fraction at both sites despite their very different depositional environments.

Chapter 5 indicated the changing source of sediment over H2 and H4 at the IRD belt in the clay size fraction. The decreased ratios of Nd and increased ratios of Sr isotopes demonstrate a change from a source with a similar ratio to the Fennoscandian ice sheet (FSIS)/Gulf of Saint Lawrence (GSL) source region during the ambient glacial, to one similar to a Hudson Strait source during H2 and H4 at site SU92-09. At the Rosemary Bank site (British Margin) during H4 there is a possible small input from the LIS source and the majority of the material is BIIS-derived. During H2 there is no discernible LIS derived material input to the Rosemary Bank site and the H2 interval is dominated by increased clay-sized material from the BIIS.

In Chapter 6 oxygen and carbon isotope data from benthic and planktonic foraminifera is presented from site SU92-09. A significant decrease in $\delta^{18}O$ of *N. pachyderma* ~1.5 ‰ are associated with H4 and H2. However, benthic stable isotopes demonstrated that there was no concomitant change in $\delta^{13}C$ during H4 potentially indicating a consistent presence of North Atlantic Deep Water (NADW) at the site during the early glacial.

7.1 British Ice sheet growth

7.1.1 41-27 ka BP (MIS 3)

Chapter 3 and Chapter 4 demonstrated the increase in fine sediment supply to the ocean margin of the BIIS over the last glacial. The trends in decreasing $\delta^{18}O_{FINE}$ and increasing supply of the fine silt end member to site MD04-2829CQ over MIS 3 are interpreted as increased delivery of continental derived carbonate material to the site. An increase in supply of continental sediments is likely due to increased calving activity and meltwater runoff at the margin of the BIIS as it grew and reached the shelf break. At site MD04-2829CQ there are low fluxes of IRD to the site until 27 ka, providing evidence of a small BIIS during MIS 3 that was not sufficiently large to have a constant ice margin (Hall *et al.* (2011).

Knutz *et al.* (2001) show a low supply of IRD before 30 ka BP in core MD95-2006 on the Barra Fan indicating the existence of glaciers largely above the marine limit in Scotland and N. Ireland. These authors interpreted the deposition of quartz IRD between 30-45 ka BP as indicative of intermittent glaciomarine conditions, and compared to the Rosemary Bank, the start of the maximum ice extent at the Barra fan is delayed by 3 ka. This could be due to the lower latitude position of the former which would cause IRD at that site to increase over a longer period as the near site marine margin develops. Peters et al. (2008) also show low inputs of BIIS sourced material during this interval using unmixed magnetic data at site MD95-2006 from the Barra Fan. In a multiple site study, Scourse *et al.* (2009) interprets the millennial scale frequency of IRD input during MIS 3 to mean that the British ice sheet was of a moderate size during this interval, until 29 ka BP when southward expansion of the ice sheet is evident by increasing IRD fluxes in cores to the south. Crocket et al. (2013) interprets Pb isotopes on the Mn/Fe phases of samples from ODP Site 980 in the Rockall Trough to be indicative of an intermittent ice sheet margin during MIS 3. Growth of the BIIS during this time is also consistent with ice sheet models, including the accumulation curve of Hubbard et al. (2009) which uses the Greenland ice sheet as a basis for growth and shows a small growing ice sheet until 27 ka BP. Growth during early MIS 2 would also be consistent with Stage 2-4 of the flow model of Hughes et al. (2014).

There is evidence from pollen records both in the British Isles and across northern Europe that there were warmer conditions during the interval between 38 and 32 Ka BP (Whittington and Hall, 2002). However, due to the paucity of records, it is not clear whether this was a continuous warm period or the sum of several interstadials. The overall record of growth in ice margin activity at the British ice sheet is punctuated by several excursions in the $\delta^{18}O_{FINE}$ record of site MD04-2829CQ to higher values of >-2.5‰. All of these intervals are characterised by low IRD flux and high SST, corresponding to Greenland interstadials at site MD042829CQ (Hall, et al., 2011).This would indicate these are intervals of warm sea surface conditions and low continental input. A similar correspondence between the absence of IRD and the occurrence of Greenland interstadials has been identified in total coarse fraction IRD counts and magnetic and XRF proxies of lithic material at sites along the Eastern Atlantic margin of the BIIS including site MD99-2281 (Zumaque et al., 2012) MD95-2006 (Peters et

al., 2008) and site MD01-2461 (Peck et al., 2007) Kroon et al. (2000) show highly variable IRD inputs prior to 25 ka BP in records of $CaCO_3$ at site MD95 2006, indicating changes in the relative supply of biogenic to lithic material, however the age model presented was not sufficient to compare directly to Greenland cycles.

7.1.2 27-18 ka BP (MIS 2)

At 27 ka there is a change in $\delta^{18}O_{FINE}$ to consistently low values indicating a constant influx of continental carbonate to the core site. This is supported by almost continuous coarse fraction IRD inputs and low SST at site MD04-2829CQ at this time. Previous studies dating the maximum extent of the British ice sheet show that the ice sheet indeed reached its maximum at ~27 ka BP in the northern British Isles (Clark et al., 2012). Marine records show a step increase in the amount of IRD deposited at the transition between MIS3 and MIS2, close to the margins of the BIIS. Several studies have alluded to a change in frequency of coarse fraction IRD inputs, for example in at site MD04-2829CQ and DAPC2 (Knutz et al., 2007) both from the Rosemary Bank, have IRD fluxes at the last glacial maximum that vary on a centennial scale as opposed to the millennial-scale that dominates during the lead up to the maximum ice sheet extent. However, the $\delta^{18}O$ record at core MD04-2829CQ from the fine fraction does not exhibit the same high frequency change after 27 ka BP and instead shows a relatively constant supply of low $\delta^{18}O$ detrital material. This is likely to be due to the different nature of coarse and fine fraction material in the sediment column, and to the nature of the two proxies. Firstly, fine fraction material is likely to be in the water column for a longer time than coarse fraction material due to the rapid settling velocity of larger grains. Therefore, coarse fraction material is not likely to undergo much lateral transport, and would need the presence of an ice sheet/icebergs in the vicinity of the core (Knies et al., 2001). Contrastingly, the fine fraction material can be transported over longer distances, making the IRD record more intermittent than the fine fraction record. The $\delta^{18}O_{FINE}$ is probably indicative of long term increase in ice rafting and melting indicating a constant presence of the BIIS at the shelf margin, whereas the IRD represents the intermittent activity of ice shelf collapse and the intermittent nature of the supply of icebergs to the site. The second reason accounting for more of the trend that is seen in $\delta^{18}O_{FINE}$ proxy is the sensitivity of $\delta^{18}O$ as a proxy for IRD. After the continental input has reached a certain threshold proportion of total carbonate it becomes difficult for the $\delta^{18}O$ signal to change further. This can be

demonstrated by the truncating the IRD at a flux of 8000 grains cm^2 ka^{-1}, which then closely resembles the $\delta^{18}O_{FINE}$ record.

7.2 Structure of H2 and H4

Previous studies which use coarse fraction and bulk data have identified changes in the source of material over H2 and H4 (Hemming, 2004). At site SU92-09 there are clear changes in the geochemistry of the sediments over the course of H2 and H4 with decreases in $\delta^{18}O_{FINE}$ and εNd, increases in $^{87}Sr/^{86}Sr$, shown in Chapter 4 and Chapter 5 and a significant change in the particle size of the silt fraction (Chapter 3). These changes in fine fraction $\delta^{18}O$, and clay sized fraction εNd and $^{87}Sr/^{86}Sr$ are consistent with a Hudson Strait source of the fine fraction and clay fraction during H2 and H4. This demonstrates that clay sized material has the same source during Heinrich events as the coarser fractions from other studies of Heinrich events in the IRD belt (e.g., Revel et al., 1996; Hemming et al., 1998; Snoeckx et al., 1999; Hodell et al., 2008; Grousset et al., 2001; Channell et al., 2012). The inputs of HS sourced material occur at site SU92-09 at the same time as negative excursions in the $\delta^{18}O$ of *N. pachyderma* which demonstrate the link between ice rafted fluxes and surface freshening that is observed across the North Atlantic see ***Figure 7.1*** and Figure 7.2.

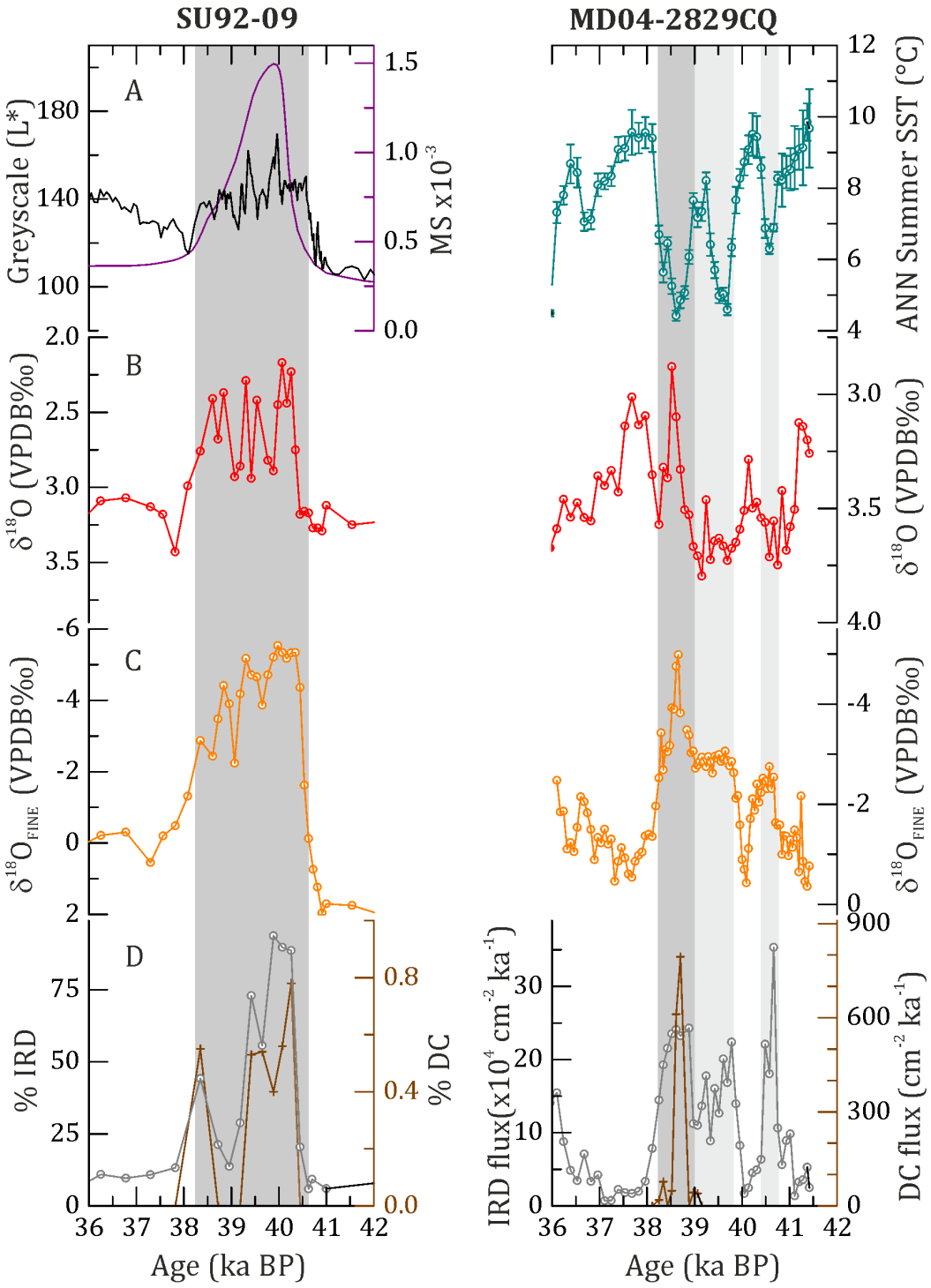

Figure 7.1: Comparison between surface conditions during H4 at site SU92-09 and MD04-2829CQ A; Greyscale and Magnetic susceptibility(purple) B; estimated sea surface temperatures, C; <u>N. pachyderma</u> D; $\delta^{18}O_{FINE}$ E; IRD abundances (total IRD in grey and DC in brown), supplementary data from Hall et al. (2011) and Elsa Cortijo pers. comms..

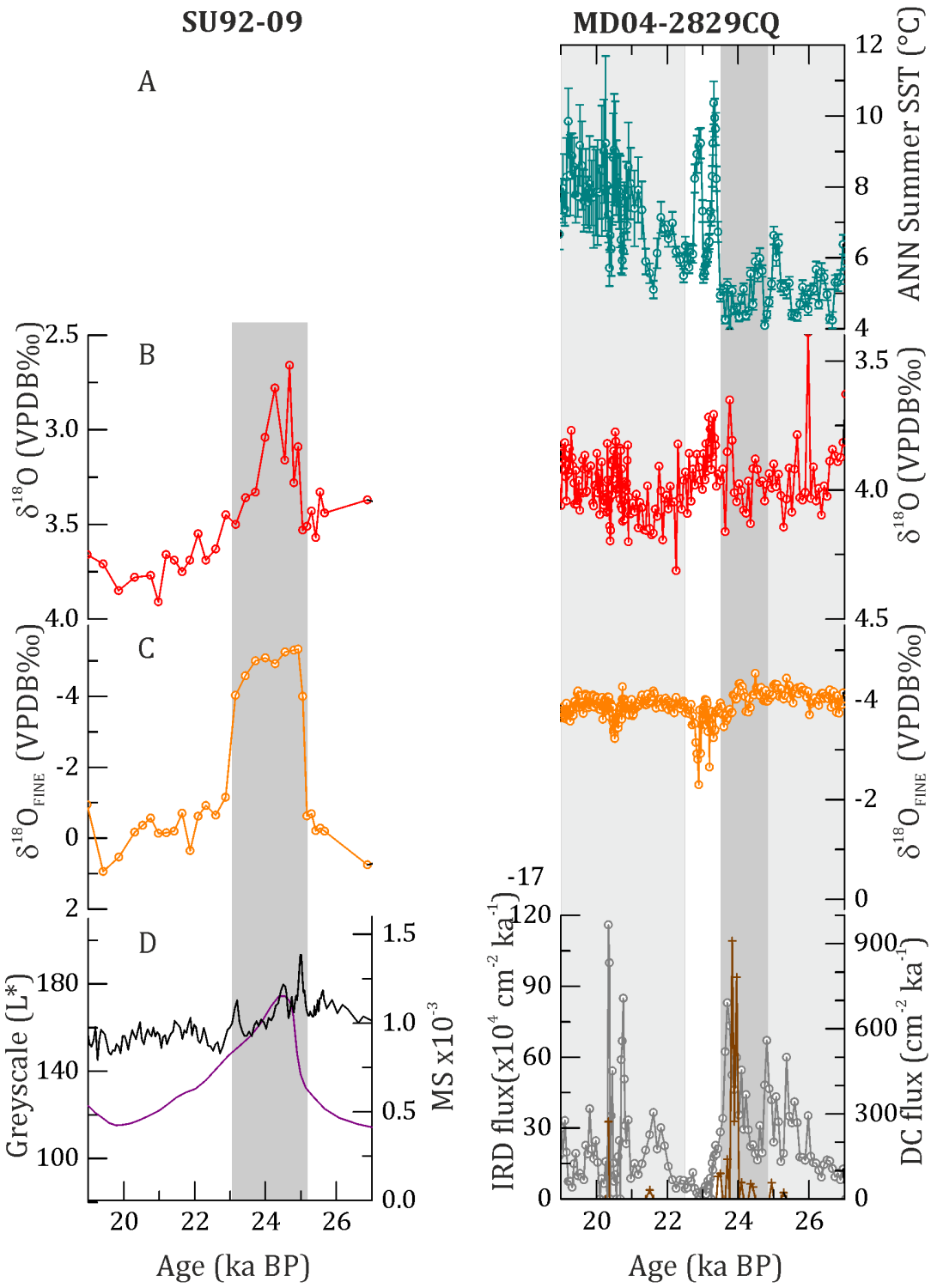

Figure 7.2: Comparison between surface conditions during H2 at site SU92-09 and MD04-2829CQ. A; Estimated sea surface temperatures, B; <u>N. pachyderma</u> C; $\delta^{18}O_{FINE}$ D; Greyscale and Magnetic susceptibility (purple) E; IRD abundances (total IRD in grey and DC in brown), supplementary data from Hall et al. (2011) and Elsa Cortijo pers. comms.

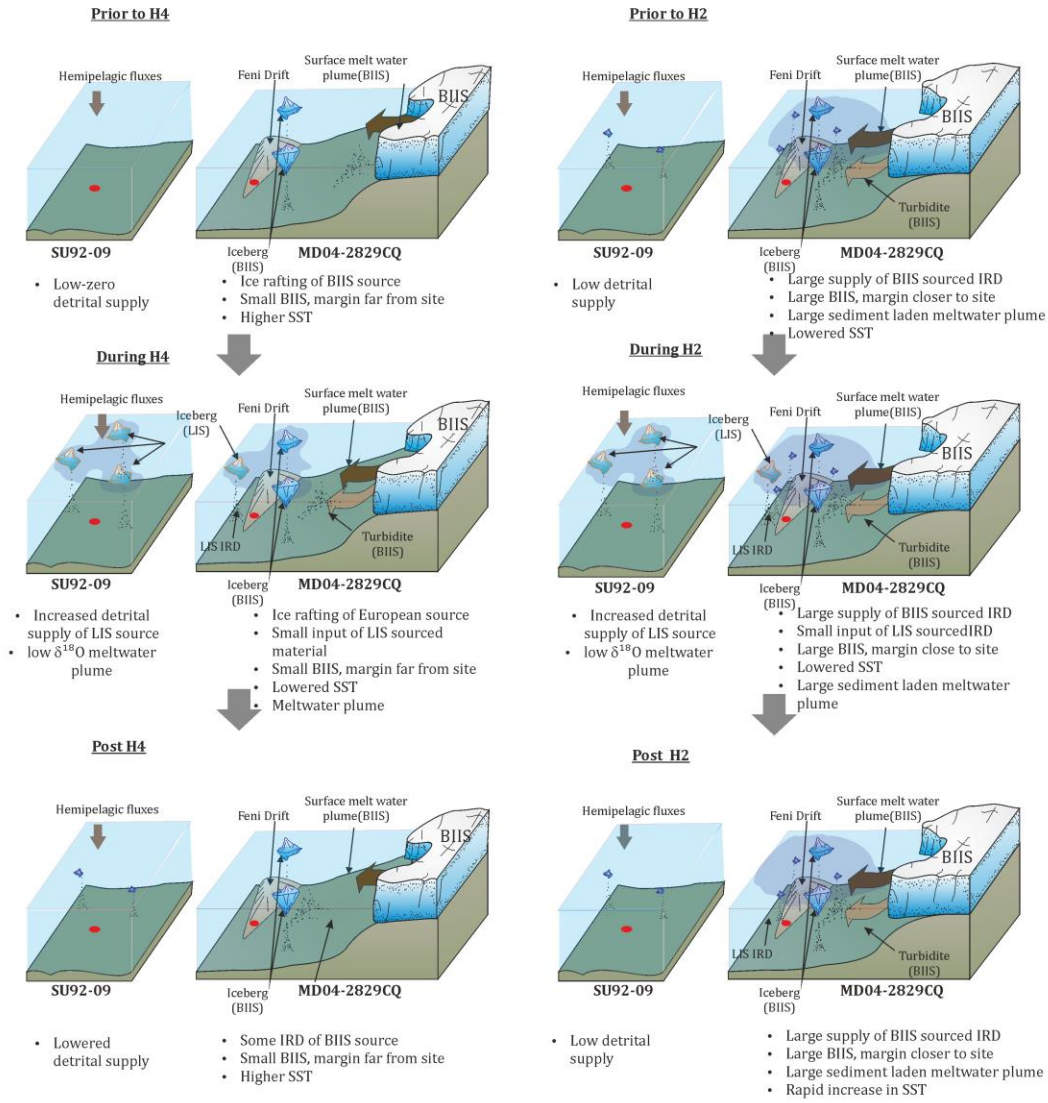

Figure 7.3: Schematic of how sediment composition changes over H2 and H4 based on changes observed at site MD04-2829CQ and site SU92-09. Red circles represent the core sites at each location.

There are several differences in the structure of H4 at the two sites that are shown by the summary data in ***Figure 7.1*** and ***Figure 7.2***. At site MD042829CQ, IRD is transported to the site prior to the main H4 event, (see schematic in Figure 7.3) whereas at the SU9209 site there is little evidence of detrital inputs prior to H4.

The duration of the event and the proportion of material that can be attributed to a LIS source during the Heinrich event is very small at the MD042829-CQ site compared to the SU9209 site, with the majority of the material at the Rockall Trough supplied by the adjacent BIIS. After H4 there is a low input of IRD at both sites. During MIS 3 the BIIS is larger and is thought to have reached the shelf break (Scourse

et al. 2009). This is evident from much increased IRD inputs and consistently low $\delta^{18}O_{FINE}$, and fining of the <63μm fraction indicating a constant input of fine grained material to site MD042829CQ, from processes occurring at the ice margin (Figure 7.3). During H2 at site MD042829CQ these processes dominate the inputs to the site particularly in the finer fraction and there is little imprint of the LIS outside of the coarse fraction lithic counts. At site SU9209, due to the distal position of the site to the ice sheets there is a clear increase in LIS sourced fine fraction material to the site.

7.3 Further Work

This study has highlighted some key issues that can help further our understanding of sediment source changes during abrupt climate change in the North Atlantic.

7.3.1 Source region investigations

Firstly, the key issue raised in Chapter 5 is the comparability of different size fractions for source regions, particularly in the case of Pb and Sr isotopes. Refining source region compositions further by including measurement on all of the >63μm, <63μm and <2μm would be an effective way of further constraining sources. A recent study by Toucanne et al. (2015) illustrated the changing Nd isotope signatures of Northern European rivers, this and the work of Farmer et al. (2003) on TMF, would be supplemented by further analyses of Pb and Sr in rivers and TMF at the European margin. This would be particularly constructive in applying radiogenic isotope analyses to sediments in the Eastern North Atlantic. Benson et al. (2003) use rare earth elements in conjunction with radiogenic isotopes in the Labrador Sea to eliminate local source regions except the Hudson Strait as the source of sediment from H2. Even though the <2μm fraction of sediments is relatively homogenous at site MD04-2829CQ, small changes in Nd and Sr isotopes are still observed, by better constraining the source region of individual ice streams of the BIIS using trace elements and Nd and Sr isotopes it may be possible to identify contributions of different ice streams to the sediment load, allowing further constrains on ice sheet dynamics and models.

7.3.2 Characterising sedimentary change associated with abrupt climate changes using particle size analysis

End member model using particle size distributions (PSD) was able to demonstrate that there are changes in the fine fraction that are associated with increases in IRD

during Heinrich events and millennial-scale changes at the BIIS margin, however it was not possible to allocate the end members to different processes. A further point of enquiry would be to use laser particle size analysis to look at the bulk sediment and see if the particle size distributions can be attributed to different mechanisms of transport more clearly using a wider particle size range.

7.3.3 Mid Atlantic Changes in bottom water ventilation

This study has successfully characterised the clay sized fraction at two sites with very different oceanographic conditions. One of the aims of this study was to use the contrasts between the fine and the coarse fraction to better understand the dynamics between ocean circulation and ice sheets. The oxygen isotope data presented in this thesis alongside the IRD data from site SU92-09 have demonstrated that the changes in surface ocean conditions, and transport of material to the site occur after changes in the deep ocean $\delta^{18}O$. However, the benthic $\delta^{13}C$ from site SU92-09 raises questions over the spatial distribution of Northern Component Waters relative to the Southern Component waters during H4. At site SU92-09 it was not possible to identify a decrease in $\delta^{13}C$ during H4, there are several explanations why this may have occurred, the simplest is that the hiatus in the *C. wuellerstorfi* $\delta^{13}C$ record means that the lowered $\delta^{13}C$ that occurs during H4 is not recorded. This hypothesis could be tested by taking further samples over the H4 interval from the same core and running replicate *C. wuellerstorfi* $\delta^{13}C$ analyses, to cover the hiatus, or if this is not possible to use *C. wuellerstorfi* $\delta^{13}C$ from local sites where no hiatus in the deposition of benthic foraminifera is found. Another potential scenario is that as site SU92-09 as the glacial $\delta^{13}C$ values of *C. wuellerstorfi* are similar to that of NADW throughout MIS 3, and the NADW does not shoal at the site until ~30 ka BP to become GNAIW, it could be that the site is not sensitive to the northward incursion of SCW as the site is 500 m shallower than the more northerly site of U1308 which does show a large $\delta^{13}C$ excursion during H4, and this could have implications for the depth of the NADW/SCW boundary in the Mid North Atlantic (Figure 7.3). In order to test this hypothesis, a multisite study of $\delta^{13}C$ of benthic foraminifera at different depths close to SU92-09 could be examined over H4 to locate the depth of the NADW/SCW during the event in the mid North Atlantic.

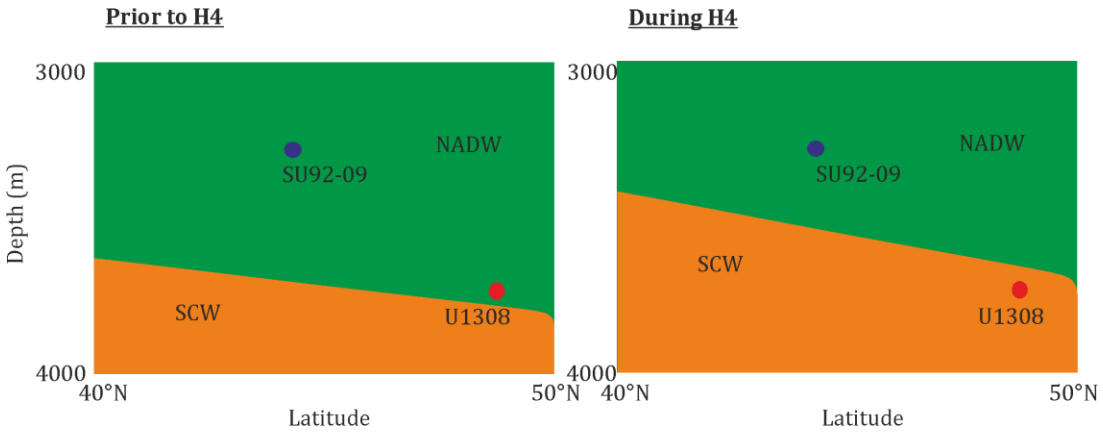

Figure 7.4 Simplified sketch hypothesis showing proposed change in depth of NADW during H4.

8 References

Abouchami, W., Galer, S.J.G., Koschinsky, A., 1999. Pb and Nd isotopes in NE Atlantic Fe–Mn crusts: Proxies for trace metal paleosources and paleocean circulation. Geochim. Cosmochim. Acta 63, 1489–1505. doi:10.1016/S0016-7037(99)00068-X

Alley, R.B., Dupont, T.K., Parizek, B.R., Anandakrishnan, S., Lawson, D.E., Larson, G.J., Evenson, E.B., 2006. Outburst flooding and the initiation of ice-stream surges in response to climatic cooling: A hypothesis. Geomorphology, Ice Sheet Geomorphology - Past and Present Processes and Landforms34th Binghampton Geomorphology Symposium 75, 76–89. doi:10.1016/j.geomorph.2004.01.011

Alvarez-Solas, J., Ramstein, G., 2011. On the triggering mechanism of Heinrich events. Proc. Natl. Acad. Sci. 108, 1359–1360. doi:10.1073/pnas.1116575108

Andersen, K.K., Azuma, N., Barnola, J.-M., Bigler, M., Biscaye, P., Caillon, N., Chappellaz, J., Clausen, H.B., Dahl-Jensen, D., Fischer, H., Flückiger, J., Fritzsche, D., Fujii, Y., Goto-Azuma, K., Grønvold, K., Gundestrup, N.S., Hansson, M., Huber, C., Hvidberg, C.S., Johnsen, S.J., Jonsell, U., Jouzel, J., Kipfstuhl, S., Landais, A., Leuenberger, M., Lorrain, R., Masson-Delmotte, V., Miller, H., Motoyama, H., Narita, H., Popp, T., Rasmussen, S.O., Raynaud, D., Rothlisberger, R., Ruth, U., Samyn, D., Schwander, J., Shoji, H., Siggard-Andersen, M.-L., Steffensen, J.P., Stocker, T., Sveinbjörnsdóttir, A.E., Svensson, A., Takata, M., Tison, J.-L., Thorsteinsson, T., Watanabe, O., Wilhelms, F., White, J.W.C., 2004. High-resolution record of Northern Hemisphere climate extending into the last interglacial period. Nature 431, 147–151. doi:10.1038/nature02805

Anderson, R.F., Ali, S., Bradtmiller, L.I., Nielsen, S.H.H., Fleisher, M.Q., Anderson, B.E., Burckle, L.H., 2009. Wind-Driven Upwelling in the Southern Ocean and the Deglacial Rise in Atmospheric CO2. Science 323, 1443–1448. doi:10.1126/science.1167441

Andrews, J.T., Tedesco, K., 1992. Detrital carbonate-rich sediments, northwestern Labrador Sea: Implications for ice-sheet dynamics and iceberg rafting (Heinrich) events in the North Atlantic. Geology 20, 1087. doi:10.1130/0091-7613(1992)020<1087:DCRSNL>2.3.CO;2

Andrews, J.T., Erlenkeuser, H., Tedesco, K., Aksu, A.E., Jull, A.J.T., 1994. Late Quaternary (Stage 2 and 3) Meltwater and Heinrich Events, Northwest Labrador Sea. Quat. Res. 41, 26–34. doi:10.1006/qres.1994.1003

Andrews, J.T., Kirby, M.E., Aksu, A., Barber, D.C., Meese, D., 1998. Late quaternary detrital carbonate (DC) layers in Baffin Bay marine sediments (67°–74° N): correlation with Heinrich events in the North Atlantic? Quat. Sci. Rev. 17, 1125–1137. doi:10.1016/S0277-3791(97)00064-4

Andrews, J.T., 2000. Icebergs and iceberg rafted detritus (IRD) in the North Atlantic: facts and assumptions. oceanography 13, 100–108.

Andrews, J.T., Principato, S.M., 2002. Grain-size characteristics and provenance of ice-proximal glacial marine sediments. Geol. Soc. Lond. Spec. Publ. 203, 305–324. doi:10.1144/GSL.SP.2002.203.01.16

Andrews, J.T., Hardardóttir, J., Kristjansdóttir, G.B., Grönvold, K., Stoner, J.S., 2003. A high-resolution Holocene sediment record from Húnaflóaáll, N Iceland margin: centuryto millennial-scale varability since the Vedde tephra. The Holocene 13, 625–638. doi:10.1191/0959683603hl651ft

Armishaw, J.E., Holmes, R.W., Stow, D.A.., 2000. The Barra Fan: A bottom-current reworked glacially-fed submarine fan system. Mar. Pet. Geol. 17, 219–238.

Arz, H.W., Lamy, F., Pätzold, J., Müller, P.J., Prins, M., 2003. Mediterranean Moisture Source for an Early-Holocene Humid Period in the Northern Red Sea. Science 300, 118–121. doi:10.1126/science.1080325

Arz, Helge W., Frank Lamy, Andrey Ganopolski, Norbert Nowaczyk, and Jürgen Pätzold. 2007. "Dominant Northern Hemisphere Climate Control over Millennial-Scale Glacial Sea-Level Variability." *Quaternary Science Reviews* 26, no. 3–4: 312–21. doi:10.1016/j.quascirev.2006.07.016.

Auffret, G., Zaragosi, S., Dennielou, B., Cortijo, E., Van Rooij, D., Grousset, F., Pujol, C., Eynaud, F., Siegert, M., 2002. Terrigenous fluxes at the Celtic margin during the last glacial cycle. Mar. Geol. 188, 79–108. doi:10.1016/S0025-3227(02)00276-1

Bailey, I., Foster, G.L., Wilson, P.A., Jovane, L., Storey, C.D., Trueman, C.N., Becker, J., 2012. Flux and provenance of ice-rafted debris in the earliest Pleistocene sub-polar North Atlantic Ocean comparable to the last glacial maximum. Earth Planet. Sci. Lett. 341-344, 222–233. doi:10.1016/j.epsl.2012.05.034

Bailey, I., Hole, G.M., Foster, G.L., Wilson, P.A., Storey, C.D., Trueman, C.N., Raymo, M.E., 2013. An alternative suggestion for the Pliocene onset of major northern hemisphere glaciation based on the geochemical provenance of North Atlantic Ocean ice-rafted debris. Quat. Sci. Rev. 75, 181–194. doi:10.1016/j.quascirev.2013.06.004

Balsam, W.L., Williams, D., 1993. Transport of carbonate sediment in the western North Atlantic: evidence from oxygen and carbon isotopes. Mar. Geol. 112, 23–34.

Barber, D.C., 2001. Laurentide ice sheet dynamics from 35 to 7 ka: Sr–Nd–Pb isotopic provenance of NW North Atlantic margin sediments. University of Colorado, Boulder.

Bard, E., 2000. Hydrological Impact of Heinrich Events in the Subtropical Northeast Atlantic. Science 289, 1321–1324. doi:10.1126/science.289.5483.1321

Barker, S., Elderfield, H., 2002. Foraminiferal Calcification Response to Glacial-Interglacial Changes in Atmospheric CO2. Science 297, 833–836. doi:10.1126/science.1072815

Barker, S., Knorr, G., Edwards, R.L., Parrenin, F., Putnam, A.E., Skinner, L.C., Wolff, E., Ziegler, M., 2011. 800,000 Years of Abrupt Climate Variability. Science 334, 347–351. doi:10.1126/science.1203580

Barker, S., Chen, J., Gong, X., Jonkers, L., Knorr, G., Thornalley, D., 2015. Icebergs not the trigger for North Atlantic cold events. Nature 520, 333–336. doi:10.1038/nature14330

Bennett, M., Glasser, N., 2009. Glacial Geology Ice Sheets and Landforms, 2nd ed. Wiley-Blackwell, Chichester.

Benson, L., Barber, D., Andrews, J.T., Taylor, H., Lamothe, P., 2003. Rare-earth elements and Nd and Pb isotopes as source indicators for Labrador Sea clay-size sediments during Heinrich event 2. Quat. Sci. Rev. 22, 881–889. doi:10.1016/S0277-3791(03)00011-8

Benway, H.M., McManus, J.F., Oppo, D.W., Cullen, J.L., 2010. Hydrographic changes in the eastern subpolar North Atlantic during the last deglaciation. Quat. Sci. Rev. 29, 3336–3345. doi:10.1016/j.quascirev.2010.08.013

Berger, A., and M. F. Loutre. 1991. “Insolation Values for the Climate of the Last 10 Million Years.” *Quaternary Science Reviews* 10 (4): 297–317. doi:10.1016/0277-3791(91)90033-Q.

Bianchi, Hall, McCave, Joseph, 1999. Measurement of the sortable silt current speed proxy using the Sedigraph 5100 and Coulter Multisizer IIe: precision and accuracy. Sedimentology 46, 1001–1014. doi:10.1046/j.1365-3091.1999.00256.x

Bianchi, G.G., McCave, I.N., 2000. Hydrography and sedimentation under the deep western boundary current on Björn and Gardar Drifts, Iceland Basin. Mar. Geol. 165, 137–169. doi:10.1016/S0025-3227(99)00139-5

Biscaye, P.E., Dasch, E.J., 1971. The rubidium, strontium, strontium-isotope system in deep-sea sediments: Argentine Basin. J. Geophys. Res. 76, 5087–5096. doi:10.1029/JC076i021p05087

Bitz, C.M., Chiang, J.C.H., Cheng, W., Barsugli, J.J., 2007. Rates of thermohaline recovery from freshwater pulses in modern, Last Glacial Maximum, and greenhouse warming climates. Geophys. Res. Lett. 34, L07708. doi:10.1029/2006GL029237

Bloemsma, M. R., M. Zabel, J. B. W. Stuut, R. Tjallingii, J. A. Collins, and G. J. Weltje. 2012. “Modelling the Joint Variability of Grain Size and Chemical Composition in Sediments.” *Sedimentary Geology* 280 (December): 135–48. doi:10.1016/j.sedgeo.2012.04.009.

Blott, S.J., Pye, K., 2001. GRADISTAT: a grain size distribution and statistics package for the analysis of unconsolidated sediments. Earth Surf. Process. Landf. 26, 1237–1248. doi:10.1002/esp.261

Blott, S.J., Pye, K., 2012. Particle size scales and classification of sediment types based on particle size distributions: Review and recommended procedures. Sedimentology 59, 2071–2096. doi:10.1111/j.1365-3091.2012.01335.x

Bond, G., Heinrich, H., Broecker, W., Labeyrie, L., McManus, J., Andrews, J., Huon, S., Jantschik, R., Clasen, S., Simet, C., Tedesco, K., Klas, M., Bonani, G., Ivy, S., 1992. Evidence for massive discharges of icebergs into the North Atlantic ocean during the last glacial period. Nature 360, 245–249. doi:10.1038/360245a0

Bond, G.C., Broecker, W.S., Johnsen, S.J., McManus, J., Labeyrie, L., Jouzel, J., Bonani, G., 1993. Correlations between climate records from North Atlantic sediments and Greenland. Nature 365, 143–147.

Bond, G.C., Lotti, R., 1995. Iceberg Discharges into the North Atlantic on Millennial Time Scales During the Last Glaciation. Science 267, 1005–1010. doi:10.1126/science.267.5200.1005

Bond, G., Showers, W., Cheseby, M., Lotti, R., Almasi, P., Priore, P., Cullen, H., Hajdas, I., Bonani, G., 1997. A pervasive millennial-scale cycle in North Atlantic Holocene and glacial climates. science 278, 1257–1266.

Bout-Roumazeilles, V., Cortijo, E., Labeyrie, L., Debrabant, P., 1999. Clay mineral evidence of nepheloid layer contributions to the Heinrich layers in the northwest Atlantic. Palaeogeogr. Palaeoclimatol. Palaeoecol. 146, 211–228. doi:10.1016/S0031-0182(98)00137-0

Boyle, E.A., Keigwin, L., 1987. North Atlantic thermohaline circulation during the past 20,000 years linked to high-latitude surface temperature. Nature 330, 35–40. doi:10.1038/330035a0

Bradwell, T., Stoker, M., 2007. Geomorphological signature and flow dynamics of The Minch palaeo-ice stream, northwest Scotland. Quat. Sci. Rev. 22, 609–617.

Broecker, W., Bond, G., Klas, M., Clark, E., McManus, J., 1992. Origin of the northern Atlantic's Heinrich events. Clim. Dyn. 6, 265–273. doi:10.1007/BF00193540

Broecker, W.S., 1994. Massive iceberg discharges as triggers for global climate change. Nature 372, 421–424.

Broecker, W.S., 1998. Paleocean circulation during the Last Deglaciation: A bipolar seesaw? Paleoceanography 13, 119–121. doi:10.1029/97PA03707

Broecker, W.S., 2003. Does the Trigger for Abrupt Climate Change Reside in the Ocean or in the Atmosphere? Science 300, 1519–1522. doi:10.1126/science.1083797

Brook, E.J., Sowers, T., Orchardo, J., 1996. Rapid Variations in Atmospheric Methane Concentration During the Past 110,000 Years. Science 273, 1087–1091. doi:10.1126/science.273.5278.1087

Calov, R., 2002. Large-scale instabilities of the Laurentide ice sheet simulated in a fully coupled climate-system model. Geophys. Res. Lett. 29. doi:10.1029/2002GL016078

Caniupán, M., Lamy, F., Lange, C.B., Kaiser, J., Arz, H., Kilian, R., Baeza Urrea, O., Aracena, C., Hebbeln, D., Kissel, C., Laj, C., Mollenhauer, G., Tiedemann, R., 2011. Millennial-scale sea surface temperature and Patagonian Ice Sheet changes off southernmost Chile (53°S) over the past ~60 kyr. Paleoceanography 26, n/a–n/a. doi:10.1029/2010PA002049

Channell, J.E.T., Hodell, D.A., Romero, O., Hillaire-Marcel, C., de Vernal, A., Stoner, J.S., Mazaud, A., Röhl, U., 2012. A 750-kyr detrital-layer stratigraphy for the North Atlantic (IODP Sites U1302–U1303, Orphan Knoll, Labrador Sea). Earth Planet. Sci. Lett. 317-318, 218–230. doi:10.1016/j.epsl.2011.11.029

Channell, J.E.T., Hodell, D.A., 2013. Magnetic signatures of Heinrich-like detrital layers in the Quaternary of the North Atlantic. Earth Planet. Sci. Lett. 369–370, 260–270. doi:10.1016/j.epsl.2013.03.034

Chappellaz, J., Bluniert, T., Raynaud, D., Barnola, J.M., Schwander, J., Stauffert, B., 1993. Synchronous changes in atmospheric CH4 and Greenland climate between 40 and 8 kyr BP. Nature 366, 443–445. doi:10.1038/366443a0

Chappellaz, J., Stowasser, C., Blunier, T., Baslev-Clausen, D., Brook, E.J., Dallmayr, R., Faïn, X., Lee, J.E., Mitchell, L.E., Pascual, O., Romanini, D., Rosen, J., Schüpbach, S., 2013. High-resolution glacial and deglacial record of atmospheric methane by continuous-flow and laser spectrometer analysis along the NEEM ice core. Clim Past 9, 2579–2593. doi:10.5194/cp-9-2579-2013

Chester, R., Hughes, M.., 1967. A chemical technique for the separation of ferro-manganese minerals, carbonate minerals and adsorbed trace elements from pelagic sediments. Chem. Geol. 2, 249–262.

Clark, C.D., Hughes, A.L.C., Greenwood, S.L., Jordan, C., Sejrup, H.P., 2012. Pattern and timing of retreat of the last British-Irish Ice Sheet. Quat. Sci. Rev. 44, 112–146. doi:10.1016/j.quascirev.2010.07.019

Clarke, G.K.C., Marshall, S.J., Hillaire-Marcel, C., Bilodeau, G., Veiga-Pires, C., 1999. A Glaciological Perspective on Heinrich Events, in: Clark, P.U., Webb, R.S., Keigwin, L.D. (Eds.), Mechanisms of Global Climate Change at Millennial Time Scales. American Geophysical Union, pp. 243–262.

Clark, P.U., Mix, A.C., 2000. Global change: Ice sheets by volume. Nature 406, 689–690. doi:10.1038/35021176

Clauer, N., Chaudhuri, S., Kralik, M., Bonnot-Courtois, C., 1993. Effects of experimental leaching on Rb□Sr and K□Ar isotopic systems and REE contents of diagenetic illite. Chem. Geol. 103, 1–16. doi:10.1016/0009-2541(93)90287-S

Cortijo, E., Labeyrie, L., Vidal, L., Vautravers, M.J., Chapman, M., Duplessy, J.-C., Elliot, M., Arnold, M., Turon, J.-L., Auffret, G., 1997. Changes in sea surface hydrology associated with Heinrich event 4 in the North Atlantic Ocean between 40° and 60° N. Earth Planet. Sci. Lett. 146, 29–45.

Cortijo, E., Duplessy, J.-C., Labeyrie, L., Duprat, J., Paillard, D., 2005. Heinrich events: hydrological impact. Comptes Rendus Geosci. 337, 897–907. doi:10.1016/j.crte.2005.04.011

Crocket, K.C., Foster, G.L., Vance, D., Richards, D.A., Tranter, M., 2013. A Pb isotope tracer of ocean-ice sheet interaction: the record from the NE Atlantic during the Last Glacial/Interglacial cycle. Quat. Sci. Rev. 82, 133–144. doi:10.1016/j.quascirev.2013.10.020

Culver, S.J., 1991. Early Cambrian Foraminifera from West Africa. Science 254, 689–691. doi:10.1126/science.254.5032.689

Curry, W.B., Oppo, D.W., 2005. Glacial water mass geometry and the distribution of $\delta^{13}C$ of ΣCO_2 in the western Atlantic Ocean. Paleoceanography 20, PA1017. doi:10.1029/2004PA001021

Dahlgren, KI Torbjørn, and Tore O. Vorren. 2003. "Sedimentary Environment and Glacial History during the Last 40 Ka of the Vøring Continental Margin, Mid-Norway." *Marine Geology* 193 (1): 93–127.

Dansgaard, W., Clausen, H.B., Gundestrup, N., Hammer, C.U., Johnsen, S.., 1982. A New Greenland Deep Ice Core. Science 218, 1274–1277.

Dansgaard, W., Johnsen, S.J., Clausen, H.B., Dahl-Jensen, D., Gundestrup, N., Hammer, C.U., Hvldberg, C.S., Steffensen, J.P., Sveinbjornsdottir, A.E., Jouzel, J., Bond, G.C., 1993. Evidence for general instability of past climate from a 250-kyr ice core record. Nature 364, 218–220.

Dasch, E.J., 1969. Strontium isotopes in weathering profiles, deep-sea sediments, and sedimentary rocks. Geochim. Cosmochim. Acta 33, 1521–1552. doi:10.1016/0016-7037(69)90153-7

Davis, J.C., 1970. Information contained in sediment-size analyses. J. Int. Assoc. Math. Geol. 2, 105–112. doi:10.1007/BF02315152

de Abreu, L., Shackleton, N.J., Schönfeld, J., Hall, M., Chapman, M., 2003. Millennial-scale oceanic climate variability off the Western Iberian margin during the last two glacial periods. Mar. Geol. 196, 1–20. doi:10.1016/S0025-3227(03)00046-X

deGelleke, L., Hill, P.S., Kienast, M., Piper, D.J.W., 2013. Sediment dynamics during Heinrich event H1 inferred from grain size. Mar. Geol. 336, 160–169. doi:10.1016/j.margeo.2012.12.007

DePaolo, D.J., Wasserburg, G.., 1979. Petrogenetic mixing models and Nd-Sr isotopic patterns. Geochim. Cosmochim. Acta 43, 615–627.

Dowdeswell, J.A., Scourse, J.D., 1990. On the description and modelling of glacimarine sediments and sedimentation. Geol. Soc. Lond. Spec. Publ. 53, 1–13. doi:10.1144/GSL.SP.1990.053.01.01

Dowdeswell, J.A., Maslin, M.A., Andrews, J.T., McCave, I.N., 1995. Iceberg production, debris rafting, and the extent and thickness of Heinrich layers (H-

1, H-2) in North Atlantic sediments. Geology 23, 301. doi:10.1130/0091-7613(1995)023<0297:IPDRAT>2.3.CO;2

Dowdeswell, J.A., ELVERHFI, A., Spielhagen, R., 1998. Glacimarine sedimentary processes and facies on the Polar North Atlantic margins. Quat. Sci. Rev. 17, 243–272.

Downing, G.E., Hemming, S.R., Jost, A., Roy, M., 2013. $^{40}Ar/^{39}Ar$ hornblende provenance clues about Heinrich event 3 (H3). Geol. Soc. Lond. Spec. Publ. 378, SP378.18. doi:10.1144/SP378.18

Duplessy, J.C., Shackleton, N.J., Fairbanks, R.G., Labeyrie, L., Oppo, D., Kallel, N., 1988. Deepwater source variations during the last climatic cycle and their impact on the global deepwater circulation. Paleoceanography 3, 343–360. doi:10.1029/PA003i003p00343

Elderfield, H., Vautravers, M., Cooper, M., 2002. The relationship between shell size and Mg/Ca, Sr/Ca, $\delta^{18}O$, and $\delta^{13}C$ of species of planktonic foraminifera. Geochem. Geophys. Geosystems 3, 1–13. doi:10.1029/2001GC000194

Elliot, M., Labeyrie, L., Bond, G.C., Cortijo, E., Turon, J.L., Tisnerat, N., Duplessy, J.-C., 1998. Millenial-scale iceberg discharges in the Irminger Basin during the last glacial period: Relationship with the Heinrich events and environmental settings. Paleoceanography 13, 433–446.

Elliot, M., Labeyrie, L., Duplessy, J.-C., 2002. Changes in North Atlantic deep-water formation associated with the Dansgaard–Oeschger temperature oscillations (60–10ka). Quat. Sci. Rev. 21, 1153–1165.

Emiliani, C., 1955. Pleistocene Temperatures. J. Geol. 63, 538–578.

Epstein, S., Buchsbaum, R., Lowenstam, H.A., Urey, H.C., 1953. Revised Carbonate-Water Isotopic Temperature Scale. Geol. Soc. Am. Bull. 64, 1315–1326. doi:10.1130/0016-7606(1953)64[1315:RCITS]2.0.CO;2

Evans, David J.A., Chris D. Clark, and Wishart A. Mitchell. 2005. "The Last British Ice Sheet: A Review of the Evidence Utilised in the Compilation of the Glacial Map of Britain." *Earth-Science Reviews* 70 (3-4): 253–312. doi:10.1016/j.earscirev.2005.01.001.

Fagel, N., Innocent, C., Stevenson, R.K., Hillaire-Marcel, C., 1999. Deep circulation changes in the Labrador Sea since the Last Glacial Maximum: New constraints from Sm-Nd data on sediments. Paleoceanography 14, 777–788. doi:10.1029/1999PA900041

Fagel, N., Innocent, C., Gariepy, C., Hillaire-Marcel, C., 2002. Sources of Labrador Sea sediments since the last glacial maximum inferred from Nd-Pb isotopes. Geochim. Cosmochim. Acta 66, 2569–2581. doi:10.1016/S0016-7037(02)00866-9

Fagel, N., Hillaire-Marcel, C., Humblet, M., Brasseur, R., Weis, D., Stevenson, R., 2004. Nd and Pb isotope signatures of the clay-size fraction of Labrador Sea sediments during the Holocene: Implications for the inception of the modern deep circulation pattern. Paleoceanography 19, PA3002. doi:10.1029/2003PA000993

Fagel, N., Hillaire-Marcel, C., 2006. Glacial/interglacial instabilities of the Western Boundary Under Current during the last 365 kyr from Sm/Nd ratios of the sedimentary clay-size fractions at ODP site 646 (Labrador Sea). Mar. Geol. 232, 87–99. doi:10.1016/j.margeo.2006.08.006

Fagel, N., Mattielli, N., 2011. Holocene evolution of deep circulation in the northern North Atlantic traced by Sm, Nd and Pb isotopes and bulk sediment mineralogy. Paleoceanography 26, PA4220. doi:10.1029/2011PA002168

Fairbanks, R.G., Mortlock, R.A., Chiu, T.-C., Cao, L., Kaplan, A., Guilderson, T.P., Fairbanks, T.W., Bloom, A.L., Grootes, P.M., Nadeau, M.-J., 2005. Radiocarbon calibration curve spanning 0 to 50,000 years BP based on paired 230Th/234U/238U and 14C dates on pristine corals. Quat. Sci. Rev. 24, 1781–1796. doi:10.1016/j.quascirev.2005.04.007

Farmer, G.L., Barber, D., Andrews, J., 2003. Provenance of Late Quaternary ice-proximal sediments in the North Atlantic: Nd, Sr and Pb isotopic evidence. Earth Planet. Sci. Lett. 209, 227–243. doi:10.1016/S0012-821X(03)00068-2

Faure, G., Mensing, T.M., 2005. Isotopes: Principles and Applications, 3rd ed. John Wiley and Sons, Hoboken.

Folk, R.L., 1966. A Review of Grain-Size Parameters. Sedimentology 6, 73–93. doi:10.1111/j.1365-3091.1966.tb01572.x

Folk, R.L., Ward, W.C., 1957. Brazos River Bar: A Study in the Significance of Grain Size Parameters. J. Sediment. Res. 27.

Forrest, J., Clark, N.R., 1989. Characterizing grain size distributions: evaluation of a new approach using a multivariate extension of entropy analysis. Sedimentology 36, 711–722. doi:10.1111/j.1365-3091.1989.tb02095.x

Francois, R., Bacon, M.P., 1994. Heinrich events in the North Atlantic: Radiochemical evidence. Deep Sea Res. Part Oceanogr. Res. Pap. 41, 315–334.

Franzese, A.M., Hemming, S.R., Goldstein, S.L., Anderson, R.F., 2006. Reduced Agulhas Leakage during the Last Glacial Maximum inferred from an integrated provenance and flux study. Earth Planet. Sci. Lett. 250, 72–88. doi:10.1016/j.epsl.2006.07.002

Gaiero, D.M., 2007. Dust provenance in Antarctic ice during glacial periods: From where in southern South America? Geophys. Res. Lett. 34, L17707. doi:10.1029/2007GL030520

Ganssen, G.M., Kroon, D., 2000. The isotopic signature of planktonic foraminifera from NE Atlantic surface sediments: implications for the reconstruction of past oceanic conditions. J. Geol. Soc. 157, 693–699. doi:10.1144/jgs.157.3.693

Garçon, M., Chauvel, C., France-Lanord, C., Limonta, M., Garzanti, E., 2014. Which minerals control the Nd–Hf–Sr–Pb isotopic compositions of river sediments? Chem. Geol. 364, 42–55. doi:10.1016/j.chemgeo.2013.11.018

Goldstein, S.J., Jacobsen, S.B., 1988. Nd and Sr isotopic systematics of river water suspended material: implications for crustal evolution. Earth Planet. Sci. Lett. 87, 249–265. doi:10.1016/0012-821X(88)90013-1

Goldstein, S.L., Hemming, S.R., 2003. Long-lived Isotopic Tracers in Oceanography, Paleoceanography and Ice-sheet Dynamics, in: Elderfield, H. (Ed.), The Oceans and Marine Geochemistry. Elsevier-Pergamon, Oxford, pp. 453–490.

Grootes, P., Stuiver, M., White, J.W.C., Johnsen, S., Jouzel, J., 1993. Comparison of oxygen isotope records from the GISP2 and GRIP Greenland ice cores. Nature 366, 552–554.

Grootes, Pieter, and M. Stuiver. 1997. "Oxygen 18/16 Variability in Greenland Snow and Ice with 10^3 to 10^5 Year Time Resolution." *Journal of Geophysical Research* 102 (12): 26455–70.

Grousset, F.E., Labeyrie, L., Sinko, J.A., Cremer, M., Bond, G.C., Duprat, J., Cortijo, E., Huon, S., 1993. Patterns of ice-rafted detritus in the glacial North Atlantic (40-55°N). Paleoceanography 8, 175–192.

Grousset, F.E., Pujol, C., Labeyrie, L., Auffret, G., Boelaert, A., 2000. Were the North Atlantic Heinrich events triggered by the behavior of the European ice sheets? Geology 28, 123. doi:10.1130/0091-7613(2000)28<123:WTNAHE>2.0.CO;2

Grousset, F.E., Cortijo, E., Huon, S., Herve, L., Richter, T., Burdloff, D., Duprat, J., Weber, O., 2001. Zoooming in on Heinrich Layers. Paleoceanography 16, 240–259.

Gwiazda, R.H., Hemming, S.R., Broecker, W.S., 1996a. Provenance of icebergs during Heinrich event 3 and the contrast to their sources during other Heinrich episodes. Paleoceanography 11, 371–378.

Gwiazda, R.H., Hemming, S.R., Broecker, W.S., 1996b. Tracking the sources of icebergs with lead isotopes: The provenance of ice-rafted debris in Heinrich layer 2. Paleoceanography 11, 77–93.

Haapaniemi, A.I., Scourse, J.D., Peck, V.L., Kennedy, H., Kennedy, P., Hemming, S.R., Furze, M.F.A., PieńKowski, A.J., Austin, W.E.N., Walden, J., Wadsworth, E., Hall, I.R., 2010. Source, timing, frequency and flux of ice-rafted detritus to the Northeast Atlantic margin, 30-12 ka: testing the Heinrich precursor hypothesis. Boreas 576–591. doi:10.1111/j.1502-3885.2010.00141.x

Hall, I.R., Scourse, J.D., 2005. Sequencing Ocean-Ice Interaction, MD141 Cruise Report.

Hall, I.R., Moran, S.B., Zahn, R., Knutz, P.C., Shen, C.-C., Edwards, R.L., 2006. Accelerated drawdown of meridional overturning in the late-glacial Atlantic triggered by transient pre-H event freshwater perturbation. Geophys. Res. Lett. 33, L16616. doi:10.1029/2006GL026239

Hall, I.R., Colmenero-Hidalgo, E., Zahn, R., Peck, V.L., Hemming, S.R., 2011. Centennial- to millennial-scale ice-ocean interactions in the subpolar northeast Atlantic 18-41 kyr ago. Paleoceanography 26, PA2224. doi:10.1029/2010PA002084

Hart, S.R., 1984. A large-scale isotope anomaly in the Southern Hemisphere mantle. Nature 309, 753–757. doi:10.1038/309753a0

Hass, H.C., 2002. A method to reduce the influence of ice-rafted debris on a grain size record from northern Fram Strait, Arctic Ocean. Polar Res. 21, 299–306. doi:10.1111/j.1751-8369.2002.tb00084.x

He, Y., Duan, T., and Gao, Z., 2008. Chapter 7 Sediment Entrainment. Developments in Sedimentology. 60, 101-119.

Hebbeln, D., 2000. Flux of ice-rafted detritus from sea ice in the Fram Strait. Deep Sea Res. Part II Top. Stud. Oceanogr. 47, 1773–1790. doi:10.1016/S0967-0645(00)00006-0

Heinrich, Hartmut. 1988. "Origin and Consequences of Cyclic Ice Rafting in the Northeast Atlantic Ocean during the Past 130,000 Years." *Quaternary Research* 29 (2): 142–52. doi:10.1016/0033-5894(88)90057-9.

Hemming, S.R., Broecker, W.S., Sharp, W.D., Bond, G.C., Gwiazda, R.H., McManus, J.F., Klas, M., Hajdas, I., 1998. Provenance of Heinrich layers in core V28-82, northeastern Atlantic: $^{40}Ar/^{39}Ar$ ages of ice-rafted hornblende, Pb isotopes in feldspar grains, and Nd–Sr–Pb isotopes in the fine sediment fraction. Earth Planet. Sci. Lett. 164, 317–333.

Hemming, S.R., Bond, G.C., Broecker, W.S., Sharp, W.D., Klas-Mendelson, M., 2000. Evidence from $^{40}Ar/^{39}Ar$ Ages of Individual Hornblende Grains for Varying Laurentide Sources of Iceberg Discharges 22,000 to 10,500 yr B.P. Quat. Res. 54, 372–383. doi:10.1006/qres.2000.2181

Hemming, S.R., Gwiazda, R.H., Andrews, J.T., Broecker, W.S., Jennings, A.E., Onstott, T.C., 2000. 40Ar/39Ar and Pb-Pb study of individual hornblende and

feldspar grains from southeastern Baffin Island glacial sediments: Implications for the provenance of the Heinrich layers. Can. J. Earth Sci. 37, 879–890.

Hemming, S.R., Hall, C.., Biscaye, P.E., Higgins, S.M., Bond, G.C., McManus, J.F., Barber, D.C., Andrews, J.T., Broecker, W.S., 2002. ^{40}Ar/^{39}Ar and ^{40}Ar concentrations of fine grained sediment fractions from North Atlantic Heinrich layers. Chem. Geol. 182, 583–603.

Hemming, S.R., Hajdas, I., 2003. Ice-rafted detritus evidence from ^{40}Ar/^{39}Ar ages of individual hornblende grains for evolution of the eastern margin of the Laurentide ice sheet since 43 14C ky. Quat. Int. 99–100, 29–43. doi:10.1016/S1040-6182(02)00110-6

Hemming, S.R., 2004. Heinrich events: Massive late Pleistocene detritus layers of the North Atlantic and their global climate imprint. Rev. Geophys. 42. doi:10.1029/2003RG000128

Heslop, D., von Dobeneck, T., Höcker, M., 2007. Using non-negative matrix factorization in the "unmixing" of diffuse reflectance spectra. Mar. Geol. 241, 63–78. doi:10.1016/j.margeo.2007.03.004

Hesse, R., Khodabakhsh, S., 1998. Depositional facies of late Pleistocene Heinrich events in the Labrador Sea. Geology 26, 103–106. doi:10.1130/0091-7613(1998)026<0103:DFOLPH>2.3.CO;2

Hesse, R., Rashid, H., Khodabakhsh, S., 2004a. Fine-grained sediment lofting from meltwater-generated turbidity currents during Heinrich events. Geology 32, 449. doi:10.1130/G20136.1

Hesse, R., Rashid, H., Khodabakhsh, S., 2004b. Fine-grained sediment lofting from meltwater-generated turbidity currents during Heinrich events. Geology 32, 449. doi:10.1130/G20136.1

Hillaire-Marcel, C., Bilodeau, G., 2000. Instabilities in the Labrador Sea water mass structure during the last climatic cycle. Can. J. Earth Sci. 37, 795–809.

Hodell, D.A., Channell, J.E.T., Curtis, J.H., Romero, O.E., Röhl, U., 2008. Onset of "Hudson Strait" Heinrich events in the eastern North Atlantic at the end of the middle Pleistocene transition (~640 ka)? Paleoceanography 23, n/a–n/a. doi:10.1029/2008PA001591

Hodell, D.A., Curtis, J.H., 2008. Oxygen and carbon isotopes of detrital carbonate in North Atlantic Heinrich Events. Mar. Geol. 256, 30–35. doi:10.1016/j.margeo.2008.09.010

Hodell, D.A., Evans, H.F., Channell, J.E.T., Curtis, J.H., 2010. Phase relationships of North Atlantic ice-rafted debris and surface-deep climate proxies during the last glacial period. Quat. Sci. Rev. 29, 3875–3886. doi:10.1016/j.quascirev.2010.09.006

Hoefs, J., 2009. Stable Isotope Geochemistry, 2nd ed. Springer-Verlag, Berlin.

Hubbard, A., Bradwell, T., Golledge, N., Hall, A., Patton, H., Sugden, D., Cooper, R., Stoker, M., 2009. Dynamic cycles, ice streams and their impact on the extent, chronology and deglaciation of the British–Irish ice sheet. Quat. Sci. Rev., Quaternary Glaciodynamics 28, 758–776. doi:10.1016/j.quascirev.2008.12.026

Hughes, A.L.C., Clark, C.D., Jordan, C.J., 2014. Flow-pattern evolution of the last British Ice Sheet. Quat. Sci. Rev. 89, 148–168. doi:10.1016/j.quascirev.2014.02.002

Hulbe, C.L., 1997. An ice shelf mechanism for Heinrich layer production. Paleoceanography 12, 711–717. doi:10.1029/97PA02014

Hulbe, C.L., MacAyeal, D.R., Denton, G.H., Kleman, J., Lowell, T.V., 2004. Catastrophic ice shelf breakup as the source of Heinrich event icebergs. Paleoceanography 19, n/a–n/a. doi:10.1029/2003PA000890

Huon, S., Jantschik, R., 1993. Detrital silicates in Northeast Atlantic deep-sea sediments during the late Quaternary: Major elements, REE, Rb-Sr isotopic data. Eclogae Geol. Helvetiae 86, 195–218.

Innocent, C., Fagel, N., Hillaire-Marcel, C., 2000. Sm–Nd isotope systematics in deep-sea sediments: clay-size versus coarser fractions. Mar. Geol. 168, 79–87. doi:10.1016/S0025-3227(00)00052-9

Jantschik, R., Huon, S., 1992. Detrital silicates in Northeast Atlantic deep-sea sediments during the Late Quaternary: Mineralogical and K-Ar isotopic data. Eclogae Geol. Helvetiae 85, 185–212.

Johnsen, S.J., Clausen, H.B., Dansgaard, W., Fuhrer, K., Gundestrup, N., Hammer, C.U., Iversen, P., Jouzel, J., Stauffer, B., Steffensen, J.P., 1992. Irregular glacial interstadials recorded in a new Greenland ice core. Nature 359, 311–313. doi:10.1038/359311a0

Johns, W.E., Baringer, M.O., Beal, L.M., Cunningham, S.A., Kanzow, T., Bryden, H.L., Hirschi, J.J.M., Marotzke, J., Meinen, C.S., Shaw, B., Curry, R., 2010. Continuous, Array-Based Estimates of Atlantic Ocean Heat Transport at 26.5°N. J. Clim. 24, 2429–2449. doi:10.1175/2010JCLI3997.1

Jonkers, L., Prins, M.A., Brummer, G.-J.A., Konert, M., Lougheed, B.C., 2009. Experimental insights into laser diffraction particle sizing of fine-grained sediments for use in palaeoceanography. Sedimentology 56, 2192–2206. doi:10.1111/j.1365-3091.2009.01076.x

Jonkers, L., Moros, M., Prins, M.A., Dokken, T., Dahl, C.A., Dijkstra, N., Perner, K., Brummer, G.-J.A., 2010. A reconstruction of sea surface warming in the northern North Atlantic during MIS 3 ice-rafting events. Quat. Sci. Rev. 29, 1791–1800. doi:10.1016/j.quascirev.2010.03.014

Jonkers, L., Prins, M.A., Moros, M., Weltje, G.J., Troelstra, S.R., Brummer, G.-J.A., 2012a. Temporal offsets between surface temperature, ice-rafting and bottom flow speed proxies in the glacial (MIS 3) northern North Atlantic. Quat. Sci. Rev. 48, 43–53. doi:10.1016/j.quascirev.2012.06.006

Jonkers, L., Prins, M.A., Moros, M., Weltje, G.J., Troelstra, S.R., Brummer, G.-J.A., 2012b. Temporal offsets between surface temperature, ice-rafting and bottom flow speed proxies in the glacial (MIS 3) northern North Atlantic. Quat. Sci. Rev. 48, 43–53. doi:10.1016/j.quascirev.2012.06.006

Jonkers, L., van Heuven, S., Zahn, R., Peeters, F.J.C., 2013. Seasonal patterns of shell flux, $\delta^{18}O$ and $\delta^{13}C$ of small and large N. pachyderma (s) and G. bulloides in the subpolar North Atlantic. Paleoceanography 28, 164–174. doi:10.1002/palo.20018

Jonkers, L., Zahn, R., Thomas, A., Henderson, G., Abouchami, W., François, R., Masque, P., Hall, I.R., Bickert, T., 2015. Deep circulation changes in the central South Atlantic during the past 145 kyrs reflected in a combined $^{231}Pa/^{230}Th$, Neodymium isotope and benthic record. Earth Planet. Sci. Lett. 419, 14–21. doi:10.1016/j.epsl.2015.03.004

Jouzel, J., Masson-Delmotte, V., Cattani, O., Dreyfus, G., Falourd, S., Hoffmann, G., Minster, B., Nouet, J., Barnola, J.M., Chappellaz, J., Fischer, H., Gallet, J.C., Johnsen, S., Leuenberger, M., Loulergue, L., Luethi, D., Oerter, H., Parrenin, F., Raisbeck, G., Raynaud, D., Schilt, A., Schwander, J., Selmo, E., Souchez, R., Spahni, R., Stauffer, B., Steffensen, J.P., Stenni, B., Stocker, T.F., Tison,

J.L., Werner, M., Wolff, E.W., 2007. Orbital and Millennial Antarctic Climate Variability over the Past 800,000 Years. Science 317, 793–796. doi:10.1126/science.1141038

Jullien, E., Grousset, F.E., Hemming, S.R., Peck, V.L., Hall, I.R., Jeantet, C., Billy, I., 2006. Contrasting conditions preceding MIS3 and MIS2 Heinrich events. Glob. Planet. Change 54, 225–238. doi:10.1016/j.gloplacha.2006.06.021

Kaiser, J., Lamy, F., Hebbeln, D., 2005. A 70-kyr sea surface temperature record off southern Chile (Ocean Drilling Program Site 1233). Paleoceanography 20, n/a–n/a. doi:10.1029/2005PA001146

Keigwin, L.D., Lehman, S.J., 1994. Deep circulation change linked to HEINRICH Event 1 and Younger Dryas in a middepth North Atlantic Core. Paleoceanography 9, 185–194. doi:10.1029/94PA00032

Kim, S.-T., O'Neil, J.R., 1997. Equilibrium and nonequilibrium oxygen isotope effects in synthetic carbonates. Geochim. Cosmochim. Acta 3461–3475. doi:10.1016/S0016-7037(97)00169-5

Klovan, J.E., 1966. The use of factor analysis in determining depositional environments from grain-size distributions. J. Sediment. Res. 36, 115–125. doi:10.1306/74D7141A-2B21-11D7-8648000102C1865D

Knies, J., Kleiber, H.-P., Matthiessen, J., Müller, C., Nowaczyk, N., 2001. Marine ice-rafted debris records constrain maximum extent of Saalian and Weichselian ice-sheets along the northern Eurasian margin. Glob. Planet. Change, The late Quaternary stratigraphy and environments of northern Eurasia and the adjacent Arctic seas - new contributions from QUEEN 31, 45–64. doi:10.1016/S0921-8181(01)00112-6

Knutz, P.C., Austin, W.E.N., Jones, E.J.W., 2001. Millennial-scale depositional cycles related to British Ice Sheet variability and North Atlantic paleocirculation since 45 kyr B.P., Barra Fan, U.K. margin. Paleoceanography 16, 53–64. doi:10.1029/1999PA000483

Knutz, P. C., E. J. W. Jones, W. E. N. Austin, and T. C. E. van Weering. 2002. "Glacimarine Slope Sedimentation, Contourite Drifts and Bottom Current Pathways on the Barra Fan, UK North Atlantic Margin." *Marine Geology* 188 (1–2): 129–46. doi:10.1016/S0025-3227(02)00278-5.

Knutz, P.C., Zahn, R., Hall, I.R., 2007. Centennial-scale variability of the British Ice Sheet: Implications for climate forcing and Atlantic meridional overturning circulation during the last deglaciation. Paleoceanography 22, n/a–n/a. doi:10.1029/2006PA001298

Kroon, D., Shimmield, G., Austin, W.E.N., Derrick, S., Knutz, P., Shimmield, T., 2000. Century- to millennial-scale sedimentological–geochemical records of glacial–Holocene sediment variations from the Barra Fan (NE Atlantic). J. Geol. Soc. 157, 643–653. doi:10.1144/jgs.157.3.643

Lamy, F., 2004. Antarctic Timing of Surface Water Changes off Chile and Patagonian Ice Sheet Response. Science 304, 1959–1962. doi:10.1126/science.1097863

Lamy, F., Kaiser, J., Arz, H.W., Hebbeln, D., Ninnemann, U., Timm, O., Timmermann, A., Toggweiler, J.R., 2007. Modulation of the bipolar seesaw in the Southeast Pacific during Termination 1. Earth Planet. Sci. Lett. 259, 400–413.

Landais, A., Masson-Delmotte, V., Stenni, B., Selmo, E., Roche, D.M., Jouzel, J., Lambert, F., Guillevic, M., Bazin, L., Arzel, O., Vinther, B., Gkinis, V., Popp, T., 2015. A review of the bipolar see–saw from synchronized and high

resolution ice core water stable isotope records from Greenland and East Antarctica. Quat. Sci. Rev. 114, 18–32. doi:10.1016/j.quascirev.2015.01.031

Leigh, S.N.B., 2007. A study of the dynamics of the British Ice Sheet during Marine Isotope Stages 2 and 3, focusing on Heinrich Events 2 and 4 and their relationship to the North Atlantic glaciological and climatological conditions (Thesis). University of St Andrews.

Lekens, W.A.H., H.P. Sejrup, H. Haflidason, G.ø. Petersen, B. Hjelstuen, and G. Knorr. 2005. "Laminated Sediments Preceding Heinrich Event 1 in the Northern North Sea and Southern Norwegian Sea: Origin, Processes and Regional Linkage." *Marine Geology* 216 (1-2): 27–50. doi:10.1016/j.margeo.2004.12.007.

Leng, M.J., Jones, M.D., Frogley, M.R., Eastwood, W.J., Kendrick, C.P., Roberts, C.N., 2010. Detrital carbonate influences on bulk oxygen and carbon isotope composition of lacustrine sediments from the Mediterranean. Glob. Planet. Change, Oxygen isotopes as tracers of Mediterranean variability: linking past, present and future 71, 175–182. doi:10.1016/j.gloplacha.2009.05.005

Lippold, J., Grützner, J., Winter, D., Lahaye, Y., Mangini, A., Christl, M., 2009. Does sedimentary $^{231}Pa/^{230}Th$ from the Bermuda Rise monitor past Atlantic Meridional Overturning Circulation? Geophys. Res. Lett. 36, L12601. doi:10.1029/2009GL038068

Lippold, J., Mulitza, S., Mollenhauer, G., Weyer, S., Heslop, D., Christl, M., 2012. Boundary scavenging at the East Atlantic margin does not negate use of $^{231}Pa/^{230}Th$ to trace Atlantic overturning. Earth Planet. Sci. Lett. 333–334, 317–331. doi:10.1016/j.epsl.2012.04.005

Lisiecki, L.E., Raymo, M.E., 2005. A Pliocene-Pleistocene stack of 57 globally distributed benthic $\delta^{18}O$ records. Paleoceanography 20, n/a–n/a. doi:10.1029/2004PA001071

Lynch-Stieglitz, J., 2003. Tracers of past ocean circulation, in: Elderfield, H. (Ed.), The Oceans and Marine Geochemistry, Treatise on Geochemistry. Elsevier-Pergamon, Oxford, pp. 433–451.

Lynch-Stieglitz, J., Schmidt, M.W., Gene Henry, L., Curry, W.B., Skinner, L.C., Mulitza, S., Zhang, R., Chang, P., 2014. Muted change in Atlantic overturning circulation over some glacial-aged Heinrich events. Nat. Geosci. 7, 144–150. doi:10.1038/ngeo2045

MacAyeal, D.R., 1993. Binge/Purge oscillations of the Laurentide Ice Sheet as a cause of the North Atlantic's Heinrich events. Paleoceanography 8, 775–784.

Madureira, L.A.S., van Kreveld, S.A., Eglinton, G., Conte, M.H., Ganssen, G., van Hinte, J.E., Ottens, J.J., 1997. Late Quaternary high-resolution biomarker and other sedimentary climate proxies in a Northeast Atlantic Core. Paleoceanography 12, 255–269. doi:10.1029/96PA03120

Manighetti, B., McCave, I.N., Maslin, M., Shackleton, N.J., 1995. Chronology for climate change: Developing age models for the biogeochemical ocean flux study cores. Paleoceanography 10, 513–525. doi:10.1029/94PA03062

Marcott, S.A., Clark, P.U., Padman, L., Klinkhammer, G.P., Springer, S.R., Liu, Z., Otto-Bliesner, B.L., Carlson, A.E., Ungerer, A., Padman, J., 2011. Ice-shelf collapse from subsurface warming as a trigger for Heinrich events. Proc. Natl. Acad. Sci. 108, 13415–13419.

Marshall, S.J., Koutnik, M.R., 2006. Ice sheet action versus reaction: Distinguishing between Heinrich events and Dansgaard-Oeschger cycles in the North Atlantic. Paleoceanography 21. doi:10.1029/2005PA001247

Martrat, B., Grimalt, J.O., Shackleton, N.J., de Abreu, L., Hutterli, M.A., Stocker, T.F., 2007. Four Climate Cycles of Recurring Deep and Surface Water Destabilizations on the Iberian Margin. Science 317, 502–507. doi:10.1126/science.1139994

Maslin, M.A., Shackleton, N.J., Pflaumann, U., 1995. Surface water temperature, salinity, and density changes in the northeast Atlantic during the last 45,000 years: Heinrich events, deep water formation, and climatic rebounds. Paleoceanography 10, 527–544. doi:10.1029/94PA03040

Mayewski, P.A., Meeker, L.D., Whitlow, S., Twickler, M.S., Morrison, M.C., Bloomfield, P., Bond, G.C., Alley, R.B., Gow, A.J., Grootes, P.M., Meese, D.A., Ram, M., Taylor, K.C., Wumkes, W., 1994. Changes in Atmospheric Circulation and Ocean ice cover over the North Atlantic during the last 41,000 years. Science 263, 1747–1751.

McCartney, M.., 1992. Recirculating components to the deep boundary current of the northern North Atlantic. Prog. Oceanogr. 29, 283–383.

McCave, I.N., Manighetti, B., Robinson, S.G., 1995. Sortable silt and fine sediment size/composition slicing: Parameters for palaeocurrent speed and palaeoceanography. Paleoceanography 10, 593–610. doi:10.1029/94PA03039

McCave, I.N., Hall, I.R., 2006. Size sorting in marine muds: Processes, pitfalls, and prospects for paleoflow-speed proxies. Geochem. Geophys. Geosystems 7, Q10N05. doi:10.1029/2006GC001284

McCave, I.N., 2007. Deep-Sea Sediment Deposits and Properties Controlled by Currents, in: Hillaire-Marcel, C., de Vernal, A. (Eds.), Proxies in Late Cenozoic Paleoceanography. Elsevier, Oxford, pp. 19–62.

McLennan, S.M., Hemming, S.R., 1992. Samarium/neodymium elemental and isotopic systematics in sedimentary rocks. Geochim. Cosmochim. Acta 56, 887–898.

McLennan, S. M., S. Hemming, D. K. McDaniel, and G. N. Hanson. 1993. "Geochemical Approaches to Sedimentation, Provenance, and Tectonics." *Geological Society of America Special Papers* 284: 21–40.

McManus, Jerry F., Gérard C. Bond, Wallace S. Broecker, S. Johnsen, Laurent Labeyrie, and S. M. Higgins. 1994. "High-Resolution Climate Records from the North Atlantic during the Last Interglacial." *Nature* 371: 326–29.

McManus, J.F., Anderson, R.F., Broecker, W.S., Fleisher, M.Q., Higgins, S.M., 1998. Radiometrically determined sedimentary fluxes in the sub-polar North Atlantic during the last 140,000 years. Earth Planet. Sci. Lett. 155, 29–43. doi:10.1016/S0012-821X(97)00201-X

McManus, J.F., Francois, R., Gherardi, J.-M., Keigwin, L.D., Brown-Leger, S., 2004. Collapse and rapid resumption of Atlantic meridional circulation linked to deglacial climate changes. Nature 428, 834–837.

Meese, D.A., Gow, A.J., Alley, R.B., Zielinski, G.A., Grootes, P.M., Ram, M., Taylor, K.C., Mayewski, P.A., Bolzan, J.F., 1997. The Greenland Ice Sheet Project 2 depth-age scale: Methods and results. J. Geophys. Res. Oceans 102, 26411–26423. doi:10.1029/97JC00269

Mojtahid, M., F. Eynaud, S. Zaragosi, J. Scourse, J.-F. Bourillet, and T. Garlan. 2005. "Palaeoclimatology and Palaeohydrography of the Glacial Stages on Celtic and Armorican Margins over the Last 360000 Yrs." *Marine Geology* 224 (1-4): 57–82. doi:10.1016/j.margeo.2005.07.007.

Mudelsee, M., 2003. Estimating Pearson's Correlation Coefficient With Bootstrap Confidence Interval From Serially Dependant Time Series. Math. Geol. 35, 651–665.

Naafs, B.D.A., Hefter, J., Grützner, J., Stein, R., 2013a. Warming of surface waters in the mid-latitude North Atlantic during Heinrich events. Paleoceanography 28, 153–163. doi:10.1029/2012PA002354

Naafs, B.D.A., Hefter, J., Stein, R., 2013b. Millennial-scale ice rafting events and Hudson Strait Heinrich(-like) Events during the late Pliocene and Pleistocene: a review. Quat. Sci. Rev. 80, 1–28. doi:10.1016/j.quascirev.2013.08.014

National Research Council (U.S.). Committee on Abrupt Climate Change, 2002. Abrupt climate change inevitable surprises. National Academy Press, Washington, D.C.

NEEM community, 2013. Eemian interglacial reconstructed from a Greenland folded ice core. Nature 493, 489–494. doi:10.1038/nature11789

Negre, C., Zahn, R., Thomas, A.L., Masqué, P., Henderson, G.M., Martínez-Méndez, G., Hall, I.R., Mas, J.L., 2010. Reversed flow of Atlantic deep water during the Last Glacial Maximum. Nature 468, 84–88. doi:10.1038/nature09508

Obrochta, S.P., Miyahara, H., Yokoyama, Y., Crowley, T.J., 2012. A re-examination of evidence for the North Atlantic "1500-year cycle" at Site 609. Quat. Sci. Rev. 55, 23–33. doi:10.1016/j.quascirev.2012.08.008

Obrochta, S.P., Yokoyama, Y., Morén, J., Crowley, T.J., 2014. Conversion of GISP2-based sediment core age models to the GICC05 extended chronology. Quat. Geochronol. 20, 1–7. doi:10.1016/j.quageo.2013.09.001

Oeschger, H., Beer, J., Siegenthaler, U., Stauffer, B., Dansgaard, W., Langway, C.C., 1984. Late glacial climate history from ice cores. Clim. Process. Clim. Sensit. 299–306.

Oppo, D.W., Fairbanks, R.G., 1987. Variability in the deep and intermediate water circulation of the Atlantic Ocean during the past 25,000 years: Northern Hemisphere modulation of the Southern Ocean. Earth Planet. Sci. Lett. 86, 1–15. doi:10.1016/0012-821X(87)90183-X

Oppo, D.W., Curry, W.B., McManus, J.F., 2015. What do benthic $\delta^{13}C$ and $\delta^{18}O$ data tell us about Atlantic circulation during Heinrich Stadial 1? Paleoceanography 30, 2014PA002667. doi:10.1002/2014PA002667

Paillard, D., Labeyrie, L., Yiou, P., 1996. Macintosh Program performs time-series analysis. Eos Trans. Am. Geophys. Union 77, 379–379. doi:10.1029/96EO00259

Papa, B.D., Mysak, L.A., Wang, Z., 2005. Intermittent ice sheet discharge events in northeastern North America during the last glacial period. Clim. Dyn. 26, 201–216. doi:10.1007/s00382-005-0078-4

Pearson, P.N., 2012. Oxygen isotopes in foraminifera: Overview and historical review. Paleontol. Soc. Pap. 18, 1–38.

Peck, V.L., Hall, I.R., Zahn, R., Elderfield, H., Grousset, F., Hemming, S.R., Scourse, J.D., 2006. High resolution evidence for linkages between NW European ice sheet instability and Atlantic Meridional Overturning Circulation. Earth Planet. Sci. Lett. 243, 476–488. doi:10.1016/j.epsl.2005.12.023

Peck, V.L., Hall, I.R., Zahn, R., Grousset, F., Hemming, S.R., Scourse, J.D., 2007. The relationship of Heinrich events and their European precursors over the past 60ka BP: a multi-proxy ice-rafted debris provenance study in the North East Atlantic. Quat. Sci. Rev. 26, 862–875. doi:10.1016/j.quascirev.2006.12.002

Peck, V.L., Hall, I.R., Zahn, R., Elderfield, H., 2008. Millennial-scale surface and subsurface paleothermometry from the northeast Atlantic, 55–8 ka BP. Paleoceanography 23, PA3221. doi:10.1029/2008PA001631

Peltier, W.R., and R.G. Fairbanks. 2006. "Global Glacial Ice Volume and Last Glacial Maximum Duration from an Extended Barbados Sea Level Record." *Quaternary Science Reviews* 25 (23-24): 3322–37. doi:10.1016/j.quascirev.2006.04.010.

Peters, C., Walden, J., Austin, W.E.N., 2008. Magnetic signature of European margin sediments: Provenance of ice-rafted debris and the climatic response of the British ice sheet during Marine Isotope Stages 2 and 3. J. Geophys. Res. Earth Surf. 113, F03007. doi:10.1029/2007JF000836

Petit, J.R., Jouzel, J., Raynaud, D., Barkov, N.I., Barnola, J.-M., Basile, I., Bender, M., Chappellaz, J., Davis, M., Delaygue, G., Delmotte, M., Kotlyakov, V.M., Legrand, M., Lipenkov, V.Y., Lorius, C., PÉpin, L., Ritz, C., Saltzman, E., Stievenard, M., 1999. Climate and atmospheric history of the past 420,000 years from the Vostok ice core, Antarctica. Nature 399, 429–436. doi:10.1038/20859

Philpotts, A.., Ague, J.., 2009. Principles of Igneous and Metamorphic Petrology, 2nd ed. Cambridge University Press, Cambridge.

Porter, S.C., 1995. Correlation between climate events in the North Atlantic and China during the last glaciation. Nature 375, 305–308.

Prange, M., 2004. Modelling tempo-spatial signatures of Heinrich Events: influence of the climatic background state. Quat. Sci. Rev. 23, 521–527. doi:10.1016/j.quascirev.2003.11.004

Prins, M.A., Postma, G., Cleveringa, J., Cramp, A., Kenyon, N.H., 2000. Controls on terrigenous sediment supply to the Arabian Sea during the late Quaternary: the Indus Fan. Mar. Geol. 169, 327–349. doi:10.1016/S0025-3227(00)00086-4

Prins, M.A., Postma, G., Weltje, G.J., 2000. Controls on terrigenous sediment supply to the Arabian Sea during the late Quaternary: the Makran continental slope. Mar. Geol. 169, 351–371. doi:10.1016/S0025-3227(00)00087-6

Prins, M.A., Troelstra, S.R., Kruk, R.W., van de Borg, K., Weltje, G.J., 2001. The late quaternary sedimentary record of reykjanes ridge, North Atlantic. Radiocarbon 43, 939–947.

Prins, M.A., Bouwer, L.M., Beets, C.J., Troelstra, S.R., Weltje, G.J., Kruk, R.W., Kuijpers, A., Vroon, P.Z., 2002. Ocean circulation and iceberg discharge in the glacial North Atlantic: Inferences from unmixing of sediment size distributions. Geology 30, 555–558. doi:10.1130/0091-7613(2002)030<0555:OCAIDI>2.0.CO;2

Prins, M.A., Vriend, M., Nugteren, G., Vandenberghe, J., Lu, H., Zheng, H., Jan Weltje, G., 2007. Late Quaternary aeolian dust input variability on the Chinese Loess Plateau: inferences from unmixing of loess grain-size records. Quat. Sci. Rev. 26, 230–242. doi:10.1016/j.quascirev.2006.07.002

Rahmstorf, S., 2002. Ocean circulation and climate during the past 120,000 years. Nature 419, 207–214.

Rahmstorf, S., Box, J.E., Feulner, G., Mann, M.E., Robinson, A., Rutherford, S., Schaffernicht, E.J., 2015. Exceptional twentieth-century slowdown in Atlantic Ocean overturning circulation. Nat. Clim. Change 5, 475–480. doi:10.1038/nclimate2554

Rashid, H., Hesse, R., Piper, D.J.W., 2003a. Evidence for an additional Heinrich event between H5 and H6 in the Labrador Sea. Paleoceanography 18, n/a–n/a. doi:10.1029/2003PA000913

Rashid, H., Hesse, R., Piper, D.J.W., 2003b. Origin of unusually thick Heinrich layers in ice-proximal regions of the northwest Labrador Sea. Earth Planet. Sci. Lett. 208, 319–336. doi:10.1016/S0012-821X(03)00030-X

Rashid, H., Boyle, E.A., 2007. Mixed-Layer Deepening During Heinrich Events: A Multi-Planktonic Foraminiferal $\delta^{18}O$ Approach. Science 318, 439–441. doi:10.1126/science.1146138

Rashid, H., Boyle, E.A., 2008. Response to Comment on "Mixed-Layer Deepening During Heinrich Events: A Multi-Planktonic Foraminiferal $\delta^{18}O$ Approach." Science 320, 1161–1162.

Rashid, H., Saint-Ange, F., Barber, D.C., Smith, M.E., Devalia, N., 2012. Fine scale sediment structure and geochemical signature between eastern and western North Atlantic during Heinrich events 1 and 2. Quat. Sci. Rev. 46, 136–150. doi:10.1016/j.quascirev.2012.04.026

Rasmussen, T.L., Oppo, D.W., Thomsen, E., Lehman, S.J., 2003. Deep sea records from the southeast Labrador Sea: Ocean circulation changes and ice-rafting events during the last 160,000 years. Paleoceanography 18, 1018. doi:10.1029/2001PA000736

Ravelo, C., Hillaire-Marcel, C., 2007. The Use of oxygen and carbon isotopes of foraminifera in paleoceanography, in: Hillaire-Marcel, C., de Vernal, A. (Eds.), Proxies in Late Cenozoic Paleoceanography. Elsevier, Oxford.

Revel, M., Sinko, J.A., Grousset, F.E., Biscaye, P.E., 1996. Sr and Nd isotopes as tracers of North Atlantic lithic particles: Paleoclimatic implications. Paleoceanography 11, 95–113.

Richter, Thomas O., Sjerry Van der Gaast, Bob Koster, Aad Vaars, Rineke Gieles, Henko C. de Stigter, Henk De Haas, and Tjeerd CE van Weering. 2006. "The Avaatech XRF Core Scanner: Technical Description and Applications to NE Atlantic Sediments." *Geological Society, London, Special Publications* 267 (1): 39–50.

Rohling, E.J., Cooke, S., 1999. Stable oxygen and carbon isotopes in foraminiferal carbonate shells, in: Gupta, B.K. Sen (Ed.), Modern Foraminifera. Kluwer academic publishers, London, pp. 239–258.

Rohling, E., Mayewski, P., Challenor, P., 2003. On the timing and mechanism of millennial-scale climate variability during the last glacial cycle. Clim. Dyn. 20, 257–267.

Rohling, E.J., Grant, K., Hemleben, C., Kucera, M., Roberts, A.P., Schmeltzer, I., Schulz, H., Siccha, M., Siddall, M., Trommer, G., 2008. New constraints on the timing of sea level fluctuations during early to middle marine isotope stage 3. Paleoceanography 23, PA3219. doi:10.1029/2008PA001617

Rohling, E.J., Liu, Q.S., Roberts, A.P., Stanford, J.D., Rasmussen, S.O., Langen, P.L., Siddall, M., 2009. Controls on the East Asian monsoon during the last glacial cycle, based on comparison between Hulu Cave and polar ice-core records. Quat. Sci. Rev. 28, 3291–3302. doi:10.1016/j.quascirev.2009.09.007

Rosell-Melé, A., Maslin, M.A., Maxwell, J.R., Schaeffer, P., 1997. Biomarker evidence for "Heinrich" events. Geochim. Cosmochim. Acta 61, 1671–1678. doi:10.1016/S0016-7037(97)00046-X

Rosell-Melé, A., Jansen, E., Weinelt, M., 2002. Appraisal of a molecular approach to infer variations in surface ocean freshwater inputs into the North Atlantic

during the last glacial. Glob. Planet. Change, From process studies to reconstruction of the palaeoenvironment: advances in palaeoceanography 34, 143–152. doi:10.1016/S0921-8181(02)00111-X

Ruddiman, W.F., 1977. North Atlantic Ice-Rafting: A major change at 75,000 years before the present. Science 196, 1208–1211.

Saito, S., 1998. Major and trace element geochemistry of sediments from East Greeland continental rise: an implication for sediment provenance and source area weathering, in: Saunders, A.D., Larsen, H.C., Wise, S.. (Eds.), Proceedings of the Ocean Drilling Program, Scientific Results.

Sacchetti, Fabio, Sara Benetti, Rory Quinn, and Colm Ó Cofaigh. 2012. "Glacial and Post-Glacial Sedimentary Processes in the Irish Rockall Trough from an Integrated Acoustic Analysis of near-Seabed Sediments." *Geo-Marine Letters* 33 (1): 49–66. doi:10.1007/s00367-012-0310-2.

Sanchez Goñi, Maria Fernanda, and Sandy P. Harrison. 2010. "Millennial-Scale Climate Variability and Vegetation Changes during the Last Glacial: Concepts and Terminology." *Quaternary Science Reviews* 29, no. 21–22: 2823–27. doi:10.1016/j.quascirev.2009.11.014.

Sarnthein, M., Winn, K., Jung, S.J.A., Duplessy, J.-C., Labeyrie, L., Erlenkeuser, H., Ganssen, G., 1994. Changes in East Atlantic Deepwater Circulation over the last 30,000 years: Eight time slice reconstructions. Paleoceanography 9, 209–267. doi:10.1029/93PA03301

Schiebel, R., Bijma, J., Hemleben, C., 1997. Population dynamics of the planktic foraminifer Globigerina bulloides from the eastern North Atlantic. Deep Sea Res. Part Oceanogr. Res. Pap. 44, 1701–1713. doi:10.1016/S0967-0637(97)00036-8

Schulz, M., 2002. On the 1470-year pacing of Dansgaard-Oeschger warm events. Paleoceanography 17, 4–1–4–9. doi:10.1029/2000PA000571

Scourse, J.D., Hall, I.R., McCave, I.N., Young, J.R., Sugdon, C., 2000. The origin of Heinrich layers: evidence from H2 for European precursor events. Earth Planet. Sci. Lett. 182, 187–195. doi:10.1016/S0012-821X(00)00241-7

Scourse, J.D., Haapaniemi, A.I., Colmenero-Hidalgo, E., Peck, V.L., Hall, I.R., Austin, W.E.N., Knutz, P.C., Zahn, R., 2009. Growth, dynamics and deglaciation of the last British–Irish ice sheet: the deep-sea ice-rafted detritus record. Quat. Sci. Rev. 28, 3066–3084. doi:10.1016/j.quascirev.2009.08.009

Seidov, D., Maslin, M., 2001. Atlantic ocean heat piracy and the bipolar climate see-saw during Heinrich and Dansgaard-Oeschger events. J. Quat. Sci. 16, 321–328. doi:10.1002/jqs.595

Shackleton, N.., Fairbanks, R.., Chiu, T., Parrenin, F., 2004. Absolute calibration of the Greenland time scale: implications for Antarctic time scales and for $\Delta^{14}C$. Quat. Sci. Rev. 23, 1513–1522. doi:10.1016/j.quascirev.2004.03.006

Sharp, Z., 2007. Principles of stable isotope geochemistry, 1st ed. Pearson Prentice Hall, London.

Siddall, M., Rohling, E.J., Thompson, W.G., Waelbroeck, C., 2008. Marine isotope stage 3 sea level fluctuations: Data synthesis and new outlook. Rev. Geophys. 46, RG4003. doi:10.1029/2007RG000226

Snoeckx, H., Grousset, F., Revel, M., Boelaert, A., 1999. European contribution of ice-rafted sand to Heinrich layers H3 and H4. Mar. Geol. 158, 197–208. doi:10.1016/S0025-3227(98)00168-6

Spindler, Michael, and Gerhard S. Dieckmann. 1986. "Distribution and Abundance of the Planktic Foraminifer Neogloboquadrina Pachyderma in Sea Ice of the

Weddell Sea (Antarctica).” *Polar Biology* 5 (3): 185–91. doi:10.1007/BF00441699.

Stoker, M., Bradwell, T., 2005. The Minch palaeo-ice stream, NW sector of the British-Irish Ice Sheet. J. Geol. Soc. 162, 425–428.

Stuut, J.-B.W., Prins, M.A., Schneider, R.R., Weltje, G.J., Jansen, J.H.F., Postma, G., 2002. A 300-kyr record of aridity and wind strength in southwestern Africa: inferences from grain-size distributions of sediments on Walvis Ridge, SE Atlantic. Mar. Geol. 180, 221–233. doi:10.1016/S0025-3227(01)00215-8

Svensson, Anders, Katrine K. Andersen, Matthias Bigler, Henrik B. Clausen, Dorthe Dahl-Jensen, Siwan M. Davies, Sigfus J. Johnsen, et al. 2006. “The Greenland Ice Core Chronology 2005, 15–42 Ka. Part 2: Comparison to Other Records.” *Quaternary Science Reviews* 25 (23–24): 3258–67. doi:10.1016/j.quascirev.2006.08.003.

Sylvain Huon, R.J., 1993. Detrital silicates in Northeast Atlantic deep-sea sediments during the late Quaternary: Major elements, REE, Rb-Sr isotopic data. Eclogae Geol. Helvetiae 86, 195–218.

Syvitski, J.P.M., Andrews, J.T., Dowdeswell, J.A., 1996. Sediment deposition in an iceberg-dominated glacimarine environment, East Greenland: basin fill implications. Glob. Planet. Change, Impact of Glaciations on Basin Evolution: Data and Models from the Norwegian Margin and Adjacent Areas 12, 251–270. doi:10.1016/0921-8181(95)00023-2

Taylor, S.R., McLennan, S.M., 1985. The continental crust: Its composition and evolution, Geoscience Texts. Blackwell Science, Malden, Mass.

Thomas, C., Graham, C., Ellam, R., Fallick, A., 2004. 87Sr/86Sr chemostratigraphy of Neoproterozoic Dalradian limestones of Scotland and Ireland: constraints on depositional ages and time scales. J. Geol. Soc. 161, 229–242. doi:10.1144/0016-764903-001

Thomson, J., Higgs, N.C., Clayton, T., 1995. A geochemical criterion for the recognition of Heinrich events and estimation of their depositional fluxes by the (230Thexcess)0 profiling method. Earth Planet. Sci. Lett. 135, 41–56. doi:10.1016/0012-821X(95)00142-Y

Thornalley, D.J.R., Barker, S., Becker, J., Hall, I.R., Knorr, G., 2013. Abrupt changes in deep Atlantic circulation during the transition to full glacial conditions. Paleoceanography 28, 253–262. doi:10.1002/palo.20025

Tjallingii, R., Claussen, M., Stuut, J.-B.W., Fohlmeister, J., Jahn, A., Bickert, T., Lamy, F., Röhl, U., 2008. Coherent high- and low-latitude control of the northwest African hydrological balance. Nat. Geosci. 1, 670–675. doi:10.1038/ngeo289

Toucanne, S., S. Zaragosi, J.F. Bourillet, F. Naughton, M. Cremer, F. Eynaud, and B. Dennielou. 2008. “Activity of the Turbidite Levees of the Celtic–Armorican Margin (Bay of Biscay) during the Last 30,000 Years: Imprints of the Last European Deglaciation and Heinrich Events.” *Marine Geology* 247 (1-2): 84–103. doi:10.1016/j.margeo.2007.08.006.

Toucanne, Samuel, Guillaume Soulet, Nicolas Freslon, Ricardo Silva Jacinto, Bernard Dennielou, Sébastien Zaragosi, Frédérique Eynaud, Jean-François Bourillet, and Germain Bayon. 2015. “Millennial-Scale Fluctuations of the European Ice Sheet at the End of the Last Glacial, and Their Potential Impact on Global Climate.” *Quaternary Science Reviews* 123 (September): 113–33. doi:10.1016/j.quascirev.2015.06.010.

Treble, P., Schmitt, A., Edwards, R., Mckeegan, K., Harrison, T., Grove, M., Cheng, H., Wang, Y., 2007. High resolution Secondary Ionisation Mass Spectrometry (SIMS) $\delta^{18}O$ analyses of Hulu Cave speleothem at the time of Heinrich Event 1. Chem. Geol. 238, 197–212. doi:10.1016/j.chemgeo.2006.11.009

Urey, H.C., 1947. The thermodynamic properties of isotopic substances. J. Chem. Soc. Resumed 562–581. doi:10.1039/JR9470000562

Veiga-Pires, C.., Hillaire-Marcel, C., 1999. U and Th isotope constraints on the duration of Heinrich events H0-H4 in the southeastern Labrador Sea. Paleoceanography 14, 187–199.

Veizer, J., Ala, D., Azmy, K., Brukschen, P., Buhl, D., Bruhn, F., Carden, G.A.F., Diener, A., Ebneth, S., Godderis, Y., Torsten, J., Korte, C., Pawellek, F., Podlaha, O.G., Strauss, H., 1999. $^{87}Sr/^{86}Sr$, $\delta^{13}C$ and $\delta^{18}O$ evolution of Phanerozoic seawater. Chem. Geol. 161, 59–88.

Veizer, J., Hoefs, J., Lowe, D.R., Thurston, P.C., 1989. Geochemistry of Precambrian carbonates: II. Archean greenstone belts and Archean sea water. Geochim. Cosmochim. Acta 53, 859–871. doi:10.1016/0016-7037(89)90031-8

Vidal, L., Labeyrie, L., Cortijo, E., Arnold, M., Duplessy, J.C., Michel, E., Becqué, S., van Weering, T.C.E., 1997. Evidence for changes in the North Atlantic Deep Water linked to meltwater surges during the Heinrich events. Earth Planet. Sci. Lett. 146, 13–27. doi:10.1016/S0012-821X(96)00192-6

Voelker, A.H.L., Workshop participants, 2002. Global distribution of centennial-scale records for Marine Isotope Stage (MIS) 3: a database. Quat. Sci. Rev. 21, 1185–1212.

Wang, Y., Cheng, H., Edwards, R.L., Kong, X., Shao, X., Chen, S., Wu, J., Jiang, X., Wang, X., An, Z., 2008. Millennial- and orbital-scale changes in the East Asian monsoon over the past 224,000 years. Nature 451, 1090–1093. doi:10.1038/nature06692

Watkins, S.J., Maher, B.A., Bigg, G.R., 2007. Ocean circulation at the Last Glacial Maximum: A combined modeling and magnetic proxy-based study. Paleoceanography 22, PA2204. doi:10.1029/2006PA001281

Weber, S.L., Drijfhout, S.S., 2007. Stability of the Atlantic Meridional Overturning Circulation in the Last Glacial Maximum climate. Geophys. Res. Lett. 34, L22706. doi:10.1029/2007GL031437

Weldeab, S., 2012. Bipolar modulation of millennial-scale West African monsoon variability during the last glacial (75,000–25,000 years ago). Quat. Sci. Rev. 40, 21–29. doi:10.1016/j.quascirev.2012.02.014

Weltje, G.J., 1997. End-member modeling of compositional data: Numerical-statistical algorithms for solving the explicit mixing problem. Math. Geol. 29, 503–549. doi:10.1007/BF02775085

Weltje, G.J., Prins, M.A., 2003. Muddled or mixed? Inferring palaeoclimate from size distributions of deep-sea clastics. Sediment. Geol. 162, 39–62. doi:10.1016/S0037-0738(03)00235-5

Weltje, G.J., Prins, M.A., 2007. Genetically meaningful decomposition of grain-size distributions. Sediment. Geol. 202, 409–424. doi:10.1016/j.sedgeo.2007.03.007

Whittington, G., Hall, A.M., 2002. The Tolsta Interstadial, Scotland: correlation with D–O cycles GI-8 to GI-5? Quat. Sci. Rev. 21, 901–915. doi:10.1016/S0277-3791(01)00068-3

Willamowski, C., Zahn, R., 2000. Upper ocean circulation in the glacial North Atlantic from benthic foraminiferal isotope and trace element fingerprinting. Paleoceanography 15, 515–527. doi:10.1029/1999PA000467

Williams, P.., Ford, D.., 2006. Global distribution of carbonate rocks. Z. Für Geomorphol. 147, 1–2.

Zahn, R., Schönfeld, J., Kudrass, H.-R., Park, M.-H., Erlenkeuser, H., Grootes, P., 1997. Thermohaline instability in the North Atlantic during meltwater events: Stable isotope and ice-rafted detritus records from core SO75-26KL, Portugese margin. Paleoceanography 12, 696–710.

Zaragosi, S., F. Eynaud, C. Pujol, G. A. Auffret, J. -L. Turon, and T. Garlan. 2001. "Initiation of the European Deglaciation as Recorded in the Northwestern Bay of Biscay Slope Environments (Meriadzek Terrace and Trevelyan Escarpment): A Multi-Proxy Approach." *Earth and Planetary Science Letters* 188 (3–4): 493–507. doi:10.1016/S0012-821X(01)00332-6.

Ziveri, P., Stoll, H., Probert, I., Klaas, C., Geisen, M., Ganssen, G., Young, J., 2003. Stable isotope "vital effects" in coccolith calcite. Earth Planet. Sci. Lett. 210, 137–149. doi:10.1016/S0012-821X(03)00101-8

Zumaque, J, Frédérique Eynaud, Sébastien Zaragosi, F. Marret, K.M Matsuzaki, Catherine Kissel, Didier M. Roche, et al. 2012. "An Ocean-Ice Coupled Response during the Last Glacial: A View from a Marine Isotopic Stage 3 Record South of the Faeroe Shetland Gateway." *Climate of the Past* 8 (6): 1997–2017. doi:10.5194/cp-8-1997-2012.

9 Appendices

9.1 Appendix 1; Tie points for site U1308 from Hodell et al. (2008)

Available from https://doi.pangaea.de/10.1594/PANGAEA.831743
Radiocarbon dates from Bond et al. (1993).
SFCP04 = Shackleton et al. (2004); LR04 = Lisiecki and Raymo (2005).

Depth (m)	Age (Ka BP)	Age Model			
0.953	17.79	radiocarbon	94-609	Marine	
0.981	19.17	radiocarbon	94-609	Marine	
1.007	19.56	radiocarbon	94-609	Marine	
1.076	20.18	radiocarbon	94-609	Marine	
1.167	22.66	radiocarbon	94-609	Marine	
1.22	23.9	radiocarbon	94-609	Marine	
1.238	24.58	radiocarbon	94-609	Marine	
1.256	25.28	radiocarbon	94-609	Marine	
1.305	25.59	radiocarbon	94-609	Marine	
1.335	27.05	radiocarbon	94-609	Marine	
1.555	30.1	radiocarbon	94-609	Marine	
1.635	30.89	radiocarbon	94-609	Marine	
1.7	31.98	radiocarbon	94-609	Marine	
1.886	33.2	radiocarbon	94-609	Marine	
1.988	33.92	radiocarbon	94-609	Marine	
2.251	35.45	%Nps	94-609	GICC05	
2.512	38.15	%Nps	94-609	GICC05	
2.917	41.45	%Nps	94-609	GICC05	
3.06	43.3	%Nps	94-609	GICC05	
3.324	46.65	%Nps	94-609	GICC05	
4.099	54.4	%Nps	94-609	GICC05	
4.308	57.8	%Nps	94-609	GICC05	
4.36	59.05	%Nps	94-609	GICC05	
4.526	63.95	%Nps	94-609	GICC05modelext	
4.734	69.6	%Nps	94-609	GICC05modelext	
4.885	72.25	%Nps	94-609	GICC05modelext	
5.163	76.5	%Nps	94-609	GICC05modelext	
5.9	86	benthic	O-18	303-U1308	LR04
6.22	93	benthic	O-18	303-U1308	LR04
7.06	104	benthic	O-18	303-U1308	LR04
8.75	127	benthic	O-18	303-U1308	LR04
9.17	136	benthic	O-18	303-U1308	LR04
11.54	191	benthic	O-18	303-U1308	LR04

12.42	201	benthic	O-18	303-U1308	LR04
13.65	220	benthic	O-18	303-U1308	LR04
15.32	243	benthic	O-18	303-U1308	LR04
18.06	281	benthic	O-18	303-U1308	LR04
18.74	292	benthic	O-18	303-U1308	LR04
21.42	325	benthic	O-18	303-U1308	LR04

9.2 Appendix 2:No. of foraminifera per sample

N. pachyderma		***G. bulloides***		***C. wuellerstorfi***		***N. pachyderma***		***G. bulloides***		***C. wuellerstorfi***	
sample depth (cm)	No. of tests	sample depth (cm)	No. of tests	sample depth (cm)	No. of tests	sample depth (cm)	No. of tests	sample depth (cm)	No. of tests	sample depth (cm)	No. of tests
34	31	34	31	42	1	110	34	110	31	121	1
36	31	36	30	43	2			111	31	125	1
40	40	40	30	44	1	112	36	112	31	133	4
		42	30	46	2			113	30	134	2
		44	30	50	3	114	36	114	30	135	6
		46	30	52	2			115	30	136	5
48	39	48	30	53	5	116	40	116	30	137	3
		50	30	54	6			117	30	138	4
		52	30	55	2	118	36	118	31	139	4
53	32	53	30	56	5	119	35	119	30	140	4
54	34	54	30	57	1	120	40	120	31	142	5
		55	30	58	4	121	40	121	30	146	3
56	35	56	30	59	2	122	39	122	29	148	5
57	31	57	30	60	5			123	30		
58	34	58	30	61	2	124	41	124	27		
59	39	59	30	71	2	125	40	125	31		
60	36	60	31	72	3	126	36	126	29		
61	34	61	30	73	2	127	28	127	11		
62	30	62	31	74	3	128	25				
63	32	63	30	75	2	130	37	129	24		
64	35	64	28	76	1	131	40	131	12		
65	38	65	30	78	3	132		132	30		
66	29	66	5	80	2			133	30		
69	30			82	3	134	41	134	31		
70	29			86	3			135	31		
71	30	71	17	88	2	136	36	136	31		
72	33	72	30	90	5			137	31		
73	33	73	30	92	6	138	33	138	30		
74	34	74	30	94	5			139	32		
75	39	75	30	96	3	140	34	140	29		
76	35	76	31	98	2	142	37	142	30		
78	31	78	28	100	4			144	29		
80	30	80	30	102	2	146	40	146	30		
82	35	82	30	102	2	148	32	148	30		
84	36	84	30	103	2						

86	32	86	30	104	2
88	34	88	30	106	4
90	31	90	30	108	3
92	39	92	32	110	2
94	38	94	30	111	5
96	40	96	31	112	2
98	38	98	30	113	2
		100	30	114	4
		102	30	115	1
		103	35	117	1
104	40	104	32	118	4
106	38	106	32	119	3
108	33	108	30	120	2

9.3 Appendix 3: Trace element initial concentrations

element	sample concentrations	
	940	628
Li	49.6234	49.51897
Be	1.452195	1.484208
Sc	16.32953	15.41419
Ti	4754.641	4893.554
V	153.9296	140.5509
Cr	120.7654	127.2099
Co	11.86422	9.639769
Ni	56.75402	56.51842
Cu	20.62591	20.00068
Zn	82.88364	80.04471
Ga	20.42744	20.42256
Rb	178.3162	174.4809
Sr	14.50939	14.97467
Y	12.1223	14.24635
Zr	115.4054	110.4449
Nb	14.08847	14.02896
Cs	11.7959	11.15394
Ba	445.2745	457.2357
Ba	438.2114	444.7059
La	33.91117	41.69871
Ce	67.47243	83.77815
Pr	7.08713	8.626474
Nd	25.18019	30.75985
Sm	4.056023	4.852582
Eu	0.758852	0.901328
Tb	0.4376	0.515785
Gd	2.86014	3.415408
Dy	2.483554	2.907365
Ho	0.519953	0.600025
Er	1.58308	1.861867
Tm	0.260557	0.300041
Yb	1.715938	2.025776
Lu	0.265138	0.301799
Hf	3.270061	3.157396
Ta	1.090147	1.156575
Pb	33.6409	37.65788
Th	10.00281	10.89535
U	2.758321	3.248629

9.4 Appendix 4: Potential source area data, Grousset et al (2001) >63µm

PSA	$^{87}Sr/^{86}Sr$	+2o	$^{143}Nd/^{144}Nd$	+2o	εNd
FramStrait	0.71818	37	0.51198	16	-12.8
FramStrait	0.72162	21	0.512	15	-12.4
VoringPlateau	0.7229		0.511903	12	-14.3
VoringPlateau	0.7235		0.512057	11	-11.3
Oslofjord	0.725039	6	0.512077	8	-10.9
Sogreford	0.735614	6	0.511923	3	-13.9
RockallTrough	0.724352	6	0.512062	14	-11.2
RockallTrough	0.724012	8	0.512001	6	-12.4
IrishShelf	0.721308	7	0.511998	5	-12.4
IrishChannel	0.729787	7	0.512011	8	-12.2
CelticSea	0.720651	30	0.511965	18	-13.1
BritishIsles(mean)	0.732519		0.511966		-13.1
BayofBiscay(mean)	0.73065		0.51203		-11.9
SWPortuguessehelf	0.723874	10	0.512054	6	-11.4
NWPortuguessehelf	0.723285	9	0.511919	11	-14
Iceland(mean)	0.70345		0.513924	7.6	
Azores	0.704172	23	0.51289	16	4.9
FaeroeIslands	0.704637	11	0.512905	17	5.3
FaeroeIslands	0.705334	29	0.512966	28	6.2
FaeroeIslands	0.703887	10	0.513037	53	7.6
BaffinBay(b)	0.74287				-33
BaffinBay(b)	0.73156				-27.4
SaintLawrence	0.720113	8	0.511738	5	-17.5
MilnesSeamount	0.72836	12	0.510991	11	-32.1
GRIPbedrock	0.7288	11	0.510403	20	-43.5
GRIPbedrock	0.73167	7	0.510739	12	-37
EastGreenlandshelf	0.713495	8	0.512094	9	-10.6
FarewellCape	0.71111	10	0.511483	12	-22.5

Appendix 4 Continued: Revel et al (1996)

Reproduced with permission from John Wiley and Sons.

PSA	facies	Sr (ppm)	1000/Sr	$^{87}Sr/^{86}Sr$	Nd (ppm)	$^{143}Nd/^{144}Nd$	εNd
Baffin Bay W. Greenland[1]	SC	185	5.4	0.74285		0.511	-32
Baffin Bay W. Greenland[1]	SC	238	4.2	0.73225	21	0.51125	-27
Baffin Bay mean value[1]		208	4.8	0.73755	20.9	0.51112	-29.5
E. Greenland Shelf[1]	SC	366	2.73	0.712	23	0.51146	-23
Southeast Canada[2]	R	286	3.5	0.722		0.51135	-25
Norwegian shelf[1]	SC	162	6.17	0.72934	22	0.51161	-20.1
Norwegian Margin[1]	SC	154	6.49	0.7223	18	0.51119	-28
Norwegian Margin[1]	SC	116	8.62	0.72815			
Baltic Shield av[3]	CS				30	0.51164	-19.4
Norway[4]	S			0.72951		0.511876	-14.83
Norway[4]	S			0.73165		0.51191	-14.22
Scandinavia mean		141	7.1	0.72819	23	0.51644	-19.3
British Isles North[5]	RR	89	11.2	0.73903	40	0.51209	-10.6
British Isles South[5]	RR	106	9.4	0.72947	37	0.51195	-13.5
British Isles mean[5]		97	10.3	0.73425	38	0.51202	-12.1
Bay of Biscay[6]	SC	90	11.11	0.7348			
Bay of Biscay[7]	SC	78	12.76	0.73024	25	0.51205	-11.5
Bay of Biscay[7]	SC	84	11.9	0.72898	26	0.51204	-11.6
Bay of Biscay mean		81	12	0.72961	25	0.51204	-11.6
Faeroe Islands [8]	SC	80	12.52	0.7047	7	0.5123	-6.5
Iceland south[8]	ES	450	2.22	0.70345	54	0.51302	7.6
Iceland SW[9]	IB			0.70325		0.51304	7.98
Reykjanes Pen.[10]	B	164	6.14	0.70317	8	0.51305	7.9
Iceland[11]	B	154	6.5	0.70304			

Sources :[1] Sinko (1994) [2] McCulloch and Wasserberg (1978) [3] Miller et al (1986) [4] Janveit (1994) [5] Davies et al. (1985) [6]Dasch (1969), [7] Biscaye et al. (1996), [8]Revel (1995), [9] O'Noins and Gronvold (1973),[10] Zindler et al (1979) [11]Schilling et al (1983).

SC=sediment core, R=rock, CS=Clastic sediments, S= Shales, RR=Rock and river sediments ES= Esturine sediments, IB= Icelandic Basalts, B= Basalts

Appendix 4 Continued: Farmer et al. (2003) Trough mouth fan <63µm Reproduced with permission of Elsevier.

Site	Litho -	Grain	Rb	Sr		$^{87}Rb/^{86}Sr$	$^{87}Sr/^{86}Sr$	2σ	Sm (ppm)	Nd	$^{147}Sm/^{144}Nd$	$^{143}Nd/^{144}Nd$	2σ	εNd	TDm	$^{208}Pb/^{204}Pb$	$^{207}Pb/^{204}Pb$	$^{206}Pb/^{204}Pb$
HU77027-002TWC	h	<63	27.4	171	5.84795	0.463	0.72729	11	1.66	10.7	0.094	0.51145	12	-23.1	2	41.419	15.444	17.727
HU77027-002PC	h	<63	61.7	135	7.40741	1.319	0.72586	14	2.38	15.8	0.091	0.51153	27	-21.7	1.9	38.286	15.324	16.815
HU76029-034PC	h	<63	42.6	176	5.68182	0.698	0.73557	15	1.98	11.9	0.101	0.51124	8	-27.2	2.4	38.064	15.456	17.448
HU74026-557PC	h	<63	34.9	183	5.46448	0.552	0.73073	10	1.86	10.7	0.105	0.51131	11	-25.8	2.4	37.608	15.466	17.173
HU90023-101	ipg	<63	53.5	170	5.88235	0.91	0.72177	18	3.17	16.9	0.114	0.51119	13	-28.2	2.8	38.952	15.463	17.953
HU90023-101	ipg	<63	189	-	-	-	-	-	-	-	-	0.51116	9	-28.9		39.134	15.449	18.093
HU90023-101	ipg	<63	54.2	127	7.87402	1.231	0.72589	10	2.57	13.2	0.118	0.5112	12	-28.1	3	39.784	15.593	18.751
MD99.2236	ipg	<63	-	326	3.06748	0	0.71695	18	3.85	22.6	0.103	0.51149	6	-22.5	2.2	36.847	15.292	16.692
MD99.2236	ipg	<63	55.1	326	3.06748	0.489	0.7159	10	3.27	19.3	0.103	0.51156	20	-21	2	-	-	-
HU90-028-010	ipg	<63	44.8	148	6.75676	0.874	0.71714	16	2.89	16.6	0.105	0.51188	10	-14.7	1.6	38.364	15.534	18.096
HU90-028-010	ipg	<63	62.9	62	16.12903	2.915	0.72643	17	2.24	11.9	0.114	0.51199	7	-12.7	1.6	38.698	15.627	18.616
HU90-028-010	mt	<63	96.9	74	13.51351	3.803	0.72663	16	2.59	13.5	0.116	0.51197	6	-13.1	1.7	-	-	-
HU90-028-010	ipg	>150	54.5	130	7.69231	1.209	0.7184	9	1.35	7.9	0.102	0.51191	13	-14.2	1.5	-	-	-
HU90-028-010	ipg	>150	54.8	120	8.33333	1.314	0.71856	9	1.94	11.3	0.104	0.51194	10	-13.5	1.5	38.12	15.587	18.209
HU90-028-010	mt	>150	51.1	89	11.23596	1.662	0.72073	13	1.6	8.4	0.115	0.51198	7	-12.9	1.6	38.241	15.603	18.309

HU90-028-020	Mt	<63	54	36	27.77778	4.395	0.72639	9	1.31	6.2	0.128	-	-	-	-	38.987	15.615	18.746
HU90-028-020	mt	<63	53	34	29.41176	4.538	0.72869	11	1.25	6.8	0.111	0.51196	8	-13.3	1.6	38.96	15.611	18.738
HU90-028-020	mt	>150	61.7	80	12.5	2.226	0.72418	7	2.25	12.4	0.11	0.51203	12	-11.9	1.5	38.648	15.64	18.612
HU90-028-020	mt	>151	64.6	67	14.92537	2.793	0.72906	8	2.02	11.9	0.103	0.5119	13	-14.5	1.6	38.72	15.635	18.719
HU93030-006	Ic/ipg	<63	2.1	285	3.50877	0.022	0.70501	130	2.71	11.6	0.141	0.51296	9	6.2	0.1	38.953	15.578	18.989
HU93030-006	Ic/ipg	<63	19.3	191	5.2356	0.292	0.70385	7	3.64	15.4	0.143	0.51295	12	6.1	0.2	-	-	-
B9-97-336	Ic/ipg	<63	5.2	148	6.75676	0.101	0.70415	8	2.11	7.85	0.162	0.51293	9	5.7	0.4	38.953	15.618	19.031
B9-97-336	Ic/ipg	<63	8.3	185	5.40541	0.129	0.70418	8	2.34	8.78	0.161	0.51295	12	6.1	0.3	38.577	15.602	18.81
HU93030-007	hpmd	<63	-	231	4.329		0.70475	12	3.4	14.1	0.146	0.51285	23	4.2	0.5	38.66	15.551	18.753
HU93030-007	IRDSD	<63	-	137	7.29927		0.71323	12	2.75	14	0.119	0.5123	20	-6.5	1.2	-	-	-
HU93030-007	SG		-	112	8.92857		0.70399	44	2.75	14	0.119	0.51284	28	3.9	0.4	-	-	-
HU93030-007	IRDSD	<63	-	201	4.97512		0.70852	12	2.94	13.7	0.13	0.51251	16	-2.5	1	-	-	-
JM96-1207	SG		-	-	-	-	-	-	-	-	-	0.51244	73	-3.8	0.4	-	-	-
JM 96 70	DF	<63	104.1	150	6.66667	2.008	0.71714	8	6.47	34.1	0.115	0.51212	7	-10.1	1.4	-	-	-
JM96 68	Gmuf	<63	100.3	160	6.25	1.808	0.71749	9	6.1	32.2	0.115	0.51205	10	-11.4	1.5	38.785	15.595	18.721
JM98 624	D	<63	125.4	243	4.11523	1.495	0.72271	10	7.56	40	0.114	0.51187	7	-15.1	1.8	-	-	-
JM98 625	D	<63	99	247	4.04858	1.157	0.72206	10	7.43	39	0.115	0.51188	14	-14.8	1.8	38.91	15.653	19.309

Facies abbreviations; h= hemipelagic, ipg= ice proximal glaciomarine, mt=middle till, hpmd= hemipelagic muddy diamict, IRDSD= IRD rich sandy diamict, SG= siltstone grains, DF= debris flow, Gmuf= glaciomarine upper fan, D=diamiction

Appendix 4 Continued: Fagel et al. (2002)

Reproduced with permission from Elsevier.

Mean data PSA	No. Nd	No. Pb	$^{147}Sm/^{144}Nd$	$^{143}Nd/^{144}Nd$	$^{206}Pb/^{204}Pb$	$^{207}Pb/^{204}Pb$	$^{208}Pb/^{204}Pb$	$^{207}Pb/^{206}Pb$	$^{208}Pb/^{206}Pb$
Mid-Atlantic volcanism[1]	52	77	0.1877	0.513006	18.641	15.515	38.308	0.841	2.076
European Variscan crust[1]	17	12	0.1144	0.51208	18.84	15.702	39.024	0.834	2.072
European Pan-African crust[1]	57	12	0.1171	0.512045	18.95	15.549	38.709	0.821	2.044
Scandinavia[1]	15	38	0.1257	0.512044	18.925	15.633	39.755	0.833	2.541
Sveconorwegian belt[1]									
Scandinavia Pan-African crust[1]	19	36	0.1052	0.512137	18.451	15.604	38.25	0.846	2.073
Scandinavian shield[1]	19		0.1153	0.511588					
Greenland Pan-African crust		3			18.596	15.594	38.895	0.839	2.092
Greenland Ketilidian belt	21	64	0.1135	0.511697	21.236	15.624	39.084	0.757	1.89
Greenland Naqssuqtoqidian belt	18	212	0.1009	0.511046	16.673	14.92	37.935	0.95	2.363
Greenland[2]	11	97	0.0894	0.510671	14.914	14.738	35.646	1.003	2.43
Archean Craton Greenland[2] Early Archaean gneisses	109	11	0.131	0.510989	12.6	13.902	35.527	1.104	2.584
Baffin Island[2]	2		0.9925	0.510925					
Labrador[3] Early Archaean gneisses		9			13.2	14.07	34.202	1.067	2.595
Labrador Nain province[3]		15			15.684	14.618	36.894	0.939	2.375

Southern Canada Grenvillian belt[3]		9			16.805	15.428	36.403	0.919	2.168
Trans-Hudsonian orogeny	34	59	0.1215	0.511828	19.263	15.61	38.202	0.834	2.031
Superior province	86	81	0.1122	0.5112	25.526	16.657	44.515	0.711	1.852
West Greenland Rivers[2]	6	2	0.094	0.509676	17.265	14.733	37.553	0.854	2.176

Sources [1] Fagel et al. (1999), [2] Goldstein and Jacobsen (1987,1988) and Asmeron and Jacobsen (1993) [3] McCulloch and Wasserberg (1978),

Median data PSA	$^{147}Sm/^{144}Nd$	$^{143}Nd/^{144}Nd$	$^{206}Pb/^{204}Pb$	$^{207}Pb/^{204}Pb$	$^{208}Pb/^{204}Pb$	$^{207}Pb/^{206}Pb$	$^{208}Pb/^{206}Pb$
Mid-Atlantic volcanism	0.1756	0.512997	18.49	15.495	38.278	0.839	2.067
Europe Variscan crust	0.1151	0.512074	18.891	15.723	39.135	0.831	2.072
Europe Pan-African crust	0.1154	0.512037	18.772	15.529	38.562	0.829	2.058
Scandinavia Sveconorwegian belt	0.1199	0.51198	17.981	15.556	38.276	0.864	2.458
Scandinavian Pan-African crust	0.1042	0.51216	18.419	15.602	38.201	0.847	2.072
Scandinavian shield	0.1122	0.511525					
Greenland Pan-African crust			18.388	15.598	38.87	0.848	2.107
Greenland Ketilidian belt	0.1137	0.511699	20.816	15.653	39.115	0.754	1.863
Greenland Naqssuqtoqidian belt	0.1007	0.510973	15.227	14.692	36.164	0.966	2.362
Greenland Archean craton	0.0916	0.510699	14.417	14.755	35.3	1.028	2.428
Greenland Early Archaean gneisses	0.1195	0.510738	12.366	13.785	32.29	1.114	2.607
Labrador Early Archaean gneisses			13.115	14.045	33.709	1.075	2.651
Labrador Nain province			15.986	14.548	36.825	0.925	2.395
Southern Canada Grenvillian belt			16.867	15.416	36.449	0.914	2.164
Trans-Hudsonian orogen	0.1105	0.511761	18.44	15.52	37.45	0.84	2.062
Superior province	0.1056	0.511068	22.719	16.226	42.301	0.714	1.835
West Greenland Rivers	0.0945	0.509658					

9.5 *Appendix 5:Calculation of $\delta^{18}O_{SW}$ from foraminifera $\delta^{18}O$ and SST*

In Chapter 4 the available SST and *N. pachyderma* $\delta^{18}O$ data is used to present a rough estimate of the $\delta^{18}O$ of seawater ($_{SW}$) to show the difference between the variability of $\delta^{18}O_{FINE}$ and biogenic $\delta^{18}O$ of calcite. This estimate was derived by rearranging the palaeotemperature equation of Kim and O'Neil (1997) as described in Chapter 2, see Equation 2.2. SST estimates from faunal transfer functions taken from Hall et al., (2011) are shown in Figure A.1. Calculation of $\delta^{18}O_{SW}$ using SST transfer functions introduces error and should be interpreted with caution. Faunal transfer functions use the abundance of many planktic foraminifera to infer temperature. Whilst the technique is a valid approach comparisons with Mg/Ca and biomarker derived SST demonstrate differences between the proxies (e.g., Nurnberg et al., 2000; Bard, 2001).

Equation A.1: Palaeo temperature equation (Kim and O'Neil, 1997)

$$T = 16.1 - 4.64\ (\delta^{18}Oc\ -\ \delta^{18}Osw)\ +\ (0.09\ (\delta^{18}Oc\ -\ \delta^{18}Osw))^2$$

Calculation of $\delta^{18}O_{SW}$ from coupled Mg/Ca temperature estimates and $\delta^{18}O$ from a single species of foraminifera is a much better method, as Mg/Ca temperature estimates and $\delta^{18}O$ are likely to have been recorded in the same water mass. For this site Mg/Ca data was only available for part of the record, however it is useful to check the result provided by faunal transfer functions. The Mg/Ca temperatures displayed are derived using equations from nearby sites with similar conditions using the equations found in Anand (2003) and Peck et al (2006) and are shown in Figure A.2. As is evident from the data in Figure A.1 there are large shifts in the $\delta^{18}O_{SW}$ of nearly 3 ‰ from 30-26 ka BP, which is due to the large changes in ANN faunal transfer function SST. However, estimates over the same period from Mg/Ca derived SST show much less variability, with shifts of ~ 1‰. This would suggest that using the SST derived from faunal transfer functions over estimates the variability in $\delta^{18}O_{SW}$ compared to Mg/Ca SST estimates.

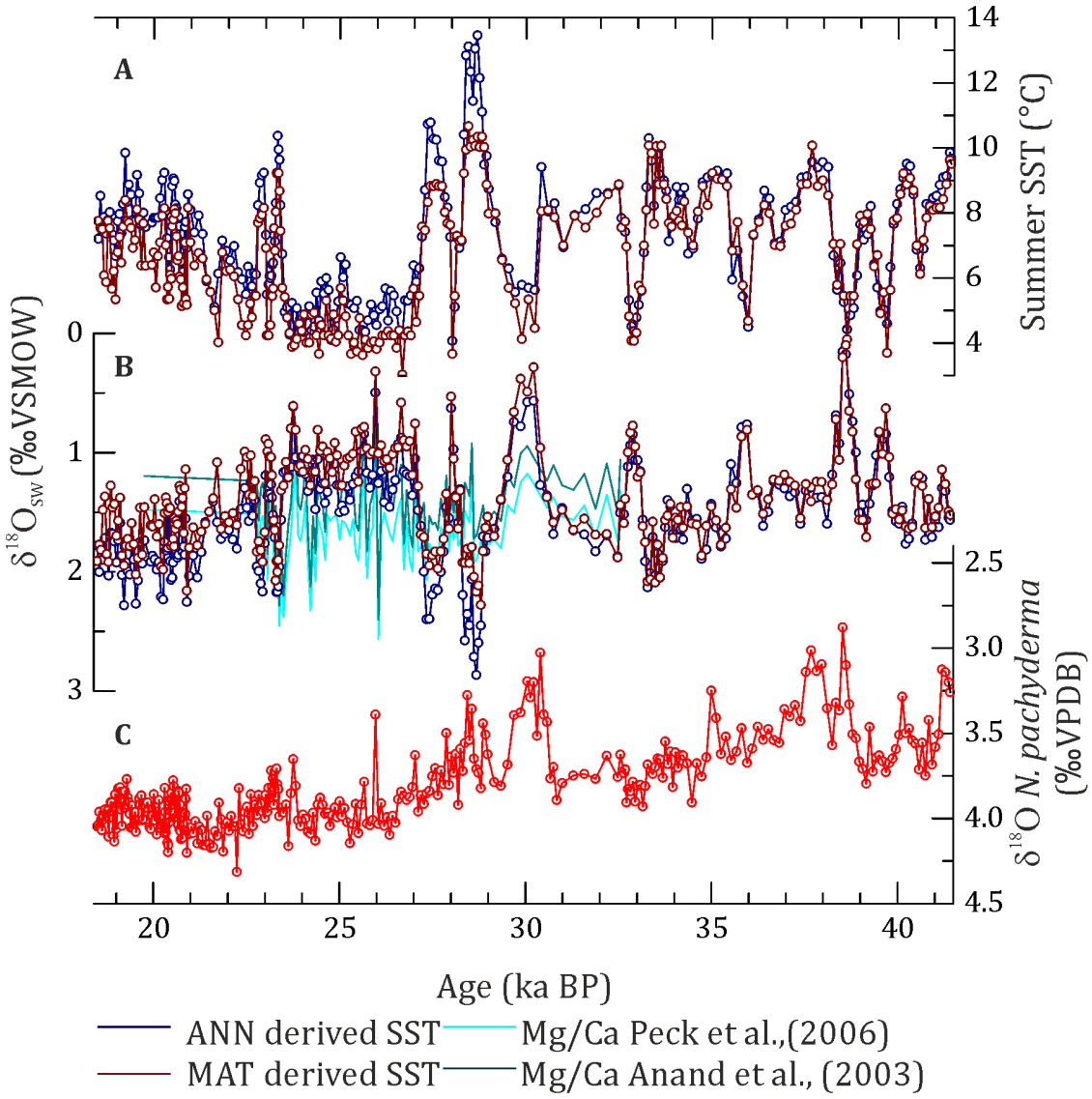

Figure A.1 $\delta^{18}O_{SW}$ derived from faunal ANN (dark blue) and MAT (brown) SST estimates and $\delta^{18}O$ of N. pachyderma. A: Summer SST estimates derived from ANN (dark blue) and MAT (brown) faunal transfer functions. B: $\delta^{18}O_{SW}$ derived from faunal SST estimates with Mg/Ca derived $\delta^{18}O_{SW}$ for comparison. C: $\delta^{18}O$ of N. pachyderma tests. Data are from Hall et al (2011) and pers. Comms. Ian Hall and Elena Colmenero-Hidalgo.

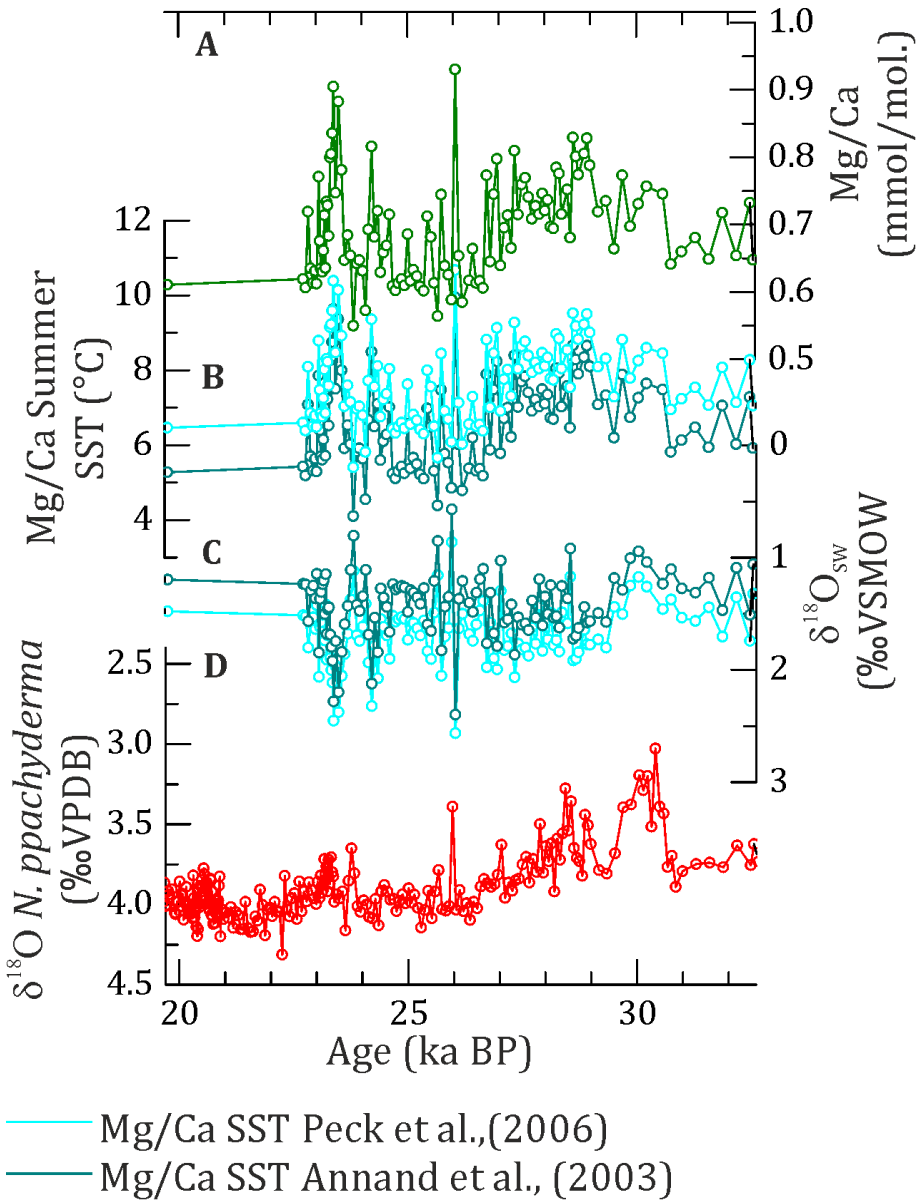

Figure A.2 Mg/Ca SST and N. pachyderma derived $\delta^{18}O_{SW}$ estimates A: Mg/Ca measurements (per mmol), B: Mg/Ca derived Summer SST estimates using the equations from Peck et al., (2006) (light blue) and Anand et al., (2003) (dark blue). C: $\delta^{18}O_{SW}$ estimates using the summer SST derived from Mg/Ca and $\delta^{18}O$ N. pachydema D: N.pachyderma $\delta^{18}O$ Data are from Hall et al (2011) and pers. Comms. Ian Hall and Elena Colmenero-Hidalgo..